ISSN 0973-8916

Current Trends in Biotechnology and Pharmacy

Volume- 19 issue 1 January 2025

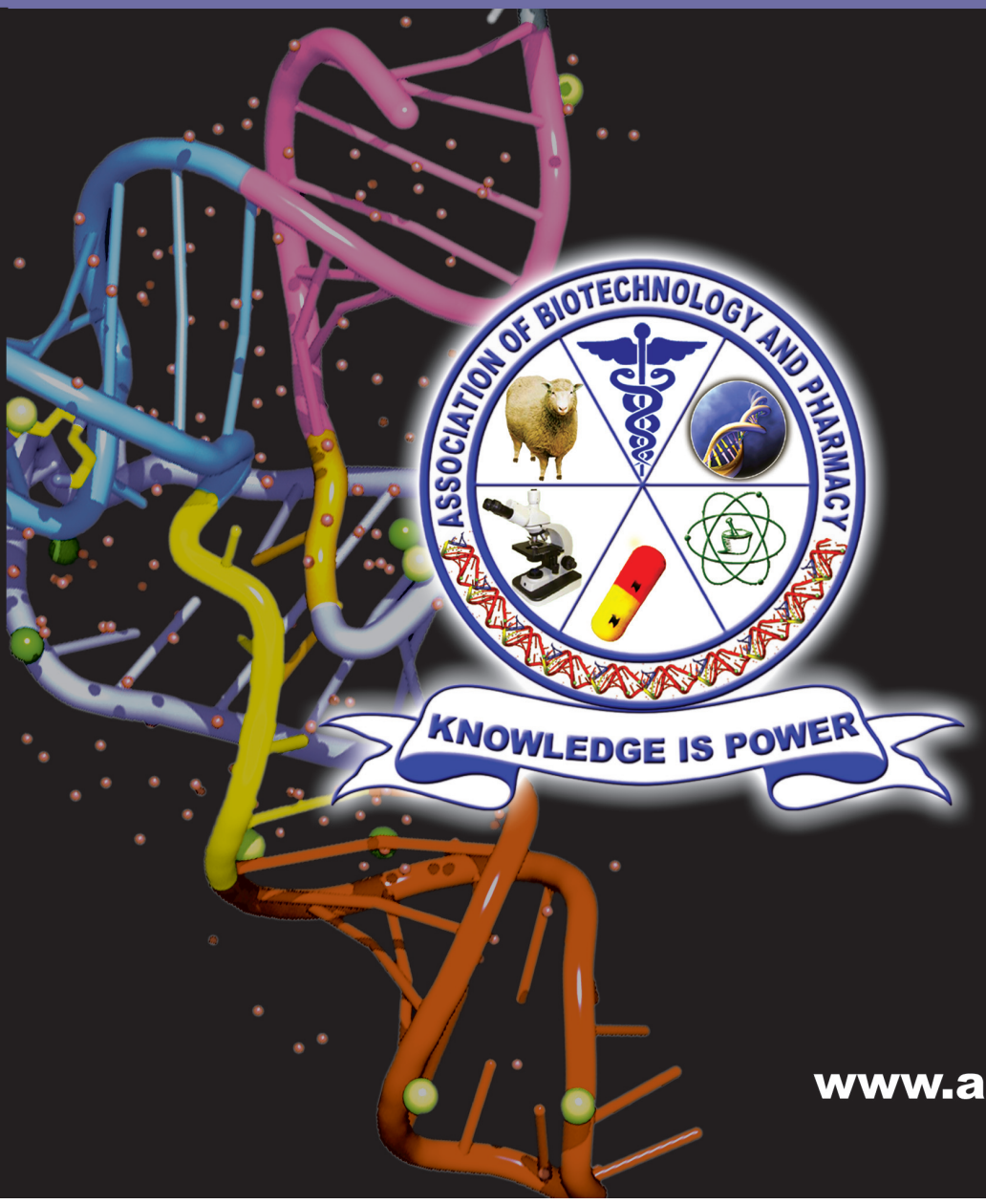

www.abap.co.in

Current Trends in Biotechnology and Pharmacy

ISSN 0973-8916 (Print), 2230-7303 (Online)

www.abap.co.in

ISSN 0973-8916

Current Trends in Biotechnology and Pharmacy

(An International Scientific Journal)

Volume- 19 issue 1 January 2025

www.abap.co.in

Indexed in Chemical Abstracts, EMBASE, ProQuest, Academic SearchTM, DOAJ, CAB Abstracts, Index Copernicus, Ulrich's Periodicals Directory, Open J-Gate Pharmoinfonet.in Indianjournals.com and Indian Science Abstracts.

Association of Biotechnology and Pharmacy
(Regn. No. 28 OF 2007)

The Association of Biotechnology and Pharmacy (ABAP) was established for promoting the science of Biotechnology and Pharmacy. The objective of the Association is to advance and disseminate the knowledge and information in the areas of Biotechnology and Pharmacy by organising annual scientific meetings, seminars and symposia.

Members

The persons involved in research, teaching and work can become members of Association by paying membership fees to Association.

The members of the Association are allowed to write the title MABAP (Member of the Association of Biotechnology and Pharmacy) with their names.

Fellows

Every year, the Association will award Fellowships to the limited number of members of the Association with a distinguished academic and scientific career to be as Fellows of the Association during annual convention. The fellows can write the title FABAP (Fellow of the Association of Biotechnology and Pharmacy) with their names.

Membership details

(Membership and Journal)		India	SAARC	Others
Individuals	– 1 year	Rs. 600	Rs. 1000	$100
LifeMember		Rs. 4000	Rs. 6000	$500
Institutions	– 1 year	Rs. 1500	Rs. 2000	$200
(Journal only)	Life member	Rs.10000	Rs.12000	$1200

Individuals can pay in two instalments, however the membership certificate will be issued on payment of full amount. All the members and Fellows will receive a copy of the journal free.

Association of Biotechnology and Pharmacy

(Regn. No. 28 OF 2007)
#5-69-64; 6/19, Brodipet
Guntur – 522 002, Andhra Pradesh, India

Current Trends in Biotechnology and Pharmacy
ISSN 0973-8916

Volume 19 (1) **CONTENTS** **January 2025**

Information to Authors

The Current Trends in Biotechnology and Pharmacy is an official international journal of Association of Biotechnology and Pharmacy. It is a peer reviewed quarterly journal dedicated to publish high quality original research articles in biotechnology and pharmacy. The journal will accept contributions from all areas of biotechnology and pharmacy including plant, animal, industrial, microbial, medical, pharmaceutical and analytical biotechnologies, immunology, proteomics, genomics, metabolomics, bioinformatics and different areas in pharmacy such as, pharmaceutics, pharmacology, pharmaceutical chemistry, pharma analysis and pharmacognosy. In addition to the original research papers, review articles in the above mentioned fields will also be considered.

Call for papers

The Association is inviting original research or review papers and short comunications in any of the above mentioned research areas for publication in Current Trends in Biotechnology and Pharmacy. The manuscripts should be concise, typed in double space in a general format containing a title page with a short running title and the names and addresses of the authors for correspondence followed by Abstract (350 words), 3 – 5 key words, Introduction, Materials and Methods, Results and Discussion, Conclusion, References, followed by the tables, figures and graphs on separate sheets. For quoting references in the text one has to follow the numbering of references in parentheses and full references with appropriate numbers at the end of the text in the same order. References have to be cited in the format below.

Mahavadi, S., Rao, R.S.S.K. and Murthy, K.S. (2007). Cross-regulation of VAPC2 receptor internalization by m2 receptors via c-Src-mediated phosphorylation of GRK2. Regulatory Peptides, 139: 109-114.

Lehninger, A.L., Nelson, D.L. and Cox, M.M. (2004). Lehninger Principles of Biochemistry, (4th edition), W.H. Freeman & Co., New York, USA, pp. 73-111.

Authors have to submit the figures, graphs and tables of the related research paper/article in Adobe Photoshop of the latest version for good illumination and allignment.

Authors can submit their papers and articles either to the editor or any of the editorial board members for onward transmission to the editorial office. Members of the editorial board are authorized to accept papers and can recommend for publication after the peer reviewing process. The email address of editorial board members are available in website www.abap.in. For submission of the articles directly, the authors are advised to submit by email to krssrao@abap.co.in or krssrao@yahoo.com.

Authors are solely responsible for the data, presentation and conclusions made in their articles/research papers. It is the responsibility of the advertisers for the statements made in the advertisements.

Current Trends in Biotechnology and Pharmacy
Vol. 19(1) 2107-2115, January 2025, ISSN 0973-8916 (Print), 2230-7303 (Online)
DOI: 10.5530/ctbp.2025.1.1

Valproic Acid Induces Zebrafish Embryonic Developmental Defects by Inducing Oxidative Stress-mediated Apoptosis: Dose and Time-dependent Analysis

Akhila Nooka [1], Hari Krishna Chilaka [1], Ravindra Kumbha [1], Bala Bhargavi Yemineni [1], Sanny Tanukonda [1], Naveen Kumar Kalagatur [2*]

[1] Department of Pharmaceutical Engineering, Kakinada Institute of Technological Sciences, Ramachandrapuram – 533 255, Andhra Pradesh, India.
[2] DRDO-BU Centre for Life Sciences, Bharathiar University, Coimbatore – 641 046, India

*** Corresponding author:** knaveenkumar.kalagatur@yahoo.co.in

Abstract

The study aimed to reveal the developmental deformities of the anticonvulsant drug valproic acid (VPA) in zebrafish embryos. The zebrafish embryos were exposed to VPA (up to 100 µM) after 4 hours post-fertilization (hpf) and examined for *in-vivo* toxicity by hatching rate, survival rate, heart rate, oxidative stress, and apoptosis. The VPA has dose and time-dependently affected embryos' hatching, survival, and heart rate. The VPA delayed hatching and noticed unusual hatching at 72 hpf. Complete death of embryos was noticed at doses of 40, 60, 80, and 100 µM VPA at 72 and 96 hpf. Furthermore, VPA has negatively affected the heart rate and was found to be depleted with the dose and time of exposure to VPA. The VPA has induced various developmental defects in embryos, including yolk sac edema, pericardial edema, spinal cord curvature, and tail deformities. DCFH-DA staining revealed that the VPA escalated ROS molecules and induced oxidative stress in embryos. Acridine orange (AO) staining revealed that VPA causes toxicity in embryos by apoptosis. Overall, the study concluded that VPA induces developmental defects in zebrafish embryos by oxidative-stress-mediated apoptosis in dose and time-dependent ways. Thus, our study suggests that VPA release into aquatic ecosystems needs to be limited.

Keywords: Valproic acid, Zebrafish, Developmental toxicity, Reactive Oxygen Species, Apoptosis.

Introduction

To preserve human and animal health, pharmaceutical consumption is expanding internationally. About 4000 compounds are mainly used for human and animal medicine. Large-scale pharmaceutical use poses potential environmental risks (1). Feces and urine excrete medicinal substances as unabsorbed forms and metabolites/byproducts. Pharmaceutical chemicals enter aquatic habitats through sewage discharges, landfill leaching, indiscriminate hospital and residential waste disposal, and stormwater runoff. Drug-resistant infections, infertility, cancer, endocrine disruption, and plant and animal development retardation can result from ng/L levels of hazardous residues. Pharmaceutical residues, such as non-steroidal anti-inflammatory medications, hormones, antibiotics, antiretrovirals, lipid regulators, and β-blockers, adversely damage aquatic ecosystems and human health. Surface water, reclaimed wastewater, and groundwater often contain ampicillin, sulphathiazole, carbamazepine, penicillin, aspirin, paracetamol, amoxicillin, diclofenac, anticonvulsants, vancomycin, efavirenz, and ibuprofen (2, 3, 4).

For more than thirty years, the anticonvulsant drug valproic acid (VPA) and its derivatives have been used to treat epilepsy because they are non-specific inhibitors of histone deacetylase. VPA works by blocking the metabolism of γ-aminobutyric acid (GABA) and interfering with GABA reuptake at nerve terminals. As a result, VPA is used to treat several mental illnesses, including epilepsy, schizophrenia, bipolar disorder, and migraine. Despite being widely regarded as safe, VPA can have serious side effects during therapy, such as significant bone loss (5). Moreover, VPA is cautiously recommended by National Institute for Health and Care Excellence (NICE) for children, young people, and adults with Idiopathic Generalized Epilepsies (IGEs) and pregnant women (6).

The VPA has been detected in municipal sewage and surface water samples, and potentially poses an environmental and health risk. The majority of VPA drugs are taken orally, and 30% to 50% are eliminated as metabolites. Uncontrolled disposal and poor wastewater treatment release VPA's unchanged/unabsorbed form and metabolites/ byproducts into waterways. Due to its limited degradation potential, constant release, and widespread use, VPA may bio-accumulate in aquatic environments while being removed at low concentrations (ng/L or sub-parts-per-billion) (7, 8, 9). VPA accumulation, destiny, and chronic exposure can alter base-of-food-chain biotic populations. Top-of-the-food-chain creatures like larger fishes may bioaccumulate these, generating somatic mutations and systemic toxicity that can cause cancer, biodiversity loss, and death. Moreover, VPA entering the human food chain may cause baldness, elevated alanine aminotransferase and aspartate aminotransferase in the liver, tinnitus, myalgia, and dyspnea. High doses of VPA can cause liver damage, hallucinations, hypothermia, murder, hyponatremia, schizophrenia, toxic epidermal necrolysis, Stevens-Johnson syndrome, allergic reactions, anaphylaxis, syndrome of inappropriate antidiuretic hormone secretion (SIADH), pancreatic inflammation, and allergic reactions. Concentrations can cause thrombocytopenia, pancytopenia, hyperammonaemia, myelosuppression, aplastic anemia, hemorrhage, erythema multiforme, polycystic ovarian syndrome, cerebral pseudoatrophy, encephalopathy, and coma (5, 6). These harmful effects of VPA are known to be caused by the activation of oxidative stress and inflammatory processes. Therefore, antioxidants and anti-inflammatory medications are being extensively investigated in current research as possible therapeutic strategies against VPA damage (10, 11, 12, 13, 14).

We need to gain more knowledge of the impact of VPA on aquatic animals. Therefore, the VPA effect on zebrafish embryonic development was studied in the present study. The reason for selecting zebrafish as a model fish for this study is that they are well suitable for phenotypic screening, embryos are transparent to observe phenotypic changes, maintenance is easy, offspring count is very high, they reproduce all over the year, embryonic development is rapid (15). Research on vertebrate gene function and human genetic illness has been conducted using zebrafish. A high-quality sequence assembly of the zebrafish genome, spanning 26,000 protein-coding genes, has been sequenced, providing insights into the relationship between zebrafish genes and human genes, with 70% of human genes having a zebrafish orthologue (16).

Our study includes toxicological analyses of VPA, including hatching rate, developmental deformities, survival rate, heart rate, oxidative stress (ROS generation), and apoptosis (acridine orange staining).

Materials and Methods

Chemicals and reagents

2',7'-Dichlorodihydrofluorescein diacetate (DCFH-DA), VPA, pure water, and acridine orange (AO) were obtained from Sigma-Aldrich, Bengaluru, India. The other

chemicals used in the study were obtained from Merck, Bengaluru, India.

Zebrafish husbandry

Wild-type adult male and female zebrafish were purchased from the local aquarium, Coimbatore, Tamil Nadu, India. The fish were thoroughly inspected for illness and infection. The fishes were maintained in a recirculating system with a 12-hour light and 12-hour dark photoperiod at 27 ± 1°C. The fish were fed with commercially available fish food twice a day. The debris and the tank were cleaned every day and once a week, respectively. The spawning was carried out with 1:2 (male and female zebrafish), and fertile eggs were used for the study (17).

Experimental design

The exposure of zebrafish embryos to VPA was carried out in accordance with FET guidelines (17). The VPA was treated to fertile embryos after 4 hrs post fertilization (hpf). VPA stock solution was prepared in pure water (500 µM) and stored in darkness at -20°C. Then, VPA stock was subjected to dilution to obtain test concentrations of up to 100 µM VPA in an E3 medium for toxicological evaluation. Each experimental group contains 25 embryos. The experiment was carried out at 27 ± 1°C with aeration. The embryos treated alone with the E3 medium were control. The embryos were observed for developmental deformities, survival rate, heart rate, oxidative stress (ROS generation), and apoptosis (acridine orange staining). The observations were noticed at 24, 48, 72, and 96 hpf (18, 19).

Assessment of survival rate and developmental defects

Following the treatment with VPA, as explained in the experimental design. The survival rate and developmental defects of embryos were recorded at specific periods: 24, 48, 72, and 96 hpf (19). The results were expressed as percentages. The observed developmental deformities include yolk sac edema, pericardial edema, somite formation defects, spinal cord curvature, and tail deformities. The developmental deformities were observed under the inverted microscope (EVOS, FLC, Thermo Fisher Scientific, USA).

Assessment of cardiotoxicity

Following the treatment with VPA, as explained in the experimental design. The zebrafish embryos were observed for cardiotoxicity under the inverted microscope. The heartbeat rate was measured at 24, 48, 72, and 96 hpf after the embryos were exposed to the VPA. The heartbeat rate of embryos was measured and expressed per minute (20).

Assessment of oxidative stress by DCFH-DA staining

Following the treatment with VPA, as explained in the experimental design. The effect of VPA on ROS generation in zebrafish embryos was determined by DCFH-DA staining (21, 22). Briefly, before DCF-DA staining, embryos were washed with embryonic media, and staining was carried out at 5 µM of DCFH-DA in water for 15 min in the dark. Following, the embryos were washed thrice with embryonic media, anesthetized, and fixed on glass slides for observation. The green fluorescent protein (GFP) images were captured using the fluorescent inverted microscope (EVOS FLC, Thermo Fisher Scientific, USA). Furthermore, a fluorescent intensity, which reflects ROS levels, was quantified at excitation and emission of 485 and 525 nm, respectively. The results were expressed as percentages with respect to the control group.

Assessment of apoptosis by AO staining

Following the treatment with VPA, as explained in the experimental design. The role of VPA on apoptosis in zebrafish embryos was observed by acridine orange (AO) staining (20). Briefly, following the VPA treatment, embryos were washed twice with water and stained with

5 µM of AO for 15 min in the dark. Following, embryos were washed thrice with embryonic media, anesthetized, and fixed on glass slides for observation. The images were captured using a fluorescent inverted microscope (EVOS FLC, Thermo Fisher Scientific, USA). A GFP filter captured the AO images. The fluorescence intensity of AO was measured at excitation and emission of 485 and 520 nm, respectively. The results were expressed in percentage with respect to the control group.

Statistical analysis

The experiments were carried out independently and in triplicates (n = 3). The results were expressed in mean ± standard deviation. The data was processed by one-way ANOVA, and statistical significance was considered at $p \leq 0.05$. The statistical difference was calculated using Dunnett's test. The analysis and graphical representation were done using GraphPad Prism version 8.

Results and Discussion

Effect of VPA on the hatching rate, survivability, and developmental defects

In the present study, the effect of VPA on the hatching rate, survivability, and developmental defects of zebrafish embryos was assessed at 20, 40, 60, 80, and 100 µM for 24, 48, 72, and 96 hpf. The VPA has been shown to negatively affect the hatching rate of zebrafish embryos (Fig. 1). At 20 µM VPA, hatching of zebrafish embryos was noticed at 48, 72, and 96 hpf. The hatching rate was delayed at 20 µM VPA compared to the control ($p \leq 0.05$). On the contrary, hatching was found completely absent at 60, 80, and 100 µM VPA. The VPA has shown a toxic effect on zebrafish embryos and has affected the survivability of zebrafish embryos, which was found to be dose-dependent and exposure-dependent (Fig. 2). Higher zebrafish embryo death was noticed at a higher tested dose of 100 µM VPA in 24 hpf. In 48 hpf, the complete death of zebrafish embryos was noticed at 80 and 100 µM VPA, and a higher death was at 60 µM VPA. In 72 and 96 hpf, complete death of zebrafish embryos was noticed at a tested concentration of 40, 60, 80, and 100 µM VPA, and a higher death rate was noticed at 20 µM VPA. Thus, the study proved that VPA has affected the survivability of zebrafish embryos and induced death in dose-dependent and time-dependent ways. Moreover, our study observed that VPA had induced various developmental defects in zebrafish embryos at 24, 48, 72, and 96 hpf (Fig. 3). The observed developmental defects include yolk sac edema, pericardial edema, spinal cord curvature, and tail deformities (23). The high concentration of VPA showed a higher intensity of malformation and dead embryos than the low concentration of VPA. In support of our report, Wang et al. have proved that up to 50 µM VPA causes the death of embryos and is responsible for neurotoxicity (20). The results of our investigation demonstrate the substantial toxic effects of VPA on zebrafish embryos, including embryonic death, delayed hatching, and apparent cellular damage in embryos. The study revealed that the toxic effects of VPA rely on the dose and exposure time. This information explains the VPA drug's toxic aberrations and detrimental effects on zebrafish embryonic development.

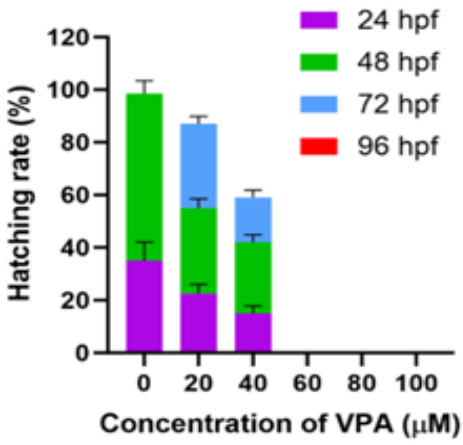

Figure 1: Effect of different concentrations of valproic acid (VPA) on hatching rate (%) of zebrafish embryos at 24, 48, 72, and 96 hpf.

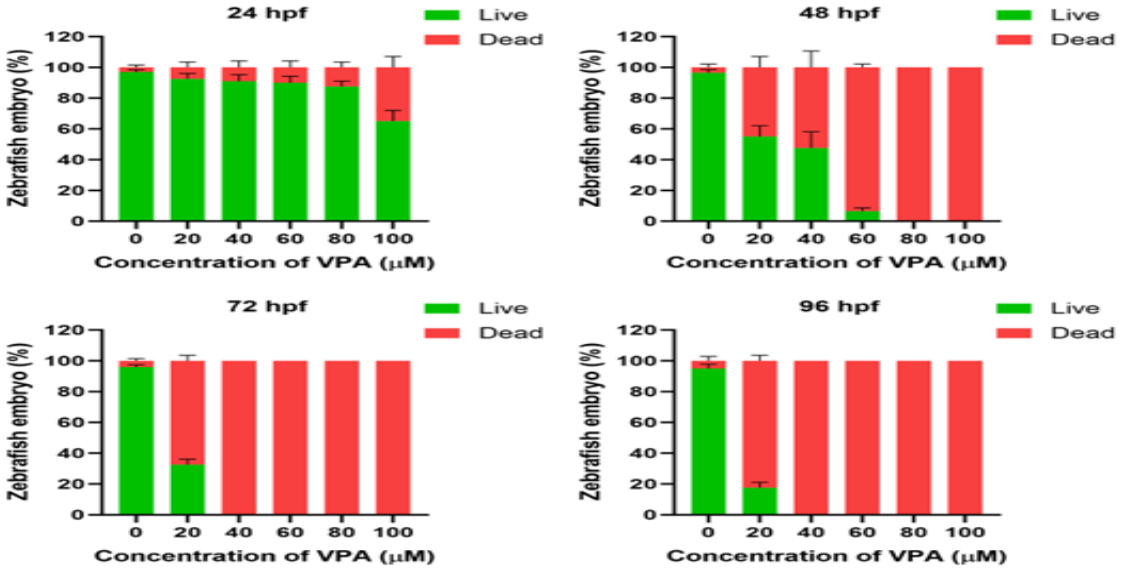

Figure 2: Effect of different concentrations of valproic acid (VPA) on survivability of zebrafish embryos at 24, 48, 72, and 96 hpf.

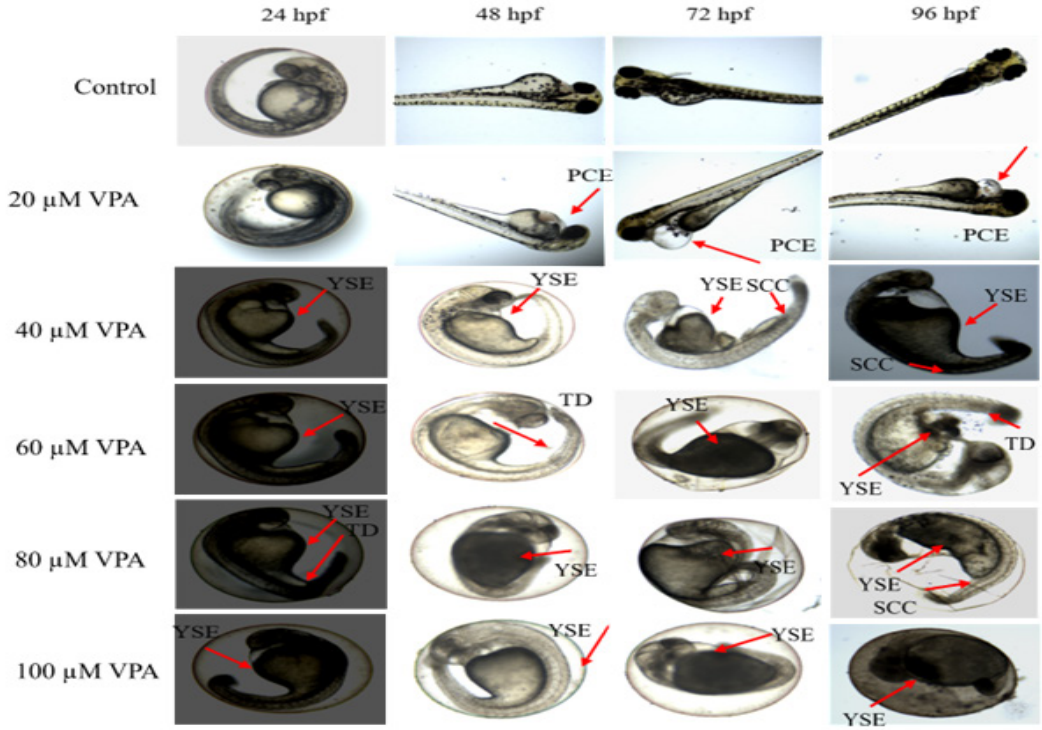

Figure 3: Effect of different concentrations of valproic acid (VPA) on developmental defects of zebrafish embryos at 24, 48, 72, and 96 hpf. YSE: yolk sac edema. PCE: pericardial edema. SCC: spinal cord curvature. TD: tail deformity.

Valproic acid induces zebrafish embryonic developmental defects by inducing oxidative stress-mediated apoptosis: dose and time-dependent analysis

Effect of VPA on heart rate

The zebrafish heart's resemblance to the human heart renders zebrafish a distinctive and essential model for genetics and drug-induced heart failure. The typical zebrafish embryo exhibits a heartbeat ranging from 120 to 180 beats per minute. An accelerated or decelerated heart rate will lead to embryonic death (24). Figure 4 depicts the heart rate of zebrafish embryos subjected to VPA treatment at 24, 48, 72, and 96 hpf. VPA exhibits a significant ($p \leq 0.05$) reduction in heart rate, with values below 80 bpm, compared to the control group. Embryos were found live at 20 µM of VPA, and a heart rate was recorded for 24, 48, 72, and 96 hpf. However, all embryos were found dead at 72 and 96 hpf at 40 and 60 µM of VPA, and the heart rate was not noted. Similarly, all embryos were found dead at 48, 72, and 96 hpf at high dosages of 80 and 100 µM VPA. In support of our report, Wang et al. proved that VPA induced developmental toxicity in zebrafish embryos by dysregulating the heart rate (20).

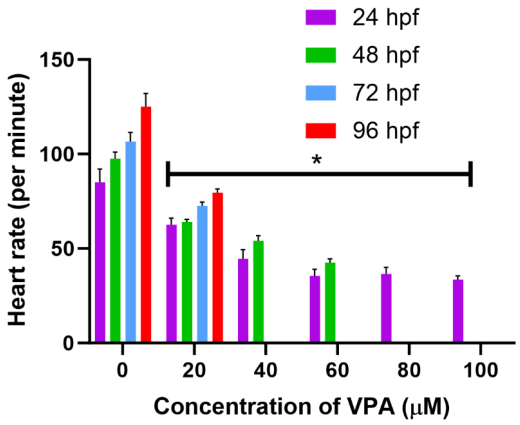

Figure 4: Effect of different concentrations of valproic acid (VPA) on heart rate (per min) of zebrafish embryos at 24, 48, 72, and 96 hpf. The statistical significance between the VPA-untreated (control) and VPA-treated groups was assessed by Dunnett's test. The significance was determined at $p \leq 0.05$ (*).

Effect of VPA on oxidative stress and apoptosis

One of the potential results of toxicity by pollutants is apoptosis. Apoptosis often occurs when a certain intracellular signaling pathway is triggered or when the cell is unable to repair DNA changes. This is the rationale behind the research that simultaneously examines apoptosis and ROS-mediated oxidative stress. In certain situations, ROS molecules harm the nucleus of cells in a way that triggers these proapoptotic signals (25, 26).

In the present study, the effect of VPA on the generation ROS molecules was assessed by DCFH-DA staining and apoptosis by AO staining in zebrafish embryos at 48 hpf (Fig. 5). The DCFH-DA is a highly selective stain for quantifying the ROS molecules and its fluorescence directly related to ROS levels (27). Figure 5A depicts that VPA has dose-dependently escalated DCFH fluoresce levels up to the tested 60 µM VPA compared to the control. The DCFH-DA staining revealed that VPA has dose-dependently escalated the ROS levels up to the tested dosage of 60 µM VPA and was found significant compared to the control ($p \leq 0.05$) (Fig. 5B). Thus, the study concluded that VPA is responsible for ROS-mediated oxidative stress. In support of our study, Wang et al. proved that VPA causes toxicity in zebrafish embryos by ROS-mediated oxidative stress (20).

Similarly, in our study, VPA's effect on apoptosis was revealed by AO staining. The intensity of AO fluorescence directly reflects the apoptosis level. Figure 5A depicts that VPA has dose-dependently escalated AO fluoresces levels up to the tested 60 µM VPA compared to the control. The AO staining revealed that VPA has dose-dependently escalated the apoptosis levels up to the tested dosage of 60 µM VPA and was found significant compared to the control ($p \leq 0.05$) (Fig. 5B). In support of our study, Wang et al. proved that VPA causes toxicity in zebrafish embryos by apoptosis through AO

staining (20). Overall, our study revealed that VPA is responsible for toxic effects in zebrafish embryos caused by oxidative-stress-mediated apoptosis.

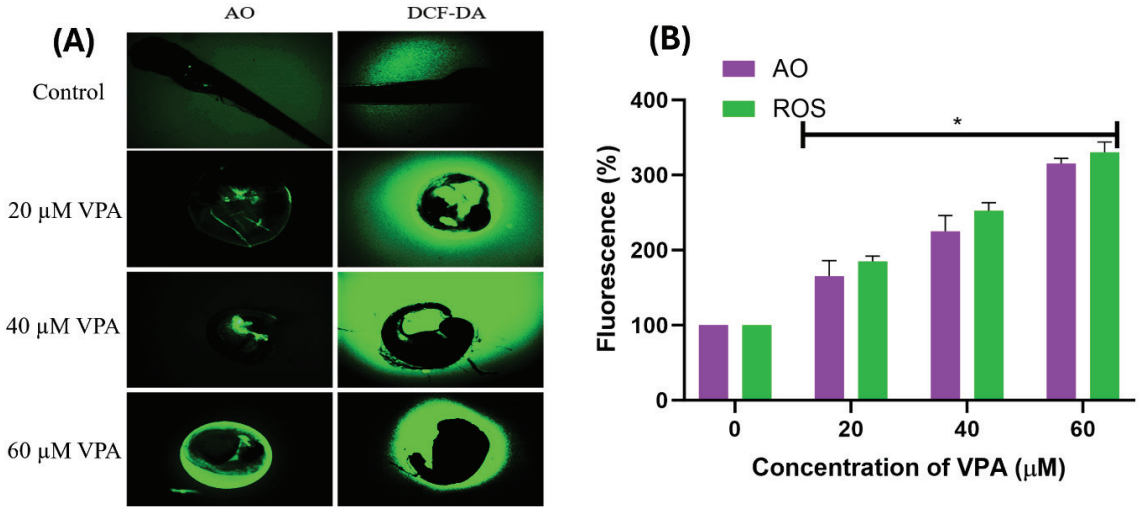

Figure 5: Effect of different concentrations of valproic acid (VPA) on apoptosis by AO staining and reactive oxygen species by DCFH-DA staining in zebrafish embryos at 48 hpf. The statistical significance between the VPA-untreated (control) and VPA-treated groups was assessed by Dunnett's test. The significance was determined at $p \leq 0.05$ (*).

Conclusion

` The study evaluated the toxic effect of the VPA on the aquatic model organism Zebrafish. VPA significantly affected the hatching rate of zebrafish embryos and induced developmental defects of zebrafish embryos. The VPA has lowered the heartbeat rate and caused cardiotoxicity. Moreover, the study showed that VPA elevated oxidative stress by causing excessive ROS accumulation. The possible mechanisms of oxidative stress and apoptosis in VPA-induced developmental defects and cardiotoxicity are elucidated in this work. Even so, substantial molecular investigations must be considered to examine the toxicological effects of VPA. Nevertheless, the relationship between VPA and different organ toxicities must thus be ascertained by assessing the toxicity at various stages of zebrafish development. Consequently, our research shows that VPA is detrimental to aquatic vertebrates during their embryonic phases, could enter the food chain, and exhibit risks to humans. Consequently, the release of VPA into aquatic environments must be constrained.

Conflicts of Interest

The authors declare that they have no conflicts of interest.

Acknowledgements

The authors are thankful to DRDO-BU-Centre for Life Sciences, Coimbatore, India, for their support and encouragement.

References

1. Rehman, M.S.U., Rashid, N., Ashfaq, M., Saif, A., Ahmad, N. and Han, J.I. (2015). Global risk of pharmaceutical contamination from highly populated developing countries. *Chemosphere*, 138, 1045-1055.
2. Waleng, N.J. and Nomngongo, P.N. (2021). Occurrence of pharmaceuticals in the environmental waters: African and Asian perspectives. *Environmental Chemistry*

and Ecotoxicology, 4, 50–66.

3. Dixit, A., Pandey, H., Rana, R., Kumar, A., Herojeet, R., Lata, R., Mukhopadhyay, R., Mukherjee, S. and Sarkar, B. (2024). Ecological and human health risk assessment of pharmaceutical compounds in the Sirsa River of Indian Himalayas. *Environmental Pollution*, 347, 123668.
4. Malviya, J. (2023). Antibiotic Resistance against E. coli Isolated from City of Lake Bhopal, Madhya Pradesh. *Current Trends in Biotechnology and Pharmacy*, 17(Supplement 3A), 1090-1096.
5. Fan, D., Miao, J., Fan, X., Wang, Q. and Sun, M. (2019). Effects of valproic acid on bone mineral density and bone metabolism: A meta-analysis. *Seizure*, 73, 56-63.
6. Gotlib, D., Ramaswamy, R., Kurlander, J. E., DeRiggi, A. and Riba, M. (2017). Valproic acid in women and girls of childbearing age. *Current psychiatry reports*, 19, 1-7.
7. Lacorte, S., Luis, S., Gómez-Canela, C., Sala-Comorera, T., Courtier, A., Roig, B., Oliveira-Brett, A.M., Joannis-Cassan, C., Aragonés, J.I., Poggio, L., Noguer, T., Lima, L., Barata, C. and Calas-Blanchard, C. (2018). Pharmaceuticals released from senior residences: occurrence and risk evaluation. *Environmental Science and Pollution Research*, 25, 6095-6106.
8. Bourioug, M., Mazzitelli, J. Y., Marty, P., Budzinski, H., Aleya, L., Bonnafé, E. and Geret, F. (2018). Assessment of Lemna minor (duckweed) and Corbicula fluminea (freshwater clam) as potential indicators of contaminated aquatic ecosystems: responses to presence of psychoactive drug mixtures. *Environmental Science and Pollution Research*, *25*, 11192-11204.
9. Al-Khazrajy, O.S. and Boxall, A.B. (2016). Risk-based prioritization of pharmaceuticals in the natural environment in Iraq. *Environmental science and pollution research*, *23*, 15712-15726.
10. Bharathi, M.P., Alagarsamy, V., Prasad, S.S., Krishna, P.V.M. and Vali, C.S. (2023). Hepatoprotective activity of Atylosia rugosa against Carbontetrachloride and Paracetamol induced hepatotoxicity in rats. *Current Trends in Biotechnology and Pharmacy*, 17(1), 609-620.
11. Salimi, A., Alyan, N., Akbari, N., Jamali, Z. and Pourahmad, J. (2022). Selenium and L-carnitine protects from valproic acid-Induced oxidative stress and mitochondrial damages in rat cortical neurons. *Drug and Chemical Toxicology*, 45(3), 1150-1157.
12. Parmar, N., Trivedi, K., Bagban, M. A., Ansari, K., Srivastava, V., Kumar, P., Maria, A., Patel, A., Chettiar, S.S. and Jhala, D. (2023). Curcumin Nanoformulation: Antioxidant, Antibacterial, and Toxicity Assessment. *Current Trends in Biotechnology and Pharmacy*, *17*(4), 1370-1382.
13. Ibrahim, I. F., Hakeem, W. A. and Rahman, S. A. (2024). A Antioxidant And Anti-Inflammatory Properties of Annona Squamosa L.: A Review. *Current Trends in Biotechnology and Pharmacy*, 18(3s), 71-96.
14. Kondabolu, U. L., Babitha, B., Kalagatur, N. K., Nagaraj, A., & Velumani, S. (2023). Phytochemical Analysis in Pithecellobium dulce Fruit Peel Extract. *Current Trends in Biotechnology and Pharmacy*, 17(3), 1052-1059.
15. Devi, M. S., Thangadurai, T. D., Nataraj, D. and Kumar, K.N. (2024). Bismuth-doped carbon quantum dots as an effective fluorescent probe for metronidazole detection through inner filter effect, cytotoxicity studies, and bioimaging in Zebrafish. *Journal of Photochemistry and*

Photobiology A: Chemistry, 450, 115429.

16. Howe, K., Clark, M. D., Torroja, C. F., Torrance, J., Berthelot, C., Muffato, M., ... and Teucke, M. (2013). The zebrafish reference genome sequence and its relationship to the human genome. *Nature*, *496*(7446), 498-503.
17. OECD. (2013). "236: fish embryo acute toxicity (FET) test," in OECD Guidelines for the Testing of Chemicals, Section, 2, (Paris: OECD).
18. Nesaragi, A.R., Ravikumar, C.H., Kalagatur, N.K., Hoolageri, S.R., Pasha, K.M., Balakrishna, R.G. and Patil, S.A. (2023). In vitro and in vivo nanomolar Hg2+ detection in live cells and zebrafish, theoretical studies. *Journal of Photochemistry and Photobiology A: Chemistry*, 445, 115079.
19. Vundela, S. R., Kalagatur, N. K., Nagaraj, A., Kadirvelu, K., Chandranayaka, S., Kondapalli, K., Hashem, A., Abd_ Allah, E.F. and Poda, S. (2022). Multi-biofunctional properties of phytofabricated selenium nanoparticles from Carica papaya fruit extract: Antioxidant, antimicrobial, antimycotoxin, anticancer, and biocompatibility. *Frontiers in Microbiology*, 12, 769891.
20. Wang, J., Zou, L., Jiang, P., Yao, M., Xu, Q., Hong, Q., Zhu, J. and Chi, X. (2024). Vitamin A ameliorates valproic acid-induced autism-like symptoms in developing zebrafish larvae by attenuating oxidative stress and apoptosis. *NeuroToxicology*, 101, 93-101.
21. Kalagatur, N.K., Nagaraj, A., Poda, S. and Salla, H.R. (2024). In vitro toxicological investigation of Fusarium graminearum toxins in Rattus norvegicus myocardial H9c2 cells. *Indian Journal of Biochemistry and Biophysics*, 61(12), 838-845.
22. Dixit, N.M., Kalagatur, N.K., Poda, S., Kadirvelu, K., Behara, M. and Mangamuri, U.K. (2022). Application of Syzygium aromaticum, Ocimum sanctum, and Cananga odorata essential oils for management of Ochratoxin A content by Aspergillus ochraceus and Penicillium verrucosum: An in vitro assessment in maize grains. *Indian Journal of Biochemistry and Biophysics*, 59, 172-182.
23. Sathiyaraj, G., Akilesh, M., Vignesh, A., Kumar, K. N., Gopinath, S., Mohanapriya, S., Malecki, J.M., Kadirvelu, K., Shankar, R. and Dharmaraj, N. (2025). Benzothiazole-based Schiff base for sensing Ca^{2+} ions: Synthesis, DFT studies, toxicity evaluation in zebrafish embryo and in silico analysis of MMP-9 inhibition. *Journal of Photochemistry and Photobiology A: Chemistry*, 458, 115985.
24. Fakhlaei, R., Selamat, J., Razis, A. F. A., Sukor, R., Ahmad, S., Khatib, A. and Zou, X. (2024). Development of a zebrafish model for toxicity evaluation of adulterated Apis mellifera honey. *Chemosphere*, 356, 141736.
25. Kalagatur, N.K., Abd_Allah, E.F., Poda, S., Kadirvelu, K., Hashem, A., Mudili, V. and Siddaiah, C. (2021). Quercetin mitigates the deoxynivalenol mycotoxin induced apoptosis in SH-SY5Y cells by modulating the oxidative stress mediators. *Saudi Journal of Biological Sciences*, 28(1), 465-477.
26. Gunasekaran, K., Thangavelu, P., Kalagatur, N. K., Jeyaraj, R. and Samiappan, S. (2024). Unveiling the Effects of Cisplatin and Diallyl Disulfide on MDA-MB-231 Breast Cancer Cells. *Current Trends in Biotechnology and Pharmacy*, 18, 1813-1821.
27. Swaminathan, S., Haribabu, J., Kalagatur, N.K., Konakanchi, R., Balakrishnan, N., Bhuvanesh, N. and Karvembu, R. (2019). Synthesis and anticancer activity of [RuCl2 (η6-arene)(aroylthiourea)] complexes—high activity against the human neuroblastoma (IMR-32) cancer cell line. *ACS omega*, 4(4), 6245-6256.

Current Trends in Biotechnology and Pharmacy
Vol. 19(1) 2116-2129, January 2025, ISSN 0973-8916 (Print), 2230-7303 (Online)
DOI: 10.5530/ctbp.2025.1.2

A Study on *Chlorella* Biomass as a Vegan Source for Omega-3 Fatty Acids and Dietary Proteins

Ananya N Nayak[1], Dhamodhar Prakash[1]*, Akash S[1, 2], Renju Raju[1]

[1] Department of Biotechnology, M S Ramaiah Institute of Technology, Bangalore 560054
[2] Biopol Biosciences, Bangalore 560100

***Corresponding author:** dhamu.bio@gmail.com

Abstract

Microalgae are one of the less-explored, nutritional treasures of the marine biosphere. With the emergence of algal technology, research has been shifting slowly towards exploring the nutraceutical values of these microorganisms, and microalgae like *Chlorella vulgaris* are gaining high market value. In addition, with the increasing demand for vegan source of omega-3 fatty acids, the *Chlorella vulgaris* biomass may be considered as a potential alternative. In this study optimization of various parameters such as culturing conditions, media composition, pH, RPM, inoculum percentage, carbon source, concentration of glucose, and salt to enhance the yield has been carried out. The best results were obtained at pH 7 with an inoculum percentage of 5 and the addition of 1.5 gm of NaCl and glucose enhanced the yield of biomass, protein, and lipid in *Chlorella vulgaris*. Optimized conditions gave a maximum yield of biomass, lipids, and protein. Among the lipids, omega-3 fatty acids have high nutraceutical value. In the fatty acid methyl esters, DHA and EPA were found to be 2.9% and 0.55 %. Estimation of omega-3 fatty acids was done using TLC and GC-MS. The Omega-3 fatty acids and dietary proteins extracted from *Chlorella vulgaris* can serve as an alternate vegan source for nutritional supplements.

Keywords: *Chlorella vulgaris*, Optimisation, Lipids, Omega-3 -Fatty acids, Protein.

Introduction

Omega-3 fatty acids are a category of fatty acids that the human body is unable to produce on its own. These are necessary fats that must be obtained from external sources. Docosahexaenoic acid (DHA) and Eicosapentaenoic acid (EPA) are the two forms of omega-3 that are majorly obtained from fish Biomass. Plants contain omega-3 fatty acids in the form of alpha-linolenic acid (ALA). Due to the abundance of non-vegetarian sources of omega-3 fatty acids and the scarcity of vegan alternatives, omega-3 fatty acid supplements derived from fish oil are not practical for vegetarians, who are unable to meet their daily needs for omega-3 fattyacids. Since fishes spawn in a specific season, the biomass of fish is not available year-round for the production of omega-3 fatty acids. Fish from contaminated waterways may have accumulated mercury, which can cause cancer[1]. Fish and fish oil allergies exist in certain people. Omega-3 fatty acid supplements derived from fish oil are not feasible for such individuals[2]. Furthermore, some people have been known to develop gastritis and indigestion after taking fish oil.

Microalgae hold great potential for the sustainable production of high-value chemicals, feed, and biofuels. Microalgae, such as *Spirulina* and *Chlorella*, are possible sources of proteins and lipids that can be utilized to make functional meals that enhance human health [3]. When

compared to other microalgae, *Chlorella vulgaris* has a high market value, with a market scope analogous to *Spirulina (Arthrospira platensis).* However, the added advantage of *Chlorella vulgaris* over Spirulina is that it does not have a cytotoxic effect on healthy cells. The Spirulina produce a compound called microcystin which is toxic to liver cells [4]. Most of the applications of *C. vulgaris* have been on its metabolism of lipids, proteins, and carbohydrates[5]. They are commercially important as they can produce a variety of essential and non-essential amino acids [6]. Apart from its nutritional value *Chlorella vulgaris* has also been known for its medical applications like cardioprotective properties [7], immunomodulatory effects [8], anticancer properties [9] and antidiabetic properties [10]. Protein makes up to 45-58% of the dry weight of the *Chlorella* biomass of which 20% of the protein is bound to the cell wall supporting the structural integrity of the cell and also serves as a transporter. The total protein content may vary 12-120 kDa of which the majority lies in the range of 39-75 kDa. Lipids constitute around 5-40% of the *Chlorella vulgaris* dry weight. The lipids are present in the form of glycolipids, waxes, hydrocarbons, fatty acids, and phospholipids. These are synthesized in the chloroplasts and directed towards the cell membrane and cell wall [11]. Concerning the type of fatty acids in *C. vulgaris*, it has been noted that 70.18% are saturated fatty acids (SFA),16.85% are monounsaturated fatty acids (MUFA) and 8.72% are polyunsaturated fatty acids (PUFA) hence, it can be considered as a storehouse of various fatty acids [12].

Microalgae can be explored as a solution for the problems related to the production of Omega-3 fatty acids from fish biomass. In comparison to higher-level plants, the growth of microalgae is quicker, they can grow in harsh conditions and give better metabolite yield[13]. Omega 3 fatty acids are produced in higher amounts in the microalgae *Chlorella vulgaris*[14]. Microalgal biomass is available throughout the year and it takes only a few days to produce the culture. The micrometer size and its unicellular nature contribute to a high surface-to-volume ratio giving efficient nutrient utilization and metabolite production[15]. It is a better alternative for people with allergies to fish and fish oil. In addition, there is no wastage in this process, as the by-products can be used as poultry/cattle feed, as they have high nutritional value.

In this study, the optimization of physical parameters and media for maximal production of lipids and proteins has been carried out through sustainable and cost-efficient processes using *Chlorella vulgaris*. The lipids and proteins that come as a byproduct in culturing processes are of high nutraceutical and pharmaceutical significance.

Materials and Methods

Revival and culturing of the microalgal strain

The pure culture of *Chlorella vulgaris* was obtained from Biopol Biosciences, Bangalore. The microalgae was revived in the BG11 media for further experiments. To find the optimal growth of the microalgae a comparative study was made between the growth, using an incubator shaker with 200 rpm at room temperature and plant tissue culture setup [16]. 200 ml of BG11 media was autoclaved and 50µl of inoculum was added to both the media under aseptic conditions and kept for incubation in their respective conditions. Once the microalgal growth was observed they were added with 40% glycerol and cryopreserved at -80ºC and used for further experiments.

Optimization studies

To enhance the yield, various parameters such as the composition of media, pH, RPM, inoculum percentage, carbon source, concentration of glucose, and salt have been optimized. The optimization experiments were done in triplicates.

Magnetic stirrer vs static condition

One ml of the culture was added to one litre of BG-11 media and kept on a magnetic stirrer with 150 rpm, at room temperature under light. Similarly, the culture was kept in static condition. The OD at 680nm was noted for every 24 hours. Microscopy was carried out at 100x to check for contamination. Wet cell weight, Dry cell weight, protein, and lipid analysis were carried out on day 9 [17].

Inoculum % optimization

Inoculum percent of 1,5 and 10, was added to BG11 media and made up to 250 ml to study the effect on yield. OD at 680nm was noted every 24 hours. Microscopy was carried out to check for contamination. Wet cell weight was measured on day 10. The pellets were dried for 24 hours at 60ºC, Dry cell weight was recorded and stored at 4ºC.

pH optimization

The initial pH of the BG11 media was set to 7,7.5,8,8.5 and 9 under aseptic conditions. The OD at 680 nm was noted for every 24 hours. The wet cell weight, dry cell weight, lipid, and protein estimations were made on day 6 [18].

Carbon source

Acetic acid and glucose were selected as carbon sources for the analysis. Bottles containing 1g/l glucose were added with BG11 media and 0.06 gm NPK and another set of bottles containing 1g/l acetic acid was added with BG11 media and 0.06gm NPK.OD at 680 nm and DCW were noted every 24 hours [19].

Growth kinetics studies for BG11 and NPK (Selection of nitrogen source)

100 ml of solution was prepared with 95 ml of BG11 media and 5 ml of inoculum. Each day optical density at 680 nm, wet cell weight, dry cell weight, protein content, and lipid content were analysed. Similar steps were carried out for NPK media which has an NPK concentration of 0.6gm/l [20].

Glucose concentration

To the BG11 media, various concentrations of glucose (1gm/l,1.5gm/l,2gm/l) were added. Estimation of OD at 680 nm, WCW, and DCW every 24 hours for 7 days was carried out. lipid and protein content was estimated for the culture on day 7 [21].

RPM optimisation

One litre of the prepared media was subjected to a magnetic stirrer at room temperature at 200 rpm. OD at 680 nm was noted down every 24 hours. The WCW, DCW, and Protein were estimated on day 7. Similarly, the experiment was repeated for 250 rpm and 300 rpm [22].

Salt stress

Various concentration of NaCl (0,1,1.5,2gm/l) was added to BG11 media. OD at 680 nm, WCW &DCW were recorded every 24 hours. Lipid and protein content were estimated on day 7 [23].

Scale up production of culture under optimized conditions

950 ml of media was prepared and 50 ml of inoculum was added to the media followed by the addition of 1.5 gm of glucose. OD at 680 nm was noted every 24 hours. The WCW, DCW, lipids, and protein were estimated only on Day 7 [24].

Analysis of omega-3 fatty acid

Confirmation by TLC

For standard preparation: Content from 1 tablet of omega-3 fatty acid soft gelatine capsule (OMEGALARK3) was dissolved in 10 ml of chloroform.

For the sample preparation, the Modified Bligh & Dyer method was used for the extraction of lipids from dried algal biomass, where 50 mg of lipid samples were mixed with a solution of water, chloroform, and methanol (0.8:1:1 v/v/v).

4 mL of a water: chloroform solution (1:1, v/v) was added after the vortex. After being vortexed, the sample was centrifuged for ten minutes at 5,000 rpm. The mobile phase was prepared using ether: benzene in the ratio 2:2.

The TLC procedure was carried out by spotting the silica gel TLC plate and the movement of the mobile phase was marked. The bands formed were observed under a UV transilluminator and marked [25].

Estimation by GC MS

The extracted lipids were measured using Gas Chromatography Mass Spectrometry[26]. Using standards (Sigma), individual FAMEs were quantified and identified. Unidentified FAMEs were estimated using the averaged RF factor [27].

Results and Discussion

Revival and culturing of the strain

The pure culture of *Chlorella vulgaris* was revived in the BG11 media. The OD at 680nm and biomass analysis on Day 8 confirmed that the plant tissue culture condition gave a yield of 0.023g DCW with an absorbance of 0.264 in comparison to the Shaker incubator. Microscopic studies revealed that there is no contamination in the culture with an appreciable level of microalgal growth.

Optimization studies

Magnetic vs static stirrer condition.

Absorbance at 680 nm showed that a stationary phase was attained on day 7 in both cultures (Figure 1). In dry biomass estimation, the higher yield was derived in the magnetic stirrer condition(0.17±0.02g/l) rather than the static condition(0.14±0.01g/l). The protein content was higher in the static condition (357.27±2.72 mg/g) when compared to the magnetic stirrer condition (319±2.67mg/g). The lipid content was higher in the magnetic stirrer condition(9.89±0.32mg/g) in comparison to the static condition (7.10±0.28mg/g) (Figure 2).

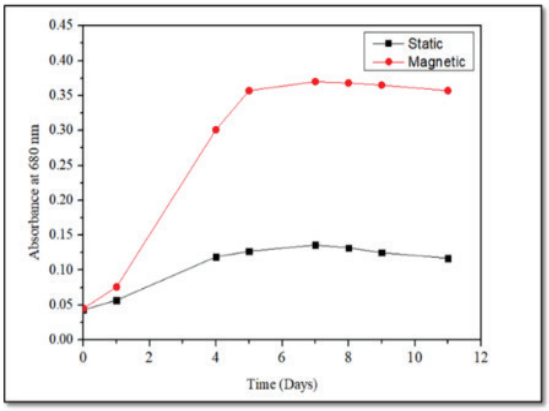

Figure 1: Growth curve for absorbance at 680 nm for static and magnetic stirrer condition.

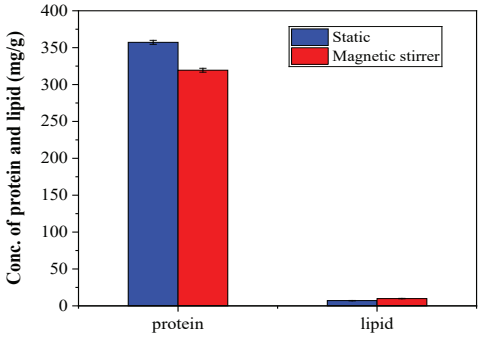

Figure 2: Protein and Lipid estimation for cultures in static vs magnetic stirrer condition.

Optimization of Inoculum

From the absorbance studies, it was observed that maximum growth was achieved by culture with an inoculum percentage of 5% on day 10 (Figure 3). However, the culture with an inoculum percentage of 10 % showed a good increase in OD initially. But started to decrease sharply from day 7 to day 10 indicating the nutrient depletion in the culture. Inoculum concentration of 5 gives the maximum yield of biomass and lipid (590.02±4.25 mg/gm) in comparison to the 1% and 10% inoculum (Table 1). From the protein analysis, it was observed that an inoculum percentage of 10 gives a maximum yield of protein (93.75±1.74 mg/g).

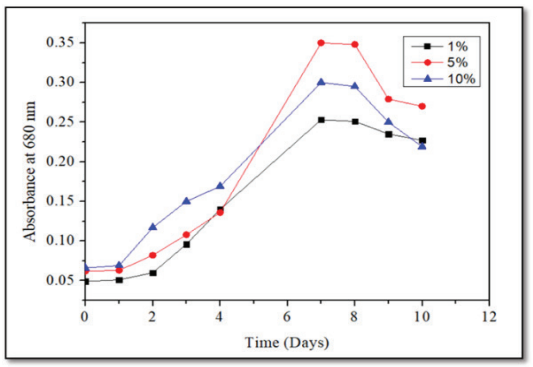

Figure 3: Growth curve for 1%,5%and 10% inoculum concentrations

pH optimization

From the absorbance studies, it was found that pH 7.5,8,9 had almost achieved the stationary phase on day 5 while pH 7 and pH 8.5 were still in the exponential phase (Figure 4). From the biomass estimation, the maximum yield of dry biomass (0.022±0.002gm/l) and lipid (509.73±3.860mg/g) was obtained from culture with an initial pH of 7 in comparison to culture with an initial pH of 7.5,8,8.5,9 (Table 1). However maximum yield of protein was obtained in culture with an initial pH of 7.5(126.57±3.521mg/g.

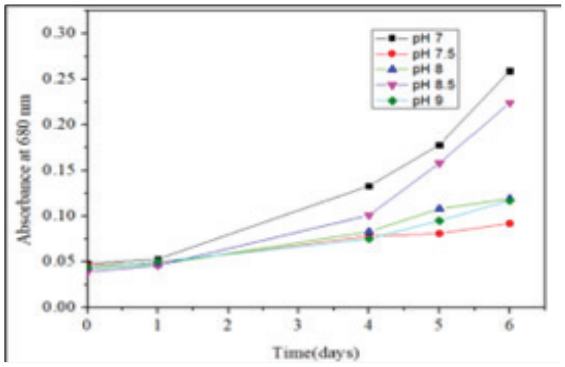

Figure 4: Growth curve for cultures of different initial pH

Growth kinetics studies (BG11)

For every 24 hours, the absorbance at 680 nm was observed till day 7. The maximum OD reading was obtained on day 7 and the absorbance was found to be linear (Figure 6). On biomass estimation, it was noted that biomass growth was exponential till day 6 however the growth declined from day 6 to day 7. The maximum biomass (4.00 g/l) (Figure 7) and protein (11.21mg/g) (Figure 5) were obtained on day 7. Specific growth and doubling time were also found to be maximum at Day 7. The maximum lipid was obtained on Day 4 (172.171±1.807 mg/g) for the cultures grown in the BG 11 media (Figure 5). The absorbance was noted at 530 nm and the lipid content was calculated based on the lipid standards.

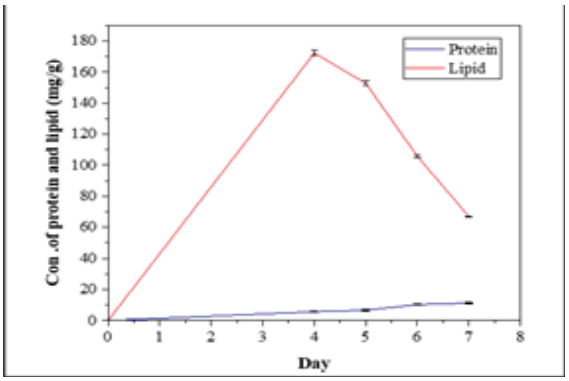

Figure 5: Protein and Lipid estimation for BG11 media culture.

NPK growth kinetics

According to biomass estimation, the absorbance at 680 nm was noted every 24 hours till Day 7, and the Growth curve was plotted (Figure 6). The graph was found to be linear, and a sharp increase in the absorbance from Day 6 to 7 indicates the culture was still in the exponential phase on day 7. The maximum biomass (0.30±0.565 gm/l) was obtained on day 7 for the NPK (Figure 7). The protein and lipid estimation was carried out for dry biomass and the growth curve was plotted. The maximum protein and lipid were obtained on day 4 and the decline of protein and lipid content was observed from day 5 to 7 (Figure 8). Absorbance was noted at 530 nm, However, the yield of biomass and lipid in NPK media was low in comparison to the BG11 media, hence BG11 is a better media for enhancing biomass growth.

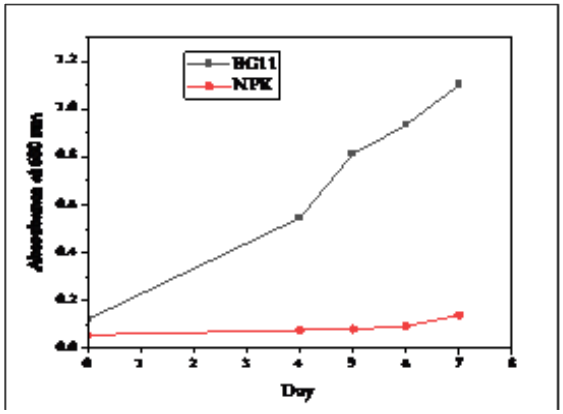

Figure 6: Absorbance growth curve for BG11 and NPK media culture.

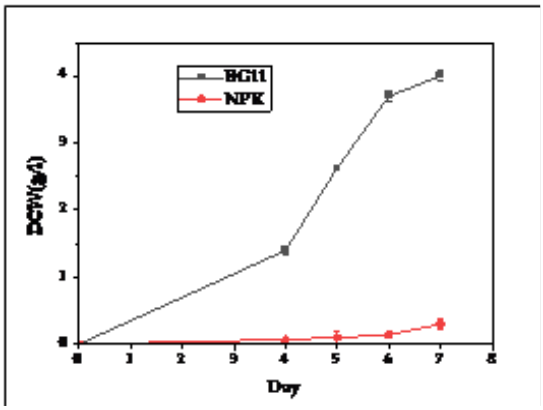

Figure 7: Biomass growth curve for BG11 and NPK media.

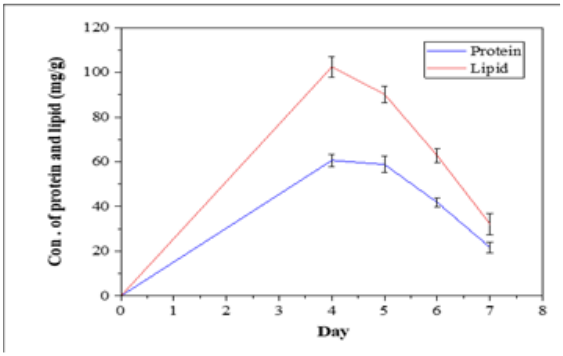

Figure 8: Protein and Lipid growth curve for NPK media.

Selection of carbon source

The growth was observed with different carbon sources. The Dry cell weight was also noted every 24 hours. From the absorbance at 680 nm (Figure 9) and dry cell estimation, it was found that glucose along with BG11 gave an appreciable amount of biomass (2.85g/l). In contrast, NPK along with acetic acid or glucose and BG11 along with acetic acid gave no biomass yield (Figure 10). Hence, glucose was selected for further studies as a carbon source.

Glucose concentration.

On day 7 the culture was harvested and the biomass estimations were carried out along with protein and lipid estimation. The maximum biomass and lipid yield was obtained in the culture with 1.5 g/l of glucose concentration in comparison to the culture with a glucose concentration of 1 g/l or 2 g/l. From the protein estimation, it was found that culture with 2g/l glucose concentration gave a maximum yield of protein.

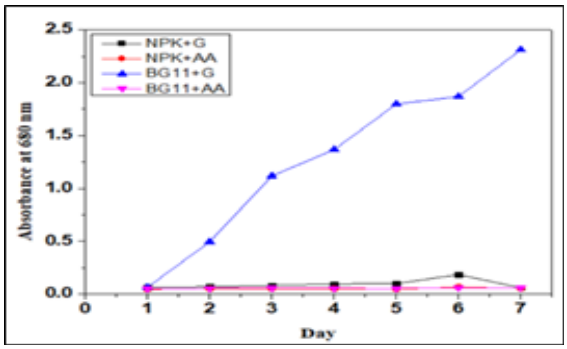

Figure 9: Growth curve for various carbon sources Based on absorbance at 680 nm.

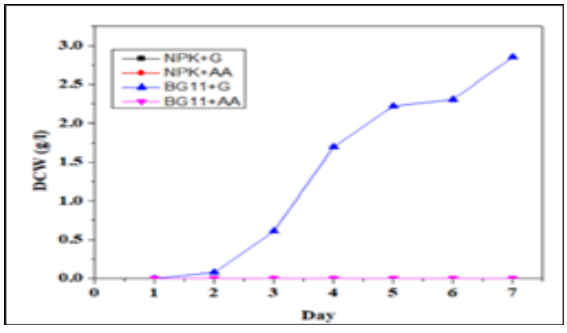

Figure 10: Dry cell weight estimation for various carbon sources.

Current Trends in Biotechnology and Pharmacy
Vol. 19(1) 2116-2129, January 2025, ISSN 0973-8916 (Print), 2230-7303 (Online)
DOI: 10.5530/ctbp.2025.1.2

RPM optimization

The biomass was harvested on day 7. The maximum yield of biomass (1.125±0.061g/l) and lipid was found in the culture subjected to 250 RPM (Table 1). At 300 rpm the yield of protein was found to be maximum.

Salt concentration

The cultures were harvested on day 7. The maximum yield of biomass was obtained for culture with an initial NaCl concentration of 0 g/l in comparison to 1.1.5,2g/l (Table 1). Maximum yield of protein and lipid was obtained in the culture with 1.5 g/l NaCl concentration in comparison to the culture with 0,1,2 g/l NaCl.

Table 1: Optimization studies of protein and lipid

		Protein (mg/gm)	Lipid content (mg/g)
Inoculum %	1%	56.58±1.45	585.15±1.96
	5%	50.18±2.37	590.02±4.25
	10%	93.75±1.74	169.50±2.12
pH	7	20.68±1.442	509.73±3.860
	7.5	126.57±3.521	499.92±2.672
	8	55.22±3.336	235.33±3.634
	8.5	15.97±2.729	436.84±1.499
	9	49.02±3.280	132.66±4.228
RPM	200	17.96±0.537	164.51±4.002
	250	25.51±2.319	286.25±3.66
	300	31.54±2.969	191.27±4.963
Concentration of glucose (gm/l)	1	21.03±3.73	259.16±2.418
	1.5	47.1±4.05	320.84±4.313
	2	66.65±3.450	288.94±2.927
Concentration of NaCl (gm/l)	0	26.46±0.791	139.30±3.874
	1	23.77±1.852	261.65±4.737
	1.5	62.37±1.152	420.80±3.323
	2	17.87±0.311	279.06±4.313

A high yield of dry cell weight was achieved at the Optimal conditions of pH 7,250 RPM, inoculum concentration of 5, with 0 and 1.5 g/l concentrations of NaCl and glucose (Figure.11). Similarly, the maximum yield of lipid was obtained at pH 7, inoculum concentration of 5%, RPM of 250, with salt and glucose concentration of 1.5mg/l (Figure 12).

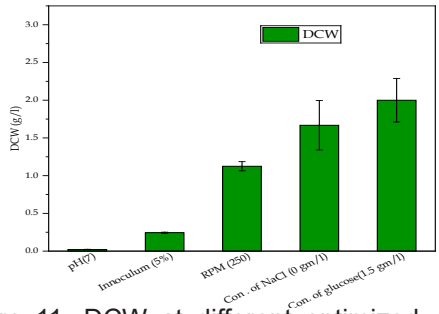

Figure 11: DCW at different optimized conditions

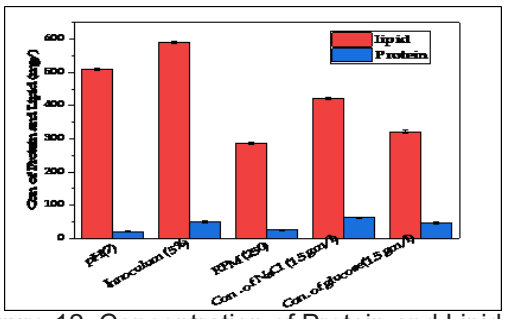

Figure 12: Concentration of Protein and Lipid at different optimized conditions

For the scale-up, pH 7, inoculum concentration of 5%, and salt, and glucose concentration of 1.5 g/l, were chosen as optimal conditions to maximize the yield of dry biomass and lipid with protein as a byproduct.

Scale-up production of culture under optimized values

In scale-up production, the culture was subjected to optimized conditions (pH 7,250 rpm,1.5gm glucose on the 1st day, and 1.5g/l NaCl on the 6th day evening). The cell was harvested on day 7, The obtained contents of dry biomass, protein, and lipid are 4.25±0.395g/l, 53.23±4.327mg/g, and 621.85±4.412 mg/g.

In comparison to the initial BG11 media culture in the optimized scale-up culture the dry biomass was found to be increased by 1.08 times (Figure 13) lipid by 8.11 times and protein by 11.18 times (Figure 14).

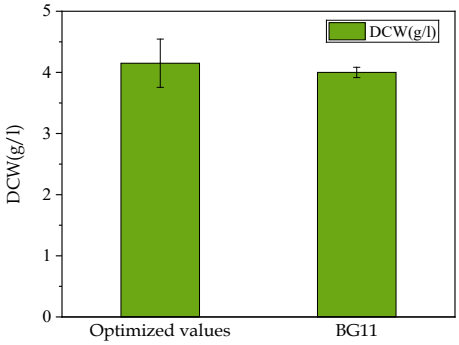

Figure 13: Biomass estimation comparison between BG11 media and optimized condition value.

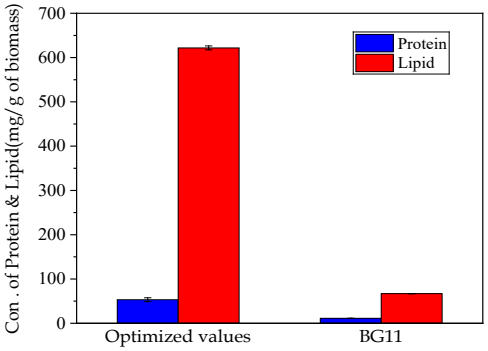

Figure 14: Protein and lipid estimation comparison between BG11 media and optimized condition value.

TLC for qualitative determination of omega-3 fatty acid

The presence of omega-3 fatty acids (DHA) was confirmed by TLC. Among the Mobile phases, ether: benzene at the ratio 2:2 gave results for the microalgae sample. The Rf value for the standard was 0.204 and 0.194 for the test sample. Which were similar to the Rf value of DHA.

Quantitative estimation of omega-3 fatty acids

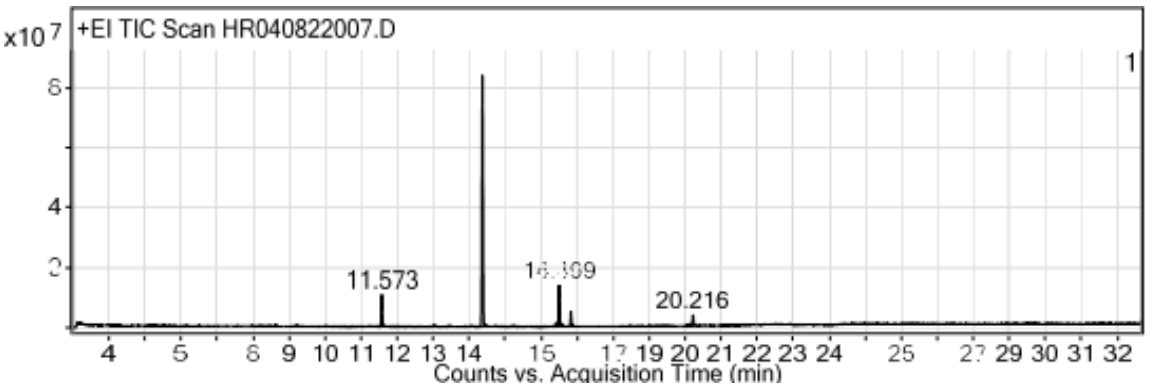

Figure 15: Results of GC-MS for fatty acid methyl esters of Chlorella vulgaris culture under optimized conditions.

Table 2: Identified fatty acids and percentage in fatty methyl esters.

Peak	Start	RT	End	Compound Name	Area	Area Sum Percent
1	11.522	11.573	11.659	Myrisitc acid	22446899.55	8.39
2	14.315	14.369	14.472	Palmaitic acid	193693525	72.43
3	16.375	16.419	16.45	Alpha-Linolenic Acid	2271729.18	0.85
4	16.453	16.499	16.546	Linoleic acid	27909906.71	10.44
5	16.546	16.567	16.603	Arachidonic Acid	1334195.15	0.5
6	16.782	16.826	16.902	Stearic Acid	9787733.04	3.66
7	20.031	20.061	20.094	Docosapentanic Acid	735398.01	0.27
8	20.108	20.146	20.177	Eicosapentanic Acid	1481883.42	0.55
9	20.177	20.216	20.287	Docosahexanic Acid	7765264.58	2.9

There were around 9 identified fatty acids such as Myristic acid, palmitic acid, Alpha-linolenic acid, linoleic acid, arachidonic acid, stearic acid, docosapentanoic acid, eicosapentanoic acid, docosahexanoic acid. In the fatty methyl esters, if we consider the omega 3 fatty acids the DHA was found to be 2. 9%, EPA was found to be 0.55 % overall the amount of omega 3 fatty acids was found to be 0.33% and omega 6 fatty acids were found to be 0.85% concerning the biomass (Figure 15, Table 2).

Discussion

Many studies conducted on microalgae are carried out conducted in photo bioreactors with CO_2 supply. Photo bioreactors being an expensive option led to this study, we investigated sustainable and effective alternatives for microalgae production. The options that were explored were the orbital shaker and plant tissue culture setup condition. From this study, we found that the plant tissue culture setup gave a better biomass yield in comparison to the shaker incubator. In the incubator shaker, the insufficiency of light might have led to the hindrance. Microalgae development depends on agitation[28], and the best RPM for maximal biomass and lipid output was discovered using a magnetic stirrer. In our studies, 250 RPM on magnetic spinner is the optimal RPM for the maximal yield of biomass (approximately 1.125g/l) and lipid (28.25% to biomass). This is the first attempt to optimize RPM for *Chlorella vulgaris* cultivation in a magnetic stirrer. In the previous study, where the RPM of the shaker incubator was optimized to 150, the biomass yield was 0.499mg/l, and the lipid yield was 15.98% of dry biomass was less in comparison to the yields of biomass and lipid at 250 rpm magnetic stirrer condition in the present study[29].

The best inoculum to use in Chlorella vulgaris cultures to maximize biomass, protein, and lipid output is 5%. When the 10% initial inoculum culture reached the nutrition depletion phase, it grew more slowly than the 5%, as reported by others [30]. Optimal temperature range for microalgal cultures is 25–35°C[13,18]. Previous studies show that 25ºC was an ideal temperature for growing *Chlorella vulgaris*[31]. pH 7 is ideal for microalgae to produce their maximum biomass and lipid output, which is in line with findings from earlier research[32–34].

Different types of media have been used in culturing of *Chlorella vulgaris* in algal research. BG11 media was found to be the optimal media in comparison to the bold basal media, Fog's medium, and M4N media[35]. In the present study, NPK and BG11 media are compared for cultivating *Chlorella vulgaris.* The

best yields of protein, lipids, and biomass of 4g/l biomass yield on day 7 which was higher compared to the previous study (approximately 1.64g/l on day 15) are obtained with BG11 medium[36]. On day 10, the proportion of lipids to biomass was 7.66%, highlighting the significance of the nutrition depletion phase in the formation of lipids. In the NPK media since the nitrogen content is high which results in a lower amount of lipid in comparison to the BG11 media. The productivity of lipids and biomass is similarly influenced by nitrogen concentration, demonstrated high lipid content over time with BG11 media. This emphasizes how important nitrogen depletion is to the lipid synthesis process in *Chlorella vulgaris.*

Glucose is the most effective carbon source for increasing biomass and lipids[36]. On the other hand, the risk of contamination was emphasized[37]. Therefore, experiments on glucose optimization were carried out to determine the ideal concentration for maximizing the yield of fat, protein, and biomass. 5g/l of glucose was found to give a maximum yield of biomass (1.39g/l) and lipid (19.29%) of biomass weight[38]. BG11 and 1.5 gm/l of glucose are the ideal concentrations with a maximum yield of biomass (approximately 2gm/l) and lipid (approximately 32.08%), varying on the specific culture conditions [36].

Under the conditions of salt stress, it was discovered that there was a reduction in biomass at the first addition of salt; yet, there was a notable rise in lipid (66.16%), which was higher than the previous report of (24%) [39]. Therefore, to reduce the possibility of salt impeding biomass growth and to increase the amount of lipids in biomass, salt was injected on the sixth day of the large-scale production of microalgae under optimal conditions.

This investigation revealed that, as compared to an orbital shaker incubator, a plant tissue culture setup was the best setting for cultivating *Chlorella vulgaris.* The goal of the study is to enhance *Chlorella vulgaris* biomass, protein, and lipid output by combining optimum conditions. Better biomass, lipid, and protein yields than individual optimized parameters are shown in the results. According to previous studies, 16.15% of lipids were obtained in the optimization studies concerning biomass[22]. 62.1% lipid was produced in this scale-up study, with yields akin to those of genetically modified strains for maximal lipid output [23]. *Chlorella vulgaris* can be employed as a source of production for DHA (2.9%) and EPA (0.55%) according to estimates of omega-3 fatty acids. This makes the *Chlorella vulgaris* a suitable option for producing omega-3 fatty acids.

Conclusion.

This study demonstrated that microalgae can be successfully cultivated in a laboratory environment with the presence of light. The ideal conditions for the growth of *C. vulgaris* biomass are pH 7 and 5% inoculum. BG11 media turned out to be the best choice when contrasted with NPK media. Maximum yield of biomass and lipid was found at 250 rpm with 1.5 g/l of glucose and NaCl. We developed a sustainable method to increase the production of protein, lipid, and omega-3 fatty acids in *Chlorella vulgaris* by combining various approaches (salt stress, glucose, and agitation). The large-scale studies combining all the optimized parameters into a single strategy demonstrated an increase in the yield of biomass, lipid, and protein. In addition to being fed to the poultry, the protein byproducts can be utilized in the production of snack bars that serve as nutritional supplements. However, maximizing agitation on a large scale and raising the yield sustainably and economically are the real challenges.

Statements and Declarations

Funding

The authors declare that no funding was received for conducting this study.

Conflict of interest /Competing interests

The authors declare that they have no

relevant financial or non-financial interests to disclose.

Authors' contribution

Ananya N Nayak, Akash S and Dhamodhar Prakash conceived and designed the research and did Data acquisition. Ananya N Nayak, Akash S, Renju Raju did data analysis. Ananya N Nayak and Renju Raju drafted the manuscript work. Dhamodhar Prakash supervised the research work and revised the manuscript. All authors have read and approved the manuscript.

References

1. Zhuzzhassarova, G., Azarbayjani, F., & Zamaratskaia, G. (2024). Fish and Seafood Safety: Human Exposure to Toxic Metals from the Aquatic Environment and Fish in Central Asia. *International Journal of Molecular Sciences*, *25*(3), 1590. https://doi.org/10.3390/ijms25031590

2. Leung, A. S. Y., Wai, C. Y. Y., Leung, N. Y. H., Ngai, N. A., Chua, G. T., Ho, P. K., Lam, I. C. S., Cheng, J. W. C. H., Chan, O. M., Li, P. F., Au, A. W. S., Leung, C. H. W., Cheng, N. S., Tang, M. F., Fong, B. L. Y., Rosa Duque, J. S., Wong, J. S. C., Luk, D. C. K., Ho, M. H. K., … Leung, T. F. (2024). Real-World Sensitization and Tolerance Pattern to Seafood in Fish-Allergic Individuals. *The Journal of Allergy and Clinical Immunology: In Practice*, *12*(3), 633-642.e9. https://doi.org/10.1016/j.jaip.2023.09.038

3. Magyar, T., Németh, B., Tamás, J., & Nagy, P. T. (2024). Improvement of N and P ratio for enhanced biomass productivity and sustainable cultivation of Chlorella vulgaris microalgae. *Heliyon*, *10*(1), e23238. https://doi.org/10.1016/j.heliyon.2023.e23238

4. Schmidt, J., Wilhelm, S., & Boyer, G. (2014). The Fate of Microcystins in the Environment and Challenges for Monitoring. *Toxins*, *6*(12), 3354–3387. https://doi.org/10.3390/toxins6123354

5. Ardila, L., Godoy, R., & Montenegro, L. (2017). Sorption Capacity Measurement of Chlorella Vulgaris and Scenedesmus Acutus to Remove Chromium from Tannery Waste Water. *IOP Conference Series: Earth and Environmental Science*, *83*(1), 012031. https://doi.org/10.1088/1755-1315/83/1/012031

6. Ursu, A.-V., Marcati, A., Sayd, T., Sante-Lhoutellier, V., Djelveh, G., & Michaud, P. (2014). Extraction, fractionation, and functional properties of proteins from the microalgae Chlorella vulgaris. *Bioresource Technology*, *157*, 134–139. https://doi.org/10.1016/j.biortech.2014.01.071

7. Barghchi, H., Dehnavi, Z., Nattagh-Eshtivani, E., Alwaily, E. R., Almulla, A. F., Kareem, A. K., Barati, M., Ranjbar, G., Mohammadzadeh, A., Rahimi, P., & Pahlavani, N. (2023). The effects of Chlorella vulgaris on cardiovascular risk factors: A comprehensive review on putative molecular mechanisms. *Biomedicine & Pharmacotherapy*, *162*, 114624. https://doi.org/10.1016/j.biopha.2023.114624

8. Srivastava, S., Rahman, Md. A., & Sundaram, S. (2023). Immunomodulatory Effects of Edible Microalgae. In *Immune-Boosting Nutraceuticals for Better Human Health* (pp. 259–288). Apple Academic Press. https://doi.org/10.1201/9781003371069-14

9. Sharma, R., Mondal, A. S., & Trivedi, N. (2023). Anticancer potential of algae-derived metabolites: recent updates and breakthroughs. *Future Journal of Pharmaceutical Sciences*, *9*(1), 44. https://doi.org/10.1186/s43094-023-00492-2

10. Shaman, A. A., Zidan, N. S., Atteia, H. H., Tayel, A. A., Alzahrani, S., AlBishi, L. A., Alsayegh, A. A., Sakran, M. I., & Elezaly, F. M. (2023). Effects of edible red sea algae (Arthrospira platensis and Chlorella vulgaris) on some antioxidants and liver

parameters of diabetic rats. *Biomass Conversion and Biorefinery*. https://doi.org/10.1007/s13399-023-04866-7

11. Montero-Sánchez, Y., Gallo, A., Gómez, L. M., Álvarez, I., Sabina, L. C., Támbara, Y., Álvarez, A., Alfonso, M. C., & Ramírez, L. R. (2012). *Investigación y Saberes 2012 PRODUCTIVIDAD DE LÍPIDOS Y COMPOSICIÓN DE ÁCIDOS GRASOS DE CINCO ESPECIES DE MICROALGAS: Vol. I* (Issue 2).

12. Shanmugam, S., Mathimani, T., Anto, S., Sudhakar, M. P., Kumar, S. S., & Pugazhendhi, A. (2020). Cell density, Lipidomic profile, and fatty acid characterization as selection criteria in bioprospecting of microalgae and cyanobacterium for biodiesel production. *Bioresource Technology*, *304*, 123061. https://doi.org/10.1016/j.biortech.2020.123061

13. Daliry, S., Hallajisani, A., Mohammadi Roshandeh, J., Nouri, H., & Golzary, A. (2017). Investigation of optimal condition for Chlorella vulgaris microalgae growth. In *Global Journal of Environmental Science and Management* (Vol. 3, Issue 2, pp. 217–230). Iran Solid Waste Association. https://doi.org/10.22034/gjesm.2017.03.02.010

14. EL-Sahar, G. E. (2014). Study on the biological effect of use flaxseed oil as a source of fat on the Biomarkers of experimental rats. In *Journal of American Science* (Vol. 10, Issue 3). http://www.americanscience.org

15. Safi, C., Zebib, B., Merah, O., Pontalier, P.-Y., & Vaca-Garcia, C. (2014). Morphology, composition, production, processing and applications of Chlorella vulgaris: A review. *Renewable and Sustainable Energy Reviews*, *35*, 265–278. https://doi.org/10.1016/j.rser.2014.04.007

16. Gao, P., Guo, L., Gao, M., Zhao, Y., Jin, C., & She, Z. (2022). Regulation of carbon source metabolism in mixotrophic microalgae cultivation in response to light intensity variation. *Journal of Environmental Management*, *302*, 114095. https://doi.org/10.1016/j.jenvman.2021.114095

17. Pawlita-Posmyk, M., Wzorek, M., & Płaczek, M. (2018). The influence of temperature on algal biomass growth for biogas production. *MATEC Web of Conferences*, *240*, 04008. https://doi.org/10.1051/matecconf/201824004008

18. Cheng, C.-L., Lo, Y.-C., Huang, K.-L., Nagarajan, D., Chen, C.-Y., Lee, D.-J., & Chang, J.-S. (2022). Effect of pH on biomass production and carbohydrate accumulation of Chlorella vulgaris JSC-6 under autotrophic, mixotrophic, and photoheterotrophic cultivation. *Bioresource Technology*, *351*, 127021. https://doi.org/10.1016/j.biortech.2022.127021

19. Li, X., Song, M., Yu, Z., Wang, C., Sun, J., Su, K., Liu, N., Mou, Y., & Lu, T. (2022). Comparison of heterotrophic and mixotrophic Chlorella pyrenoidosa cultivation for the growth and lipid accumulation through acetic acid as a carbon source. *Journal of Environmental Chemical Engineering*, *10*(1), 107054. https://doi.org/10.1016/j.jece.2021.107054

20. Farooq, W., Naqvi, S. R., Sajid, M., Shrivastav, A., & Kumar, K. (2022). Monitoring lipids profile, CO2 fixation, and water recyclability for the economic viability of microalgae Chlorella vulgaris cultivation at different initial nitrogen. *Journal of Biotechnology*, *345*, 30–39. https://doi.org/10.1016/j.jbiotec.2021.12.014

21. Yu, L., Li, T., Ma, J., Zhao, Q., Wensel, P., Lian, J., & Chen, S. (2022). A kinetic model of heterotrophic and mixotrophic cultivation of the potential biofuel organism microalgae Chlorella sorokiniana. *Algal Research*, *64*, 102701. https://doi.

org/10.1016/j.algal.2022.102701

22. Nordin, N., Yusoff, N., Md Nadzir, S., Kamari, A., & Mohd Yusoff, M. Z. (2022). OPTIMISATION OF BIOMASS, LIPID AND CARBOHYDRATE PRODUCTIVITIES IN Chlorella vulgaris FOR BIOFUEL PRODUCTION. *Jurnal Teknologi*, *84*(2), 47–57. https://doi.org/10.11113/jurnalteknologi.v84.17079

23. Rismani, S., & Shariati, M. (2017). Changes of the Total Lipid and Omega-3 Fatty Acid Contents in two Microalgae Dunaliella Salina and Chlorella Vulgaris Under Salt Stress. *Brazilian Archives of Biology and Technology*, *60*(0). https://doi.org/10.1590/1678-4324-2017160555

24. Xie, D., Ji, X., Zhou, Y., Dai, J., He, Y., Sun, H., Guo, Z., Yang, Y., Zheng, X., & Chen, B. (2022). Chlorella vulgaris cultivation in pilot-scale to treat real swine wastewater and mitigate carbon dioxide for sustainable biodiesel production by direct enzymatic transesterification. *Bioresource Technology*, *349*, 126886. https://doi.org/10.1016/j.biortech.2022.126886

25. Dąbrowska, M., Sokalska, K., Gumułka, P., Binert-Kusztal, Ż., & Starek, M. (2019). Quantification of omega-3 fatty acids in dietary supplements and cooking products available on the polish market by thin-layer chromatography–densitometry. *JPC - Journal of Planar Chromatography - Modern TLC*, *32*(1), 13–24. https://doi.org/10.1556/1006.2019.32.1.2

26. Abdo, S. M., Ali, G., & Kamel El-Baz, F. (2015). Potential production of omega fatty acids from microalgae. In *Article in International Journal of Pharmaceutical Sciences Review and Research* (Vol. 34, Issue 2). https://www.researchgate.net/publication/291057193

27. Siahbalaei, R., Kavoosi, G., & Noroozi, M. (2021). Manipulation of *Chlorella vulgaris* polyunsaturated <scp>ω-3</scp> fatty acid profile by supplementation with vegetable amino acids and fatty acids. *Phycological Research*, *69*(2), 116–123. https://doi.org/10.1111/pre.12449

28. Ugwu, C. U., & Aoyagi, H. (2012). Microalgal Culture Systems: An Insight into their Designs, Operation and Applications. *Biotechnology(Faisalabad)*, *11*(3), 127–132. https://doi.org/10.3923/biotech.2012.127.132

29. Kasimani, R., Priya Mookiah, V., Pandian, S., Asokan, T., Mookiah, V. P., & Praxis, T. (n.d.). *Study on the Effects of Initial pH, Temperature and Agitation Speed on Lipid Production by Yarrowia lipolytica and Chlorella vulgaris using Sago Wastewater as a Substrate*. https://www.researchgate.net/publication/354381832

30. Heidari, M., Kariminia, H.-R., & Shayegan, J. (2016). Effect of culture age and initial inoculum size on lipid accumulation and productivity in a hybrid cultivation system of Chlorella vulgaris. *Process Safety and Environmental Protection*, *104*, 111–122. https://doi.org/10.1016/j.psep.2016.07.012

31. AWAN, J., Rehman, A., Mubarak, M. U., Shafiq, M. I., Rahim, U., & Ahmad, M. (2022). Effect of Temperature, Light Cycle, Non-Aeration, Aeration and Aeration + Co2 Conditions on Lipid and Biomass Production of Chlorella Vulgaris. *SSRN Electronic Journal*. https://doi.org/10.2139/ssrn.4055811

32. Wang, L., Wang, Y., Chen, P., & Ruan, R. (2010). Semi-continuous Cultivation of Chlorella vulgaris for Treating Undigested and Digested Dairy Manures. *Applied Biochemistry and Biotechnology*, *162*(8), 2324–2332. https://doi.org/10.1007/s12010-010-9005-1

33. Sakarika, M., & Kornaros, M. (2016). Effect of pH on growth and lipid accumulation

kinetics of the microalga Chlorella vulgaris grown heterotrophically under sulfur limitation. *Bioresource Technology*, *219*, 694–701. https://doi.org/10.1016/j.biortech.2016.08.033

34. Ma, X., Zheng, H., Addy, M., Anderson, E., Liu, Y., Chen, P., & Ruan, R. (2016). Cultivation of Chlorella vulgaris in wastewater with waste glycerol: Strategies for improving nutrients removal and enhancing lipid production. *Bioresource Technology*, *207*, 252–261. https://doi.org/10.1016/j.biortech.2016.02.013

35. Sharma, A. K., Sahoo, P. K., Singhal, S., & Joshi, G. (2016). Exploration of upstream and downstream process for microwave assisted sustainable biodiesel production from microalgae Chlorella vulgaris. *Bioresource Technology*, *216*, 793–800. https://doi.org/10.1016/j.biortech.2016.06.013

36. Sharma, A. K., Sahoo, P. K., Singhal, S., & Joshi, G. (2016). Exploration of upstream and downstream process for microwave assisted sustainable biodiesel production from microalgae Chlorella vulgaris. *Bioresource Technology*, *216*, 793–800. https://doi.org/10.1016/j.biortech.2016.06.013

37. Caetano, N., Melo, A. R., Gorgich, M., Branco-Vieira, M., Martins, A. A., & Mata, T. M. (2020). Influence of cultivation conditions on the bioenergy potential and bio-compounds of Chlorella vulgaris. *Energy Reports*, *6*, 378–384. https://doi.org/10.1016/j.egyr.2019.08.076

38. Gupta, P. L., Choi, H.-J., Pawar, R. R., Jung, S. P., & Lee, S.-M. (2016). Enhanced biomass production through optimization of carbon source and utilization of wastewater as a nutrient source. *Journal of Environmental Management*, *184*, 585–595. https://doi.org/10.1016/j.jenvman.2016.10.018

39. Yun, H.-S., Kim, Y.-S., & Yoon, H.-S. (2020). Characterization of Chlorella sorokiniana and Chlorella vulgaris fatty acid components under a wide range of light intensity and growth temperature for their use as biological resources. *Heliyon*, *6*(7), e04447. https://doi.org/10.1016/j.heliyon.2020.e04447

Current Trends in Biotechnology and Pharmacy
Vol. 19(1) 2130-2143, January 2025, ISSN 0973-8916 (Print), 2230-7303 (Online)
DOI: 10.5530/ctbp.2025.1.3

Phytochemical, GC-MS Analysis and Acute Toxicity Evaluation of Algerian *Ocimum basilicum L* in Rats

Islam Boulaares [1,2], Samir Derouiche [1,2*], Janetta Niemann[3]

[1]Department of Cellular and Molecular Biology, Faculty of Natural Sciences and Life, University of El-Oued, El-Oued 39000, Algeria.
[2]Laboratory of Biodiversity and Application of Biotechnology in the Agricultural Field, Faculty of Natural Sciences and Life, University of El-Oued, El-Oued 39000, Algeria.
[3]Department of Genetics and Plant Breeding, Poznan University of Life Sciences, Dojazd 11, 60-632 Poznan, Poland

***Corresponding author**: dersamebio@gmail.com

Abstract

Sweet Basil (*Ocimum basilicum* L.) is regarded as a significant plant. They include a wide variety of bioactive substances, particularly phenolic substances which contribute to the plant's alleged health advantages. The objective of this study was to identify and characterize the phytochemical profile of sweet basil using GC-MS analysis. By using standard protocols, Bioactive molecules were extracted and qualitative tests of phytochemicals were also released as well as quantitative analyses of total phenols, total flavonoids, and total hydrolysable tannins. Using GC-MS, volatile compounds can be identified. About 147 volatile compounds in this plant were identified by the GC-MS analysis. The chemical constituents higher than 0.5 % found in aqueous extract were propanoic acid, 2-hydroxy-, ethyl ester (3.503%), butanoic acid, 4-hydroxy- (1.657%), cyclopentasiloxane, decamethyl- (1.346%), cyclotetrasiloxane, octamethyl- (0.983%), heptadecane, 2,6,10,15-tetramethyl- (0.785%), bis(tert-butyldimethylsilyl) 2,3-bis((tert-butyldimethylsilyl)oxy) fumarate (0.703%), cyclononasiloxane, octadecamethyl- (0.672%), phthalic acid, 8-bromoctyl isobutyl ester (0.655%), 3-isopropoxy-1,1,1,7,7,7-hexamethyl-3,5,5-tris(trimethylsiloxy)tetrasiloxane (0.535%), and cyclononasiloxane, octadecamethyl- (0.506%). Moreover, the TPC, TFC, and THTC of sweet basil was systematically assessed. The results demonstrate the value of sweet basil (*Ocimum basilicum L*.) which may be used in the food and health industries as promising sources of phenolic and volatile chemicals.

Key word: *GC-MS; Ocimum basilicum L.; Phytochemical screening; Phenolic compounds.*

Introduction

Medicinal plants have long played important roles in the treatment of diseases all over the world (1). Their pharmaceutical properties are based on the presence and abundance of secondary metabolites, such as terpenoids, phenolics, alkaloids, and flavonoids (2). Since 2600 BC, people have utilized plant metabolites and during the next 4,000 years, secondary metabolites were mostly used for food, medicine, and poison (3). Many of these herbal products exhibit medicinal properties as anticancer, anti-inflammatory, antioxidant, antiviral, and antimicrobial actions (4). Furthermore, medicinal plants are used in various food, beverage, and pharmaceutical industries (5). Plant-based bioactives have drawn a significant interest due to

Current Trends in Biotechnology and Pharmacy
Vol. 19(1) 2130-2143, January 2025, ISSN 0973-8916 (Print), 2230-7303 (Online)
DOI: 10.5530/ctbp.2025.1.3

their advantageous effects on health, especially polyphenolic chemicals (6). Common basil is among the most essential aromatic plants (7) belonging to the family Lamiaceae and is also a yearly herb that is planted in numerous diverse parts of the world (8). Since ancient times, *Ocimum basilicum* L. has been growing and used (9). This plant named usually as sweet basil (10) and was famous as a medicinal plant and culinary herb due to its phytochemical contents (11). Different basil extracts have been found to contain a various of chemical functionalities, including phenolic acids and their esters, flavonoids, anthocyanins, tannins, phytosterols, phenylpropanoid derivatives, monoterpenes, and triterpenes (12). Because of their antioxidant, anti-inflammatory characteristics, plant-based natural compounds are being investigated more and more for pharmacological uses, either as preventative or therapeutic agents (13). Common basil is one of the most significant species from the genus of *Ocimum* (14) that including more than 60 species comprising *basilicum* (15). The aim of this study was to screen the phytochemicals of an aromatic medicinal plant (*Ocimum basilicum* L.) leaves qualitatively and based on the presence of metabolites study further restricted to explore the plant extract to quantify the volatile compounds by GC-MS studies.

Materials and Methods

Plant and extract preparation

The *Ocimum basilicum* L. plant utilized in the present research was collected in August 2022 from the El-Oued (Guemar) region. The leaves were cleaned and then dried away from direct sunlight and at room temperature. By using a mechanical grinder, the dry leaves were ground into a fine powder. Until the experiment begins, *Ocimum basilicum* L. powder is kept at room temperature in airtight containers. Prof. Youcef Hellis identified the plant material (Arid Region Scientific and Technical Research Center, Station of Touggourt).

Figure 1. Sweet basil leaves.

Aqueous extract was prepared by boiling 10 g of dried *Ocimum basilicum* L. leaves powder in 100 ml of distilled water for two hours at 50 °C. The extract was first filtered through Whatman filter paper, then cooled and macerated to room temperature for 24 hours. After that, it was evaporated using a rotary evaporator and dried in an oven (16). A yield percentage of plant extract product was calculated according to the following equation used by Okoduwa et *al*. (17):

Plant aqueous extract was subjected to standard methodology for the qulitative phytochemical analysis.

$$Percentage\ yield\ \%\ (\frac{w}{w}) = \ (\frac{Weight\ of\ extract\ (g)}{Weight\ of\ plant\ sample\ (g)})\ x\ 100 \qquad (1)$$

Quantitative phytochemical contents

The Folin-Ciocalteu method was used to estimate the total phenolic content (18). Briefly, 1000 µl of Folin-Ciocalteu (10%) reagent was mixed with 200 µl of basil aqueous extract. 800 µl of saturated sodium carbonate (7.5%) was added after 4 minutes. The absorbance at 765 nm was measured following a 2 hours incubation period at room temperature. For the standard calibration curve, gallic acid was used.

The method of (19) was used to determine the flavonoid content of plant extract.

Briefly, 500 µl of $AlCl_3$ (2%) reagent was added to 500 µl of the basil extract. The absorbance was measured at 420 nm after 1 hour at room temperature. The calibration curve established with quercetin.

Using the Folin-Ciocalteu colourimetric method, the total hydrolysable tannin content was calculated. A calibration curve was created using tannic acid as the standard. Briefly, 1 ml of plant extract was added to a 10 ml test tube together with 0.7 ml of Na_2CO_3 (7%) solution, 0.5 ml of Folin-Ciocalteu (10%) reagent, and 8.4 ml of distilled water. After 30 minutes of incubation, the absorbance was measured at 700 nm against a blank (20).

The results were expressed as milligrams of gallic acid, quercetin and tannic acid equivalents per gram of dry extract (mg of GAE, QE and TAE / g). All the experiments were carried out in triplicate.

GC-MS analysis

Plant extract of leaves were prepared in universal solvent methanol and for which 1µl plant extract was employed to quantify the volatile compounds by GC-MS analysis. For extraction of volatiles headspace solid-phase micro-extraction (SPME) with DVB/CAR/PDMS fibre was used. Firstly, the fibre was conditioned in the GC injection port at 270°C for 4 h. Then the fibre was putted to the vial with the sample using adapter for 15 min at room temperature. After that the fibre was putted to the injection port of a gas chromatograph for desorption. Desorption time was 10 min at 260°C in the splitless mode. For analysis was used a 7890A GC system (Agilent Technologies, Santa Clara, United States) coupled to a 5975C VL Triple-Axis mass detector (Agilent Technologies, Santa Clara, United States). Separation was run on a DB-5MS capillary column (25 m × 0.2 mm; 0.33 µm film thickness; J&W, Folsom, California) with helium as a carrier gas at a flow rate of 0.6 mL/min. The temperature of injector and transfer line were 260°C and 280°C, respectively. The oven program of temperature was: the initial temperature at 40°C was held for 3 min, then increased at 4°C/min to 160°C and further increased at 10°C/min to 280°C, with the final temperature held for 3 min. The masses were scanned from 33 to 333 Da. The ionization energy value was set to 70 eV.

Result interpretation of GC-MS data was estimated with the aid of the database of National Institute Standard and Technology (NIST). The comparative estimation aided to characterize unknown volatile compounds when compared with stocked NIST library to explore the available data of basil extract.

In-vivo acute toxicity

In vivo acute toxicity was performed using healthy albino rats of Wistar strain. The animals were divided into three groups of two rats each and administered orally with a single dose of aqueous extract of *Ocimum basilicum* L (control, 2 and 5 g/kg of the rat's body weight). The rats were observed for 24h to monitor their behaviour as well as mortality. The results were expressed as mean ± standard deviation (SD), calculated from duplicate determinations and the linear relationship was visually determined.

Results and Discussion

The aqueous extraction of basil (*Ocimum basilicum* L.) dried leaves allowed us to obtain yield of approximately 19.063 ± 0.321 % (Table 1).

Table 1. Percentage yield of crude extract.

Plant species	Percentage yield (%)
Ocimum basilicum L.	19.063 ± 0.321

Phenols, flavonoids, catechic tannins, saponins, reducing sugars, alkaloids, and terpenes were present in this *Ocimum basilicum* L. aqueous extract (Table 2).

Table 2. Phytochemical compounds of *Ocimum basilicum* L. aqueous extract.

Phytochemical compounds	Test	Basil extract
Phenols	Ferric chloride test	+
Flavonoids	Magnesium test	+
Catechic tannins	Ferric chloride test	+
Saponins	Froth test	+
Reducing sugars	Fehling test	+
Alkaloids	Dragendorff's test	+
Terpenes	Salkowki's test	+

Total phenols, flavonoids and hydrolysable tannins contents of *Ocimum basilicum* L. obtained from water solvent revealed important concentrations; 63.60 ± 1.53 mg of GAE, 13.537 ± 0.281 mg of QE, and 27 ± 0.830 mg of TAE/g extract respectively (Figure 2,3,4,5).

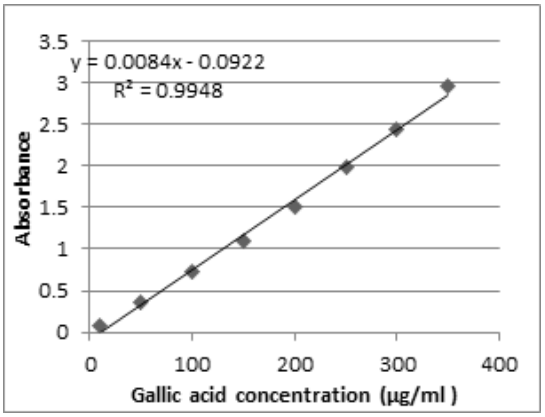

Figure 2. Gallic acid calibration curve for the quantitative determination of phenols.

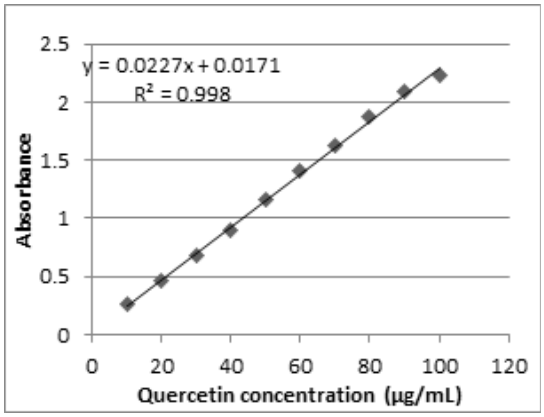

Figure 3. Quercetin calibration curve for the quantitative determination of flavonoids.

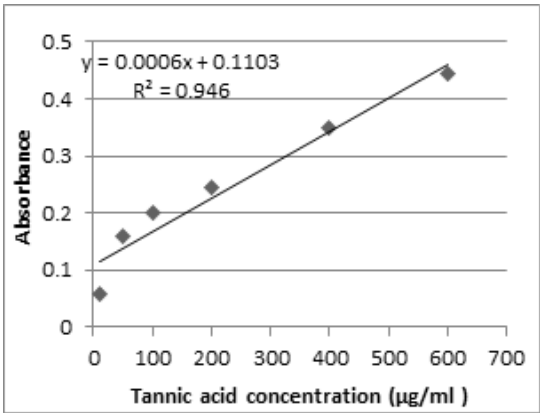

Figure 4. Tannic acid calibration curve for the quantitative determination of hydrolysable tannins.

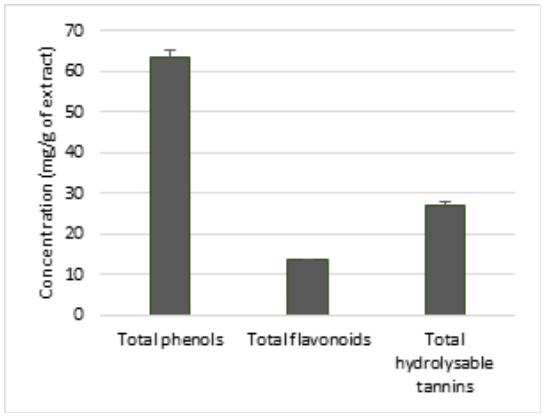

Figure 5. Total phenols, total flavonoids and total hydrolysable tannins concentrations in basil extract.

Gas chromatography-mass spectroscopy analysis

Characterization of volatile compounds from *Ocimum basilicum* L. extract was conducted through GC-MS chromatogram (Figure 6). Using GC-MS technique, about 147 components were identified (Table 3). GC-MS result showed that the chemical constituents higher than 0.5 % found in aqueous extract were propanoic acid, 2-hydroxy-, ethyl ester (3.503%), butanoic acid, 4-hydroxy- (1.657%), cyclopentasiloxane, decamethyl- (1.346%), cyclotetrasiloxane, octamethyl- (0.983%), heptadecane, 2,6,10,15-tetramethyl- (0.785%), bis(tert-butyldimethylsilyl) 2,3-bis((tert-butyldimethylsilyl)oxy)fumarate (0.703%), cyclononasiloxane, octadecamethyl- (0.672%), phthalic acid, 8-bromoctyl isobutyl ester (0.655%), 3-isopropoxy-1,1,1,7,7,7-hexamethyl-3,5,5-tris(trimethylsiloxy)tetrasiloxane (0.535%), and cyclononasiloxane, octadecamethyl- (0.506%).

Table 3: Quantification of volatile compounds by GC-MS of extract leaves of *Ocimum basilicum* L. plant and their various characters.

Peak	Name	Formula	RT (s)	Area (%)
1	Propanoic acid, 2-hydroxy-, ethyl ester	$C_5H_{10}O_3$	289.405	3.503
2	Butanoic acid, 4-hydroxy-	$C_4H_8O_3$	427.257	1.657
3	Lycorenan-7-one,9,10-dimethoxy-1-methyl-	$C_{18}H_{21}NO_4$	430.676	0.006
4	Cyclotetrasiloxane, octamethyl-	$C_8H_{24}O_4Si_4$	525.997	0.983
5	2-Propanol, 1-(2-methoxypropoxy)-	$C_7H_{16}O_3$	544.928	0.038
6	Benzene, 1-methyl-3-(1-methylethyl)-	$C_{10}H_{14}$	558.773	0.056
7	1-Hexanol, 2-ethyl-	$C_8H_{18}O$	560.792	0.144
8	Cyclohexene, 4-ethenyl-1,4-dimethyl-	$C_{10}H_{16}$	563.79	0.071
9	Benzyl alcohol	C_7H_8O	567.088	0.119
10	Benzeneacetaldehyde	C_8H_8O	578.822	0.237
11	Linalyl acetate	$C_{12}H_{20}O_2$	637.621	0.45
12	Nonanal	$C_9H_{18}O$	642.028	0.096
13	1,5,7-Octatrien-3-ol, 3,7-dimethyl-	$C_{10}H_{16}O$	642.329	0.074
14	Cyclopentasiloxane, decamethyl-	$C_{10}H_{30}O_5Si_5$	691.471	1.346
15	Octanoic acid	$C_8H_{16}O_2$	705.073	0.214
16	1,5,5-Trimethyl-6-methylene-cyclohexene	$C_{10}H_{16}$	734.686	0.075
17	Benzene, 1-methoxy-4-(1-propenyl)-, (Z)-	$C_{10}H_{12}O$	741.029	0.099
18	(3S,4R,5R,6R)-4,5-Bis(hydroxymethyl)-3,6-dimethylcyclohexene	$C_{10}H_{18}O_2$	744.729	0.048
19	Benzothiazole	C_7H_5NS	770.123	0.118
20	1,4-Benzenedicarboxaldehyde	$C_8H_6O_2$	776.346	0.015
21	Carvone	$C_{10}H_{14}O$	786.8	0.019
22	(+)-3-Carene	$C_{10}H_{16}$	792.754	0.055
23	Nonanoic acid	$C_9H_{18}O_2$	798.399	0.136
24	1H-Indene-4-carboxaldehyde, 2,3-dihydro-	$C_{10}H_{10}O$	813.245	0.045

25	Tetrasiloxane, 3,5-diethoxy-1,1,1,7,7,7-hexamethyl-3,5-bis(trimethylsiloxy)-	$C_{16}H_{46}O_7Si_6$	820.45	0.015
26	1-[p-Chlorophenyl]-3-[4-[[2-(diisopropylamino)ethyl]amino]-6-methyl-2-pyrimidinyl]-guanidine	$C_{20}H_{30}ClN_7$	839.416	0.021
27	Pentadecane	$C_{15}H_{32}$	858.385	0.026
28	Pentanoic acid, 2,2,4-trimethyl-3-hydroxy-, isobutyl ester	$C_{12}H_{24}O_3$	888.138	0.163
29	Hexadecane	$C_{16}H_{34}$	922.883	0.221
30	Dodecanal	$C_{12}H_{24}O$	931.63	0.096
31	Caryophyllene	$C_{15}H_{24}$	953.638	0.285
32	Phthalic acid, 4-fluoro-2-nitrophenyl methyl ester	$C_{15}H_{10}FNO_6$	974.316	0.02
33	2,5-Cyclohexadiene-1,4-dione, 2,6-bis(1,1-dimethylethyl)-	$C_{14}H_{20}O_2$	988.069	0.124
34	Ethanone, 1-(6,6-dimethylbicyclo[3.1.0]hex-2-en-2-yl)-	$C_{10}H_{14}O$	999.114	0.027
35	Decyl octyl ether	$C_{18}H_{38}O$	1013.58	0.036
36	Oxirane, dodecyl-	$C_{14}H_{28}O$	1017.11	0.034
37	Butylated Hydroxytoluene	$C_{15}H_{24}O$	1023.99	0.111
38	1H-Indene, 1-methyl-3-propyl-	$C_{13}H_{16}$	1026.14	0.006
39	Lilial	$C_{14}H_{20}O$	1036.3	0.038
40	Benzene, (1-butylhexyl)-	$C_{16}H_{26}$	1041.35	0.072
41	Undecane, 5-methyl-	$C_{12}H_{26}$	1044.53	0.015
42	3-[(4-Fluoroanilino)carbonyl]-1,2,2-trimethylcyclopentanecarboxylic acid	$C_{16}H_{20}FNO_3$	1045.61	0.007
43	Tetradecane, 3-methyl-	$C_{15}H_{32}$	1057.89	0.023
44	Oxirane, tetramethyl-	$C_6H_{12}O$	1085.53	0.003
45	Hexadecane	$C_{16}H_{34}$	1086.64	0.167
46	Diethyl Phthalate	$C_{12}H_{14}O_4$	1087.54	0.093
47	Pentanoic acid, 2,2,4-trimethyl-3-carboxyisopropyl, isobutyl ester	$C_{16}H_{30}O_4$	1089.69	0.166
48	Hexestrol, O-trifluoroacetyl-	$C_{20}H_{21}F_3O_3$	1096.71	0.006
49	Benzene, (1-pentylhexyl)-	$C_{17}H_{28}$	1115.07	0.025
50	Benzene, (1-butylheptyl)-	$C_{17}H_{28}$	1117.68	0.05

51	Phenol, 2,6-bis(1,1-dimethyleth-yl)-4-(1-methylpropyl)-	$C_{18}H_{30}O$	1121.14	0.029
52	Cyclopentaneacetic acid, 3-oxo-2-pentyl-, methyl ester	$C_{13}H_{22}O_3$	1132.63	0.137
53	Octane, 1,1'-oxybis-	$C_{16}H_{34}O$	1135.59	0.042
54	3-Isopropoxy-1,1,1,7,7,7-hexa-methyl-3,5,5-tris(trimethylsiloxy)tetrasiloxane	$C_{18}H_{52}O_7Si_7$	1138.39	0.535
55	Nonane, 3,7-dimethyl-	$C_{11}H_{24}$	1140.85	0.015
56	Decane, 1-chloro-	$C_{10}H_{21}Cl$	1146.63	0.011
57	Salicylic acid, isopropyl ether, isopropyl ester	$C_{13}H_{18}O_3$	1152.88	0.026
58	Decyl acrylate	$C_{13}H_{24}O_2$	1157.24	0.019
59	1-(2-Aminopropoxy)-2-methoxyethane	$C_6H_{15}NO_2$	1163.35	0.001
60	Pentadecane, 2,6,10,14-tetramethyl-	$C_{19}H_{40}$	1166.7	0.06
61	Hydrazinecarboxamide	CH_5N_3O	1167.88	0.005
62	2-(4,5-Dihydroxy-2-methylphenyl)-4-hy-droxy-6-methoxybenzoic acid, 4TMS	$C_{27}H_{46}O_6Si_4$	1172.97	0.142
63	Phenethyl isocyanate	C_9H_9NO	1191.03	0.021
64	Tetradecanoic acid	$C_{14}H_{28}O_2$	1203.52	0.036
65	Hexadecane, 2,6,10,14-tetramethyl-	$C_{20}H_{42}$	1240.94	0.045
66	Benzene, (1-methylnonadecyl)-	$C_{26}H_{46}$	1243.15	0.016
67	Salicylic acid, 1-methylpropyl ester	$C_{11}H_{14}O_3$	1245.87	0.021
68	Pentadecanal-	$C_{15}H_{30}O$	1246.84	0.063
69	Bis(tert-butyldimethylsilyl) 2,3-bis((tert-bu-tyldimethylsilyl)oxy)fumarate	$C_{28}H_{60}O_6Si_4$	1253.32	0.703
70	Nickel tetracarbonyl	C_4NiO_4	1264.2	0
71	Isoamyl laurate	$C_{17}H_{34}O_2$	1265.09	0.188
72	Dodecanoic acid, 1,1-dimethylpropyl ester	$C_{17}H_{34}O_2$	1267.65	0.034
73	4-Fluorobenzylamine, N,N-dibutyl-	$C_{15}H_{24}FN$	1275.68	0.009
74	Phthalic acid, 8-bromoctyl isobutyl ester	$C_{20}H_{29}BrO_4$	1285.64	0.655
75	Semioxamazide	$C_2H_5N_3O_2$	1288.89	0.002
76	Sulfurous acid, 2-ethylhexyl nonyl ester	$C_{17}H_{36}O_3S$	1301.97	0.028
77	Hydrazinecarboxamide	CH_5N_3O	1309.44	0.007
78	2-(Diethylamino)ethyl 4-amino-2-hydroxy-benzoate	$C_{13}H_{20}N_2O_3$	1312.77	0.404
79	Pentadecanoic acid, 14-methyl-, methyl ester	$C_{17}H_{34}O_2$	1319.53	0.049

80	Nickel tetracarbonyl	C_4NiO_4	1324.45	0
81	n-Hexadecanoic acid	$C_{16}H_{32}O_2$	1340.11	0.057
82	1,4-Dibutyl benzene-1,4-dicarboxylate	$C_{16}H_{22}O_4$	1348.04	0.128
83	Cyclononasiloxane, octadecamethyl-	$C_{18}H_{54}O_9Si_9$	1355.76	0.672
84	Decane, 6-ethyl-2-methyl-	$C_{13}H_{28}$	1367.14	0.019
85	Hydrazinecarboxamide	CH_5N_3O	1391.66	0.001
86	Piceatannol, 4TMS	$C_{26}H_{44}O_4Si_4$	1395.26	0.324
87	Hydrazinecarboxamide	CH_5N_3O	1406.69	0
88	Hydrazinecarboxamide	CH_5N_3O	1430.48	0.005
89	(1-Methoxy-pentyl)-cyclopropane	$C_9H_{18}O$	1436.74	0.009
90	Pentadecanoic acid, 14-methyl-, methyl ester	$C_{17}H_{34}O_2$	1446.12	0.035
91	Cyclononasiloxane, octadecamethyl-	$C_18H_{54}O_9Si_9$	1449.57	0.506
92	5-Hexyl-5-methyloxolan-2-one	$C_{11}H_{20}O_2$	1457.25	0.004
93	Hydrazinecarboxamide	CH_5N_3O	1482.2	0.001
94	Benzoic acid, tetradecyl ester	$C_{21}H_{34}O_2$	1494.32	0.028
95	Semicarbazide	CH_5N_3O	1500.05	0.002
96	Nickel tetracarbonyl	C_4NiO_4	1509.8	0.005
97	Hydrazinecarboxamide	CH_5N_3O	1511.62	0.001
98	Cyclononasiloxane, octadecamethyl-	$C_{18}H_{54}O_9Si_9$	1534.56	0.364
99	Hydrazinecarboxamide	CH_5N_3O	1540.15	0.001
100	Hydrazinecarboxamide	CH_5N_3O	1553.07	0.001
101	Benzoic acid, tridecyl ester	$C_{20}H_{32}O_2$	1553.75	0.036
102	Semicarbazide	CH_5N_3O	1573.77	0.001
103	Semicarbazide	CH_5N_3O	1577.54	0.002
104	2-Hexanamine	$C_6H_{15}N$	1580.48	0.005
105	Benzoic acid, hexadecyl ester	$C_{23}H_{38}O_2$	1610.8	0.036
106	Cyclononasiloxane, octadecamethyl-	$C_{18}H_{54}O_9Si_9$	1612.91	0.29
107	Semicarbazide	CH_5N_3O	1621.61	0.002
108	L-Alanine, α-N-methyl-N-benzyl-, methyl ester	$C_{12}H_{17}NO_2$	1637.98	0.02
109	Semicarbazide	CH_5N_3O	1645.43	0.007
110	Carbonic acid, bis(2-ethylhexyl) ester	$C_{17}H_{34}O_3$	1656.43	0.017
111	Semicarbazide	CH_5N_3O	1664.98	0.001
112	Benzoic acid, pentadecyl ester	$C_{22}H_{36}O_2$	1665.58	0.031
113	Benzyldiethyl-(2,6-xylylcarbamoylmeth-yl)-ammonium benzoate	$C_{28}H_{34}N_2O_3$	1680.52	0.086

114	Phthalic acid, 2-ethylhexyl pentadecyl ester	$C_{31}H_{52}O_4$	1682.77	0.031
115	Cyclononasiloxane, octadecamethyl-	$C_{18}H_{54}O_9Si_9$	1686.3	0.274
116	Sulfurous acid, 2-ethylhexyl hexyl ester	$C_{14}H_{30}O_3S$	1712.83	0.04
117	Vinyl 2-ethylhexanoate	$C_{10}H_{18}O_2$	1717.17	0.175
118	dl-Alanyl-l-alanine	$C_6H_{12}N_2O_3$	1730.68	0.003
119	Heptadecane, 2,6,10,15-tetramethyl-	$C_{21}H_{44}$	1732.27	0.785
120	Hydrazinecarboxamide	CH_5N_3O	1733.46	0.004
121	Hydrazinecarboxamide	CH_5N_3O	1754.55	0.001
122	Cyclononasiloxane, octadecamethyl-	$C_{18}H_{54}O_9Si_9$	1757.18	0.304
123	Carbonic acid, bis(2-ethylhexyl) ester	$C_{17}H_{34}O_3$	1758.38	0.011
124	Semicarbazide	CH_5N_3O	1760.82	0.001
125	Hydrazinecarboxamide	CH_5N_3O	1768.11	0.001
126	1,3-Benzenedicarboxylic acid, bis(2-ethyl-hexyl) ester	$C_{24}H_{38}O_4$	1785.34	0.041
127	Semicarbazide	CH_5N_3O	1805.8	0.001
128	Benzenemethanol, α-(1-aminoethyl)-	$C_9H_{13}NO$	1833.93	0.013
129	Squalene	$C_{30}H_{50}$	1835.62	0.108
130	Semicarbazide	CH_5N_3O	1836.47	0.001
131	Cyclononasiloxane, octadecamethyl-	$C_{18}H_{54}O_9Si_9$	1839.37	0.28
132	2-Hydroxybenzene-1,3-dicarboxylic acid, trimethylsilyl ether, bis(trimethylsilyl) ester	$C_{17}H_{30}O_5Si_3$	1850.8	0.311
133	Semicarbazide	CH_5N_3O	1863.63	0.001
134	Hydrazinecarboxamide	CH_5N_3O	1880.66	0.002
135	Hydrazinecarboxamide	CH_5N_3O	1882.03	0.001
136	Hydrazinecarboxamide	CH_5N_3O	1891.75	0.001
137	Semicarbazide	CH_5N_3O	1893.9	0.005
138	Benzenemethanol, α-(1-aminoethyl)-	$C_9H_{13}NO$	1904.71	0.003
139	Hydrazinecarboxamide	CH_5N_3O	1909.88	0.001
140	Benzenemethanol, α-(1-aminoethyl)-	$C_9H_{13}NO$	1911.59	0.001
141	Semicarbazide	CH_5N_3O	1917.4	0.001
142	Semicarbazide	CH_5N_3O	1927.25	0.001
143	Semicarbazide	CH_5N_3O	1932.07	0.001
144	Cyclononasiloxane, octadecamethyl-	$C_{18}H_{54}O_9Si_9$	1941.29	0.485
145	Semicarbazide	CH_5N_3O	1945.74	0.001
146	Semicarbazide	CH_5N_3O	1946.04	0.001
147	Semicarbazide	CH_5N_3O	1958.37	0.001

In-vivo acute toxicity

Wistar albino rats were used in this experiment to test acute toxicity over the course of 24 hours. Our plant is administered at doses of 2 g and 5 g per kilogram of rats. No mortality and no alteration in the other physiological parameters of the rats, which indicates that the aqueous extract of *Ocimum basilicum* L. had no toxic and no adverse effects on the rats during the treatment period (Table 4).

Table (4) : Effect of basil extract on physiological parameters of Wistar albino rats.

Parameter	Dose	Toxicity time				
		0 h	3 h	7 h	14 h	24 h
Death rats	Control	None	None	None	None	None
	2 g/ kg	None	None	None	None	None
	5 g/ kg	None	None	None	None	None
Eyes	Control	Normal	Normal	Normal	Normal	Normal
	2 g/ kg	Normal	Normal	Normal	Normal	Normal
	5 g/ kg	Normal	Normal	Normal	Normal	Normal
Sleep	Control	Normal	Normal	Normal	Normal	Normal
	2 g/ kg	Normal	Normal	Normal	Normal	Normal
	5 g/ kg	Normal	Normal	Normal	Normal	Normal
Diarrhea	Control	Normal	Normal	Normal	Normal	Normal
	2 g/ kg	Normal	Normal	Normal	Normal	Normal
	5 g/ kg	Normal	Normal	Normal	Normal	Normal

Discussion

The bioactive substances in *Ocimum basilicum* L. leaves aqueous extract were qualified and quantified using the qualitative and quantitative phytochemical analysis and GC-MS methodology.

Our study revealed the presence of phenols, flavonoids, catechic tannins, saponins, reducing sugars, alkaloids, and terpenes in basil aqueous extract. The results of the current study on phytochemical screening are consistent with those of Nadeem et *al*. who found that basil leaves water extract consist of phenols, alkaloids, tannins, flavonoids, steroids, terpenoids, and glycosides (21). Moreover; tannins, flavonoids, terpenoids, saponins, and reducing sugars were reported as the present phytochemical compounds aqueous extract from sweet basil leaves (22). According to Pushpalatha et *al*., preliminary secondary metabolites screening of aqueous extract of *Ocimum basilicum* L. showed the existence of phytochemicals such as carbohydrates, tannins, saponins, flavonoids, anthocyanin, cardiac glycosides, terpenoids, triterpenoids, phenols, and steroids (23). According to reports, the active substances in medicinal plants that give them their pharmacological potentials are their phytochemicals (24). Phenolic and flavonoids compounds found in plant secondary metabolites have pharmacological effects such as anti-allergic, antibacterial, antiviral, anti-inflammatory, antioxidant, anti-diabetic, anticancer and neurodegenerative effect (25).

Concerning the quantification of phytochemical molecules, the present results are supported by the by the results of Nadeem et *al*. who found 70.7 mg GAE/g of total phenolic content, 6.49 mg QE/g of total flavonoids and 13.3 mg GAE/g of total tannins content in O*. basilicum* aqueous extract (21).

In this work, the identification and characterisation of 147 volatile compounds from basil water extract were conducted through GC-MS. The identification of basil extracts was carried out by Kaya and Keskin using GC-MS Which showed the presence of various bioactive compounds (26). GC-MS result showed that the compounds higher than 4 % found in aqueous extract by Ababutain were Propane, 3-chloro-1,1,14,5-Dichloro-1,3-dioxolan-2-one (49.87 %), phenol (6.22 %), propane, 3-chloro-1,1,1-trifluoro (4.26 %), and gamma-sitosterol (4.19 %) (27). D´ıaz-Maroto et *al.* in their study could identifying various volatile components in basil extracts using (GC/MS), linalool being the major component (28). Numerous investigations of the volatile composition of *Ocimum basilicum* L. have been conducted (29). Volatile organic components in plant, the low-molecular-weight molecules, have elevated chemical reactivities due to their functional groups, such as the structure with hydroxy, α, β-unsaturated carbonyl, phenyl, alkoxyl and sulfhydryl, and ester groups, bringing high polarity or electrophile capacity to these molecules (30). The basil volatile components, as well as their antifungal, antibacterial, and antioxidant properties, have been extensively studied (31). A previous study has shown that the chemical profiles of leaf volatile compounds from a plant genus are highly diverse (32). The results of the acute toxicity study revealed that the oral administration of basil aqueous extract to rats at doses of 2 and 5 g/kg did not result in any toxicity symptoms or animal death. Acute toxicity is a single-dose test that identifies symptoms and the extent to which toxicity affects animals (33). The principal aim of evaluating the safety of any medicinal plant is to identify the nature and significance of adverse effect and to establish the exposure level at which this effect is observed (34). Based on their long-term use by humans one might expect plants used in traditional medicine to have low toxicity (35). The pharmacological potential of a medicinal plant depends on its secondary metabolites (36).

Conclusion

The volatile components from *Ocimum basilicum* L. were successfully identified using the GC-MS analysis; it has a distinctive compounds content, ester, alcohols, ketones, fatty acids, aldehydes and hydrocarbons. From this plant, about 147 chemicals were provably discovered. Basil was tentatively found to include phenols, flavonoids, catechic tannins, saponins, reducing sugars, alkaloids and terpenes. This research will help the extensive use of basil in the food, nutrition, and pharmaceutical industries and will provide useful information for the future utilization of volatile chemicals.

Acknowledgments

The authors thank the members of Pedagogic Laboratories, El-Oued, Algeria and department of food and biotechnology, Poznan university of life sciences, Poznan for providing research facilities to carry out the present work.

Conflict of interests: None declared

References

1. Boulaares I., Derouiche S. Effect of Garlic and Onions Extract Enriched with Honey Treatment on the Lipid Profile, Biochemical and Hematological Biomarker Status in Healthy Women. of Pharm Biosci Journal. 2021; 9(1): 22-27.
2. Thokchom SD, Gupta S, Kapoor R. An appraisal of arbuscular mycorrhiza-mediated augmentation in production of secondary metabolites in medicinal plants. Journal of Applied Research on Medicinal and Aromatic Plants. 2023; 37(4): 100515.
3. Twaij BM, Hasan MN. Bioactive Secondary Metabolites from Plant Sources: Types, Synthesis, and Their Therapeutic Uses. Int J Plant Biol. 2022; 13: 4-14.
4. Parham S, Kharazi AZ, Bakhsheshi-Rad HR, Nur H, Ismail AF, Sharif S, RamaKrishna S, Berto F. Antioxidant, antimicrobial and antiviral properties of herbal materials.

Antioxidants. 2020; 9(12): 1309.

5. Tang J, Dunshea FR, Suleria HA. Lc-esi-qtof/ms characterization of phenolic compounds from medicinal plants (hops and juniper berries) and their antioxidant activity. Foods. 2019; 9(7): 1-25.

6. Boulaares I, Derouiche S, Niemann J. HPLC-Q-TOF-MS analysis of phenolic compounds, in vitro biological activities and in vivo acute toxicity evaluation of Ocimum Basilicum L. Fresenius Environmental Bulletin. 2024; 33(2): 73-82

7. Taha R, Alharby H, Bamagoos A, Medani R, Rady M. Elevating tolerance of drought stress in *Ocimum basilicum* using pollen grains extract; a natural biostimulant by regulation of plant performance and antioxidant defense system. S Afr J Bot. 2020; 128: 42-53.

8. Derouiche S, Guemari IY, Boulaares I. Characterization and acute toxicity evaluation of the MgO Nanoparticles Synthesized from Aqueous Leaf Extract of *Ocimum basilicum* L. Alger J Biosciences. 2020; 1(1): 1-6.

9. Georgiadou EC, Kowalska E, Patla K, Kulbat K, Smolińska B, Leszczyńska J, Fotopoulos V. Influence of heavy metals (Ni, Cu, and Zn) on nitro-oxidative stress responses, proteome regulation and allergen production in basil (*Ocimum basilicum* L.) plants. Front Plant Sci. 2018; 9: 862.

10. Ahmed AF, Attia FA, Liu Z, Li C, Wei J, Kang W. Antioxidant activity and total phenolic content of essential oils and extracts of sweet basil (*Ocimum basilicum* L.) plants. Food Sci Hum Wellness. 2019; 8(3): 299-305.

11. Rumengan I, Mandey L, Citraningtiyas G, Luntungan A: Antihyperglicemic capacity of basil (*Ocimum basilicum* L.) leaves extracts coated with the marine fish scales derived nanochitosan. In: *IOP Conference Series: Materials Science and Engineering: 2019*. IOP Publishing: 012023.

12. Rezzoug M, Bakchiche B, Gherib A, Roberta A, Kilinçarslan Ö, Mammadov R, Bardaweel SK. Chemical composition and bioactivity of essential oils and Ethanolic extracts of *Ocimum basilicum* L. and *Thymus algeriensis* Boiss. & Reut. from the Algerian Saharan Atlas. BMC Complement Altern Med. 2019; 19(146): 1-10.

13. Picos-Salas MA, Heredia JB, Leyva-López N, Ambriz-Pérez DL, Gutiérrez-Grijalva EP. Extraction Processes Affect the Composition and Bioavailability of Flavones from Lamiaceae Plants: A Comprehensive Review. Processes. 2021; 9(9): 1675.

14. Zahedifar M, Moosavi AA, Zarei Z, Shafigh M, Karimian F. Heavy metals content and distribution in basil (*Ocimum basilicum* L.) as influenced by cadmium and different potassium sources. Int J Phytoremediation. 2019; 21(5): 435-447.

15. Murali M, Prabakaran G. Effect of different solvents system on antioxidant activity and phytochemical screening in various habitats of *Ocimum basilicum* L.(Sweet basil) leaves. Int J Zool Appl Biosci. 2018; 3(5): 375-381.

16. Derouiche S, Chetehouna S, Atoussi W. The Effects of aqueous leaf extract of *Portulaca oleracea* on haemato-biochemical and histopathological changes induced by Sub-chronic Aluminium toxicity in male wistar rats. Pharmacol Res - Mod Chin Med. 2022; 3: 100101.

17. Okoduwa SIR, Umar IA, James DB, Inuwa HM, Habila JD. Evaluation of extraction protocols for anti-diabetic phytochemical substances from medicinal plants. World J Diabetes. 2016; 7(20): 605-614.

18. Li H-B, Cheng K-W, Wong C-C, Fan K-W, Chen F, Jiang Y. Evaluation of antioxidant capacity and total phenolic content of dif-

ferent fractions of selected microalgae. Food Chem. 2007; 102: 771-776.

19. Ahn M-R, Kumazawa S, Usui Y, Nakamura J, Matsuka M, Zhu F, Nakayama T. Antioxidant activity and constituents of propolis collected in various areas of China. Food Chem. 2007; 101(4): 1383-1392.

20. Poudel M, Rajbhandari M. Phytochemical Analysis of Ampelopteris Prolifera (Retzius) Copeland. Nepal J Sci Technol. 2020; 19(1): 78-88.

21. Nadeem HR, Akhtar S, Sestili P, Ismail T, Neugart S, Qamar M, Esatbeyoglu T. Toxicity, Antioxidant Activity, and Phytochemicals of Basil (*Ocimum basilicum* L.) Leaves Cultivated in Southern Punjab, Pakistan. Foods. 2022; 11: 1239.

22. Nguyen V, Nguyen N, Thi N, Thi C, Truc T, Nghi P: Studies on chemical, polyphenol content, flavonoid content, and antioxidant activity of sweet basil leaves (*Ocimum basilicum* L.). In: *IOP conference series: Materials Science and Engineering: 2021*. IOP Publishing: 012083.

23. Pushpalatha M, Ponvel M, Narayanan PS. Phytochemical screening and antioxidant, antibacterial activities of Ocimum basilicum L. Journal of Cardiovascular Disease Research. 2021; 12(1):

24. Seema R, Hindole G, Muddasir B. Phytochemical characterization and antioxidative property of *Ocimum canum*: effect of ethanolic extract of leaves and seeds on basic immunologic and metabolic status of male rats. J Immunol Res. 2016; 1(2): 1-7.

25. Shoker R, Raheema RH, Shamkhi IJ. Antimicrobial activity, HPLC analysis of phenolic extract of *Ocimum basilicum* and *Ocimum sanctum*. Biochem Cell Arch. 2021; 21(2): 1-8.

26. Kaya G, Keskin M. Biochemical properties and urease, α-amylase inhibitory effects of *Ocimum basilicum* L.(Reyhan). Journal of Medicinal Herbs and Ethnomedicine. 2020; 6(52-55.

27. Ababutain IM. Antimicrobial Activity and Gas Chromatography-Mass Spectrometry (GC-MS) Analysis of Saudi Arabian *Ocimum basilicum* Leaves Extracts. Journal of Pure & Applied Microbiology. 2019; 13(2): 823-833.

28. Díaz-Maroto MC, Sánchez Palomo E, Castro L, González Viñas M, Pérez-Coello MS. Changes produced in the aroma compounds and structural integrity of basil (*Ocimum basilicum* L) during drying. Journal of the Science of Food and Agriculture. 2004; 84(15): 2070-2076.

29. Calín-Sánchez Á, Lech K, Szumny A, Figiel A, Carbonell-Barrachina ÁA. Volatile composition of sweet basil essential oil (*Ocimum basilicum* L.) as affected by drying method. Food Research International. 2012; 48(1): 217-225.

30. Frahtia A, Derouiche S, Niemann J. GC-MS Analysis and Quantification of Some Secondary Metabolites of the Algerian Phragmites australis Leaf Extract and Their Biological Activities. Current Trends in Biotechnology and Pharmacy. 2024; 18(4) 2024-2035,

31. Du P, Yuan H, Chen Y, Zhou H, Zhang Y, Huang M, Jiangfang Y, Su R, Chen Q, Lai J *et al*. Identification of Key Aromatic Compounds in Basil (*Ocimum* L.) Using Sensory Evaluation, Metabolomics and Volatilomics Analysis. Metabolites. 2023; 13(1): 85.

32. Osei-Owusu J, Heve WK, Aidoo OF, Jnr Opoku M, Apau J, Dadzie KN, Vigbedor BY, Awuah-Mensah KA, Appiah M, Acheampong A *et al*. Repellency Potential, Chemical Constituents of *Ocimum* Plant Essential Oils, and Their Headspace Volatiles against Anopheles gambiae ss, Malaria Vector. J Chem. 2023; 2023(5): 1-12.

33. Benrahou, K., Mrabti, H.N., Assaggaf, H.M., Mortada, S., Salhi, N., Rouas, L., El Bacha, R., Dami, A., Masrar, A., Alshahrani, M.M. (2022) Acute and Subacute Toxicity Studies of Erodium guttatum Extracts by Oral Administration in Rodents. *Toxins*, **14**(11),735.

34. Ugwah-Oguejiofor, C.J., Okoli, C.O., Ugwah, M.O., Umaru, M.L., Ogbulie, C.S., Mshelia, H.E., Umar, M., Njan, A.A. (2019) Acute and sub-acute toxicity of aqueous extract of aerial parts of Caralluma dalzielii NE Brown in mice and rats. *Heliyon*, **5**(1),e01179.

35. Yuet-Ping, K., Darah, I., Chen, Y., Sreeramanan, S., Sasidharan, S. (2013) Acute and subchronic toxicity study of Euphorbia hirta L. methanol extract in rats. *BioMed research international*, **2013**,1-14.

36. Sánchez-Ramos, M., Marquina-Bahena, S., Alvarez, L., Román-Guerrero, A., Bernabé-Antonio, A., Cruz-Sosa, F. (2021) Phytochemical, Pharmacological, and Biotechnological Study of Ageratina pichinchensis: A Native Species of Mexico. *Plants*, **10**(10),2225.

Current Trends in Biotechnology and Pharmacy
Vol. 19(1) 2144-2158, January 2025, ISSN 0973-8916 (Print), 2230-7303 (Online)
DOI: 10.5530/ctbp.2025.1.4

Molecular Modelling, Hirshfeld Surface Analysis, Molecular Docking and Therapeutic Potential of Phenothiazine Derived Quinizarin

Shiny P. Laila[a], Vidya V. G.[a], Sherin G. Thomas[a], Arunkumar B[b], Viju Kumar V. G.[a]*

[a] Department of Chemistry, University College, Thiruvananthapuram, Kerala, 695034, India
[b] Department of Computational Biology and Bioinformatics, University of Kerala, Thiruvananthapuram, Kerala,695034, India

***Corresponding author:** *viju@universitycollege.ac.in

Abstract

Phenothiazine derivative synthesized from hydroxy anthraquinone, characterized by X-ray crystallography, spectroscopic, Hirshfeld surface, DFT studies and molecular docking investigation intent to ascertain its anti-cancer activity. The title compound 7-hydroxy-8-H-naptho[2,3-α]phenothiazine-8,13(14H)-dione crystallizes in orthorhombic lattice. UV-VIS, IR, NMR and mass spectrometric data were employed for characterization. Computational chemistry studies are conducted to further detail its geometrical and spectroscopic characteristics performed with unrestricted DFT method at of B3LYP/ 6-311+G (d, p) level and a comparison between the experimental and simulation results was performed. Non-covalent interactions primarily H-bonding and π-π stacking close contacts were observed at intermolecular levels. Small HOMO-LUMO energy gap of 2.2902 eV, shows the stability of molecule and effectiveness towards charge transfer interactions. Furthermore, MEP is used for predicting reactive sites. Based on Hirshfeld surface analysis, there is evidence for a wide range of interactions and a significant contribution from several non-covalent interactions to crystal packing. The bio-viability study was done using pre ADMET tool. The study elaborates the antitumor activity employing *in silico* molecular docking studies using the protein over-expressed in lymphoma cell lines namely p53 and BCL2 and when compared with standard drug doxorubicin revealed promising results. The study's results may inspire to develop more potent derivatives and similar scaffolds for cancer treatment and to explore phenothiazine's role in fields of material science, photochemistry, and catalysis, that can be analyzed from its structural and electronic properties. Hirshfeld surface analysis sheds light on the role of non-covalent interactions in crystal packing, influencing the compound's solid-state properties.

Keywords: hydroxyanthraquinone, phenothiazine, quinizarin, ADMET, DFT

Introduction

The anthracycline drugs comprise a number of chemotherapy medications commonly employed for the treatment of cancer and are popular for their potent anti-tumor activity and have been widely used for several decades. It works by inhibiting DNA replication and interfering with the function of topoisomerase enzymes, which are essential for DNA repair Studies on quinone compounds revealed that

anthraquinone ring when fused with oxazine moiety resembles that of anthracyclines, and exhibits various biological activity, involving a reduction in multidrug resistance [1]. Phenothiazines are related to oxazine in such a way that both came under the class of heterocyclic compounds which exhibits diversified pharmacological property in which the oxygen atom in the oxazine ring is replaced by sulphur atom which is an isostere of oxygen that forms the phenothiazine ring. These compounds can show varied biological activities like antimicrobial, antitumor, anticancer, and anti-inflammatory properties. It is believed that the diverse biological activity of phenothiazines is due to the presence of a folded axis along sulphur and nitrogen-containing heterocyclic ring. The reports on the bioactivity of DAQ are very few and less likely to be bioactive so an attempt was made to modify the structure of 1,4-dihydroxy anthraquinone by coupling reaction. Various amino and acetyl derivatives of anthraquinone have been reported [2]. There are several reports related to phenothiazine derivative of hydroxy benzoquinones and naphthaquinones, but the phenothiazine derivatives synthesized from hydroxy anthraquinone with C=O group in the 9 and 10 positions are very rare.

Cancer is caused mainly by the uncontrolled growth of cells or through different mutations which block the normal defenses that protect against unnatural growth. High levels of expression of p53 were found in many cancers so p53 was originally believed to be an oncogene [3,4]. The p53 protein is a phosphoprotein made of 393 amino acids and about 50% of all human tumors contain p53 mutants [5]. Though p53 is a tumor suppressor gene that shows a key role in the protection of our body from cancer. Mutated p53 could allow abnormal cells to proliferate, resulting in malignancy. Protein p53 gets mutated by the error caused due to placing an incorrect amino acid at a point in the protein chain. Thus, the normal functions of it will be blocked thereby, it is unable to repair the damaged cell. The work published by Zhen W *et al.,* [6] about the p53 protein state that synthetic drugs identified was selectively used to kill mutant p53-containing cancer cells and are very much helpful for chemoprevention. The certain synthetic drug can eliminate mutant p53-containing cancer-prone cells, at their early stage of carcinogenesis but one of the main adverse effects of drugs against mutated p53 is, normal cells containing non-mutated p53 will also be get destroyed. If the cell has other mutations, then that also causes uncontrolled growth which leads to the formation of the tumor. To prevent cell proliferation and to reduce genotoxic stress thereby maintaining genome integrity, tumor suppressor drugs are essential. The family of BCL2 protein consists of mainly 3 subgroups; BCL-2(anti-apoptotic/pro-survival proteins), BAX and Bak (pro-apoptotic proteins), BAD and BID (pro-apoptotic BH3-only proteins) [7]. Over-expression of the BCL2 gene is involved in cancer development. A large number of B-cell leukemias and lymphomas have the BCL2 gene transferred to a different chromosome. In this way, the BCL2 protein is produced in larger amounts, which may keep cancer cells alive. Thus it is found as a protein target within the breakpoint region of the t(14;18) translocation carried by persons with the follicular variant of B-cell lymphoma. The overexpression of BCL-2 can be found in 80% of B-cell Lymphomas. It is one of the key anti-cancer targets, which is chosen in the present study. One of the major roles of BCL-2 is it represses apoptosis by blocking the release of *cytochrome* complex from the mitochondria.

Owing to its multifunctional properties, this investigation focuses on the synthesis of an o-amino thiophenol derivative of anthraquinone. 1,4-dihydroxy anthraquinone (DAQ), also known as quinizarin, is a dye containing anthraquinone moiety. The interaction of the pharmacophoric substituent, via interaction of the multicyclic ring system improves the lipophilic character and allows the penetration of molecule into the biological membranes. From the study it has been revealed that the formation of

the phenothiazine core is a very potent pharmacophoric moiety which can be a rich source of desirable biological activities. In the present work the in silico biological activity was studied using iGEMDOCK software. Predicted poses of protein and ligand can be further understood from the post-analyzing tag. This can guide the biological researchers to explore better binding sites and interacting aminoacid. It was reported by Hamda M *et al.,* [8] 1996 that p53 mutations are associated with lymphoma. The apoptosis of cancer cells could be achieved by inhibition of this protein. In the present work, the synthetic derivative of hydroxyquinone and the standard drug doxorubicin was taken as the ligands and it is then docked with the targeted proteins. Though numerous in vitro methods are available to predict the absorption, distribution, metabolism and toxicity studies, all are time consuming so it is a common trend to predict and determine the toxicity and the ADME properties using different soft wares like SWISS ADME, preADMET etc. This the method to identify the effectiveness of a molecule to reach its target site. In the present work preADMET is used for predicting the various ADME parameters and Toxicity properties. The present study also investigates the electronic structure of the title compound, its quantum computational studies and supramolecular non-covalent contacts present in the crystal structure.

Materials and M ethods

Synthesis of 7-hydroxy-14-H-naptho[2,3-α] phenothiazine-8,13-dione (HNPD)

Quinizarin, o-aminothiophenol, and iodobenzene diacetate were purchased from Merck and used as such. All the solvents used for synthesis and purification were double distilled and dried using anhydrous calcium sulphate. A pre-coated aluminum plate of silica gel 60F 254 plates (0.25mm) was used for TLC. Column Chromatography is performed using silica gel of mesh size 100-200.

The derivative HNPD was synthesized as reported [9]. For the synthesis, 0.024 g of DAQ was dissolved in 20 ml of dichloromethane and a solution of 0.2 ml of o-aminothiophenol dissolved in 5 mL dichloromethane is added followed by the addition of a catalytic quantity of iodobenzenediacetate (IDA) and is shown in Scheme 1. The mixture is refluxed under a nitrogen atmosphere for 5 hours. The progress of the reaction was ascertained by TLC. After distilling CH_2Cl_2, the crude product is then washed with dil. HCl and neutralized with $NaHCO_3$ solution, extracted with ethyl acetate. The water content of the extract was removed by the addition of anhydrous sodium sulphate. precipitate was subjected to column chromatography by gradient elution method, using petroleum ether and ethyl acetate (60:80). The required product was eluted using pet ether: ethyl acetate in the ratio 8:2. Product was obtained as dark blue precipitate (55% yield). It was recrystallized by vapor deposition method using a mixture of CH_2Cl_2 and methanol, in which the product was highly soluble in CH_2Cl_2 and partially soluble in methanol. Thus obtained a dark blue colored needle-like crystals.

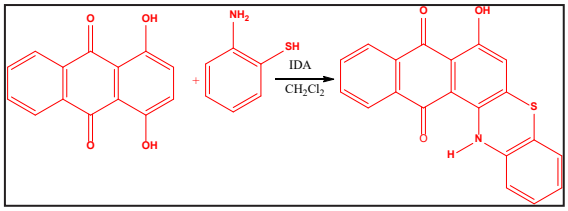

Scheme 1. Synthesis of HNDP

Spectroscopic analysis

Infrared spectra were recorded on a Shimadzu IR Prestige-21 FTIR spectrometer using KBr pellets. Proton NMR was taken in Bruker advanced spectrometer of 500 MHz with $CDCl_3$ as the solvent. The mass spectrum was recorded in the Shimadzu GCMS spectrometer. UV-Vis spectrum was recorded in Shimadzu-UV-3600. Single crystal X-ray diffraction was performed in Bruker AXS Kappa Apex2 CCD diffractometer with Mo Kα radiation using ωϕ scan mode at ambient temperature. The program SAINT/XPREP was used for data reduction and APEX2/SAINT for cell refinement. The

Current Trends in Biotechnology and Pharmacy
Vol. 19(1) 2144-2158, January 2025, ISSN 0973-8916 (Print), 2230-7303 (Online)
DOI: 10.5530/ctbp.2025.1.4

structure was solved using SIR 92 and refinement was carried out by full-matrix least square of F^2 using SHELXL-97.

Quantum computational investigations and molecular docking

Density Functional Theory calculations are aimed to study electronic structure of molecules using *Gaussian 16W* software with B3LYP/6-311+G(d,p) level of theory and graphical representations are generated using *GaussView 6.1*. Corresponding Molecular graphics are generated by MERCURY and PLATON. *Crystal explorer 21* sketches and quantitatively express interactions in molecular crystal, through Hirshfeld surfaces and corresponding 2D- fingerprint plots. It can be used to calculate and visualize various properties of crystals, such as electron density, electrostatic potential and electron localization function. It also analyzes intermolecular interactions and chemical bonding in crystals. The B3LYP/6-311G (d,p) level of theory was used for generating energy framework in crystal fabrication.

iGEMDOCK is a computational software that works on empirical scoring functions that integrate; docking, post-analysis, visualization, and screening. iGEMDOCK is used for finding the interactions of the compounds with the targeted protein molecules BCL2 and p53. The predicted pose generated after the docking procedure is visualized and then analyzed by post-analysis tool Discovery Studio visualizer [10,11]. iGEMDOCK provides the post-analysis tools using k-means and hierarchical clustering methods based on the docked poses and atomic compositions. The ADMET results were obtained from PreADMET tool [12, 13].

To start a docking/screening procedure, two files are to be prepared, a protein structure file and a ligand file. The protein structure file can be obtained from a protein data bank. Selection and identification of a drug target or receptor is the first step involved in the drug-designing process. Different computational tools are being used to find out excellent drug targets. For a drug target to be ideal, it must be linked closely to the selected human disease. In the present investigation, BCL2 and mutated p53 were taken as the drug targets.

Results and Discussion

Commentary on crystal structure

The crystal structure was reported by our research group earlier. [9]. The space group of phenothiazine derivative HNPD is P2(1)2(1)2(1) and crystallizes in orthorombic space lattice. The ORTEP diagram of the molecule is given (Fig.1). C-O bond distance C19-O1 1.249 Å and C6-O21.242 Å, indicated that the molecule existed in the keto form. From SCXRD analysis, bond distance of C8-N1 and C9-N1 were 1.365 Å and 1.393 Å respectively which was found to be greater than 1.28 Å and this confirmed the presence of C-N bond rather than C=N bond. The bond angle of C9-N1-C8 was found to be 128.94°. The bond angle between C15-S1-C14 was observed at 103.6 Å which revealed that the S atom has taken part in the cyclisation leading to the formation of heterocyclic phenothiazine ring system [14].

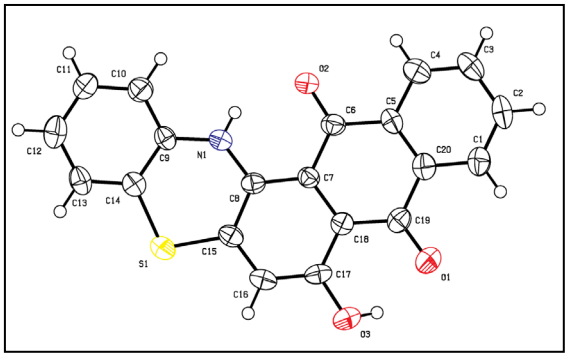

Fig. 1. Crystal structure of HNPD

Prediction of ADMET Properties

Different biological parameters like blood-brain barrier permeability (BBB), solubility, various inhibitions, skin permeability, plasma protein binding affinity, partitions coefficient, and different toxicity study to find the mutagenic activity, liver toxicity, etc. were determined using

preADMET software. All the parameters were then compared with the sample compound and the standard drug Doxorubicin. HNPD and Doxorubicin got a human intestinal absorption ability of 95.91%, 56.84%. There is CYP2C9 and CYP3A4 enzyme inhibition observed with HNPD while no inhibitory activity on CYP2D6, which is essential for metabolism of many drugs and toxic chemicals. Doxorubicin inhibits the enzymes CYP2C9, CYP2D6 but a substrate of CYP3A4.

The MDCK (Madin Darby Canine Kidney Cell line) evaluation, which is helpful for the rapid screening of cell permeability gave a low value of 16.10 for HNPD which means its diffusivity through the cell membrane is low. A value of 1.02 has been observed for the standard drug doxorubicin, means good diffusivity through the cell membrane. The HNPD compounds can act as an inhibitor of Pgp (glycoprotein) but doxorubicin has no Pgp(glycoprotein) inhibition. The solubility of HNPD in water is 0.001 but the standard drug doxorubicin has got high water solubility (8.34). The permeability though the skin is the next important parameter. The skin permeability value is -3.624 which means the HNPD compound provides good absorption via skin. The doxorubicin has also good value (-4.737). The more the negative value of permeability, lower will be the solubility. The toxicity prediction of all HNPD compounds were conducted by Ames test, and from the results HNPD is mutagen exhibiting carcinogenic activity in rat and mouse model. The doxorubicin is non mutagenic. The negative values for TA1535_10RLI indicates non mutagenic while TA100_NA is positive for HNPD compound. The negative values for doxorubicin which means non mutagenic. The hERG (The Human Ether-a-go-go-Related Gene) analysis when done using the PreADMET software displays high risk for HNPD but was ambiguous in the case of standard drug doxorubicin. All the data of ADME and toxicity are given in Table 1 and Table 2 respectively.

Table 1. ADME-parameters

ID For ADME	Values	
	HNPD	DOXO
BBB	1.02598	0.0355281
Buffer_solubility_mg_L	0.196846	3963.51
$CaCO_3$	3.41067	17.7263
CYP_2C19_inhibition	Non	Inhibitor
CYP_2C9_inhibition	Non	Inhibitor
CYP_2D6_substrate	Non	Non
CYP_3A4_inhibition	Non	Weakly
CYP_3A4_substrate	Weakly	Inhibitor
HIA	95.910386	Weakly
MDCK	16.1011	56.840587
Pgp_inhibition	Inhibitor	1.0236
Plasma_Protein_Binding	97.123298	Non
Pure_water_solubility_mg_L	0.0014759	31.160238
Skin_Permeability	3.62419	8.34623
SKlogD_value	4.379130	4.73786
SKlogP_value	4.379130	0.314800
SKlogS_buffer	-6.244160	-2.137140
SKlogS_pure	8.369230	-4.813730

Table 2. Toxicity parameters

ID For Toxicity	Values	
	DOXO	HNPD
algae_at	0.0118035	0.0202937
Ames_test	non-mutagen	mutagen
Carcino_Mouse	negative	negative
Carcino_Rat	negative	negative
daphnia_at	0.553548	0.0092121
hERG_inhibition	ambiguous	high_risk
medaka_at	0.704316	0.000247842
minnow_at	0.511881	0.000340659
TA100_10R	negative	positive
TA100_NA LI	negative	positive
TA1535_10RLI	negative	positive
TA1535_NA	negative	positive

Current Trends in Biotechnology and Pharmacy
Vol. 19(1) 2144-2158, January 2025, ISSN 0973-8916 (Print), 2230-7303 (Online)
DOI: 10.5530/ctbp.2025.1.4

Computational chemistry studies

Geometry optimization

The optimized molecular geometry of HNPD was reported using B3LYP/6-311+G(d,p) and is shown in fig.2. The C28-O32 bond length is found to be 1.2488 Å close to actual value of 1.249 Å. The newly formed bonds between C13-N15 & C21-S30 are found to have an optimized bond lengths of 1.3901 Å & 1.7701 Å which coincides with 1.393 Å & 1.767 Å respectively in crystal structure. The bond lengths C25-O26 & C10-O33 are found be 1.3336 & 1.2437 that agrees to values 1.329 Å & 1.242 Å. The other optimized bond lengths N15-C12, C29-C9, C27-C28, C10-C9, C23-S30, C25-C27, C23-C12, C10-C11 and C28-C29 are 1.3698, 1.4053, 1.4542, 1.485, 1.7707, 1.4055, 1.4313, 1.4664 Å and 1.476 that concede to speculative results of 1.365, 1.402, 1.436, 1.476, 1.747, 1.435, 1.435, 1.462 &1.438 Å respectively. All the optimized bond angles are exploratory to crystal structure values. The bond angle ranges from 117.8^0- 122.7^0 throughout the molecule, except C21-S30-C23, C12-N15-C36, C24-C23-S30, C25-O26-H35 and C12-N15-C13 bond angles are 103.2^0, 112.6^0, 116.4^0, 106.0^0 and 128.4^0 respectively. The newly formed bond angles show maximum deviation of 103.2^0 and 128.4^0. A tremendous amount of agreement exists between experimental and theoretical values.

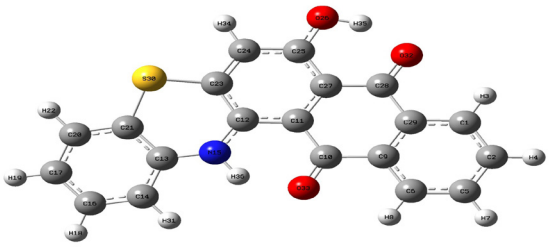

Fig. 2. Optimized geometry of HNPD

As shown in the simulated FT-IR spectrum, -OH and -NH stretching frequencies are detected peak at 3230 cm-1 and 3104 cm^{-1} along with aromatic C-H at 3066cm^{-1}. A strong peak at 1609 $cm^{-1}$is due to >C=O group. The band at 1262cm-1 and 1350cm^{-1} are due to the C-N and C-S stretching frequencies. The C-S-C stretching frequency was seen at 734cm^{-1}. The experimental IR spectrum gave peaks at 1350 cm^{-1} which corresponds to C-N stretching. The C-S stretching frequency was observed at 1262 $cm^{-1}$and stretching frequency due to C-S-C gave an absorption in the finger print region 744 cm^{-1}. Aromatic C-H stretch was observed at 3066 cm^{-1}. N-H and O-H functional groups gave absorption bands in the range 3452-3200 cm^{-1}. These values are in tune with the simulated values.

In the UV-Visible spectrum, the absorption maxima λ_{max} in $CHCl_3$ were observed at 692 nm, 641 nm and 597 nm. A bathochromic shift which was observed in HNPD indicated the intra molecular charge transfer transition (ICT) between electron donor and electron acceptor moiety. We computed the UV-Visible spectrum using TD-DFT method with maximum absorbance at 604 nm and the theoretically calculated absorption wavelength of the title compound shows variation as it is calculated for a single molecule in vacuum and not in solid state.

The structure was further confirmed by NMR and mass spectral analysis. The ^1H NMR spectrum of HNPD in $CDCl_3$ gave peaks at δ 6.717, δ 6.801, δ 6.816, δ 6.833, δ 6.8796, δ 8.967, δ 7.052, δ 7.071, δ 7.800 which corresponded to the aromatic protons. -NH and -OH protons are observed at δ 12.698 and δ 14.202 respectively. The ^{13}C NMR in $CDCl_3$ revealed the presence of different aromatic carbon environment at δ 115.23, δ 115.93, δ 117.26, δ 118.25, δ 102.83, δ 123.81, δ 125.77, δ 126.35, δ 126.84, δ 127.08, δ 128.32, δ 131.60, δ 133.28, δ 133.88, δ 134.51 and δ 136.83. The -C=O groups of anthraquinone moiety were obtained at δ 180.90 and δ 181.25. The presence of one hydroxyl group was indicated by the presence of a peak in the region δ 160.60. In the mass spectrum of HNPD the molecular ion peak was observed at 345(100%) which was the base peak, M+1 peak at 346 and (M+OH) at 328.

Current Trends in Biotechnology and Pharmacy
Vol. 19(1) 2144-2158, January 2025, ISSN 0973-8916 (Print), 2230-7303 (Online)
DOI: 10.5530/ctbp.2025.1.4

Thermodynamic parameters of HNPD obtained through DFT studies are given in Table 3.

Table 3. Thermodynamic properties of HNPD

Thermal energy	175.053845 kcal/mol
Heat Capacity (Cv)	74.263 cal/mol-kelvin
Entropy (S)	137.78 cal/mol-kelvin
Electronic Energy (EE)	-908452.43665 kcal/mol
Zero-point Energy Correction	163.703452 kcal/mol
Enthalpy	175.64621 kcal/mol
Free Energy	134.567553 kcal/mol
EE + Zero-point Energy	-908288.71939 kcal/mol
EE + Thermal Energy Correction	-908277.36147 kcal/mol
EE + Thermal Enthalpy Correction	-908276.79671 kcal/mol
EE + Thermal Free Energy Correction	-908317.83584 kcal/mol

Mulliken population analysis

In quantum chemical calculations, Mulliken charge calculations have a significant role because they affect electronic structures, dipole moments, polarization, and other properties of molecules. By studying each atom's electronic population, Mulliken charges can be determined. The total atomic charges of HNPD obtained by Mulliken population analysis with 6-311+G(d,p) basis set is given in fig. 3. The Mulliken atomic charge of C_{21} atom of phenyl group attached to Sulphur has highest positive value of 1.060576 and is acidic in nature. An increased electron density is seen in carbon atoms C_2, C_5, C_{10}, C_{12}, C_{13}, C_{14}, C_{16}, C_{17}, C_{20}, C_{25}, C_{26} and C_{28} that has values -0.3647, -0.4353, -0.1321, -0.2387, -0.532, -0.2092, -0.3735, -0.0585, -0.3894, -0.3017, -0.3106, -0.120. All other carbon atoms are positively charged. Here in HNPD all eleven hydrogen atoms shows positive charge, among which the highest positive charge is on hydrogen atom attached to nitrogen atom, H_{36} with value 0.3406 and oxygen, H_{35} having value 0.3348. The nitrogen atom has a net charge of 0.0297. All the three oxygen atoms are negatively charged O_{26}, O_{32}, O_{33} with -0.3106, -0.322 and -0.2879 values. The Sulphur atom is negative and has a value of -0.5083 value. The electrophilic substitution can happen on Sulphur rather than on nitrogen.

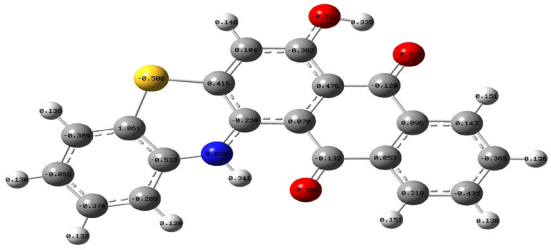

Fig. 3. Mulliken charges of HNPD

Molecular electrostatic potential (MEP)

The MEP was evaluated using DFT to investigate the reactive sites of HNPD. The distribution of electrostatic charge is illustrated in three dimensions by molecular electrostatic potential energy maps. Fundamentally, electrostatic potential energy computes the strength of nearby charges, nuclei, and electrons. The MEP can be used to predict chemical reactions by giving insight into the active sites of attack by electrophile or nucleophile [15]. Hydrogen bond interactions and behavior towards charged species can be sketched with the help of MEP. Interactions towards various receptors like proteins, enzymes can be recognized by MEP plots as shown (Fig. 4).

Those regions with attractive potential are red, while those with repulsive potential are blue. So, the red region holding negative potential depicts the minimum electrostatic potential. In the present system the alcoholic oxygen and two carbonyl oxygen atoms act as site for electrophilic attack. The blue regions can receive nucleophile, hydrogen atoms on aromatic rings in present case. To generate and display

difference in electron density, the difference in electron density between the first excited state from total CI density matrix and the ground state based on total SCF density is mapped to SCF density and is shown in Fig.5. The blue contour maps positive values of difference density where excited state density is larger than ground state density and red contour denotes the opposite. In present system, the electron density flows from the left side to anthraquinone ring as the transition happens from ground state to excited state.

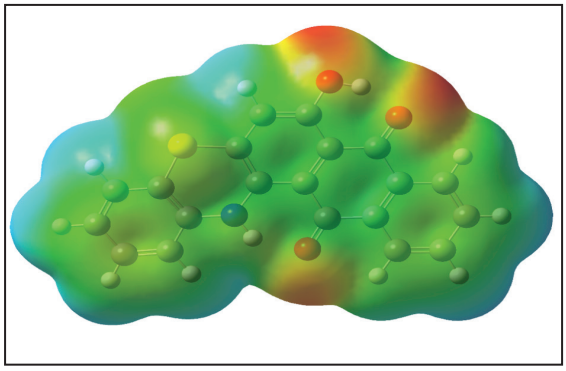

Fig.4. Plot of ESP on electron density surface

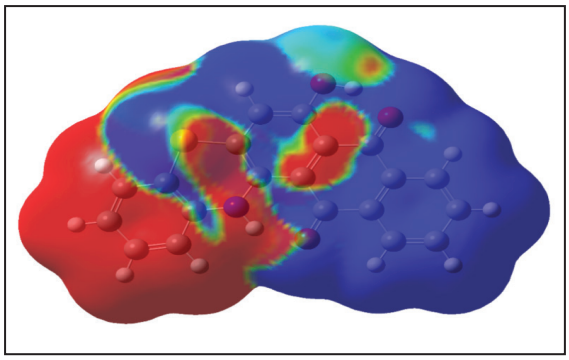

Fig. 5. MEP plot of difference of SCF and CI into ground state

Frontier molecular orbital analysis (FMO)

Analyzing FMOs can provide insight into organic compounds' optical and electronic properties. The properties of molecular orbitals, including energy, help us predict the most reactive site in two-electron systems and also describe many different types of reactions that occur in conjugated systems. To evaluate the chemical reactivity of molecules, it is useful to know how HOMO and LUMO interact, as well as their properties, such as their energy. As electrons transfer from the LUMO to the HOMO during molecular interactions, the LUMO's energy correlates with electron affinity, and the HOMO's energy corresponds to the ionization potential (IP). HOMO-LUMO energy gaps are useful for determining molecular electrical transport properties and explaining charge transfer interactions within molecules. FMO of HNPD is shown in fig. 6.

In HNPD the electron density is localized on phenyl ring on C_{25}, C_{27}, C_{28} Sulphur and Nitrogen atom and in HOMO-1 it is seen entirely on phenyl ring alone. In HOMO and HOMO+1, the third hexagon of anthracene ring lacks electron density. On moving from HOMO to LUMO the electron density shifts towards anthracene ring, where phenyl ring has nil electron density. In LUMO+1 the electron density occurs throughout the whole molecule. There is an energy gap of 2.2902 eV in this system [16]. Structure's firmness is highlighted by the energy gap. In contrast to a high HOMO-LUMO gap, a low HOMO-LUMO gap indicates a more stable molecule with higher charge transfer. Especially in conjugated and soft molecules, a small energy gap can cause low excitation energies and high levels of intramolecular charge transfer.

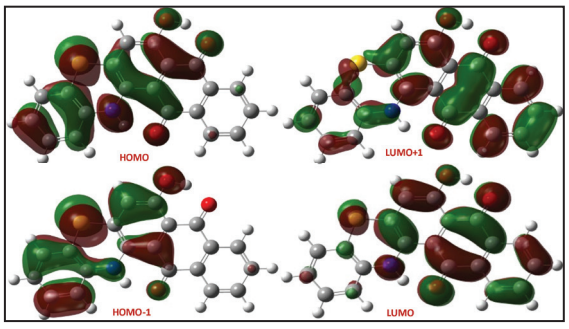

Fig. 6. HOMO and LUMO of HNPD

Hirshfeld surface (HS) analysis

Hirshfeld surface analysis is a valuable tool in computational chemistry that allows for

Current Trends in Biotechnology and Pharmacy
Vol. 19(1) 2144-2158, January 2025, ISSN 0973-8916 (Print), 2230-7303 (Online)
DOI: 10.5530/ctbp.2025.1.4

the visualization and quantification of intermolecular interactions with a detailed emphasis on the spatial distribution and nature of these interactions, aiding in the interpretation of molecular behavior and properties in crystal architecture. The analysis is based on the concept of the Hirshfeld surface, which is constructed by mapping the density distribution of one molecule onto a surface surrounding another molecule or group of molecules. This surface represents the region of space where the interacting molecule or group of molecules influence the electron density of the molecule of interest.

The following expression generates a Hirshfeld surface formed by the continuous scalar function on 0.5 isosurface.

$$w_A(r) = \rho_{promol}(r) / \rho_{procrystal}(r) = \frac{\sum_{A \in molecule} \rho_A(r)}{\sum_{C \in crystal} \rho_C(r)}$$

Where $w_A(r) = \rho_{promol}(r) / \rho_{procrystal}(r) \rho_A(r)$ are weight function, promolecule electron density, procrystal electron density and atomic electron density respectively.

The *Crystalexplorer 21* program maps the normalized contact distance depicted by d_{norm} in terms of the closest nucleus externally and internally to the Hirshfeld surface which is d_e and d_i. The blue shade denotes atoms in close contacts with longer vdW than the red patched regions, whereas the red spots denote the opposite. In cases where distances are approximately vdW, white is predominant.

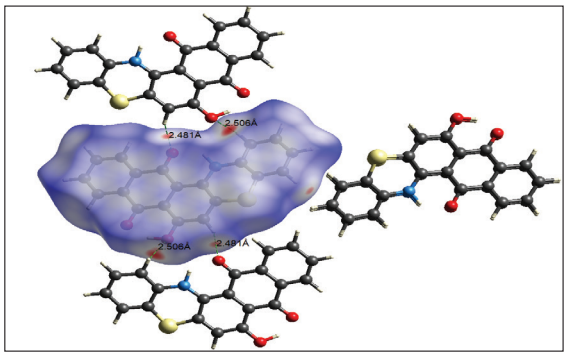

Fig. 7. d_{norm} mapped on Hirshfeld surface showing the intermolecular contacts

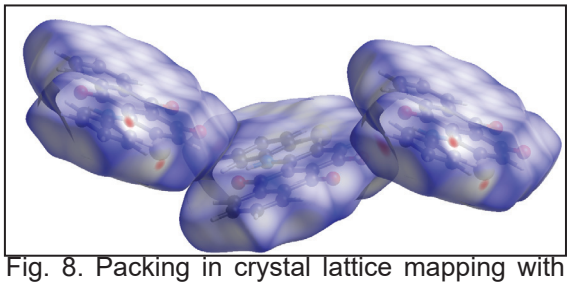

Fig. 8. Packing in crystal lattice mapping with Hirshfeld surface

Bright red spots in Fig.7 are due to C-H--O- interaction at an internuclear distance of 2.49±0.01Å. these major interactions held the molecules in XY plane as shown in Fig.8. The aromatic rings are spatially arranged through parallel displaced π-π stacking interactions where all the carbon atoms and heteroatoms of two layers keeps the exact interacting distance. The average distance between two adjacent layers is 3.806 Å (Fig. 10). Ideal distance between two aromatic platform keeps a centroid-centroid distance of ~3.5 Å [17] and in present case its slightly higher due to higher Van der Waals radius of sulphur and oxygen atoms of the ring system and forms a see-saw motif (Fig.9).

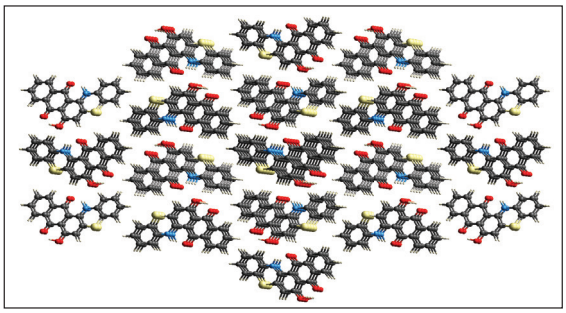

Fig. 9. The ring system forming a see-saw motif

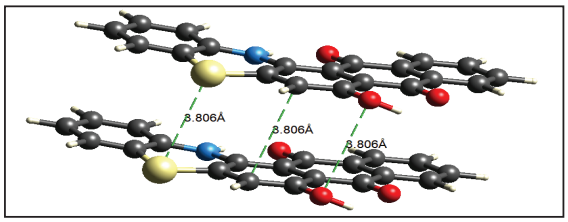

Fig. 10. Crystal packing showing molecular array with π-π stacking interactions

Current Trends in Biotechnology and Pharmacy
Vol. 19(1) 2144-2158, January 2025, ISSN 0973-8916 (Print), 2230-7303 (Online)
DOI: 10.5530/ctbp.2025.1.4

It is possible to better understand the interactions occurring within a crystal by using two-dimensional fingerprint plots, shown in Fig.11, associated with the Hirshfeld surface. A molecule's immediate surroundings influence 2D fingerprint plots, and filtering is done by the type of element and surface area, which enumerates close contacts between atoms inside and outside the HS surface, shown in fig.12 [18]. H—H close contacts are characterized by blunt peak which is positioned at $d_i+d_e \approx 2.4$ Å. Remarkable and well-defined O—H/H—O interactions are observed as sharp peaks at $d_i+d_e \approx 2.8$ Å which spans around 17.9 % of the total HS area. The pale green region falls diagonally in the fingerprint plot of C--C contacts at $d_i \cong d_e$ □ 1.7 Å reinforces the existence of characteristic π-π stacking, comprising 19.8 % of HS area [19]. C--H and S--H close contacts are also prominent which appears as two sharp wings comprising 12.3 and 5.2 % respectively of total area.

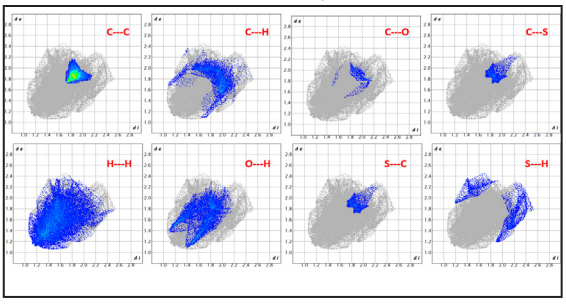

Fig. 11. Decomposed 2-D fingerprint plots of HNPD

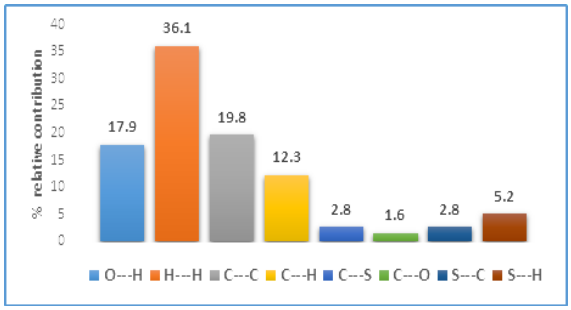

Fig. 12. Relative contributions of major close contacts in crystal lattice

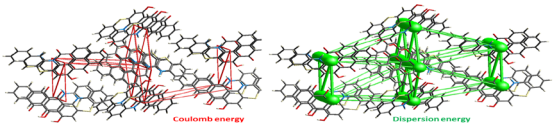

Fig. 13. Energy frameworks in 3D molecular packing (Energies <10 kJ mol^{-1} have been discarded)

For fabricating energy frameworks, single point wavefunctions with B3LYP functional incorporating 6-31G(d,p) basis set in order to compute interaction energies inside a cluster of molecules [Fig. 13]. Total energies, benchmarked for B3LYP/6-31G(d,p) energy model and scaled appropriately, are provided as the sum of four principal energy components namely electrostatic (E_{ele}), polarization (E_{pol}), dispersion (E_{disp}) and exchange-repulsion (E_{rep}) (Table). For simplification, close contacts with energies below 10 kcal/mol have been discarded. The distinct 3D topology with respect to b-axis., give different infrastructure for coulomb energy and dispersion energy. Stacked layers are maneuvered into a hexagon motif and larger tubes of dispersion energy fame work passed between NH and CO groups which seems to run along with the crystallographic c-axis. The packing of crystal lattice of the title complex is majorly driven by the dispersion energy component.

Table 4. Interaction energies generated within a cluster of radius 3.8 Å

N	Symop	R	E_{-ele}	E_{-pol}	E_{-dis}	E_{-rep}	E_{-tot}
2	x, y, z	3.81	-9.2	-2.7	-111.9	54.8	-67.5
2	-x, y+1/2, -z+1/2	7.86	-8.9	-2.3	-22.6	14.5	-19.3
2	x+1/2, -y+1/2, -z	13.13	-3.3	-1.0	-11.8	7.3	-8.7
2	-x+1/2, -y, z+1/2	14.04	-1.5	-0.7	-9.2	4.5	-6.6
2	x+1/2, -y+1/2, -z	12.66	-6.9	-1.6	-10.0	3.7	-14.1
2	-x, y+1/2, -z+1/2	7.77	-6.3	-2.4	-22.2	8.1	-21.5
2	-x+1/2, -y, z+1/2	14.50	2.3	-0.9	-8.0	3.7	-2.5

'N' corresponds to the number of molecules with centroid-to centroid distance 'R'.
Energy values in kJ mol^{-1} and R in Å.

Molecular docking studies

iGEMDOCK (integrated GEMDOCK) is a molecular docking software used for predicting the binding modes and affinities of small

molecules with protein targets. It is specifically designed for high-throughput virtual screening and drug discovery applications. iGEMDOCK employs a combination of a genetic algorithm and an empirical scoring function to perform molecular docking simulations. The software takes a protein structure and a small molecule ligand as input and generates a set of possible binding conformations. These conformations are then scored using an empirical scoring function that evaluates the intermolecular interactions between the protein and the ligand. The genetic algorithm is used to optimize the conformational search and exploration of the ligand binding space. The tool is used to predict the affinity of the molecule towards two proteins BCL2 and p53 which are the mutated proteins responsible for the cancer in lymph nodes. Both the proteins were selected from the Protein Data bank with PDB id 2X0W (p53 protein) and 4LVT (BCL2 protein). By preparing two files, the protein structure file, and Ligand file docking was performed using iGEMDOCK software, and the results obtained were expressed in terms of free energy. Both the standard drug and sample compound HNPD were subjected to computational studies and the results were compared. Discovery Studio Visualizer is used to sketch the docked poses and to shine light upon different types of interactions existing between the ligand and proteins [20].

The most frequently interacting amino acids with compounds of anthraquinone moiety were PRO, THR and LEU. The interactions of major amino acid residues present in p53 protein with ligands of a particular class having better docking affinity along with the docking pose of standard drug (Doxorubicin) is given below. Interactions of amino acids with ligands in the active site of mutated p53(2XOW) protein indicates that Hydrogen bonded interactions, pi-alkyl, pi-sigma and van der Waals interactions are dominant in the case of derivative while van der Waals and hydrogen bonded interactions are exist in Doxorubicin. Different types of interactions of p53 with the standard drug and HNPD are given. (Table 5) From the in-silico studies the interaction of amino acids with ligands in the active site of mutated BCl2(4LVT) protein with various amino acid residues indicate that the title compound is found to be higher than that of the standard drug Doxorubicin The derivative is found to possess all types of interactions like pi-sigma, pi-alkyl, Pi-Anion, Pi-Donor Hydrogen Bond, Pi-sulfur and van der Waals interactions while the standard drug Doxorubicin has got pi-alkyl interactions alone. (Table 6)

Table 5. Docked files of ligand and standard drug with 2X0W(p53)

Sl.No.	Ligand	Amino acid residues				
		van der Waals	Hydrogen bond	Pi-sigma	Pi-alkyl	Pi-donar hydrogen bond
1	HNPD	PROB153	GLYB:154 THRB:155 CYSB:220	PROB:151	PROB:222 VALB:147 PROB:223	THR B:150 GLU B:220
2	DOXO (STD)	THRB:230,155, 150 VALB:147 PROB:151, 223, 219 GLYB:154 GLUB:221 ARGB:202	CYSB:220	-	-	-

Current Trends in Biotechnology and Pharmacy
Vol. 19(1) 2144-2158, January 2025, ISSN 0973-8916 (Print), 2230-7303 (Online)
DOI: 10.5530/ctbp.2025.1.4

Table 6. Docked files of ligand and standard drug with 4LVT(BCL2)

Sl. No.	Ligand	Amino acid residues				
		van der Waals	Pi-Anion	Pi-Donor hydrogen bond	Pi-sulfur	Pi-Alkyl
1	HNPD	GLUB:133 ALAB:146 VALB:130 PHEB:150 GLUB:149 SERB:113	ASPB:108	TYR B:105	PHEB:109 PHEB:101	LEUB:134 VALB:134 METB:112
2	DOXO (STD)	-	-	ASPB:108	-	PHEB:150 ALAB:146 METB:112

Table 7. Docking parameters of proteins with title compound and standard drug

Docking score of p53 (pdb-2X0W)					
Sl. No.	Name	Energy	VDW	H bond	Electrostatic force
1	HNPD	-112.57	-100.62	-12.15	0
2	DOXO(STD)	-117.99	-100.08	-17.91	0
Docking score of BCL2 (pdb-4LVT)					
Sl. No.	Name	Energy	VDW	H bond	Electrostatic force
1	HNPD	-79.68	-54.65	-25.03	0
3	DOXO(STD)	-99.21	-68.43	-30.77	0

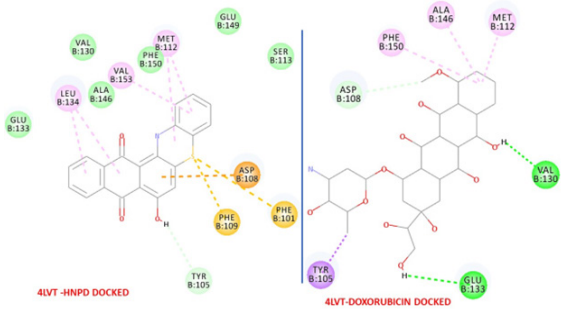

Fig. 11. 2D representation of ligands inside 4LVT receptor pocket

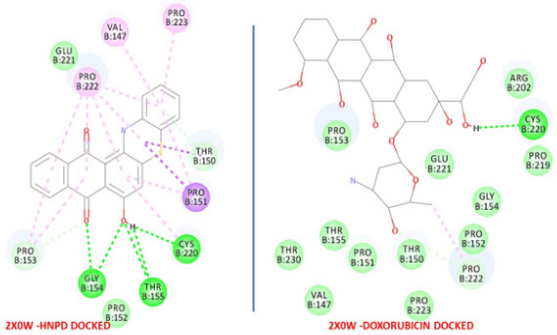

Fig. 12. 2D representation of ligands inside 2X0W receptor pocket

Potential as drug candidate of a molecule can be inferred from the ligand (drug)- protein interaction in terms of binding energy. The docked scores of the molecules are given in Table 7. Various interactions like van der Waals, Pi-alkyl, Pi-sigma and hydrogen bonded interactions were found to be exist between ligand and protein pocket. HNPD and standard drug Doxorubicin has got van der Waals and hydrogen bond interactions in common with p53 and all other interactions like Pi-sigma, pi-alkyl and pi-donor hydrogen bond is present only within HNPD that is all the latter interactions are absent. In the case of binding affinity towards BCL2 the standard drug Doxorubicin has got Pi-Donor Hydrogen Bond and Pi-alkyl interaction. The van der Waals, Pi-sulphur and Pi-alkyl interactions are dominant in the case of HNPD.

Conclusion

One of the most feared cancers is lymphoma, which spreads easily and is extremely deadly, but effective drugs are a few. The present investigation purports to synthesize an o-amino thiophenol derivative of anthraquinone with potent biological activity. The SCXRD data of 7-hydroxy-8-H-naptho[2,3-α]phenothiazine-8,13(14H)-dione suggests an orthorhombic lattice. UV-VIS, IR, NMR and mass spectrometric data were collected and analyzed and supports the formation of intended compound. A potential for drug candidate was assessed for its ADMET and toxicological properties to assess drug likeness and therapeutic efficacy. IR, UV-Visible, Mulliken charge analysis, geometry optimization and thermochemical investigation were performed with unrestricted DFT method at the level of B3LYP/6-311+G(d,p) and the results were in consistent with experimental data. Small HOMO-LUMO energy gap of 2.2902 eV of shows the stability and effectiveness of the title molecule to incorporate charge transfer interactions. Numerous non-covalent interactions have been revealed in crystal packing, according to Hirshfeld surface analysis. Aromatic rings are arranged spatially through π-π stacking interactions in which carbon atoms and heteroatoms of two layers maintain the exact same distance between them. Separating adjacent molecular layers require 3.806 Å internuclear distance. The predominant C---C, O--H and H--H close contacts comprise 73.8 % of the total HS area. An in silico inhibitory activity of HNPD on two over expressed protein in lymphoma namely p53and BCL2 were carried out using iGEMDOCK tool which gave comparable score with standard drug Doxorubicin. The bio-viability study of HNPD using preADMET software also gave a promising result. Thus, HNPD can be used as a lead molecule against Lymphoma. There are remarkable weak interactions involving hydrogen bonds and aromatic stacking close contacts that can be tuned with high selectivity which in turn are responsible for the enhanced pharmacological activity revealed through molecular docking studies.

Acknowledgment

The authors would like to express deep gratitude to the Department of Chemistry, University College Thiruvananthapuram for providing computational laboratory facility. We also thank Department of Computational Biology and Bioinformatics, Kriyavattom, Thiruvananthapuram for laboratory facility.

Declarations

Conflicts of interest

The authors do not have any conflict of interest.

Ethical Approval

Not applicable.

Funding

No funding recieved

Availability of data and materials

Data will be made available on request.

References

1. Dzieduszycka, B., Stefa_nska, M., Gawro

nska, M., Arciemiuk, E., Borowski, Synthesis of new polycyclic anthracenedione analogs with hetero- or carbocyclic ring(s) fused to the chromophore system, *Pol. J. Chem*., **81**, 2007, 535-546.

2. Supranee, S., Helen, H., Thapong, T., Nattaya, N., Nouri, N., Nongnuj, M., Overcoming doxorubicin-resistance in the NCI/ADR-RES model cancer cell line by novel anthracene-9,10-dione derivatives*, Bioorg. Med. Chem. Lett.,* **23**, 2013, 6156-6160.

3. Meek, D., Regulation of the p53 response and its relationship to cancer, *Biochem. J.,* **469(3)**, 2015, 325-46.

4. Muller, P., Vousden, K.H., p53 mutations in cancer, *Nature Cell Biology*. **15(1)**, 2013, 2-8.

5. Ling, B., Wei-Guo, Z., p53: Structure, Function and Therapeutic Applications, *J. Cancer Mol.,* **2(4)**, 2006. 141-153.

6. Zhen, W., Yi S., Targeting p53 for Novel Anticancer Therapy, *Transl Oncol.,* **3(1)**, 2010,1-12.

7. Blaineau, S. V., Aouacheria, A., BCL2DB: Moving "helix-bundled" BCL-2 family members to their database. *Apoptosis* **14**, 2009 923–925

8. Hamda, M., Fujiwara, T., Hizuta, A., Gochi, A., Naomoto,Y Takakura, N., Takahashi, K., Roth, J.A., Tanaka, N., Orita, K., The p53 gene is a potent determinant of chemosensitivity and radiosensitivity in gastric and colorectal cancers, *J. Cancer Res. Clin. Oncol.,* **122(6)**,1996, 360-365.

9. Shiny, P. L**.**, Annette, F., Arun, K. B, Vishnu, V. S., Rema, D. K., Archana, P. D., Thomas, O., Synthesis, Single Crystal Study, in silico Analysis, in vitro Anti-inflammatory and Anticancer Activities of 7-hydroxy-14H-naphtho[2,3- a]phenothiazine-8,13-dione*, Drug Delivery Letters*, **5(2)**, 2015, 140-150.

10. Priya, R.P., Indu, P.I., Sangeetha, K., Raja, R.S.R., discovery of a novel Binding trench in BMRF1 of Epstein BARR Virus an in silico approach, *Int J Pharm Pharm Sci.*, **6(1)**, 2014, 578-584

11. Kumar, A., Ram, T., Goel, B., Bansal, E., Srivastava, V.K., Synthesis and anti-inflammatory activity of some potential cyclic phenothiazines. *Boll. Chim*. *Farm,* **137**, 1988, 152-156.

12. Lipinski, C.A., Lambardo, F.M., Doming, B.W., Feeney, P.J., Experimental and computational approaches to estimate solubility and permeability in drug discovery and development settings, *Adv. Drug Delivery Rev.,* **46**, 2001, 3-26.

13. Daina, A., Michielin, O. & Zoete, V. SwissADME: a free web tool to evaluate pharmacokinetics, drug-likeness and medicinal chemistry friendliness of small molecules. Sci Rep 7, 42717 (2017)

14. Dandia, A., Sarawgi, P., Hursthouse M.B., Bingham, A.L., Elight M., Drake J.K., Ratnani R., Vibrational spectrostroscopic (FT-IR,FT-Raman) and quantum chemical calculations of 1-(5,5-dioxido-10H-Phenothiazine-10-yl)ethanone, *J. Chem. Res*., 2006, 445-448.

15. Anila Raj S., Vidya, V. G., Preethi V., Viju Kumar V. G., Single Crystal XRD and DFT investigation of 1,5-dimethyl-4-[(2-oxo-1,2-diphenylethylidene) amino]-2-phenyl-1,2-dihydro-3H-pyrazol-3-one. *Results in Chemistry*, **4,** 2022, 100665. 10.5267/j.ccl.2022.9.006

16. Abhijith, V. H., Vidya, V. G., Viju Kumar, V. G. DFT computations, Spectral investiga-

tions and Antimicrobial studies of Zn (II) complex with α-diketimine ligand. *Results in Chemistry*, **8(6)**, 2022 100420**.** https://doi.org/10.1016/j.rechem.2022.100420.

17. Leslie-Joana Riwar, Nils Trapp, Bernd Kuhn, and Francois Diederich, Substituent Effects in Parallel-Displaced π-π Stacking Interactions: Distance Matters, Angew. Chem. Int. Ed. 2017, **56,** 11252 –11257, DOI: 10.1002/anie.201703744).

18. V.G. Viju Kumar, V.G. Vidya, Crystal architecture, DFT and Hirshfeld surface analysis of novel 'double open-end spanner' type dimer derived from 4-aminoantipyrine, Journal of Molecular Structure 1270 (2022) 133882, https://doi.org/10.1016/j.molstruc.2022.133882.

19. Joshua J McKinnon, Mark A Spackman, Anthony S Mitchell, Novel tools for visualizing and exploring intermolecular interactions in molecular crystals, Acta Crystallogr B. 2004 Dec;60(Pt 6):627-68, Doi:10.1107/S0108768104020300.

20. Meenukutty, M. S., Mohan, A. P., Vidya, V. G., Viju Kumar, V. G. Synthesis, characterization, DFT analysis and docking studies of a novel Schiff base using 5-bromo salicylaldehyde and β-alanine. ***Heliyon***, e09600, **2022**. https://doi.org/10.1016/j.heliyon.2022.e09600

Current Trends in Biotechnology and Pharmacy
Vol. 19(1) 2159-2169, January 2025, ISSN 0973-8916 (Print), 2230-7303 (Online)
DOI: 10.5530/ctbp.2025.1.5

Formulation and Characterization of Transdermal Patch Containing Eucalyptus, Curcumin and Ginger Oils with its In-vitro Permeability Study Using Goat Skin and GC-MS Analysis

Gaurav Lokhande [1], Amol Sherikar [1*], John Disouza [1]

[1]Department of Quality Assurance, SWVSM's Tatyasaheb Kore College of Pharmacy, Warananagar, 416 113, Maharashtra, India.

***Corresponding author:** assherikar.tkcp@gmail.com

Abstract

The present research has been carried out to formulate the transdermal patch containing medicinal oils like eucalyptus, curcumin, and ginger with its characterization and in-vitro permeability checking by GC-MS analysis. Three formulations (F1, F2, and F3) of transdermal patches containing different concentrations of oils were prepared. The patches were evaluated for thickness, weight uniformity, percentage moisture content, and percentage moisture uptake. The average thickness was found to be 0.434, 0.433, and 0.438 mm for F1, F2, and F3 respectively. 0.1876, 0.1861, and 0.1866 gm weight uniformity were observed for F1, F2, and F3 respectively. The moisture content for F1 was 3.96 %, for F2 was 2.48 % and for F3 was 3.67 %. The moisture uptake for F1 was 5.68 %, for F2 was 4.32 % and for F3 was 4.82 %. The F2 formulation produced optimum results, so it is better than F1 and F3. The in-vitro permeation of oils from the transdermal patch was checked by Franz diffusion cell using goat skin as a semi-permeable membrane. The transferred sample was collected and investigated by chemical identification tests at time intervals of 1, 2, 3, 4, and 5 hours for the presence of active chemical constituents. The GC-MS analysis showed the presence of active chemical moieties which transferred through the goatskin including D-limonene, (+)-4-carene, Fenchone, linalool, endo-borne, citronellal, 2,6-octadienal,3,7-dimethyl-,(Z)-,longifolene, caryophyllene, carotol, diethyl phthalate, etc. The above research proves our approach to formulation and delivery of polyherbal oils in a single transdermal patch which may open the door for delivery of formulation containing herbal oils through the skin.

Keywords: Transdermal patch**,** In-vitro permeability, GC-MS, Franz diffusion cell, D-Limonene, Caryophyllene.

Introduction

The transdermal drug delivery system (TDDS) has an essential component of emerging technologies for the release of medications (1). A TDDS applies a reasonably prescribed amount of the medicine to the inside of a patch; that is applied on the local site of the skin for an incredibly longer effect. The medication reaches the systemic circulation via the skin by diffusion mechanism (2). From the patch a balanced concentration of drug diffuses into the bloodstream for an extended period, ensuring a constant concentration of drug in the systemic circulation. This not only improves the drug effectiveness and safety, but it also improves patient fulfilment and overall gives therapeutic benefit (3). TDDS has some benefits such as

being less invasive or non-invasive, avoiding first-pass metabolism, being easy to apply, not requiring expert personnel, and having the potential to reduce the rate of administration (4).

Several transdermal therapeutic systems have been developed for topical administration to regulate therapeutic drug delivery. There are several topical ayurvedic drugs formulated and reported as an herbal patches (5-8). There are different types of transdermal patches reported like Drug-in adhesive with a single layer type of patch, Drug-in adhesive with multiple layers, Matrix type of patch, etc (9). Eucalyptus oil is obtained from Eucalyptus spp. and has a variety of biological activities like anti-microbial, anti-fungal, cardinal, insecticidal, herbicidal, anti-inflammatory, and analgesic, etc (10-11). The chemical moieties responsible for all the above biological activities present in eucalyptus oil are 1, 8-cineole, piperitone, citronellal, citronellol, linalool, *p*-cymene, a -phellandrene, a-pinene, a -terpineol, limonene, alloocimene, g -terpinene, geranyl acetate, spathulenol, a -thujene, etc (10).

Curcumin essential oil is obtained from *Curcuma longa* and reported many biological activities such as antihyperlipidemic (12), antidiabetic and hypoglycaemic (14), antiobesity (15), antioxidant (14-16), neuroprotective (17-19), antiplatelet and antithrombosis (20-21), cytotoxic (22-23), anti-inflammatory (19, 24), antiarthritic and joint-protective (25), hepatoprotective and antihepatotoxic (26), antiatherosclerotic (27), hypothermic (28), anxiolytic (28), anticonvulsant (28), pasmolytic (29), antimutagenic (30), sedative and anesthetic (28, 31), antivenom (32), antibacterial (33), antifungal (34, 35), insecticidal (36, 37), mosquitocidal (38), phytotoxic (39), antitumor (40), hypoglycemic (41), larvicidal (42) etc. The above reported biological activities are because of presence of phytochemical constituents such as a-turmerone, b-turmerone, a-curcumene, zingiberene, curcumenol, xanthorrhizol, curcumol, germacrone, curdione, curzerenone, curzerene, 8,9-dehydro-9-formyl-cycloisolongifolene, b-caryophyllene, (E)-b-farnesene, b-elemenone, b-elemene, b-pinene, camphor, 1,8-cineole, piperitenone, b-myrcene (43) etc.

Ginger oil is obtained from dried rhizomes of the *Zingiber officinale* having a variety of reported biological activities like antioxidant (44), anti-tumour (45-46), anti-inflammatory and analgesic activity (47), anti-microbial activity (48), hepato-protective activity (49-50), etc. All above reported biological activities are because of the active phytoconstituents present and reported in ginger oil and which are paradol, shogoal, zingerone, zerumbone, 1-dehydro-(10) gingerdione, gingerol, gingerenone A, etc (51).

By considering all the above information from the literature, we are reporting here an attempt to formulation and characterization of a transdermal patch containing eucalyptus, curcumin, and ginger oils for treating inflammation and pain. The in-vitro permeability study by using goat skin and GC-MS analysis was carried out for the formulated transdermal patch.

Materials and Methods

Collection of volatile oils (Eucalyptus, Curcumin and Ginger), chemicals, polymers etc.

The oils were procured from a local ayurvedic drug supplier from Kolhapur (Bawadekar ayurvedic shop). The oil samples were then checked for their purity by organoleptic tests (physical state, color, odor, etc), density, and refractive index. The collected oil samples were stored in an airtight amber-colored container at room temperature. HPMC K4M, EC 7 cps, PVP K30, and propylene glycol (PG) were procured from Sigma-Aldrich. Synthetic PVA was procured from Loba Chemie Pvt. Ltd., Mumbai, India. PEG-4000 was obtained as a gift sample from BASF Mumbai, India. All other materials and chemicals used were of either pharmaceutical or analytical grade.

Current Trends in Biotechnology and Pharmacy
Vol. 19(1) 2159-2169, January 2025, ISSN 0973-8916 (Print), 2230-7303 (Online)
DOI: 10.5530/ctbp.2025.1.5

Formulation of herbal transdermal patches

The herbal transdermal patches were prepared by different methods.

Method 1

Transdermal patches containing volatile oils were prepared using 4 gm of polymer PVA as a backing membrane and as a dispersion polymer. The patches were formulated by first preparing PVA as a backing membrane and then dispersing HPMC polymer in different concentrations in water and ethanol. The backing membrane was prepared and allowed to dry for 24 hours at room temperature. 2 ml of curcumin oil and HPMC were mixed with the appropriate solvent for 1 hour, then 1gm of PEG and plasticizer PEG 4000 were added and the stirring was continued for another hour. Then using a pipette, 5 ml of a dispersion-containing mixture was poured over the previously prepared backing layer of PVA. By placing an inverted funnel over the glass Petri plate, the solvent was allowed to evaporate at room temp. The film was collected and analyzed 24 hrs after drying at room temperature.

Method 2

PVP (1000 mg) and EC (1000 mg) was used as the skeletal type of polymeric material. PG as a penetration enhancer and PEG-4000 was used as a plasticizer. The polymer PVA and EC were weighted in required ratios and mixed into a 50 ml solution containing methanol and distilled water (1:1) ratio. Stirred the mixture over a hot water bath until dissolved, after the mixture was cooled down to 25 ^{0}C the volatile was added. After that, PG (0.5 ml), was added, and the mixture was then poured into a glass Petri dish and dried at room temperature for 24 hrs. The Petri dish was left and placed at room temperature for one day. The patch was obtained intact by slowly lifting from the Petri dish and collected, and stored until further use.

Method 3

PVA (1000 mg) and PVP (1000 mg) and drug were weighted in requisite ratios and mixed in 10 ml distilled water. Stirred the mixture over a hot water bath until it dissolved. After that mixture was cooled down to 25 ^{0}C, added glycerol (0.5ml), PG (0.5 ml), and pressure-sensitive adhesive such as Di-n-butyl phthalate (2 ml). PEG-4000 was used as a plasticizer. The solution was mixed by using a mechanical stirrer at 600 to 800 rpm for 20 min. under occluded condition, and then the mixture was cast on the Petri dish and kept at room temperature for 24 hrs. In table 1 the different ingredients with their quantity used in formulation F1, F2, and F3 are given.

Table 1: Showing different polymers and oils used for preparation of transdermal patches

F1 (Method 1)		F2 (Method 2)		F3 (Method 3)	
Name of Ingredient	Quantity	Name of Ingredient	Quantity	Name of Ingredient	Quantity
PVA	1000 mg	EC	1000 mg	PVP	1000 mg
HPMC	1000 mg	PVP	1000 mg	PVA	1000 mg
PG	0.5 ml	PEG-4000	1000 mg	PEG-4000	1500 mg
Glycerol	0.5 ml	PG	0.5 ml	Glycerol	0.5 ml
Dist. Water : Ethanol (1:1)	50 ml	Dist. water: methanol (1:1)	50 ml	PG	0.5 ml
Curcumin oil	1 ml	Glycerol	0.5 ml	Di-n-butyl phthalate	2 ml
Eucalyptus oil	1 ml	Curcumin oil	1 ml	Dist. water: methanol (1:1)	50 ml
Ginger oil	1 ml	Eucalyptus oil	1 ml	Curcumin oil	1 ml
		Ginger oil	1 ml	Eucalyptus oil	1 ml
				Ginger oil	1 ml

F1 = formulation 1, F2= formulation 2 and F3 = formulation 3

Evaluation of patches (53, 56, 57)

The patch thickness

The thickness of prepared drug-loaded patches was measured at different points by using a vernier calliper and determined the average thickness (56-57).

Weight uniformity

Specified areas of prepared patches were cut into different parts and weighed on a digital balance, and the average weight was calculated (56).

Percentage moisture content

The prepared films were weighed individually and kept in desiccators with fused calcium chloride at room temp for 24 hrs. After 24 hrs the film was reweighed and determined percentage moisture content (53, 56).

Percentage moisture uptake

The weighted films were kept in desiccators at room temp for 24 hours in a saturated potassium chloride solution. After 24 hrs the films were reweighed and determined the percentage of moisture uptake (53).

In-vitro oil constituents release study (Permeation study) by Franz diffusion cell method

Preparation of goat skin

The goatskin was used as semi-permeable membrane, collected from local slotter house nearby college campus. Freshly excised skin was placed for 1 min in distilled water maintained at 55°C to remove fats and subcutaneous tissues. The skin was washed with fresh distilled water and dipped in a phosphate buffer at pH 7.4 for 5 min. The excised skin was carefully checked visually for integrity. Any damaged skin was rejected. The prepared skin was wrapped in aluminium foil, stored at -20°C, and used within 2 weeks of storage (58-59).

Permeation Experiment

The in-vitro oil constituents release (permeation) study was carried out by the Franz diffusion cell method. Franz diffusion cells consist of two compartments i.e. donor and acceptor with an outer jacket. The outer jacket was placed in a water bath at 37 °C to provide a temperature of 32°C±1°C in the receptor compartment. The goatskin was used as a semi-permeable membrane. The skin was allowed to maintain a temperature of 32 °C by placing the skin in a phosphate buffer of pH 7.4 for 1 hour. The receptor compartment was filled with a phosphate buffer pH 7.4.

The goatskin was mounted between the donor and the receptor compartments in such a way that the stratum corneum was facing toward the donor compartment. A circular piece of the patch was cut from a larger patch with the help of a cutter. A circular patch was placed on the skin with the releasing side facing toward the mounted skin. The receptor fluid was continuously stirred at a speed of 120 rpm with magnetic bars on a magnetic stirrer (REMI equipment Pvt ltd., India) to provide sink conditions. At predetermined intervals of 1, 2, 3, 4, and 6 hrs, 1 mL of receptor fluid was withdrawn from the sampling port with the help of a long needle syringe.

The receptor fluid was replaced with fresh phosphate buffer. Care was taken during sampling to avoid any bubble formation in the receptor compartment, because trapped air may reduce the permeation area. In case of air entrapment, the Franz diffusion cell was tilted to remove the trapped air through the sampling port. The donor compartment was covered with aluminium foil (59).

GC-MS study

The GC-MS study was conducted in the common facilities center (CFC), Shivaji University, Kolhapur. The analysis was carried out on a Shimadzu instrument (model TQ8050). The sample collected at 6 hrs time interval

of formulation F3 was injected into the gas chromatography. The method setting and programming details are given in table 2.

Table 2: Showing Gas Chromatographic programming and method details (60).

Column oven Temperature programme	50 hold for 2 minutes at 10 ^{0}C, 200 hold for 5 minutes, 250 hold for 5 minutes, 275 holds for 5 minutes.
Injection temperature	25 ^{0}C
Injection mode	Splitters
Carrier gas	Helium (He)
Column flow	1 ml/min.
Sample volume	1µl

The separated compounds in the form of different peaks at different retention times (Rt) were transferred into the MS. The MS was carried out by setting of programming parameters given in table 3.

Table 3: MS programming parameters [60]

In source temperature	24 ^{0}C
Interface temp	25 ^{0}C
Solvent cut time	5.8 min.
m/z range	45 to 650
Detector voltage	0.76

The ionization, filtration and detection were carried out and the fragments of different ions were recorded.

Result and Discussion

Physicochemical characterization of procured oils

Organoleptic tests

The organoleptic tests for eucalyptus, curcumin, and ginger oils resemble the official monographs.

Density

The relative density is a basic physical property of an oil/substance that can be used to characterise it. The density is the ratio of mass of a substance to volume of substance at given temperature. The relative densities for all three oils i.e. eucalyptus, ginger, and curcumin were 0.866g/ml, 0.970g/ml, and 0.871/ml respectively. The standard values for the same are 0.865g/ml, 0.960 mg/ml and 0.871 g/ml respectively at room temperature.

Refractive Index

The Refractive indeces of volatile oils were determined by using Abbe's refractometer. The refractive index is one of the physicochemical properties of the substance. The refractive index (n) of a substance with reference to air is the ratio of the sine of the angle of incidence to the sine of the angle of refraction of a beam of light passing from air into the substance. It is mostly applied for identify a particular substance, confirm its purity, or measure its concentration. Generally it is used to measure the concentration of a solute in an aqueous solution. It can be used also in determination of drug concentration in pharmaceutical industry (52). The refractive indeces of Eucalyptus, Ginger, and Curcumin oil were 1.461, 1.400, and 1.450 respectively, and the standard refractive index is 1.450, 1.485, and 1.500 respectively.

Formulation and evaluation of herbal transdermal patches

The patches were prepared by using combinations of polymers such as hydroxyl propyl methyl cellulose K4M (HPMC), ethyl cellulose 7 cps (EC), synthetic polyvinyl alcohol (PVA), polyvinyl pyrrolidone K30 (PVP), and polyethylene glycol 4000 (PEG-4000). The formulated patches get softened and extend because of plasticizers. The formulation was subjected to a physical examination; films appeared slightly translucent suggesting that the transdermal patch containing oils was successfully prepared. Further, the patches were evaluated for thickness, weight uniformity, moisture content, and moisture uptake, and the results are tabulated in Table 1.

Current Trends in Biotechnology and Pharmacy
Vol. 19(1) 2159-2169, January 2025, ISSN 0973-8916 (Print), 2230-7303 (Online)
DOI: 10.5530/ctbp.2025.1.5

Table 1: Showing result of thickness, weight uniformity, moisture content, moisture uptake of prepared transdermal patches

Name of formulation	Average thickness (mm)	Weight uniformity (gm)	Moisture content (%)	Moisture uptake (%)
F1	0.434	0.1876	3.96	5.68
F2	0.433	0.1861	2.48	4.32
F3	0.438	0.1866	3.67	4.82

Each patch's thickness was measured with a vernier calliper at different points on the patch, the average thickness for F1, F2 and F3 was 0.434, 0.433 and 0.438 mm respectively. All the patches were found to be having uniform thickness. The average weight for F1, F2 and F3 was 0.1876, 0.1861 and 0.1866 gm respectively. It was found that the weights were uniform for all prepared formulations and the weight variation was within acceptable range. The moisture content for F1, F2 and F3 was 3.96, 2.48 and 3.67% respectively. The moisture uptake for F1, F2 and F3 was 5.68, 4.32 and 4.82 respectively. The moisture content and moisture uptake studies provide information regarding stability of the formulations. For maximum stability the moisture content and moisture uptake of transdermal patch should be minimum (53-55). In this case formulation F2 showed optimum results so it is better than F1 and F3. The results obtained were promising and the prepared transdermal patches were stable.

Permeation study

The permeation studies of the transdermal patches helps to predict the in vivo absorption of the drug. The permeation studies were performed by Franz diffusion cell method using goat skin as a semi-permeable membrane. The drug samples were collected at an interval of 1,2,3,4 and 6 hrs. The GC-MS study was carried out for the presence of different chemical moieties in the receptor compartment.

GC-MS analysis

The GC-MS analysis of batch F3, for 6 hrs receptor sample was carried out. The GC spectra are shown in figure 1 showing different peaks at different retention times (Rt). The detailed chromatographic separation data with retention time (Rt), initial time (It), final time (Ft), peak area, % area, and name of chemical moiety representing it is given in table no. 2. The major components were D-limonene (14.95), +)-4-carene (2.20), fenchone (1.71), linalool (1.67), acetaldehyde (9.27), camphor (6.09), endo-borneol (1.39), L-.alpha.-terpineol (4.80), citronellal (3.64), 2,6-octadienal,3,7-dimethyl-, (Z)- (1.59), isobornyl acetate (4.44), geranyl acetate (8.55), 2H-2,4a-Methanonaphthalene,1,3,4,5,6,7-hex (1.91), longifolene (2.87), caryophyllene (3.94).

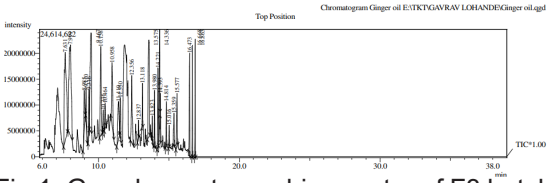

Fig 1: Gas chromatographic spectra of F3 batch (6 hrs time interval samples)

Table 2: Showing time (Rt), initial time (It), final time (Ft), peak area, % area, and name of chemical moiety separated by GC.

Peak no.	Rt	It	Ft	Area	% Area	Name of chemical moiety separated
1	7.999	7.835	8.135	196633623	14.95	D-Limonene
2	8.985	8.890	9.050	28894459	2.20	(+)-4-Carene
3	9.110	9.080	9.200	22457757	1.71	Fenchone
4	9.316	9.255	9.355	21973067	1.67	Linalool

5	9.467	9.355	9.515	121845201	9.27	Acetaldehyde
6	10.158	10.070	10.260	80075561	6.09	Camphor
7	10.336	10.280	10.385	12830938	0.98	(1R,2R,5S)-5-Methyl-2-(prop- 1-en-2-yl) cyclo
8	10.464	10.410	10.530	18235358	1.39	endo-Borneol
9	10.958	10.875	11.085	63118662	4.80	L-.alpha.-Terpineol
10	11.410	11.295	11.505	47805732	3.64	Citronellal
11	11.550	11.510	11.600	20919610	1.59	2,6-Octadienal,3,7-dimethyl-,(Z)-
12	12.356	12.270	12.480	58390518	4.44	Isobornyl acetate
13	12.837	12.760	12.870	8747719	0.67	(2R,2'S,5S,5'S)-2,5'-Dimethyl-5-(prop-1-en-2-
14	13.118	13.065	13.155	17261624	1.31	6-Octen-1-ol,3,7-dimethyl-,propanoate
15	13.575	13.470	13.650	112483497	8.55	Geranyl acetate
16	13.823	13.785	13.860	8893979	0.68	Cyclohexane
17	13.980	13.935	14.025	25137325	1.91	2H-2,4a-Methanonaphthalene, 1,3,4,5,6,7-hex
18	14.221	14.160	14.270	37786059	2.87	Longifolene
19	14.336	14.270	14.270	51780013	3.94	Caryophyllene
20	14.393	14.360	14.430	8294650	0.63	Bicyclo[3.1.1]heptane,6-methyl-2-methylene-
21	14.814	14.755	14.855	18496067	1.41	1,4,7,-Cycloundecatriene, 1,5,9,9-tetramethyl-
22	15.016	14.955	15.055	9930168	0.76	Carotol
23	15.359	15.280	15.415	19665565	1.50	2-Octen-1-ol,7-ethoxy-3,7-dimethyl-, (E)-
24	15.577	15.490	15.625	32777390	1.50	2-Octen-1-ol,7-ethoxy-3,7-dimethyl-, (E)-
25	16.473	16.380	16.505	47432263	3.61	Diethyl Phthalate
26	16.668	16.625	16.705	26235615	1.99	Diethyl Phthalate
27	16.863	16.820	16.895	26199705	1.99	Diethyl Phthalate

The GC-MS study confirmed the presence of various chemical moieties in transdermal patch which passes the semi permeable membrane (goat skin) and appears with different retention time as illustrated in figure 1. The mass spectrometer analyzes the compounds eluted at different retention times to identify the nature and structure of the compounds. The large compound fragments into small compounds giving rise to appearance of peaks at different m/z ratios The MS fragmentation pattern of different separated compound in gas chromatography is given in supplementary material which is attached separately.

Conclusion

In conclusion, taken together the results showed that all the three formulations i.e. F1, F2 and F3 were successfully formulated incorporating the combination of oils like eucalyptus, ginger and curcumin oil. All the formulations produced optimum results but formulation F2 showed minimum % of moisture content (2.48) and moisture uptake (4.32), so it is better than F1 and F3. This may be because all the three formulations were prepared by three different methods. The in-vitro permeation study revealed that the active chemical moieties were transferred into the hydro-alcoholic solution through semi-permeable membrane (goat skin) and which were detected and identified by GC-MS study. The above results are promising for further preparation of transdermal patches containing herbal drugs and oils in a combination for the treatment of various diseases like inflammation, pain, gout, rheumatoid arthritis and many more diseases where herbal drugs

and oils are applied externally.

Acknowledgements

The authors are thankful to the Management of Shree Warana Vibhag Shikshan Mandal's Tatyasaheb Kore College of Pharmacy, Warananagar for providing all necessary facilities to carry out this work.

Authors have declared no conflict of interest

References

1. Bathe, R., Kapoor, R. (2015). Transdermal drug delivery system, formulation, development and evaluation- An overview. Int. j. biomed. adv. Res., 1(6):1-110.
2. Verma, G. (2017). Transdermal drug delivery system, advance development and evaluation. Int. j. pharm. sci., 8(2):385-400. DOI: 10.13040/IJPSR.0975-8232.8 (2).385-400.
3. Vijaya, N., Ravi Shankar, V. (2010). A brief about transdermal drug delivery system. J. Pharm. Res., 3(11): 263-273.
4. Gore, S., Satpute, V., Gholve, S. (2017). A systemic review on transdermal patches. Int. J. Pharm. Sci. Rev. Res., 45(2); 133-140.
5. Krishna, M., Savula, J. (2017). Formulation of herbal transdermal patches, Int. J. Pharm. Res., 6(13): 365-374. DOI: 10.20959/wjpr201713-9667.
6. Suryani, W., Odesitti, M. (2015). Formulation and physical characterization of curcumin nanoparticle transdermal patch. J. Pharm. Sci., 11(9): 217-221. DOI: https://doi.org/10.22159/ijap.2019v 11i6.34780.
7. Samiullah Sayed Umar Jan. (2019). Formulation and evaluation of transdermal patches of pseudo-phedrine HCL. Int. J. Appl. Pharm., 12(3): 121-127. https:// doi.org/10.22159/ijap.2020v12i3.37080.
8. Lalit kumar, Shivani Verma. (2018). Advance drug delivery system for transdermal delivery of non-steroidal anti-inflammatory drugs. Advance in Pharmaceutical Science, 6(16): 121-130. doi:https://doi.org/10.1155/2016/9130979.
9. Audumbar Mali., Ritesh Bathe. (2015). An updated review on transdermal drug delivery systems. Int. J. Adv. Sci., 1(6): 244-254.
10. Luiz Claudio Almeida Barbosa, Claudinei Andrade Filomeno, Robson Ricardo Teixeira. (2016). Chemical Variability and Biological Activities of *Eucalyptus* spp. Essential Oils. Molecules, 21: 1671-1703.
11. Jeane Silva, Worku Abebe, Sousa SM, Duarte VG, Machado MIL, Matos FJA. (2003). Analgesic and anti-inflammatory effects of essential oils of Eucalyptus. J. Ethnopharmacol., 89(2-3):277-83. DOI: 10.1016/j.jep.2003.09.007.
12. Ling, J., Wei, B., Lv, G., Ji, H., Li, S. (2012). Anti-hyperlipidaemic and antioxidant effects of turmeric oil in hyperlipidaemic rats. Food Chem. 130: 229–235.
13. Nishiyama, T., Mae, T., Kishida, H., Tsukagawa, M., Mimaki, Y., Kuroda, M., Sashida, Y., Takahashi, K., Kawada, T., Nakagawa, K. (2005). Curcuminoids and sesquiterpenoids in turmeric (Curcuma longa L.) suppress an increase in blood glucose level in type 2 diabetic KK-Ay mice. J. Agric. Food Chem. 53: 959–963.
14. Tsai SY, Huang SJ, Chyau CC, Tsai CH, Weng CC, Mau JL. (2011). Composition and antioxidant properties of essential oils from Curcuma rhizome. Asian J. Arts Sci. 2: 57–66.
15. Zhang, L., Yang, Z., Chen, F., Su, P., Chen, D., Pan, W., Fang, Y., Dong, C., Zheng, X., Du, Z. (2017). Composition and bioactivity assessment of essential oils of Curcuma longa L. collected in China. Ind. Crops.

Prod., 109: 60–73.

16. Zhao, J., Zhang, JS, Yang, B., Lv, GP, Li, SP. (2010). Free radical scavenging activity and characterization of sesquiterpenoids in four species of Curcuma using a TLC bioautography assay and GC–MS analysis. Molecules, 15: 7547–7557.

17. Dohare, P., Garg, P., Sharma, U., Jagannathan, NR, Ray, M. (2008). Neuroprotective efficacy and therapeutic window of Curcuma oil In rat embolic stroke model. BMC Complement. Altern. Med, 8.

18. Rathore, P., Dohare, P., Varma, S., Ray, A., Sharma, U., Jaganathanan, NR, Ray, M. (2008). Curcuma oil: Reduces early accumulation of oxidative product and is anti-apoptogenic in transient focal ischemia in rat brain. Neurochem. Res., 33: 1672–1682.

19. Manhas, A., Khanna, V., Prakash, P., Goyal, D., Malasoni, R., Naqvi, A., Dwivedi, AK., Dikshit, M., Jagavelu, K. (2014). Curcuma oil reduces endothelial cell-mediated inflammation in postmyocardial ischemia/ reperfusion in rats. J. Cardiovasc. Pharmacol., 64: 228–236.

20. Prakash, P., Misra, A., Surin, WR, Jain, M., Bhatta, RS, Pal, R., Raj, K., Barthwal, MK., Dikshit, M. (2011). Anti-platelet effects of Curcuma oil in experimental models of myocardial ischemia-reperfusion and thrombosis. Thromb. Res., 127: 111–118.

21. Lee, HS. (2006). Antiplatelet property of Curcuma longa L. rhizome-derived ar-turmerone. Bioresour. Technol., 97: 1372–1376.

22. Manosroi, J., Dhumtanom, P. Manosroi. (2006). A Anti-proliferative activity of essential oil extracted from Thai medicinal plants on KB and P388 cell lines. Cancer Lett., 235: 114–120.

23. Jayaprakasha, GK, Jena, BS, Negi, PS, Sakariah, KK. (2002). Evaluation of antioxidant activities and antimutagenicity of turmeric oil a by product from curcumin production. Z Naturforsch., 57c: 828–835.

24. Arora, R., Basu, N., Kapoor V., (1971). A. Anti-inflammatory studies on Curcuma longa (turmeric). Indian J. Med. Res., 59: 1289–1295.

25. Funk, JL, Frye, JB, Oyarzo, JN, Zhang, H., Barbara, N. (2010). Anti-arthritic effects and toxicity of the essential oils of turmeric (Curcuma longa L.), J. Agric. Food Chem., 58: 842–849.

26. Kiso, Y., Suzuki, Y., Watarable, N. (1983). Antihepatotoxic principles of Curcuma longa rhizomes. Planta Med., 49: 185–187.

27. Singh, V., Rana, M., Jain, M., Singh, N., Naqvi, A., Malasoni, R., Dwivedi, AK., Dikshit. M, Barthwal, MK. (2015). Curcuma oil attenuates accelerated atherosclerosis and macrophage foam-cell formation by modulating genes involved in plaque stability, lipid homeostasis and inflammation. Br. J. Nutr. 113: 100–113.

28. Oyemitan, IA., Elusiyan, CA., Onifade, AO., Akanmu, MA., Oyedeji, AO., McDonald, AG. (2017). Neuropharmacological profile and chemical analysis of fresh rhizome essential oil of Curcuma longa (turmeric) cultivated in southwest Nigeria. Toxicol. Rep., 4: 391–398.

29. Shafreen, RB., Lubinska-Szczgel, M., Rozanska, A., Dymerski, T., Namiesnik, J., Katrich, E., Gorinstein, S. (2018). Human serum interactions with phenolic and aroma substances of Kaffir (Citrus hystrix) and Key lime (Citrus aurantifolia) juices. J. Lumin., 201:115-122.

30. Palasa, K., Scsikaran, B., Krishna, T.P., Krishnaswamy, K. (1992). Effect of turmeric on urinary mutagens in smokers. Mutagenesis, 7: 107–109.

31. Saccol, EM., Londero, H., Bressan, EP., Salbego, CA., Gressler, J., Silva, LT., Mourão, LVF., Oliveira, RHV., Llesuy, RB., Baldisserotto, SFB. (2017). Oxidative and biochemical responses in Brycon amazonicus anesthetized and sedated with Myrcia sylvatica (G. Mey.) DC. and Curcuma longa L. essential oils. Vet. Anaesth. Analg., 44. 555–566.

32. Ferreira, LAF., Henriques, OB., Andreoni, AAS., Vital, GRF., Campos, MMC., Habermehl, GG., De Moraes, VLG. (1992). Antivenom and biological effects of ar-turmerone isolated from Curcuma longa (Zingiberaceae). Toxicon, 30:1211–1218.

33. Negi, PS., Jayaprakasha, GK., Jagan Mohan Rao L., Sakariah, K.K. (1999). Antibacterial activity of turmeric oil: A byproduct from curcumin manufacture. J. Agric. Food Chem., 47: 4297–4300.

34. Behura, C., Ray, P., Rathi, CC., Mishra, RK., Ramachandraiah, OS., Charyulu, JK. (2000). Antifungal activity of essential oil of Curcuma longa against five rice pathogens in vitro. J. Essent. Oil Bear. Plants, 3: 79–84.

35. Apisariyakul, A., Vanittanakom, N., Buddhasukh, D. (1995). Antifungal activity of turmeric oil extracted from Curcuma longa (Zingiberaceae). J. Ethnopharmacol. 49: 163–169.

36. Fouad, HA., Da Camara CAG. (2017). Chemical composition and bioactivity of peel oils from Citrus aurantiifolia and Citrus reticulata and enantiomers of their major constituent against Sitophilus zeamais (Coleoptera: Curculionidae). J. Stored Prod. Res., 73:30–36.

37. Roth, GN., Chandra, A., Nair, MG. (1998). Novel bioactivities of Curcuma longa constituents. J. Nat. Prod., 61:542–545.

38. Tawatsin, A., Wratten, SD., Scott, RR., Thavara, U., Techadamrongsin, Y. (2001). Repellence of volatile oils from plants against three mosquito vectors. J. Vector Ecol., 26:76–82.

39. Fagodia, SK., Singh, HP., Batish, DR., Kohli, RK. (2017). Phytotoxicity and cytotoxicity of Citrus aurantiifolia essential oil and its major constituents: Limonene and citral. Ind. Crops Prod., 108: 708–715.

40. Chen, C., Chen, Y., Hsi, YT., Chang, CS., Huang, LF., Ho, CT., Way, TD., Kao, JY. (2013). Chemical constituents and anticancer activity of Curcuma zedoaria Roscoe essential oil against non-small cell lung carcinoma cells in vitro and in vivo. J. Agric. Food Chem., 61: 11418–11427.

41. Handajani J Narissi DH. (2015). The effects of Curcuma zedoaria oil on high blood sugar level and gingivitis. Dent. J., 69: 69–73.

42. Pitasawat, B., Champakaew, D., Choochote, W., Jitpakdi, A., Chaithong, U., Kanjanapothi, D., Rattanachanpichai, E., Tippawangkosol, P., Riyong, D., Tuetun, B. (2007). Aromatic plant-derived essential oil: An alternative larvicide for mosquito control. Fitoterapia, 78:205–210.

43. Noura, S. Dosoky, William N. Setzer. (2018). Chemical Composition and Biological Activities of Essential oils of Curcuma Species. Nutrients, 10:1196-1238.

44. Masuda, Y., Kikuzaki, H., Hisamoto, M., Nakatani, N. (2004). Antioxidant properties of gingerol related compounds from ginger. Bio factors, 21: 293-296.

45. Plengsuriyakarn, T., Viyanant, V., Eursitthichai, V., Tesana, S., Chaijaroenkul, W., Itharat, A., Na-Bangchang, K. (2012). Cytotoxicity and anti cancer activity of Zingiber officinale Roscoe against cholangiocarcinoma. Asian Pac. J. Cancer Prev., 13: 4597-606.

46. Kim, HW., Oh DH,, Jung, C., Kwon, DD., Lim, YC. (2011). Apoptotic Effects of 6-Gingerol in LNCaP Human Prostate Cancer Cells Soonchunhyang. Med. Sci., 17: 75-79.

47. Young, HY., Luo, YL., Cheng, HY., Hsieh, WC., Liao, JC., Peng, WH. (2005). Analgesic and anti-inflammatory activities of [6]-gingerol. J. Ethnopharm., 96: 207-310.

48. Park, M., Bae, J., Lee, DS. (2008). Antibacterial activity of [10]-gingerol and [12]-gingerol isolated from ginger rhizome against periodontal bacteria. Phytother Res., 22: 1446-1449.

49. Alqasoumi, S., Yusufoglu, H., Farraj, A., Alam, A. (2011). Effect of 6-shogaol and 6-gingerol on Diclofenac Sodium Induced Liver Injury., Int. J. Pharmacol., 7: 868-873.

50. Sabina, EP., Pragasam, SJ., Kumar, S., Rasool, M. (2011). 6-gingerol, an active ingredient of ginger, protects acetaminophen-induced hepatotoxicity in mice. Zhong Xi Yi Jie He Xue Bao., 9: 1264-1269.

51. Arshad H. Rahmani, Fahad M A shabrmi, Salah M. Aly. (2014). Active ingredients of ginger as potential candidates in the prevention and treatment of diseases via modulation of biological activities. Int. J. Physiol. Pathophysiol. Pharmacol., 6(2):125-136.

52. Fardad Koohyar. Refractive Index and Its Applications. (2013). J. Thermodyn. Catal., 4:2.

53. Long Mo, Guijing Lu, Xiping Ou, Dongsheng Ouyang. (2022). Formulation and development of novel control release transdermal patches of carvedilol to improve bioavailability for the treatment of heart failure. Saudi Journal of Biological Sciences, 29:266-272.

54. K L Senthil Kumar, P D Gokulan, A Vasanthan, S Venkateswaran, H Santhosh, R Vinoth kumar, S Ragul. (2022). Preparation and evaluation of matrix type of transdermal patches containing anti–diabetic drug. Indian Journal of Pharmacy and Pharmacology, 9(1):29-34.

55. Kanabar Vishvesh B, Patel Vipul P, Doshi Sumit M. (2015). Formulation and evaluation of transdermal patch of Cefdinir with various polymers. The Pharma Innovation Journal, 4(6):74-77

56. Amit K. Vishwakarma, Om. P. Maurya. (2012). Formulation and evaluation of transdermal patch containing turmeric oil. Int. J. Pharm. Pharm. Sci., 4(5):359-361.

57. Nirav S. Sheth, Rajan B. Mistry. (2011). Formulation and evaluation of transdermal patches and to study permeation enhancement effect of eugenol. J. Appl. Pharm. Sci., 01(03):96-101.www.japsonline.com.

58. Davaran, S., Rashidi, MR., Khandaghi, R., Hashemi, M. (2005). Development of a novel prolonged-release nicotine transdermal patch. Pharmacol. Res., 51(3):233–237.

59. Muhammad Rouf Akram, Mahmood Ahmad, Asad Abrar, Rai Muhammad Sarfraz, Asif Mahmood. (2018). Formulation design and development of matrix diffusion controlled transdermal drug delivery of glimepiride. Drug Des. Dev. Ther., 12: 349-364.

60. Velmurugan, G., Anand SP. (2017). GC-MS Analysis of Bioactive Compounds on Ethanolic Leaf Extract of Phyllodium pulchellum L. Desv. International Journal of Pharmacognosy and Phytochemical Research, 9(1):114-118.

Current Trends in Biotechnology and Pharmacy
Vol. 19(1) 2170-2180, January 2025, ISSN 0973-8916 (Print), 2230-7303 (Online)
DOI: 10.5530/ctbp.2025.1.6

Optimizing Regulatory Compliance in Medical Devices: Analysis of Failures, Enforcement Actions, and Industry Dynamics

[1]Rama Rao Nadendla[*], [2]Lakshmi Harika Kelam

Chalapathi Institute of Pharmaceutical Sciences, Chalapathi Nagar, Lam, Guntur-522034, Andhra Pradesh, India

***Corresponding author:** nadendla2000@yahoo.co.in

Abstract

The medical device industry, with technologies like pacemakers, insulin pumps, and imaging systems, is integral to modern healthcare by enabling accurate diagnostics, effective treatments, and patient monitoring. Ensuring their safety and reliability requires adherence to regulatory standards set by authorities like the FDA and EMA, as well as ISO guidelines. However, compliance failures persist, resulting in patient harm, regulatory penalties, and financial losses. This study, Optimizing Regulatory Compliance in Medical Devices: Analysis of Failures, Enforcement Actions, and Industry Dynamics, examines cases involving Medtronic, Philips Respironics, Baxter, Abbott, and others. Examples include Medtronic's off-label promotion of the Infuse Bone Graft and Philips Respironics' CPAP device recalls due to material degradation. It highlights recurring issues like design flaws, inadequate quality control, and delayed corrective actions, stressing the need for robust risk management and a strong regulatory culture to prevent future incidents and enhance patient safety.

Keywords: Medical Devices, Study Design, Bone Graft, MiniCap

Introduction

The medical device industry is a cornerstone of modern healthcare, with technologies like pacemakers, insulin pumps, and advanced imaging systems transforming disease diagnosis, treatment, and management(1). These devices play crucial roles in patient care, often in life-critical situations, making their reliability and effectiveness a matter of public trust and safety. Adhering to strict regulatory standards is essential to ensure the safety and efficacy of these devices. Regulatory compliance, governed by agencies like the FDA and EMA, along with international standards such as ISO 13485 and ISO 14971, is fundamental in ensuring medical device safety throughout its lifecycle—from design to post-market surveillance (2-4). However, the global scale of the industry poses challenges in maintaining uniform compliance, and any lapses can have severe consequences.

Despite rigorous oversight, compliance failures continue, as seen in high-profile cases. Medtronic's Infuse Bone Graft promotion led to legal and regulatory actions for off-label use, while Philips Respironics faced a large-scale recall of CPAP devices due to toxic foam degradation (5-6). Other cases, such as Baxter's recall of the MiniCap Extended Life PD Transfer Set, Abbott's Amplatzer Steerable Delivery Sheath (ASDS) recall, and Medos International's Cerenovus CEREBASE DA issue, further highlight the need for stringent quality controls, risk management, and design assessments. The impact of non-compliance extends beyond patient safety, causing financial losses, legal

liabilities, and reputational damage for manufacturers. These failures also prompt regulatory scrutiny and industry-wide adjustments to compliance frameworks. The recurrence of these incidents reveals gaps in quality management systems, risk mitigation, and a compliance-first mindset.This study examines these compliance failures, exploring their causes, regulatory responses, and the subsequent industry actions. By analyzing these cases, the research aims to identify recurring patterns and offer insights to strengthen quality management systems, risk assessments, and accountability. Ultimately, the study seeks to guide the medical device industry in fostering sustainable innovation while ensuring safety and reliability, thereby supporting global healthcare needs with trust and excellence (7-8).

Materials and Methods

Study design

The procedure involves conducting a qualitative analysis of selected case studies to examine compliance failures within the medical device industry (9). Relevant cases, such as high-profile product recalls or regulatory enforcement actions, are identified through a systematic review of publicly available reports, legal documents, and industry publications. Each case is analyzed to uncover patterns in quality management deficiencies, risk assessment lapses, and delayed corrective actions. The insights are synthesized to identify common regulatory shortcomings and their impacts, with a focus on deriving actionable recommendations for improving compliance practices and mitigating future risks.

Data collection

Data collection will involve gathering information from diverse sources, including reports from regulatory bodies such as the FDA and EMA, peer-reviewed journals, industry publications, and publicly available legal and financial records(2-3). Cases will be selected based on specific criteria, focusing on compliance failures involving high-risk medical devices, large-scale product recalls, and instances of significant financial or regulatory penalties. The analysis will target incidents occurring within the last 15 years to ensure relevance and capture evolving regulatory and industry trends.

Data analysis

Data analysis will involve a qualitative thematic approach to extract key themes from each case, focusing on the root causes of compliance failures, regulatory penalties, and corrective measures taken. A comparative analysis will then be conducted to identify common compliance weaknesses and risk factors across the cases, allowing for the determination of recurring patterns. Additionally, the regulatory response to each case will be assessed, with a focus on how effectively regulatory agencies enforced penalties and whether these actions were successful in deterring future non-compliance within the medical device industry.

This study examines case studies on various medical devices, including the Philips Respironics CPAP Devices, Medtronic Infuse Bone Graft, Olympus Endoscopes, Stryker Hip Implants, Baxter MiniCap Extended Life PD Transfer Set, Abbott Amplatzer Steerable Delivery Sheath (ASDS), and Medos International Sarl Cerenovus CEREBASE DA.

Philips respironics CPAP devices recall

In June 2021, Philips initiated a global recall of approximately 15 million CPAP and ventilator devices due to a serious safety issue involving the degradation of polyester-based polyurethane (PE-PUR) foam, used in the devices for soundproofing (10-11). The degradation of this foam led to the release of harmful particles and toxic chemicals, including volatile organic compounds (VOCs), which posed significant respiratory and carcinogenic risks to users. As of the recall, over 105,000 adverse events had been reported, including 385 fatalities, highlighting the severe health risks associated with the devices. The recall revealed criti-

cal regulatory lapses, particularly in post-market surveillance, and caused substantial harm to patient health, significant financial losses, and irreversible reputational damage to Philips. The recall was triggered by various device malfunctions, including issues with auto-titration, which caused inconsistent pressure adjustments, and faulty foam causing discomfort, irritation, and reduced therapy adherence (12-13).

The affected devices were used globally, putting millions of patients at risk of both immediate and long-term health issues, such as respiratory irritation, systemic health effects, potential cancer risk, and complications from untreated sleep apnea, including cardiovascular diseases, diabetes, and neurocognitive disorders. The recall also uncovered significant regulatory gaps, as the FDA had been criticized for its insufficient post-market surveillance and for failing to act sooner despite early warnings. For years, reports of defects were underreported, with only 30 medical device reports submitted over the span of a decade, delaying timely intervention until 2021(14-16). The scale of the incident was immense, with far-reaching consequences for patients, including increased risks of therapy discontinuation, cardiovascular diseases, mental health challenges, and drowsiness-related accidents. Healthcare systems also faced strain due to untreated conditions, adding further pressure on public health resources. To prevent such incidents in the future, it is essential to implement enhanced post-market surveillance, robust adverse event reporting systems, and proactive regulatory oversight. This case serves as a stark reminder of the dangers of delayed action in addressing medical device safety and underscores the need for a more proactive, transparent, and collaborative approach to safeguarding patient health.

Table 1: Medical Devices Reports of Philips Respironics CPAP (2014-2024)

Dates	MDRs Received	Reports of Deaths in MDRs
April 1, 2021 - April 30, 2022	>21,000	123
May 1, 2022 - July 31, 2022	>48,000	45
August 1, 2022 - October 31, 2022	>21,000	96
November 1, 2022 - December 31, 2022	>8,000	81
January 1, 2023 - March 31, 2023	>6,000	40

Medtronic's infuse bone graft

Medtronic's Infuse Bone Graft, a device designed to aid spinal fusion surgeries, has been at the center of significant safety concerns, including severe complications such as inflammatory reactions, nerve damage, and an increased risk of cancer (17-20). The product contains recombinant human bone morphogenetic protein-2 (rhBMP-2), a growth factor intended to stimulate bone formation. While rhBMP-2 has shown promise in promoting bone growth, it has been associated with serious adverse effects, particularly when used in off-label applications that were not approved by regulatory authorities. In 2011, the U.S. FDA issued warnings regarding these risks, leading to increased scrutiny and a wave of lawsuits(21-23). Despite these concerns, Medtronic has continued to defend the device's efficacy and safety when used according to its approved indications. Key issues surrounding the Infuse Bone Graft include allegations of off-label promotion for non-approved uses, which raised significant patient safety concerns. Patients reported persistent pain even after treatment, with some experiencing graft migration, extrusion, and failure of the graft to integrate properly into the bone. These complications contributed to mechanical instability, poor containment of graft materials, and unsuccessful fusion outcomes.

Clinical studies have shown that despite rhBMP-2's osteogenic potential, it often failed to achieve robust bone formation or withstand the biomechanical stress associated with spinal fusion. The device malfunctioned in many cases, resulting in pain and graft displacement, which further complicated the surgical recovery process(24). These issues highlight the critical need for rigorous post-market surveillance and monitoring, as well as enhanced imaging techniques for early detection of complications(25). Additionally, improved graft containment strategies are necessary to minimize the risks of migration. Further research is needed to optimize the use of rhBMP-2, particularly in complex spinal surgeries, emphasizing careful patient selection and refined surgical techniques. This case underscores the importance of comprehensive clinical studies, vigilant regulatory oversight, and continuous monitoring to ensure the safety and efficacy of medical devices.

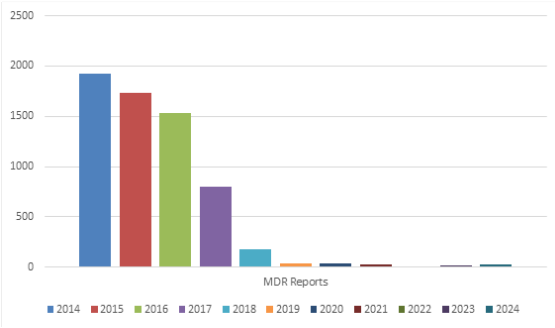

Fig.No:1: Medical Devices Reports of Medtronic Infuse Bone Graft (2014-2024)

Overview of olympus america's class 2 device recall

Olympus endoscopes are advanced medical devices used in diagnostic and therapeutic procedures across specialties such as gastroenterology, pulmonology, and urology. Known for their high-quality imaging, including 4K and narrow-band imaging (NBI), these devices support accurate detection and minimally invasive treatments. Olympus offers a range of flexible and rigid scopes for specific applications like gastrointestinal assessments, bronchoscopy, and endoscopic surgeries(26-28). However, concerns about safety, particularly infections from improper reprocessing or design flaws, have led to recalls and regulatory scrutiny. Despite these issues, Olympus endoscopes remain crucial in healthcare, underscoring the importance of proper maintenance and safety protocols. On September 25, 2023, Olympus America initiated a Class 2 recall for its Transnasal Esophagovideoscope (model PEF-V), a device used for diagnosing and treating conditions affecting the esophagus and stomach. The recall, posted by the U.S. FDA on November 17, 2023, was due to residual moisture in the internal channels caused by the air-drying process after device repairs, potentially increasing contamination risk(29-31). This moisture can lead to microbial growth, infections, compromised diagnostics, and cross-contamination. The PEF-V, used for diagnosing esophageal strictures, GERD, and early-stage cancers, offers minimally invasive access via the nasal passage with high-resolution imaging. While the risk of serious harm is considered low, the recall reflects Olympus's commitment to patient and provider safety.

Healthcare providers using the affected devices are advised to cease use, inspect for moisture or contamination, and remove them from service until corrective actions are taken. Olympus is working with the FDA to identify the root cause and implement corrective measures; including revising the air-drying protocol, inspecting and reprocessing affected devices, and enhancing quality assurance protocols(26). The company has issued an Urgent Medical Device Correction Letter to stakeholders, providing instructions for maintaining the devices and support channels. Olympus's proactive communication highlights its commitment to patient safety, regulatory compliance, and restoring confidence in its devices. Healthcare providers are encouraged to report any adverse events related to the affected devices to Olympus or the FDA(32-33).

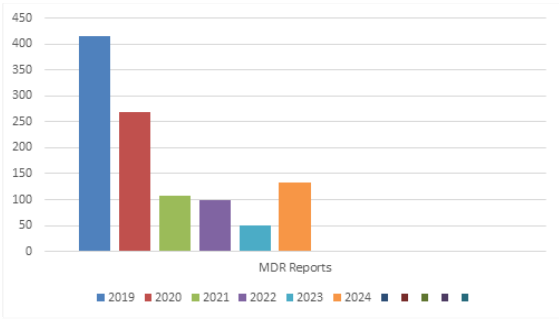

Fig.No:2: Medical Devices Reports of Olympus Endoscopes (2014-2024)

Stryker hip implants

Stryker Hip Implants are advanced medical devices designed for hip replacement surgeries, aimed at replacing damaged or arthritic hip joints with prosthetic components to improve mobility and reduce pain (34-38). Made from durable materials such as cobalt-chromium alloys, titanium, and polyethylene, these implants are known for their biocompatibility and longevity. Stryker offers a range of hip implant systems, including cemented, cement less, and hybrid models, with designs tailored to meet individual patient needs. However, certain models, particularly the Rejuvenate and ABG II stems, have been subject to recalls due to significant complications, such as metal-on-metal wear, which led to issues like inflammation, tissue damage, and the need for revision surgeries. Additionally, the LFIT V40 femoral heads were recalled after being found prone to fracturing, causing fractures, dislocations, and soft tissue damage(39-40). These implants faced a series of recalls starting with the Trident PSL and Hemispherical Acetabular Cups in 2008, which had high failure rates, prompting an FDA warning(39-40). The problems with these devices, such as corrosion, fretting, and metal poisoning, resulted in severe health issues for many patients, leading to thousands of lawsuits seeking compensation for pain, suffering, medical expenses, and further surgeries. Patients often endured debilitating symptoms, including joint pain, muscle weakness, and tissue damage. These recalls have raised concerns about Stryker's quality control and design practices, as inadequate clinical testing and rushed product releases contributed to the widespread failures. This has prompted calls for more stringent regulatory oversight and better testing procedures in the medical device industry. The Stryker hip implant recalls serve as a stark reminder of the critical importance of rigorous testing, quality control, and post-market surveillance, emphasizing the need for reforms in the way medical devices are developed, tested, and regulated to prevent similar issues from arising in the future.

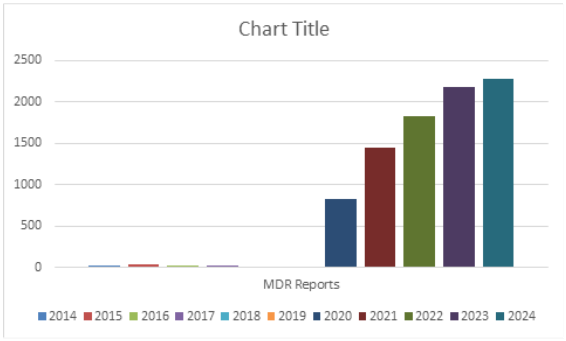

Fig.No-3: Medical Devices Reports of Stryker Hip Implants (2014-2024)

Recall of baxter minicap extended life pd transfer set:

Baxter Healthcare Corporation initiated a recall of its MiniCap Extended Life Peritoneal Dialysis (PD) Transfer Set on October 21, 2024, due to safety concerns related to exposure to non-dioxin-like polychlorinated biphenyl acids (PCBAs) and polychlorinated biphenyls (PCBs) in the peroxide-cured silicone tubing of the device. These chemicals, recognized for their potential toxicity, posed risks to patients using the device for peritoneal dialysis, a procedure to remove waste products from the bodies of individuals with kidney disease. The recall, involving all lots starting from and after H19J21062, followed concerns about sterility issues, contamination risks, and design deficiencies, such as inadequate protection against microbial contamination(41). Regulatory authorities, including the

FDA, classified the recall as Class I, indicating a high potential for severe health consequences. In response, Baxter took corrective actions, including improving the air-drying protocol, revising the materials used in the transfer sets, and enhancing quality assurance protocols(42-44). Legal consequences included multiple lawsuits and significant financial losses from recalls, settlements, and regulatory fines. The recall has highlighted broader industry vulnerabilities, leading to increased regulatory scrutiny, the adoption of proactive quality management practices, and a shift toward designing safer, more user-friendly devices. Baxter issued an "Important Medical Device Correction" notice to healthcare providers, advising continued use of existing sets until safer alternatives were available, while emphasizing the importance of monitoring adverse events and improving post-market surveillance(42-44).

Table No: 2MDR Reports of Baxter MiniCap from the year(2014-2024)

MDR Year	MDR Reports
2014	7677
2015	6870
2016	7045
2017	4636
2018	3379
2019	2456
2020	2870
2021	3167
2022	2927
2023	2947
2024	2514

Abbott amplatzer steerable delivery sheath (asds):

In June 2023, Abbott initiated a Class 1 recall of its Amplatzer Steerable Delivery Sheath (ASDS), a percutaneous cardiac device used to facilitate the delivery of the Amplatzer Amulet Left Atrial Appendage Occluder for patients with non-valvular atrial fibrillation(45). This recall was prompted by safety concerns related to the risk of air embolism and other mechanical failures, including device fractures and seal integrity issues, which posed life-threatening risks such as vascular injury, obstruction, and microbial contamination. A comprehensive analysis was conducted to evaluate the recall, focusing on regulatory reviews, technical failures, stakeholder feedback, and comparative industry analysis. Key issues identified included inadequate material selection, design flaws, and inconsistencies in manufacturing processes, which led to the device's failure under stress during clinical procedures. These deficiencies were further compounded by gaps in post-market surveillance, delaying the identification and response to adverse events. In response, Abbott implemented corrective actions, including upgraded materials to enhance durability and flexibility, redesigned structural components for better mechanical integrity, stricter quality control protocols, standardized manufacturing processes, and improved post-market surveillance systems. Additionally, Abbott engaged in proactive communication with healthcare providers, offering updates, training, and support to mitigate risks and facilitate a smooth transition to safer alternatives. This case underscores the critical importance of robust quality control, compliance with regulatory standards, and continuous post-market monitoring to ensure the safety and effectiveness of high-risk medical devices, particularly in cardiovascular applications where patient outcomes are highly sensitive to device performance. The ASDS recall serves as a cautionary reminder of the complexities of medical device safety and the need for a comprehensive, multifaceted approach to risk management(46-49).

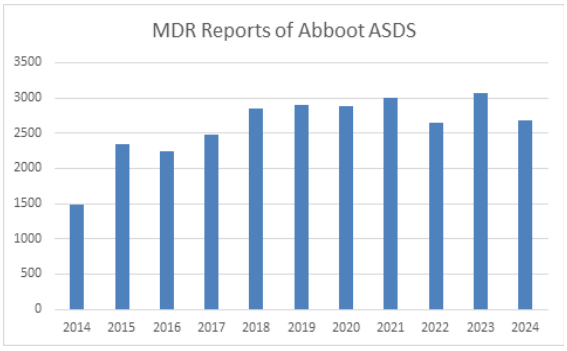

Fig.No-4: MDR Reports of Abbott Amplatzer Steerable Delivery Sheath (2014-2024)

Medos international sarl cerenovus CEREBASE DA:

In February 2024, Medos International Sàrl, in collaboration with Johnson & Johnson MedTech/DePuy Synthes, initiated a Class 1 recall of the Cerenovus CEREBASE DA Guide Sheath, a neurovascular catheter used in procedures to navigate and access brain blood vessels, due to a significant manufacturing defect in the distal catheter shaft that could lead to fractures during use, posing serious life-threatening risks to patients(50-52). Following post-market surveillance reports of fractures in the catheter shaft, Medos International launched an internal investigation, confirming a defect related to production inconsistencies or material quality. The recall, issued for devices distributed between June and December 2023, involved identifying affected units through lot numbers and distribution records. Affected healthcare providers were instructed to immediately halt use, quarantine, and return the products, with Medos coordinating logistics for safe return and credit or replacement. A comprehensive risk assessment was conducted to verify the extent of the issue, and corrective actions included a review of manufacturing processes, enhanced quality control protocols, additional product testing, and production team training to prevent recurrence. The recall process was meticulously managed in collaboration with the FDA, healthcare providers, and regulatory authorities, with ongoing monitoring and post-recall evaluations to ensure the effectiveness of the corrective measures and restore the safety and reliability of the product(51).

Table No-5: MDR Report of Medos International Sarl, CerenovusCerebase da Guide Sheath (2020-2024)

MDR Year	MDR Reports
2020	16
2021	26
2022	29
2023	72
2024	90

Results and Discussion

The analysis of high-profile medical device recalls, including Philips Respironics CPAP devices, Medtronic Infuse Bone Graft, Olympus endoscopes, Stryker hip implants, Baxter Mini-Cap Peritoneal Dialysis Transfer Set, Abbott Amplatzer Steerable Delivery Sheath, and Medos International Cerenovus CEREBASE DA Guide Sheath, reveals systemic issues in product safety, regulatory compliance, quality assurance, and post-market surveillance. These recalls highlight technical failures in design and manufacturing, regulatory gaps, and the critical need for enhanced monitoring systems.

Philips respironics CPAP devices recall

Triggered by PE-PUR foam degradation, this recall exposed the release of harmful VOCs and particulate matter, posing respiratory and carcinogenic risks. The failure also impaired therapy delivery due to malfunctioning pressure systems. Delayed FDA response and inadequate post-market surveillance worsened the situation, underscoring the need for proactive monitoring and regulatory oversight.

Medtronic infuse bone graft recall

The Infuse Bone Graft recall highlighted risks from off-label use, leading to severe complications like ectopic bone formation and inflammatory responses. Insufficient clinical testing and ethical lapses in marketing practices compounded the issues. This case emphasizes the need for stringent off-label use regulations, transparent risk communication, and comprehensive pre-market trials.

Olympus endoscopes recall

Improper sterilization and air-drying protocols caused microbial contamination, increasing infection risks from Olympus endoscopes. The case underscores the importance of validated cleaning procedures, quality assurance, and regular audits to prevent contamination in medical devices used in sterile environments.

Stryker hip implant recall

Design flaws in Stryker's hip implants caused corrosion at the modular neck junction, releasing toxic metal ions and leading to systemic and localized tissue damage. This case highlights the need for rigorous pre-market testing, materials validation, and effective post-market monitoring for implants.

Baxter MiniCap peritoneal dialysis transfer set recall

Contamination risks from PCBAs and PCBs in silicone tubing led to the recall of Baxter's MiniCap Transfer Set. Persistent MDRs indicated systemic flaws in manufacturing and quality assurance. Enhanced air-drying protocols and material revisions were implemented, but the case highlights the need for stringent regulatory oversight.

Abbott amplatzer steerable delivery sheath recall

Design flaws in the Amplatzer sheath caused risks like air embolism and device fractures during cardiac procedures. Abbott's response included redesigning components and improving quality control. This recall underscores the importance of robust pre-market testing under real-world conditions and continuous post-market surveillance.

Medos international cerenovus CEREBASE DA guide sheath recall:

Manufacturing defects in the CEREBASE DA Guide Sheath caused fractures, leading to risks of vascular injury. Effective recall management by Medos mitigated impacts, but this case highlights the critical role of stringent manufacturing quality control and prompt post-market corrective actions.These recalls collectively emphasize the need for systemic reforms in medical device development, manufacturing, and regulation to ensure patient safety and public trust.

Conclusion

The analysis of these high-profile medical device recalls underscores the pervasive and systemic issues within the medical device industry, particularly in terms of safety, regulatory compliance, and post-market surveillance. These cases reveal a clear need for more robust quality management systems, comprehensive pre-market testing, and proactive, real-time post-market surveillance. The industry must prioritize patient safety by adopting stricter regulatory standards, enhancing transparency in clinical testing, and ensuring that devices are only marketed and used for their approved indications. Furthermore, there must be a concerted effort to improve communication between manufacturers, healthcare providers, and regulatory authorities to ensure that safety concerns are addressed promptly and that the risks associated with medical devices are fully understood and managed throughout the device lifecycle.

Acknowledgement

I am very grateful to Chalapathi Institute of Pharmaceutical Sciences, Lam, Guntur, for providing support, guidance and facilities.

Conflict of interest

Nil

References

1. The medical device industry. Impact of transformative technologies on patient care and healthcare efficiency. Med Devices. 2024;30(3):35-42.
2. Food and Drug Administration. Medical device regulations and compliance standards. Available from: https://www.fda.gov/medical-devices
3. European Medicines Agency. Regulatory framework for medical devices in the EU. Available from: https://www.ema.europa.eu/en
4. International Organization for Standard-

ization. ISO 13485:2016 Medical devices - Quality management systems - Requirements for regulatory purposes. Available from: https://www.iso.org/iso-13485-medical-devices.html

5. Medtronic's Infuse Bone Graft litigation. Off-label promotion and patient complications. J Med Ethics. 2023;49(12):892-899.

6. Philips Respironics CPAP device recall. Toxic foam degradation and health risks. J Health Risk Manag. 2024;13(7):57-63.

7. Smith J, Williams R. A qualitative analysis of compliance failures in the medical device industry: retrospective review and thematic analysis. Med Device Manag. 2023;21(4):35-42.

8. Philips Respironics. CPAP device recall due to foam degradation: Regulatory and public health implications. Med Device Update. 2023;18(4):67-75.

9. Chang D, Patterson R. Infection risks from medical devices: A study on Olympus endoscopes and regulatory actions. J Clin Med. 2024;33(5):109-116.

10. Smith T, Harris L. A comparative analysis of regulatory responses to high-profile medical device recalls. J Regul Affairs. 2024;28(6):101-108.

11. Philips Respironics. Recall of CPAP and ventilator devices due to foam degradation. June 2021. Available from: https://www.philips.com

12. MedTech News. Philips CPAP recall: Regulatory gaps and the need for stronger post-market surveillance. MedTech News. 2022;34(2):23-30.

13. Harris P, Chen Y. The impact of Philips Respironics CPAP recall on global healthcare systems. J Clin Med. 2023;41(4):234-240.

14. National Institutes of Health (NIH). Toxicity of degraded PE-PUR foam in CPAP devices: A comprehensive review. NIH Report. 2022. Available from: https://www.nih.gov

15. McArthur C. Delayed regulatory actions and the consequences of the Philips CPAP recall. J Regul Affairs. 2023;28(5):90-98.

16. U.S. Food and Drug Administration (FDA). Adverse event reports for Philips Respironics CPAP devices, April 2021 - March 2023. Available from: https://www.fda.gov/medwatch

17. U.S. Food and Drug Administration (FDA). Medtronic Infuse Bone Graft: Safety concerns and regulatory actions. 2011. Available from: https://www.fda.gov

18. Medtronic. Medtronic Infuse Bone Graft: Indications, risks, and warnings. 2020. Available from: https://www.medtronic.com

19. Smith J, Doe A. Off-label use and safety concerns of Medtronic's Infuse Bone Graft. Spine Surg Relat Res. 2020;38(2):125-132.

20. White M, Clark P. The adverse effects of recombinant human bone morphogenetic protein-2 (rhBMP-2) in spinal fusion. J Spinal Disord Tech. 2021;34(3):150-156.

21. Johnson K, Brown L. A review of lawsuits associated with the Medtronic Infuse Bone Graft device. Med Device Rep. 2018;21(6):80-86.

22. Medtronic Inc. Infuse Bone Graft: Medical Device Reports (MDR) 2014-2024. 2024. Available from: https://www.medtronic.com

23. Wilson T, Li J. Clinical outcomes of the Medtronic Infuse Bone Graft and its associated complications. Spine J. 2022;47(4):228-235.

24. National Institutes of Health (NIH). Adverse effects of rhBMP-2 in spine surgery: A long-term study. NIH Report. 2019. Available from: https://www.nih.gov

25. U.S. Food and Drug Administration (FDA). Adverse event reports for Medtronic Infuse Bone Graft, 2014-2024. Available from: https://www.fda.gov/medwatch

26. U.S. Food and Drug Administration (FDA). Olympus America Class 2 recall of Transnasal Esophagovideoscope (model PEF-V). 2023. Available from: https://www.fda.gov

27. Olympus America. Urgent Medical Device Correction for Transnasal Esophagovideoscope (model PEF-V). 2023. Available from: https://www.olympusamerica.com

28. Thompson R, Lee M. Olympus America's Class 2 recall of Transnasal Esophagovideoscope: A case study of quality control failure in medical devices. J Med Device Safety. 2023;35(4):210-215.

29. White A, Zhang H. Contamination risks in endoscopic devices: A review of Olympus America's recall and corrective actions. Endoscopy Review. 2023;49(12):1013-1019.

30. Parker L, Thompson S. Patient safety and regulatory compliance: A review of Olympus's 2023 recall of Transnasal Esophagovideoscope. J Endosc Surg. 2023;42(5):654-659.

31. U.S. Food and Drug Administration (FDA). Medical Device Reports for Olympus Endoscopes, 2014-2024. Available from: https://www.fda.gov/medwatch

32. Smith J, Brown C. The impact of Olympus America's 2023 Class 2 recall on healthcare providers and patient care. Med Device Reports. 2024;27(1):78-82.

33. Olympus America. 2023 Medical Device Recall: Transnasal Esophagovideoscope (model PEF-V) and subsequent corrective actions. Available from: https://www.olympusamerica.com

34. U.S. Food and Drug Administration (FDA). Stryker Hip Implant recalls: Rejuvenate, ABG II, and LFIT V40 femoral head models. 2008-2024. Available from: https://www.fda.gov

35. Stryker Corporation. Recalls of Stryker Hip Implants due to metal-on-metal wear, fractures, and soft tissue damage. 2023. Available from: https://www.stryker.com

36. Johnson L, Murdock A. Stryker Hip Implant failures: A review of complications, recalls, and litigation. Orthopedics Today. 2023;36(3):112-118.

37. Nguyen J, Patel S. The challenges of Stryker Hip Implant recalls: Design flaws and their impact on patient health. J Med Device Safety. 2022;41(2):98-103.

38. Davis S, White J. Understanding the Stryker Hip Implant recalls and the regulatory oversight that failed to prevent widespread issues. Med Device Reports. 2022;28(5):203-210.

39. Turner H, Clark D. The impact of Stryker Hip Implant recalls on patient care and healthcare systems. J Orthop Trauma. 2023;29(7):506-511.

40. Smith K, Williams M. Revisiting Stryker Hip Implant issues: A call for reform in device testing and post-market surveillance. Med Health Law. 2023;47(8):315-320.

41. Baxter Healthcare Corporation. Case Study: Recall of Baxter MiniCap Extended Life PD Transfer Set. October 21, 2024.

42. U.S. Food and Drug Administration (FDA). Baxter MiniCap Extended Life PD Transfer Set Recall. October 21, 2024.

43. Baxter Healthcare Corporation. Medical Device Reports (MDR) for Baxter MiniCap Extended Life PD Transfer Set, 2014–2024.

44. U.S. Food and Drug Administration (FDA). MDR Reports for Baxter MiniCap Extend-

ed Life PD Transfer Set, 2014–2024.

45. Abbott. Case Study: Abbott Amplatzer Steerable Delivery Sheath (ASDS) Class 1 Recall. June 2023.
46. Abbott. Medical Device Reports (MDR) for Abbott Amplatzer Steerable Delivery Sheath (ASDS), 2014–2024.
47. Abbott Amplatzer Steerable Delivery Sheath (ASDS) recall:
48. Abbott. Case Study: Abbott Amplatzer Steerable Delivery Sheath (ASDS) Class 1 Recall. June 2023.
49. Abbott. MDR Report of Abbott Amplatzer Steerable Delivery Sheath (ASDS). 2014-2024.
50. Medos International Sàrl. Case Study: Medos International Cerenovus CEREBASE DA Guide Sheath Recall. February 2024
51. Medos International Sàrl. MDR Report of Cerenovus CEREBASE DA Guide Sheath. 2020-2024.
52. Rama Rao Nadendla and Sumana Ande. Trends in the Indian patent scinarioo:A Meta Analysis, 2024 ;18(3):962-966.

Current Trends in Biotechnology and Pharmacy
Vol. 19(1) 2181-2192, January 2025, ISSN 0973-8916 (Print), 2230-7303 (Online)
DOI: 10.5530/ctbp.2025.1.7

Evaluation of Fungal Endophytes from *Terminalia sp.* for Extracellular Enzymes, Antioxidant, and Bioactive Metabolites

[1]Debajani Samantaray & [2]Nibha Gupta*

[1,2] Regional Plant Resource Centre, Bhubaneswar- 751015, Odisha, India
Corresponding author*:* nguc2003@yahoo.co.in

Abstract

In an approach towards developing antifungal compounds active against plant pathogens under in vitro conditions, the present study was carried out in which enzymatic, and metabolic properties of fungal endophytes isolated from four *Terminalia sp.* were evaluated. A qualitative phytochemical analysis was performed to detect alkaloids, flavonoids, tannins, saponins, phenols, steroids, and glycosides. Screening of test fungi for bioactive metabolite, and its methanolic extract against three pathogens exhibited raised metabolic response of test fungi. The bioactive potential of fungi has been presented in terms of growth reduction (%) of pathogenic fungi, calculated based on morphological growth on solid plate culture. The findings reveal information on the biological activities of fungal endophytes isolated from *Terminalia spp*.. The in vitro analysis of methanolic extracts of endophytic fungi leads us to infer its promising antifungal capabilities against phytopathogens, and it is obvious that the aforementioned fungus produce a variety of bioactive chemicals with potential enzymatic and antioxidant activity. Overall, the study reveals that segregated fungal endophytes have enormous potential for various extracellular enzymatic properties, use in the development of new antifungal drugs, and as a therapeutic model in the agricultural and pharmaceutical industries. However, more study is needed to uncover and understand bioactive components that have a variety of biological functions and might be used for human and environmental benefits.

Keywords*:* Bioactive, Endophytes, Enzymatic activity, Fungi, Phytochemical, *Terminalia*

Introduction

In the 21st century global concern focuses on infectious diseases. 25 % of total deaths are caused by pathogenic microorganisms given by the World Health Organization (WHO). Many antibiotics are produced to remove fungal and bacterial infections, but the problem that remains is antibiotic resistance. Due to the development of multi-drug resistance microorganisms which show resistance in two or more classes of antibiotics, this kind of difficulty is displayed nowadays (1). There is a challenge for the development of a better understanding of resistance and finding newer drugs against microbial disease (WHO). Several antimicrobial assays are well-known and commonly used in microbial laboratories nowadays (2). This promotes research for novel antimicrobial agents to prevent resistance and provide relief from diseases (3).

Historically plants contribute a potential source of compounds and species like *Combretum, Terminalia, and Pteleopsis* have found profound antimicrobial effects. The second largest genus, *Terminalia* has nearly about 200

species of the family Combretaceae after Combretum. Plants from the *Terminalia* genus (Combretaceae family) are utilized as traditional medicines all over the world. *Terminalia arjuna, Terminalia belerica,* and *Terminalia chebula* are the most commonly utilized *Terminalia* species in medicine. Members of *Terminalia* are used for the treatment of Cardiovascular problems, wound healing, colds, conjunctivitis, ulcers, headaches, hypertension, jaundice, leprosy, pneumonia & skin diseases, and also for the treatment of HIV and other microbial disease (4, 5). Root, stem-bark samples of *Terminalia arjuna* contain some bioactive compounds like tannins, glycoside, alkaloids, steroids, triterpenoids, etc are known to display both pharmacological and physiological properties (6, 7). It has been found that tannin, a secondary metabolite from *Terminalia sp.* is responsible for anticancer properties (8, 9). *Terminalia* contains ingredients that help for the stimulation of the heart & also help the heart by lowering cholesterol and blood pressure. *T. arjuna* is used for bile duct disorder, asthma, scorpion stings, and poisonings whereas *T.belerica* is used for respiratory tract infections, cough, and sore throat & *T. chebula* is used for treating vaginal infections, and dysentery. In the field of Ayurvedic medicine *Terminalia belerica* in combination with *Terminalia chebula* has been used as a “Health harmonizer” & both are used for lowering cholesterol which prevents the destruction of heart tissue.

Plants and microbes endowed some natural products that have an established record of providing new pharmaceutical medicines (10). Many medicinal plants are recognized for housing endophytic fungi, which are key sources of many bioactive secondary metabolites and enzymes useful in the pharmaceutical business (11-13). Therefore, increasing efforts are made to identify and focus on endophytic fungi from medicinal plants. Fungal organisms that reside in the plant without forming disease or damage to their host, this definition of endophytic fungi includes the symbiotic interaction in which plants and endophytic fungi participate: Parasitism, Commensalism, and Mutualism (14). Endophytes have recently known as a major source of a variety of new physiologically active secondary metabolites possibly useful for human treatment, and a recent study found that 51% of compounds extracted from endophytes (15, 16). Fungi present inside the plant could be a very promising way to produce various metabolites for medicinal, agricultural, and industrial uses (17). Fungal endophytes form a mutual relationship with the plant in which the plant gives shelter & nutrients to the endophytes whereas endophytes produce bioactive substituent which increases the resistance & benefits the plant growth (18, 19).

A great number of antifungal compounds may be found in endophytic fungi isolated from plant *Terminalia* and exploring natural compounds synthesized by endophytic fungus is thought to be a strategy to eliminate resistance while also meeting the demand for the discovery of extremely cost-effective, less toxic antibiotics to treat infectious diseases caused by microorganisms (20).

Materials and Methods

Plant sample collection

Samples like leaves and barks of four *Terminalia sp.* were collected from the campus of Regional Plant Resource Centre, Nayapalli, Bhubaneswar, Odisha. The samples were taken to the laboratory, rinsed to eliminate any dirt, and air-dried. Leaf and bark samples were chopped into with sterile scalpels. Sample fragments were successively surface sterilized in 70% ethanol for 1 minute, 2.5% sodium hypochlorite for 2 minutes, and sterile distilled water 2 times for 1 minute each (21).

Isolation and purification

The inner tissues of the leaves and barks were removed, and approximately 2-3 segments were put in SD agar media and incubated. Daily observations were made un-

til endophytic fungi began to proliferate (22, 23). Following incubation, fungal colonies were collected, streaked on agar plates, and incubated at 30°C for three days, so that the microbial cells were well spaced from each other. The processes like streak plate and central inoculation were repeated 3-4 times until we got purified pathogens.

Preliminary plate test of endophytic fungi for extracellular enzymes and mineral solubilization potential

To carry out the screening of fungi for extracellular enzyme production and mineral solubilization potential, a plate test was performed by inoculating 7days old culture of fungal isolates on media specified for amylase, cellulase, xylanase, L-asparaginase, Lipase, IAA, organic acid production and Phosphate solubilization, Zinc solubilization potential (24-26). A clear zone enclosing the fungal colony formed after 3-5 days of incubation was considered an indicator of enzyme production and mineral solubilizing potential (27).

Preliminary phytochemical screening of isolated fungal extracts

SD broth was prepared for phytochemical screening of fungal isolates. Inoculation of isolated endophytic fungi into the broth and after incubation filtration occurs to separate the mycelial mat. The mat was pulverized in a pestle and mortar with ethyl acetate, methanol, and ethanol individually, and the grounded mycelia were then put into three distinct flasks and stored for 5 days (28). The extract was partitioned into ethyl acetate, aqueous ethanol, and aqueous methanol soluble fractions, and the filtrate of the above fungal isolates was taken for biochemical test. Different biochemical tests like alkaloids, phenols, flavonoids, saponins, steroids, tannins, and glycosides were done with the four samples (Ethanol, Methanol, Ethyl acetate, and Culture filtrate) to know the availability of metabolites.

Biological screening of methanolic extract of fungal endophytes

Three references of plant pathogens, i.e., *Fusarium sp*. were taken for antifungal assay. Endophytic fungi isolated from *Terminalia sp.* were examined for antifungal activity against three pathogens of *Fusarium sp.* by inoculating them using the co-inoculation method on agar media and incubated for 5- 7 days (29). Two pieces of growing mycelial disc of endophytic fungi were inoculated into SD broth & incubated for 10 days. After the incubation period, filtration occurred to separate the culture filtrate and mycelial mat through Whatmann no. 1 filter paper (30). The culture filtrate was concentrated by the Soxhlet apparatus and solvent was added to the concentrated filtrate for 72 hours. The upper layer was separated and evaporated by Soxhlet. Evaporated samples were dissolved in methanol and preparation of methanolic extract was completed. Methanolic extract samples were screened for qualitative phytochemical screening to know the availability of secondary metabolites discussed earlier. A qualitative free-radical scavenging activity test occurred with the methanolic sample and the antimicrobial activity test was done through the pour plate method to find the best test organism (31). The bioactive potential of fungi has been presented in terms of growth reduction (%) of pathogenic fungi, calculated based on morphological growth on solid plate culture.

Results and Discussions

Occurance of fungi on leaf and bark of Terminalia sp.

A total of 29 nos. of fungi have been isolated from samples collected from different species of *Terminalia.* All were characterized morphologically and evaluated for their extracellular enzyme and mineral solubilization potential.

Profiling of endophytic fungi for extracellular enzymes and mineral solubilization potential

Profiling of fungi for enzymes and sol-

ubilization potential is described in Table 1. Cellulase has been used in biofuel, agriculture, food, detergent, and also in textile industries. Cellulase is present in *Phoma sp., Penicillium sp.,* etc. (32). Among all, 6 fungi (24.13%) were found to be producers of cellulase and 11 fungi (37.93%) for xylanase activity. Almost all fungi exhibited zinc-solubilization potential but no IAA, lipase, and L-asparaginase activity could be observed in these fungi. Phosphate solubilization potential has been observed in 4 fungi (13.79%). Many fungal isolates have been observed as organic acid producers in the present study (27.58%). There is limited information about amylase enzymes from endophytic fungus (33). In the present study, 51.7% of the isolates tested positive including *Aspergillus sp., Penicillium sp., Trichoderma sp., Fusarium sp.* etc. As shown in Figure 1, amylase-producer fungi are more in number as well as Zinc solubilization potential. Another fungal extracellular enzyme is lipase which is dominantly used in the food industry. The report says that there are very less findings regarding lipolytic activity. In the present study, no lipolytic activity was found in the fungi isolated from *Terminalia sp.* Microbial L-asparaginase is secreted extracellularly and considered to be intracellular in nature (34), in the present study, no L-asparaginase activity is found positive. A report from (35) says that if tryptophan is used as a substrate then fungi are capable of synthesizing IAA. In the present study, fungi show no activity for producing IAA. Results obtained for extracellular enzyme production and mineral solubilization potential are given in Table 1 and the percentage of incidence is given in Figure 1.

Table 1: Preliminary plate screening tests of fungi for extracellular enzymes, mineral solubilization potential

Sl no	Name of fungal isolates	Extracellular activity, mineral solubilization potential								
		A	B	C	D	E	F	G	H	I
1	*Aspergillus sp. 1*	-	-	-	-	-	-	-	-	+
2	*Aspergillus sp. 2*	-	-	-	-	-	-	-	-	-
3	*Aspergillus sp. 3*	-	+	-	-	+	-	+	+	-
4	*Aspergillus sp. 4*	-	-	-	-	-	-	-	-	-
5	*Aspergillus sp. 5*	-	+	-	-	+	-	+	+	+++
6	*Aspergillus sp. 6*	-	+	-	+++	+	-	-	+	-
7	*Aspergillus sp. 7*	-	+	-	-	+	-	-	+	-
8	*Aspergillus sp. 8*	-	+	-	-	+	-	-	+	-
9	*Aspergillus sp. 9*	-	+	-	+	+	-	+	+	-
10	*Aspergillus sp. 10*	-	+	-	-	-	-	-	+	-
11	*Aspergillus sp. 11*	-	+	-	-	-	-	-	+	++
12	*Aspergillus sp. 12*	-	-	-	-	-	-	-	+	-
13	*Aspergillus sp. 13*	-	+	-	+	+	-	-	+	+
14	*Aspergillus sp. 14*	-	-	-	-	+	-	-	-	+
15	*Aspergillus sp. 15*	-	-	-	+++	+	-	-	+	-
16	*Penicilium sp. 1*	-	+	-	-	-	-	-	+	-

17	*Penicilium sp. 2*	-	-	-	-	-	-	-	+	++
18	*Penicilium sp. 3*	-	+	-	+++	-	-	-	+	-
19	*Penicilium sp. 4*	-	-	-	+	+	-	+	-	+
20	*Trichoderma sp. 1*	-	+	-	-	-	-	-	+	-
21	*Trichoderma sp. 2*	-	-	-	-	-	-	-	+	-
22	*Trichoderma sp. 3*	-	-	-	-	-	-	-	-	-
23	*Myceloid sp. 1*	-	-	-	-	-	-	-	+	-
24	*Myceloid sp. 2*	-	+	-	-	-	-	-	+	+
25	*Fusarium sp. 1*	-	+	-	-	-	-	-	+	++
26	*Fusarium sp. 2*	-	-	-	-	-	-	-	-	-
27	*Nectria sp.*	-	+	-	-	-	-	-	-	-
28	*Acladium sp.*	-	-	-	+++	+	-	-	+	-
29	*Colletotrichum sp.*	-	-	-	-	-	-	-	-	+

Abbreviations: +, (Present) ; ++, (Present Significantly); +++, (Present in excess) ; -, (Absent)

A, Indole acetic acid (IAA); B, Amylase; C, Lipase ;D, Cellulase ;E, Xylanase; F, L-asparaginase; G, Phosphate solubilisation; H, Zinc-solubilization; I, Organic acid.

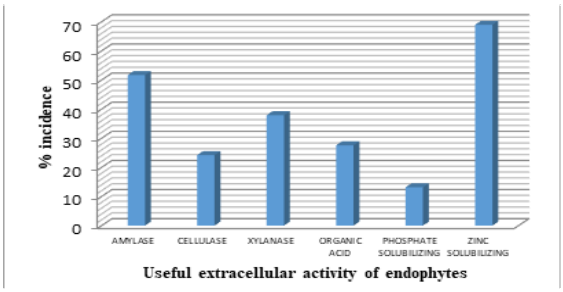

Figure 1: Incidence of fungal endophytes (%) isolated from *Terminalia sp.*

% of incidence= Fungi tested positive/Total isolated fungi × 100

Preliminary phytochemical screening of isolated fungi and plant sample

Phytochemicals, like phenols, tannins, flavonoids, saponins, glycosides, and steroids present in plant extracts which is revealed in the present study (Table 2). *T. arjuna* is a widely used medicinal plant responsible for the treatment of degenerative diseases considered a pharmacological system of medicine (36). Phytochemical screening of extract of endophytes isolated from leaf, and bark sample of four *Terminalia sp.* were completed. This was done to know the presence of bioactive metabolite. Ethanolic, Methanolic, and ethyl acetate extract of crude extract of 29 endophytes and plant samples contain alkaloids, flavonoids, steroids, phenols, saponins, tannins, and glycosides. Alkaloid, the secondary metabolite resides in plant extract which hinders the microorganism by inhibiting the enzymes involved in energy generation. *Terminalia bellerica* containing tannins in plant extract might have hampered the growth of microorganisms by precipitating the microbial protein and making nutritious proteins inaccessible to them (37). There are several reports available on the phytochemical screening of fruit & stem extract but comparatively fewer reports on leaf and bark samples. In one report, ethanolic extract contains all biomolecules, methanolic extract contains all biomolecules except tannins and saponins whereas ethyl acetate extract except saponins, steroids & tannins but in our study it shows the better result that all extract contains all biomolecules (28).

Table 2: Preliminary Phytochemical screening of isolated fungal extracts.

Name of fungal isolates	Secondary metabolites																																	
	Alkaloids				Phenols				Flavanoids				Tanins				Glycosides				Steroids				Saponins			
	M	E	EA	CF	M	E	EA	CF	M	E	EA	CF	M	E	EA	CF	M	E	EA	CF	M	E	EA	CF	M	E	EA	CF
Aspergillus sp. 1	+	+	+	-	+	+	-	+++	-	-	-	-	+	+	+	+++	+	+	+	-	-	-	-	-	-	+	-	-
Aspergillus sp. 2	-	-	-	-	+	+++	+++	-	-	-	-	+	+	+	+	-	-	+	+	-	-	-	+	-	-	-	-	
Aspergillus sp.3	+	++	-	-	+	-	++	++	-	-	-	-	+	+	+	+	-	-	+	+	+++	+++	+++	-	-	-	-	-
Aspergillus sp. 4	++	+	-	-	++	+	++	+	-	-	-	-	+	+	+	+	+	++	+	-	+	+	+	-	-	-	-	-
Aspergillus sp. 5	+	+	+	+	++	++	+	+	-	-	-	-	+	+	+	+	+	+	+	-	+	+	+	-	+	+	+	-
Aspergillus sp. 6	+	+	-	-	+	+++	++	+++	+	-	-	-	+	+	+	++	++++	++	-	+	-	+	+++	+	-	-	-	-
Aspergillus sp. 7	+	+	-	-	+	++	++	+	-	-	+	-	+	+	+	+	++	+++	+	-	-	-	-	-	-	-	-	-
Aspergillus sp. 8	+	-	-	-	+	+	+	+	-	-	-	-	+	+	+	+	++	+	+	+	-	-	-	-	-	-	-	-
Aspergillus sp. 9	+	+	-	+	+	+	+	++	-	+	-	-	+	+	-	+	++	-	-	-	++	-	++	-	-	-	-	-
Aspergillus sp. 10	+	+	-	-	+	-	+	+	-	-	-	+	+	+	+	+	++	+++	+	-	+	+	++	+	-	-	-	-
Aspergillus sp.11	+	+	-	-	+	+	+	+	-	-	-	+	+	+	+	-	-	-	-	-	+	-	+	+	-	-	-	+
Aspergillus sp. 12	-	+	-	-	+++	++	++	+	-	-	-	-	+	+	+	-	+	+	+	-	-	+	++	-	-	-	-	-
Aspergillus sp. 13	+	+	-	-	+++	+++	+++	-	-	-	-	+	+++	+	+++	+	+	+	+	+	+++	+	+	-	-	-	-	-
Aspergillus sp. 14	-	+	-	-	+	++	-	-	-	-	-	+	+	+	-	+	-	-	-	+	-	-	-	-	-	+	-	-
Aspergillus sp. 15	+	+	+	+	+	+	-	+	-	-	-	-	+	+	-	+	+	+	+	-	-	-	+	-	-	+	-	-
Penicillium sp. 1	+	+	-	+	++	+	+	-	-	-	-	-	+	+	+	+	-	-	-	-	-	+	+	-	-	-	-	+
Penicillium sp. 2	+	-	-	-	+	+	+	-	-	-	-	-	+	+	+	-	+	+	-	+	-	-	-	+	-	-	-	-
Penicillium sp. 3	-	+	-	+	+	+	+	-	-	-	-	-	+	+	+	++	+++	+	-	+	-	+	++	-	-	-	-	-
Pernicilium sp. 4	+	+	-	+	+	+	-	+	-	-	-	-	+	+	-	+	-	-	-	-	-	-	-	-	-	-	-	+
Trichoderma sp. 1	+	+	-	+	+	+	+	++	+	+	-	-	+	+	-	+	-	-	-	++	+	+	+	+	-	-	-	-
Trichoderma sp. 2	+	+	-	-	+	+	+	++	+	-	+	-	+	+	+	+	+	+	-	+	+	-	+	-	-	-	-	-
Trichoderma sp. 3	+	+	-	-	+	+	+	++	-	-	-	-	+	+	-	+	+++	+++	-	+	+	-	+	+	-	-	-	-
Myceloid sp. 1	+	+	-	-	++	+	+	+	-	-	-	-	+	+	+	+	-	-	-	-	-	+	+	+	-	-	-	-
Myceloid sp. 2	+	-	-	+	+	-	+	+	-	-	-	-	+	+	+	-	+	+	-	-	-	-	+	+	-	-	-	-
Fusarium sp. 1	-	+	-	-	+++	+	+	++	-	-	+	+	+	+	+	-	-	-	-	-	-	+	+	+	-	-	-	-
Fusarium sp. 2	-	-	-	+	+	+	-	+	-	-	-	-	+	+	-	+	-	-	-	-	-	-	-	-	-	-	-	-
Nectria sp.	-	+	-	-	++	++	-	+	+	+	+	-	+	+	-	+	-	-	-	-	-	-	-	-	+	-	-	-
Acladium sp.	+	+	-	-	++	+++	+	+	-	-	-	+	+	+	-	+	-	+	-	-	+	-	++	+	-	-	-	+
Colletotrichum sp.	+	+	-	-	+	+	-	+	-	-	-	-	+	+	-	+	-	-	-	-	-	-	-	-	-	-	-	-

Abbreviations: +, (Present) ; ++, (Present Significantly); +++, (Present in excess) ; -, (Absent)

M, Methanol; E, Ethanol; EA, Ethyl acetate; CF, Culture filtrate

Biological Screening of methanolic extract of fungal endophytes

Several studies have described the antioxidant properties of different parts of various medicinal plants. Antioxidant activity test, and qualitative biochemical estimation to know the best endophytic fungi for further experiment (Table 3)**.** Some positive results of the test for alkaloids, flavonoids, phenols, tannins, saponins, steroids, and glycosides were recorded. DPPH is a stable nitrogen-centered, lipophilic free radical that is extensively used to evaluate antioxidant activity in a shorter period of time than other techniques. The odd electron in DPPH is coupled with hydrogen from a free radical scavenging antioxidant, resulting in decreased DPPH. The ensuing decolorization from purple to yellow revealed a favorable result (38). After completion of the biological screening test, we selected the best fungal strain. Among all fungi, the methanolic extract of *Aspergillus sp.* 14 indicated the greatest result.

Table 3: Phytochemical and qualitative antioxidant activity test of solvent extract of 29 fungal isolates

Sl no	Fungal isolate	Alkaloids	Phenols	Flavonoids	Tannins	Glycosides	Steroids	Saponins	DPPH
1	*Aspergillus sp. 1*	+	+	-	+	-	+	+	+++
2	*Aspergillus sp. 2*	+	-	-	+	-	+	-	++
3	*Aspergillus sp. 3*	-	+	-	+++	+	+	+	++
4	*Aspergillus sp. 4*	-	-	-	+	+	+	-	-
5	*Aspergillus sp. 5*	+	-	-	+	+	+	+	-
6	*Aspergillus sp. 6*	-	+	-	+	+	+	-	+
7	*Aspergillus sp. 7*	-	-	-	+	+	+	-	-
8	*Aspergillus sp. 8*	-	+	-	+	+	-	-	++
9	*Aspergillus sp. 9*	+	+	++	+	+	+	+	+++
10	*Aspergillus sp. 10*	-	-	-	-	+	-	-	+
11	*Aspergillus sp. 11*	-	+	-	+++	+	++	-	+++
12	*Aspergillus sp. 12*	-	-	-	+	+	-	-	-
13	*Aspergillus sp. 13*	-	-	-	+	-	+	-	+
14	*Aspergillus sp. 14*	+	+	-	++	+	+	+	+
15	*Aspergillus sp. 15*	-	-	-	+	+	-	-	+
16	*Penicillium sp. 1*	+	-	-	+	+	+++	-	+
17	*Penicilium sp. 2*	-	-	-	+	+	+++	-	+++
18	*Penicilium sp. 3*	+	+	+	+	+	+	+	+
19	*Penicilium sp. 4*	+	-	+	++	+	++	+	+++
20	*Trichoderma sp. 1*	+	+	-	+	-	++	+	-
21	*Trichoderma sp. 2*	-	+	-	+++	+	+++	-	++
22	*Trichoderma sp. 3*	+	+	-	++	+	++	-	++
23	*Myceloid sp.1*	-	+	+	+	++	++	+	+
24	*Myceloid sp. 2*	-	+	-	+	++	+	-	++
25	*Fusarium sp. 1*	-	-	-	+	+	++	-	-
26	*Fusarium sp. 2*	-	-	-	+	+	+	-	++
27	*Nectria sp.*	-	-	-	+	+	-	-	++
28	*Acladium sp.*	+	-	++	-	+	+++	+	+++
29	*Colletotrichum sp.*	-	-	-	+	-	-	-	-

Abbreviations: +, (Present) ; ++, (Present Significantly) ; +++, (Present in excess) ; -, (Absent)

The solvent extract of *T. bellerica* was tested against *S. aureus* and *K. pneumonia*, which are two respiratory pathogens that indicated the greatest activity (39). The antimicrobial activity of different solvent extracts of *Terminalia sp.* was conducted against four bacteria and two viruses and the various solvent extracts were hexane, benzene, chloroform, Ethyl acetate, Acetone, Ethyl alcohol and methanolic extracts, among all the extracts studied, methanol and ethyl acetate extracts exhibited good effects against NDV, PV virus, S. aureus, and E. coli (40). In our study, the prepared methanolic sample of 29 fungi undergoes antimicrobial activity test against three *Fusarium sp.,* result denoted in Table 4**.** This was demonstrated in terms of growth reduction (%) of pathogenic fungi, calculated based on morphological growth on solid plate culture, indicating that there was an inhibition of growth of the test microbe. So *Aspergillus 14* was considered a good source of antimicrobial compounds. This finding suggested that the antimicrobial compounds generated by active fungal endophytes might have specialized applications where disease control is needed.

Table 4: Antimicrobial activity test of methanolic extract of 29 fungal isolates

Pathogens				
		D1	D2	D3
Sl no	Fungal isolate	% of growth reduction	% of growth reduction	% of growth reduction
1	*Aspergillus sp. 1*	1.45±0.77	11.83±2.305	13.3±0
2	*Aspergillus sp. 2*	10.82±1.666	17.84±0.749	16.51±2.142
3	*Aspergillus sp. 3*	13.1±4.101	18.76±0.657	17.6±1.088
4	*Aspergillus sp. 4*	1.1±0.42	12.85±0.855	5.78±1.103
5	*Aspergillus sp. 5*	12.82±1.661	1.96±0.063	16.52±0.975
6	*Aspergillus sp. 6*	7.81±2.559	1.74±0.424	19±0.219
7	*Aspergillus sp. 7*	6.68±0.417	3.38±1.640	16.5±3.344
8	*Aspergillus sp. 8*	4.35±2.877	7.88±1.725	14.63±1.845
9	*Aspergillus sp. 9*	11.5±1.195	14.59±1.364	3.66±0.049
10	*Aspergillus sp. 10*	13.36±0.841	5.63±1.675	7.32±0.919
11	*Aspergillus sp. 11*	4.35±2.863	8.99±0.141	2.55±1.52
12	*Aspergillus sp. 12*	12.8±1.93	15.52±1.067	13.53±2.375
13	*Aspergillus sp. 13*	13.9±0.378	8.07±1.774	8.88±0.41
14	*Aspergillus sp. 14*	15.4±1.209	20.69±3.549	16.4±2.59
15	*Aspergillus sp. 15*	11.93±0.806	12.64±0.205	19.43±3.146
16	*Penicillium sp. 1*	4.99±1.774	17.5±1.64	6.6±0.077
17	*Penicilium sp. 2*	9.01±3.705	1.68±0.763	1.83±0.48
18	*Penicilium sp. 3*	6.58±2.729	6.74±0.113	8.07±1.159
19	*Penicilium sp. 4*	5.49±1.873	8.03±1.491	18.6±0.806
20	*Trichoderma sp. 1*	2.9±1.272	4.92±1.195	19.2±1.131
21	*Trichoderma sp. 2*	*2.4±2.26*	10.83±1.852	5.77+1.294

22	*Trichoderma sp. 3*	9.65±4.023	8.63±0.961	6.59±0.106
23	*Myceloid sp.1*	4.7±4.101	16.8±1.944	2.48±1.195
24	*Myceloid sp. 2*	8.2±0.84	6.74±0.106	1.09±0.502
25	*Fusarium sp. 1*	12.5±0.318	21.32±4.426	11.35±0.339
26	*Fusarium sp. 2*	11.93±0.799	15.5±1.117	4.54±0.53
27	*Nectria sp.*	2.18±0.141	17.23±1.286	9.37±0.891
28	*Acladium sp.*	2.23±0.141	10.06±4.617	6.6±1.138
29	*Colletotrichum sp.*	7.58±1.074	6.9±0.113	5.79±1.23

Abbreviations: D1, *Fusarium sp.* 1 ; D2, *Fusarium sp.* 2 ; D3, *Fusarium sp.*3 ;

Conclusion

We can conclude that endophytic fungi isolated from four *Terminalia sp.* may be a valuable natural resource for producing physiologically active chemicals with significant antifungal activity against *Fusarium sp.* We also reported that the endophytic fungi are very effective in eliciting the production of secondary metabolite that acts against plant pathogens. Further research into the compounds' purity and structure is underway. It is thought that finding natural compounds formed by endophytes may be a viable strategy to overcome the problem of resistance and meet the emerging desire for highly effective, low-toxicity, and environmentally friendly antibiotics to combat infections.

Conflicts of interest

The authors declare that there are no conflicts of interest.

Acknowledgements

The financial support from the Forest, Environment and Climate Change department, Govt. of Odisha (State plan- 2023-24) is gratefully acknowledged. The authors are thankful to the Chief Executive, Regional Plant Resource Centre, Bhubaneswar, Odisha, for providing the necessary laboratory, and administrative facilities for this research project and also highly grateful to Dr. U.C. Basak, Senior Scientist, Regional Plant Resource Centre, Bhubaneswar, Odisha, for the identification of plant species.

References

1. Bou, G., Otero, F.M., Santiso, R., Tamayo, M., Fernández, M.D.C., Tomás, M., & Fernández, J.L. (2012). Fast assessment of resistance to carbapenems and ciprofloxacin of clinical strains of Acinetobacter baumannii. Journal of clinical microbiology, 50(11): 3609-3613.
2. Balouiri, M., Sadiki, M., & Ibnsouda, S.K. (2016). Methods for in vitro evaluating antimicrobial activity: A review. Journal of pharmaceutical analysis, 6(2): 71-79.
3. Levy, S.B. (2005). Antibiotic resistance—the problem intensifies. Advanced drug delivery reviews, 57(10): 1446-1450.
4. Debnath, S., Dey, D., Hazra, S., Ghosh, S., Ray, R., & Hazra, B. (2013). Antibacterial and antifungal activity of Terminalia arjuna Wight & Arn. bark against multi-drug resistant clinical isolates. Journal of Coastal Life Medicine, 1(4): 312-318.
5. Dwevedi, A., Dwivedi, R., & Sharma, Y.K. (2016). Exploration of phytochemicals found in Terminalia sp. and their antiretroviral activities. Pharmacognosy Reviews, 10(20): 73.
6. Mandal, S., Patra, A., Samanta, A., Roy, S., Mandal, A., Mahapatra, T.D., & Nandi, D.K. (2013). Analysis of phytochemical profile of Terminalia arjuna bark extract with antioxidative and antimicrobial prop-

erties. Asian Pacific journal of tropical biomedicine, 3(12): 960-966.

7. Adebayo, E.A., & Ishola, O.R. (2009). Phytochemical and antimicrobial screening of crude extracts from the root, stem bark, and leaves of Terminalia glaucescens. African journal of pharmacy and pharmacology, 3(5): 217-221.

8. Jain, S., Yadav, P.P., Gill, V., Vasudeva, N., & Singla, N. (2009). Terminalia arjuna a sacred medicinal plant: phytochemical and pharmacological profile. Phytochemistry Reviews, 8: 491-502.

9. Saxena, V., Mishra, G., Saxena, A., & Vishwakarma, K.R. (2013). A comparative study on quantitative estimation of tannins in Terminalia chebula, Terminalia belerica, Terminalia arjuna and Saraca indica using spectrophotometer. Asian Journal of Pharmaceutical and Clinical Research, 6(3): 148-149.

10. Balagurunathan, R., & Radhakrishna, M. (2007). Exploiting the less explored-microbial endophytes. Adv Biotechnol, 6: 20-3.

11. Zou, W.X., Meng, J.C., Lu, H., Chen, G.X., Shi, G.X., Zhang, T.Y., & Tan, R.X. (2000). Metabolites of Colletotrichum gloeosporioides, an endophytic fungus in Artemisia mongolica. Journal of Natural Products, 63: 15.

12. Strobel, G., Daisy, B., Castillo, U., & Harper, J. (2004). Natural products from endophytic microorganisms. Journal of Natural Products, 67: 257–268.

13. Krishnamurthy, Y.L., Naik, S.B., & Jayaram, S. (2008). Fungal communities in herbaceous medicinal plants from the Malnad region, southern India. Microbes and Environments, 23: 24–28.

14. Stone, J.K., Polishook, J.D., & White, J.F. (2004). Endophytic fungi. Biodiversity of fungi: inventory and monitoring methods, 241: 270.

15. Schulz, B., Boyle, C., Draeger, S., Römmert, A.K., & Krohn, K. (2002). Endophytic fungi: a source of novel biologically active secondary metabolites. Mycological research, 106(9): 996-1004.

16. Strobel, G.A. (2003). Endophytes as sources of bioactive products. Microbes and infection, 5(6): 535-544.

17. Huang, W.Y., Cai, Y.Z., Hyde, K.D., Corke, H., & Sun, M. (2008). Biodiversity of endophytic fungi associated with 29 traditional Chinese medicinal plants. Fungal diversity, 33: 61-75.

18. Bills, G.F. (1996). Isolation and analysis of endophytic fungal communities from woody plants. Endophytic fungi in grasses and woody plants: systematics, ecology, and evolution, pp. 31-65.

19. Kouipou Toghueo, R.M., & Boyom, F.F. (2019). Endophytic fungi from Terminalia species: a comprehensive review. Journal of Fungi, 5(2): 43.

20. Toghueo, R.M., Zabalgogeazcoa, I., de Aldana, B.V., & Boyom, F.F. (2017). Enzymatic activity of endophytic fungi from the medicinal plants Terminalia catappa, Terminalia mantaly and Cananga odorata. South African Journal of Botany, 109: 146-153.

21. Tejesvi, M.V., Mahesh, B., Nalini, M.S., Prakash, H.S., Kini, K.R., Subbiah, V., & Shetty, H.S. (2005). Endophytic fungal assemblages from inner bark and twig of Terminalia arjuna W. & A.(Combretaceae). World Journal of Microbiology and Biotechnology, 21: 1535-1540.

22. Basha, N.S., Ogbaghebriel, A., Yemane, K., & Zenebe, M. (2012). Isolation and screening of endophytic fungi from Eritrean traditional medicinal plant Terminalia brownii leaves for antimicrobial activity. International Journal of Green Pharmacy (IJGP), 6(1): 40-44.

23. Phongpaichit, S., Rungjindamai, N., Rukachaisirikul, V., & Sakayaroj, J. (2006). Antimicrobial activity in cultures of endophytic fungi isolated from Garcinia species. FEMS Immunology & Medical Microbiology, 48(3): 367-372.

24. Rajoriya, A., & Gupta, N. (2016). Useful extracellular enzymatic activity of mycelial culture of some edible mushrooms of Odisha. Agricultural Research & Technology: Open Access Journal, 3(1): 23-27.

25. Kumar, R., Sedolkar, V.K., Triveni, A.G., Kumar, M.S., Shivannavar, C.T., & Gaddad, S.M. (2016). Isolation, screening and characterization of L-asparaginase producing fungi from medicinal plants. Int J Pharm Pharm Sci, 8*(*1): 281-283.

26. Shrivastava, U.P., & Kumar, A. (2011). A simple and rapid plate assay for the screening of Indole-3-Acetic Acid (IAA) producing microorganisms.

27. Hankin, L., & Anagnostakis, S.L. (1975). The use of solid media for detection of enzyme production by fungi. Mycologia, 67(3): 597-607.

28. Shivaputrappa, J., & Vidyasagar, G.M. (2018). Evaluation of Phytochemical and Antimicrobial Potential of Endophytic Fungi Nigrospora Oryzae Isolated from Terminalia BellericaRoxb. International Journal of Health Sciences and Research, 8(8): 81-88.

29. Sabat, J., & Gupta, N. (2009). Development of modified medium for the enhancement in antifungal activity of P. steckii (MF1 Mangrove Fungi) against Verticillium Wilt pathogenic fungi of rose. *Brazilian* Archives of Biology and Technology, 52: 809-818.

30. Arivudainambi, U.E., Kanugula, A.K., Kotamraju, S., Karunakaran, C., & Rajendran, A. (2014). Antibacterial effect of an extract of the endophytic fungus and its cytotoxic activity on MCF-7 and MDA MB-231 tumour cell lines. Biological Letters, 51(1): 7-17.

31. Rout, P., & Basak, U.C. (2012). Antioxidant properties in leaf and root extracts of some medicinally important mangrove species of Odisha coast. Am. J. Pharm. Tech. Res, 4: 1-13.

32. Kuhad, R.C., Gupta, R., & Singh, A. (2011). Microbial cellulases and their industrial applications. Enzyme research, 2011(1): 280696.

33. Spier, M. R. (2005). *PRODUÇÃO DE ENZIMAS AMILOLÍTICAS FÚNGICAS α-AMILASE e AMILOGLUCOSIDASE POR FERMENTAÇÃO NO* (Doctoral dissertation, Universidade Federal do Paraná).

34. Narayana, K.J.P., Kumar, K.G., & Vijayalakshmi, M. (2008). L-asparaginase production by Streptomyces albidoflavus. Indian Journal of Microbiology, 48: 331-336.

35. Bose, A., Shah, D., & Keharia, H. (2013). Production of indole-3-acetic-acid (IAA) by the white rot fungus Pleurotus ostreatus under submerged condition of Jatropha seedcake. Mycology, 4(2): 103-111.

36. Nema, R., Jain, P., Khare, S., Pradhan, A., Gupta, A., & Singh, D. (2012). Antibacterial and antifungal activity of Terminalia arjuna leaves extract with special reference to flavonoids. Basic Res J Med Clin Sci, 1(5): 63-65.

37. Huang, J.W., & Chung, W.C. (2003). Management of vegetable crop diseases with plant extracts. In Advances in plant disease management, 2003, pp.153-163.

38. Gupta, R., Singh, R.L., & Dwivedi, N. (2016). In vitro antioxidant activity and GC-MS analysis of the ethanolic extracts of Terminalia bellerica ROXB (Baheda). Int J Pharm Pharm Sci, 8(11): 275-282.

39. Sabnis, S. (2014). Antimicrobial efficacy of Terminalia bellerica against virulence factors of respiratory pathogens. Int. J Curr. Microbiol & Appl Sci, 3(5): 215-218.

40. Nagendraswamy, G., Lakshmi Ranganatha, V., Bushra Begum, A., Prashanth, T., Alghorbani, M., & Zameer, F. (2013). Extraction and Evaluation of Antimicrobial and Antiviral Efficacy of Terminalia bellirica. Fruits. Indo, 4262-4268.

Current Trends in Biotechnology and Pharmacy
Vol. 19(1) 2193-2203, January 2025, ISSN 0973-8916 (Print), 2230-7303 (Online)
DOI: 10.5530/ctbp.2025.1.8

Formulation and evaluation of Azithromycin Dihydrate Niosomes for the Effective Treatment of Bacterial Infection

Neha Srivastava* [1], Seema Thakur [2], Kamaljeet Kaur[2]

[1]School of Pharmaceutical Sciences, RIMT University, Mandi Gobindgarh, Punjab.
[2]PCTE Group of Institutes, Faculty of Pharmaceutical Sciences, Baddowal Cantt, Ludhiana, Punjab

Corresponding Author: nehasrvstva@gmail.com

Abstract

Azithromycin dihydrate is a semi-synthetic macrolide antibiotic of the azalide class for the treatment of bacterial infection. Niosomes are microscopic lamellar structures of non-ionic surfactant bilayer vesicular structures that allow the medications to be encapsulated within, allowing for regulated delivery of the drugs over an extended period. The niosomes were designed which serve the combined advantages of loading the suitable amount of drug required for treatment, modulating its release at the target site, and controlling the bacterial resistance. It also helps to reduce the dose and frequency of the drugs leads to reduction in side effects. In the present work, niosomes of Azithromycin dihydrate were prepared and evaluated for the treatment of bacterial infection. Different formulations of niosomes were designed and prepared by hand shaking method using different ratios of cholesterol, non-ionic surfactant, sodium deoxycholate, chloroform, and methanol. The prepared niosomes were evaluated for different parameters such as entrapment efficiency, vesicle size and shape, and *in vitro* release study. The drug-excipient interaction was evaluated with the help of FTIR spectra and all the peaks in physical mixtures as well. The efficiency of entrapment was found to be highest for F6 (92.4%). The particle size of the optimized formulation was shown 226.2 nm. SEM analysis indicated that the niosomes are spherical and the size of the niosomes vesicle was in range. *In vitro* drug release studies of the optimized formulation F6 showed maximum drug release of 88.4% after 24 h. The release profiles were subjected to different mathematical models and the best-suited model was found to be the Korsemeyer Peppas model with the highest regression value (0.9225) via the fickian diffusion mechanism.

Keywords Azithromycin, niosomes, vesicular system, drug release kinetics

Introduction

The vesicular drug delivery system is a novel system designed with multiple concentric lipid layers of amphiphilic surfactants and water. Vesicular delivery systems have proven beneficial over conventional delivery systems due to prolonging systemic circulation, improving bioavailability, surpassing metabolic pathways, and reducing drug-related toxicity (1). This system is also highly beneficial as it can hold hydrophilic as well as lipophilic drugs in the multiple-layer concentric vesicular structure. Along with the several advantages the vesicular delivery system also possesses several disadvantages such as lower drug loading capacity, and leakage of drugs from the vesicles during storage and transportation. The efficacy of vesicles highly depends on the size of the vesicle, type, loading capacity, lamellarity, and construction of the vesicle. The vesicular drug delivery system plays a promising role in the target specificity of the drug, can deliver the drug in a controlled

and sustained fashion, and can be administered through multiple routes. Drug delivery systems including nanovesicles are broadly classified as liposomes, niosomes, proniosomes, ethosomes, polymersomes, phytosomes, aquazomes, and many more (2).

Niosomes are microscopic lamellar structures of non-ionic surfactant vesicles that are formed by combining cholesterol with an alkyl or dialkyl polyglycerol ether class non-ionic surfactant, then hydrating the combination in aqueous medium. These lipid vesicular structures resemble liposomes and can transport both lipophilic and amphiphilic medications (3). Figure 1 represents the structure of niosomes. Niosomes are lamellar particles that range in size from 10 to 1000 nm and belong to the nano-size range (4). Niosomes are made of cholesterol and surfactant, which is followed by lipid film hydration. The main component of niosomes, which gives them greater stability than liposomes, is a non-ionic surfactant. These niosomes are less expensive, less prone to oxidation, and less vulnerable to the material's quality affecting their size and shape (5). Numerous non-ionic surfactant types, such as Brij, Tweens, Spans, polyglycerol alkyl ethers, crown ethers, ester-linked surfactants, glucosyl dialkyl ethers, and polyoxymethylene alkyl ethers, have the potential to generate niosomes (6). These carriers show great promise for topical medication delivery and may enhance therapeutic efficacy while mitigating adverse effects (7).

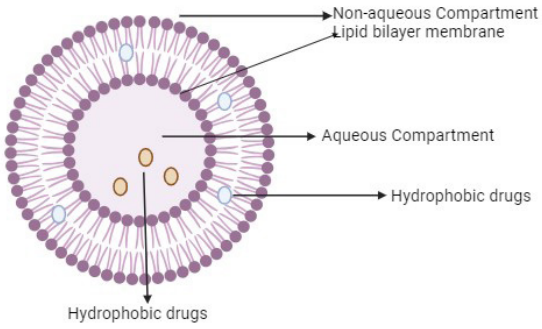

Figure 1: Structure of niosomes

Niosomes are made of bilayer structures that allow the medications to be encapsulated within, allowing for regulated delivery of the drugs over an extended period. This is a new method of medication targeting by surface modification by decreasing the amount that must be given to produce the intended result (8). By encapsulating the medication, lowering its rate of clearance, and directing it to a particular location, the therapeutic efficacy of the medications is increased. Medication targeting aids in drug localization and generates therapeutic benefits at low dose concentrations with fewer adverse effects (9). These could serve as the reservoirs, which release the drug in a controlled manner targeting the affected organs or cells (10).

Although niosomes are less stable physically, they show good chemical stability. The stability of niosomes is caused by a variety of forces, such as van der Waals forces between surfactant molecules, entropic repulsive forces of the head groups of surfactants, short-acting repulsive forces, etc. These are the forces that support the preservation of the noisome's vesicular structure (11).

Azithromycin is one member of the azalide class of semi-synthetic macrolides. By attaching itself to the 50S ribosomal subunit of the bacterial 70S ribosome, it prevents the synthesis of proteins by bacteria. Depending on the organism, it may have bacteriostatic or bactericidal effects (12). Azithromycin undergoes phagocytotic uptake by phagocytic cells and fibroblasts which take the drug and deliver it to the site of infection. On arrival at the site of infection, azithromycin is released to the surface of the cell membrane of the bacteria cell where it binds with ribosomes. The binding of the drug with ribosomes leads to cell death or inhibits the growth of bacteria (13). The current study aims to develop niosomes loaded with the required amount of Azithromycin for the treatment of bacterial infection. The niosomes were designed which serve the combined advantages of loading the suitable amount of drug required for treatment and modulating its release at the

target site. It also improves the penetrability of the drug and helps to deliver the drug to the target site. The controlled delivery system also presents an additional advantage toward bacterial resistance as the dose of the drug in the system remains controlled which reduces the bacterial resistance.

Material and Method

The drug Azithromycin was a gift sample from Biomedica International, Ludhiana. Sodium deoxycholate was obtained from Molychem., Badlapur, Dist., Thane. Cholesterol was obtained from Avarice Laboratories Pvt. Ltd., Ghaziabad. Sorbitan ester 20, Sorbitan ester 40, Sorbitan ester 60, and Sorbitan ester 80 were obtained from Central Drug House (P) Ltd., New Delhi. All the other reagents and solvents were of AR grade.

Methods

Drug excipient interaction

Drug-excipient interaction was done by using FTIR spectrophotometry. KBr pellet technique was used for FTIR studies. The spectrum for the drug Azithromycin in pure form and its physical mixture with other excipients were obtained and studied for any interactions between the drug and excipients (14).

Preparation of Azithromycin dehydrate niosomes

The niosomes of Azithromycin dihydrate with different excipients in different ratios were prepared by the handshaking method. 10 mL of organic solvent (2:1 ratio of methanol and chloroform) was taken in the round bottom flask. To this cholesterol, non-ionic surfactants and drugs were dissolved.

Different ingredients used in the formation of niosomes such as surfactant, cholesterol, and drug are dissolved in 10 ml of organic solvents (2:1 ratio of methanol and chloroform) in a round bottom flask. The organic solvent was allowed to evaporate at room temperature by rotating the flask, which led to the deposition of the thin film on the wall of the flask. The dried film of surfactant was reconstituted with 10 ml of Phosphate buffer pH 7.4 for 1 hour at 60 °C with gentle agitation. The prepared noisomes were kept overnight at 4 °C and then stored in a refrigerator for further use (15, 16). Formulations were prepared using changing ratios of cholesterol, surfactant, and drug are listed in Table 1.

Table 1: Compositions (W/W) Of Niosomes of Azithromycin Dehydrate

Formulation code	Ratios	Span 60	Span 80	Span 20	Cholesterol	Azithromycin dihydrate	SDC
F1	1:1	1	-	-	1	-	-
F2	1:1:1	1	-	-	1	1	1
F3	2:1:1	2	-	-	1	-	1
F4	2:1	2	-	-	1	1	-
F5	1:1:1	-	1	-	1	1	1
F6	1:1:1	1	-	-	1	1	1
F7	1:1:0.5	1	-	-	0.5	1	1
F8	1:1:1	-	-	1	1	1	1

Evaluation of Azithromycin dehydrate niosomes

Particle size analysis and Zeta potential analysis

The size of the particle of the prepared niosomes was determined by Malvern Zeta sizer (Zeta sizer 3, Malvern, UK) at 25 °C using a dynamic light scattering technique (17, 18). The sample of particle size was prepared in demineralized water. The niosome's stability depends upon the zeta potential of niosomal preparation. For nanosized molecules, the zeta potential indicates the strength of repulsion between neighboring particles having similar charges. A higher value of zeta potential indicates stability, or the capacity of the solution or dispersion to withstand aggregation. Zeta potential was determined using a Malvern zeta sizer.

Surface morphology

The surface morphology of the prepared niosomes was studied using a scanning electron microscope (SEM) (JSM 6100, Jeol, Japan), and the noisome were examined. The sample was directly mounted onto the SEM sample stub using the stick tape and coated with a 200 nm thick gold layer at a lowered pressure of 0.001 mmHg. An appropriate magnification was used to take photographs (19, 20).

Entrapment efficiency

The difference between the total amount of drug and the unentrapped amounts was used to calculate the entrapment efficiency. Each formulation was centrifuged using a Remi centrifuge (REMI LJ01*, Mumbai)* for 30 minutes at room temperature (25°C) at 5000 rpm to separate the drug in supernatant liquid which was entrapped in the niosomal structure. The sample was analyzed using a UV spectrophotometer (Shimadzu, Japan), and the amount of drug was determined at 214 nm. % entrapment efficiency was calculated (21). The below mention equation was used to study the entrapment efficiency:

Entrapment efficiency = (Amount entrapped / total amount) x 100

In-vitro drug release study

In vitro, the release of Azithromycin dihydrate from the niosomal structure was carried out using a slightly modified version of Hu's technique. Drug release experiments were conducted on each formulation. The glass cylinder used to construct the diffusion cell was hollow and made of Borosil glass, measuring 14.5 cm in length and 2.50 cm in diameter on inner wall of the tube. Himedia dialysis membrane (molecular weight cut-off: 12000–14000), which had been soaked in warm water beforehand, was placed over one end of the cylinder. The 250 ml beaker that was used as the receptor compartment held the manufactured diffusion cell. The magnetic bead inside the receptor cell rotated at a steady speed. With the use of a thermostat, the temperature inside the manufactured diffusion cell and receptor cells was kept at 37°C. The receiving cell was filled with phosphate buffer saline (100 ml) with a pH of 7.4. Each formulation's 1 ml sample was added to the dissolution cell. The receiving compartment was sampled (5 mL) at predetermined intervals of 1, 2, 3, 5, 6, 7, 8, 9, 10, 11, 12, 16, and 24 hours—every time the sample was replaced with phosphate buffer saline (pH 7.4). The Azithromycin dihydrate content of the samples was determined using a UV spectrophotometer (Shimadzu UV-160, Japan) set to 214 nm as the λmax (22, 23). The temperature of the system was maintained at 37ºC.

Drug release kinetics

The selected formulations were subjected to kinetics equations for drug release such as first-order kinetics, zero-order kinetics, Korsymeyer-Peppas model, Higuchi model, and Hixon Crowell model. The best-fitted model is selected based on regression value, the model with the highest regression is the governing release pattern for the prepared formulations. The drug release kinetics indicated the release

mechanism pattern from the niosomes. The equation of the different models is as follows:

$$\text{Zero order model}: \ M_t = kt + M_0$$

$$\text{First order model}: \ M_t = M_0^{e^{kt}}$$

$$\text{Higuchi model}: \ \frac{M_t}{M_\infty} = kt^{1/2}$$

$$\text{Korsmeyer} - \text{Peppas model}: \ \frac{M_t}{M_\infty} = kt^n$$

Where M_t stands for the drug amount released from the conjugated system at time t, and M_0 is the total amount of the drug in the conjugated system. M_t/M_∞ is the fraction of the released drug, n is the diffusion exponent and k is the rate constant.

The value of n in the Korsmeyer Peppas model indicated the release mechanism from the formulated structures. If the value ranges between 0.45 to 0.89, indicating the release mechanism. Suppose the value is less than 0.45 the release was considered to follow Fick's law and termed as fickian diffusion from a non-swellable matrix type. If the value of n is between 0.45 to 0.89, the release is non-fickian and considered to be released both by diffusion and erosion. If the value of n is more than 0.89, it is case II transport and if the value is more than 1 it is super case II transport (24).

Result and Discussion

Different formulations were prepared using Azithromycin dehydrate niosomes for ocular delivery along with other ingredients. Azithromycin is a macrolide antibiotic that is semi-synthetic and efficient against a broad range of bacteria. Its main application is the treatment of bacterial illnesses linked to weakened immune systems. It was observed that Azithromycin dehydrate has poor solubility and low bioavailability which makes it a suitable candidate for drug delivery (19). Noisomes are prepared using non-ionic surfactants and cholesterol. Typically, cholesterol is added to non-ionic surfactants to give the niosomal bilayer stiffness and orientational order. It increases stability, lessens aggregation, and permits vesicle formation. It is also known that cholesterol prevents the niosomal systems' gel-to-liquid phase transition, making the niosomes less prone to leakage (25). Span 60 is a non-ionic surfactant. It has a higher alkyl chain length and phase transition temperature. Span 60 has shown higher entrapment efficiency due to their higher alkyl chain length (26). Span 80 has an unsaturated alkyl chain and a lower phase transition temperature. Span 80 has shown lower entrapment efficiency due to the unsaturated alkyl chain in their structure. Sodium deoxycholate is a negative charge inducer (27). It was observed that formulations F1, F2, F3, and F4 vesicle were not formed due to lower content of cholesterol and surfactants in the formulations while from F5 to F8 vesicles were formed due to high concentration. The results of different formulations are tabulated in Table 2.

Drug excipient interaction

FTIR spectra of pure Azithromycin dihydrate and the polymers individually as well as the combination of the drug with all the other polymers are shown in Figures 2 and 3 and tabulated in Tables 3 and 4. The spectra indicated the presence of prominent peaks at 1720 cm^{-1} corresponding to carboxylic acid; another peat of C-O stretching was present at 1378.19 cm^{-1}. The stretching of the OH group is observed at 1188.48 cm^{-1}. The physical mixture exhibits similar peaks at 1720.77 for carboxylic acid, 1378.36 cm^{-1} for C-O stretching, and 1188.48 cm^{-1} for OH stretching. No significant changes in intensity of the FTIR bands of Azithromycin dihydrate were observed with polymers indicating the absence of interaction. The peak wavelength is shown in Table 2**.** Figures 2 and 3 represent the FTIR spectrum of the pure drug azithromycin dihydrate and the physical mixture of azithromycin dihydrate-excipient

Table 2: FTIR peak frequency and their corresponding functional groups of physical Mixture of drug and excipients

S . No	(KBr disc) peaks at	Indications
1.	1720.77	C=O group stretching is present (1500 - 2000)
2.	1378.36	C-O stretching is present (1400 - 1310)
3.	1188.86	O-H group stretching is present (1100-1200)
4.	955.73	C-H group bending is present (700-950)

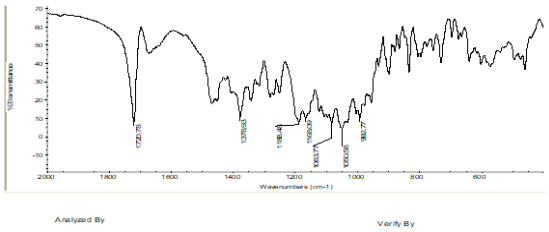

Figure 2: FTIR spectrum of pure drug azithromycin dihydrate

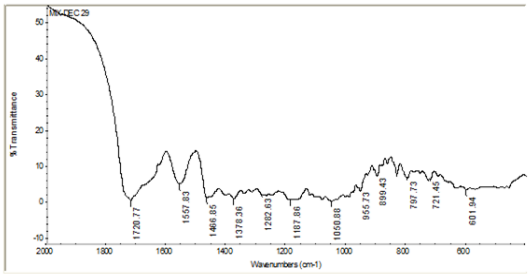

Figure 3: FTIR spectra of the physical mixture of azithromycin dihydrate-excipient

Entrapment efficiency

The drug content analysis of different formulations was done according to the procedure given in the methodology section. The results were tabulated in Table 3. It was observed that the entrapment efficiency of the vesicle of span 60 was found to be higher due to higher alkyl chain length. Very low cholesterol content in formulation also causes low entrapment efficiency which might lead to leakage of the vesicle. The entrapment efficiency was enhanced by increasing the cholesterol along with span 60 due to higher phase transition temperature (28).

The highest entrapment efficiency for the formulation F6 was found to be 92.4% and F5 was found to be 88.2%. The highest entrapment was due to the optimum concentration of span 60 and cholesterol. This leads to higher entrapment of the drug Azithromycin dihydrate.

The head groups of Span 60 and Span 80 are similar, the difference is in the chain length and branching of the chain. The Alkyl chain of span 80 is unsaturated. The permeability of liposomes is markedly enhanced upon the introduction of double bonds into paraffin chains, which may account for the Span 80 systems' lower entrapment efficiency (29). The entrapment efficiency was lower in the formulations F7 (81.8%) and F8 (79.3%) due to the unsaturated alkyl chain length of their surfactant and lower transition temperature.

Table 3: Entrapment efficiency of F5-F8 formulations

Sr. No.	Formulation Code	Entrapment Efficiency (%)
1	F5	88.2±0.56
2	F6	92.4±0.12
3	F7	81.8±0.43
4	F8	79.3±0.14

Particle size and polydispersibility

By using the Malvern Zetasizer (Zets sizer, 3, Malvern, UK) at 25 °C based on dynamic light scattering, the noisome size distribution was determined. Niosome particle size is depicted in Figures 4 and 5. When a drug is encapsulated in nonionic surfactant vesicles, the particle size typically rises. This is likely because of the interaction of the drug with the surfactant head groups. This leads to a rise in the charges and results in mutual repulsion of the bilayer of surfactant (30).

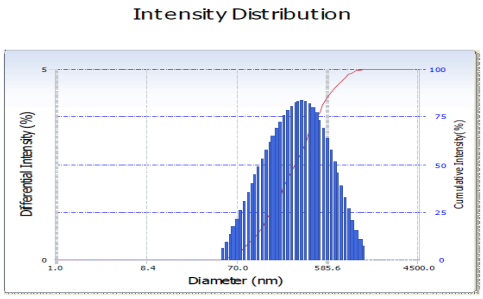

Figure 4: Particle Size of Niosomes

Cumulants Results			
Diameter	(d)	: 226.2	(nm)
Polydispersity Index	(P.I.)	: 0.304	
Diffusion Const.	(D)	: 2.175e-008	(cm²/sec)
Measurement Condition			
Temperature		: 25.0	(°C)
Diluent Name		: Buffer	
Refractive Index		: 1.3318	
Viscosity		: 1.0788	(cP)
Scattering Intensity		: 9840	(cps)

Figure 5: Polydispersity index of Niosomes

The polydispersity index was calculated as a polydispersity index of 1 indicating that globule size is varying on the larger scale. The observed value of 0.3 indicated that size variation is narrow and acceptable. Figure 5 shows the polydispersity index of niosomes.

Scanning electron microscopy

SEM images shown in Figure 6 confirm the preparation of niosomes. By field emission SEM image of the best formulation confirms that there is no aggregation the photograph reveals a smooth surface and the average length of the structure was in the nm range (31). Figure 6 represents the SEM images of prepared niosomes.

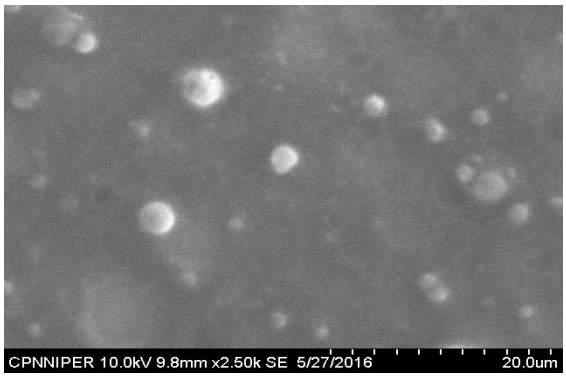

Figure 6: SEM image of prepared niosomes

The *in vitro* permeation of Azithromycin dihydrate was carried out by cellophane membrane. Vesicle suspensions were placed over the membrane. The donor compartment was clamped over it with the help of springs. Samples of 3 ml were withdrawn at predetermined (1, 2, 3, 4, 5, 6, 7, 8, 9, 10, 11, 12, 16, 20 and 24 hrs) time intervals from the receptor compartment. Graphs plotted between the percent cumulative drug releases versus time are shown in Figure 7**.** It was observed that a 1:1:1 ratio of Span: Cholesterol: Azithromycin shows maximum drug release and is considered as optimum formulation (32). Figure 7 represents the in vitro drug release profile of different formulations.

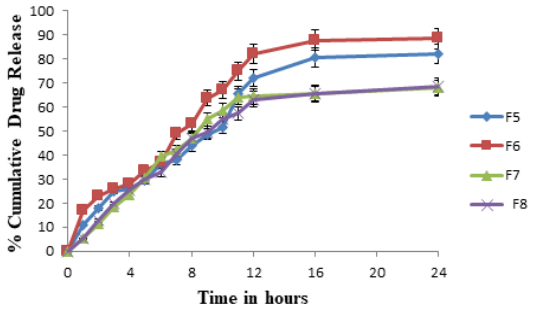

Figure 7: *In vitro* release profile of niosomes of Azithromycin dehydrate

Drug release kinetics

The drug release profile of Azithromycin dehydrates was subjected to release kinetics such as first order, zero order, Korsemeyer Peppas, Higuchi, and Hixon-Crowell methods. The best-fitted model was selected based on the R^2 value of the different models. The Regression value of different formulations using different release kinetic models is tabulated in Table 4.

Table 4: Drug release kinetics of formulation F5-F8

S.No	Formulation Code	Release kinetics					
		First-order	Zero-order	Korsmeyer-Peppas	n value	Higuchi	Hixon
1	F5	0.9201`	0.8798	0.8841	0.96821	0.9201	0.9154
2	F6	0.9031	0.8356	0.8538	0.9462	0.9225	0.891
3	F7	0.9197	0.7668	0.8247	0.8248	0.9032	0.8075
4	F8	0.9218	0.8088	0.8573	0.8256	0.9183	0.8455

All the formulations are subjected to different release kinetics models and found that all the formulation follows the Korsmeyer-Peppas model. The best-fitted model was selected as the R^2 was found to be the highest for Korsmeyer-Peppas. F6 is the optimized formulation that follows the Korsmeyer-Peppas model with the highest R^2 value (0.9225). Korsmeyer-Peppas model governs the drug release through the polymeric matrix system. This model helps to understand the release mechanism through the diffusion of water into the matrix, swelling of the matrix, and dissolution of the matrix. n value was found to be 0.0462 indicating that the release is through fickian diffusion. Figure 8 represents (a) First order kinetics of optimized formulation F6 (b) Zero order kinetics of optimized formulation F6 (c) Higuchi release kinetics of optimized formulation F6 (d) Korsmeyer-Peppas kinetics of optimized formulation F6 (e) Hixon Crowell kinetics of optimized formulation

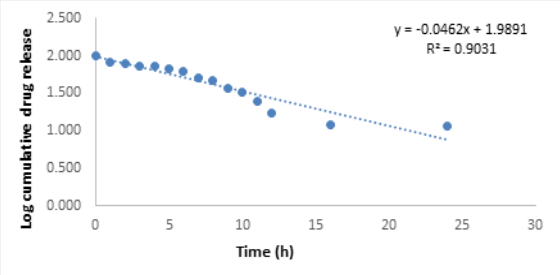

(a) First-order release kinetics of optimized formulations F6

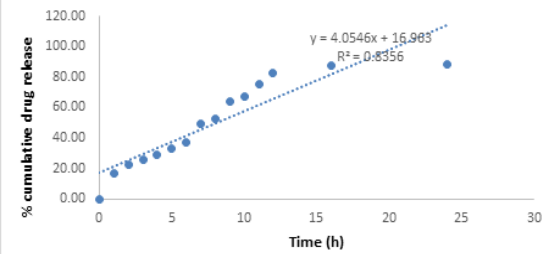

(b) Zero order release kinetics of optimized formulations F6

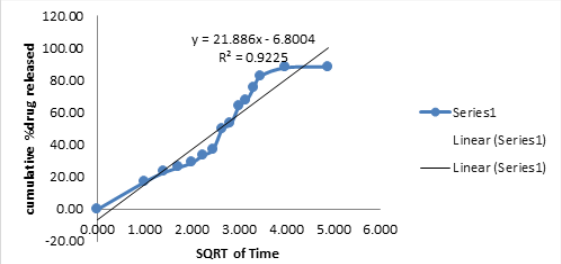

(c) Higuchi release kinetics of optimized formulations F6

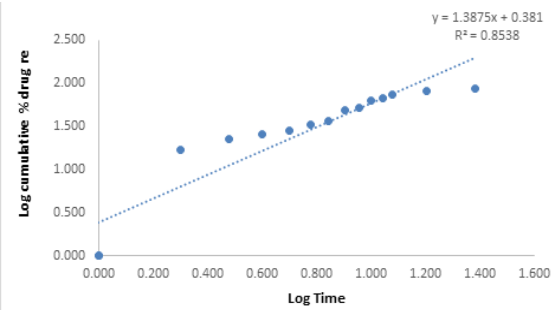

(d) Korsmeyer-Peppas release kinetics of optimized formulations F6

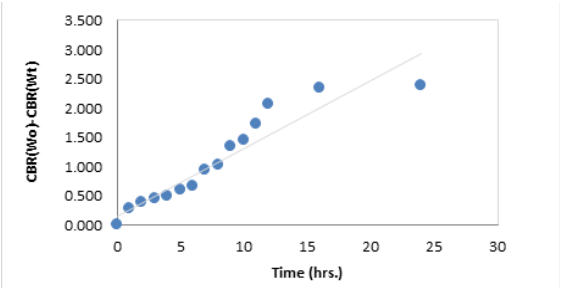

(e) Hixon-Crowel release kinetics of optimized formulations F6

Figure 8: (a) First order kinetics of optimized formulation F6 (b) Zero order kinetics of optimized formulation F6 (c) Higuchi release kinetics of optimized formulation F6 (d) Korsmeyer-Peppas kinetics of optimized formulation F6 (e) Hixon Crowell kinetics of optimized formulation

Conclusion

The study finding reveals that the prepared niosomes help to prolong the release of the drug for 24 hr. The formulation with a 1:1:1 ratio of span 60:cholesterol: drug showed good results with 92.4% entrapment efficiency and 88.4% drug release. The SEM results show the spherical and smooth vesicles without aggregations. From the study, it can be concluded that vesicle delivery can be used to improve the rate of release of drugs as well as improve bioavailability.

Release Kinetics

Conflict of interest

No conflict of interest.

References

1. Myneni, G. S., Radha, G., & Soujanya, G. V. R. L. (2021). Novel vesicular drug delivery systems: a review. Journal of Pharmaceutical Research, 11, 1650-1664.
2. Chacko, I. A., Ghate, V. M., Dsouza, L., & Lewis, S. A. (2020). Lipid vesicles: A versatile drug delivery platform for dermal and transdermal applications. Colloids and Surfaces B: Biointerfaces, 195, 111262.
3. Jain, A. K., & Mishra, K. (Eds.). (2022). Nanoparticles and Nanocarriers Based Pharmaceutical Formulations. Bentham Science Publishers, pp.333.
4. Mishra, D. K., Shandilya, R., & Mishra, P. K. (2018). Lipid based nanocarriers: a translational perspective. Nanomedicine: Nanotechnology, Biology and Medicine, 14(7), 2023-2050.
5. Chen, S., Hanning, S., Falconer, J., Locke, M., & Wen, J. (2019). Recent advances in non-ionic surfactant vesicles (niosomes): Fabrication, characterization, pharmaceutical and cosmetic applications. European journal of pharmaceutics and biopharmaceutics, 144, 18-39.
6. Rashwan, A. K., Karim, N., Xu, Y., Xie, J., Cui, H., Mozafari, M. R., & Chen, W. (2023). Potential micro-/nano-encapsulation systems for improving stability and bioavailability of anthocyanins: An updated review. Critical Reviews in Food Science and Nutrition, 63(19), 3362-3385.
7. Biswasroy, P., Pradhan, D., Kar, B., Ghosh, G., & Rath, G. (2021). Recent advancement in topical nanocarriers for the treatment of psoriasis. AAPS Pharmscitech, 22(5), 164.
8. Gharbavi, M., Amani, J., Kheiri-Manjili, H., Danafar, H., & Sharafi, A. (2018). Niosome: a promising nanocarrier for natural drug delivery through blood-brain barrier. Advances in Pharmacological and Pharmaceutical Sciences, 2018.
9. Chenthamara, D., Subramaniam, S., Ramakrishnan, S. G., Krishnaswamy, S., Essa, M. M., Lin, F. H., & Qoronfleh, M. W. (2019). Therapeutic efficacy of nanoparticles and routes of administration. Biomaterials Research, 23(1), 1-29.
10. Mehrarya, M., Gharehchelou, B., Haghighi Poodeh, S., Jamshidifar, E., Karimifard, S., Farasati Far, B., ... & Seifalian, A. (2022). Niosomal formulation for antibac-

terial applications. Journal of Drug Targeting, 30(5), 476-493.

11. Kauslya, A., Borawake, P. D., Shinde, J. V., & Chavan, R. S. (2021). Niosomes: a novel carrier drug delivery system. Journal of Drug Delivery and Therapeutics, 11(1), 162-170.
12. Zitouni, K. (2021). Structural exploration and study of the QSAR properties of several series of macrolide antibiotics (Doctoral dissertation, Université de mohamed kheider biskra).
13. Vázquez-Laslop, N., & Mankin, A. S. (2018). How macrolide antibiotics work. Trends in biochemical sciences, 43(9), 668-684.
14. Bhattacharyya, S., Pasha, I., Verma, A., Kothapalli, R., Jafar, F., & Hr, K. (2019). Formulation and evaluation of liquisolid compact of azithromycin dihydrate. Journal of Research in Pharmacy, 23(6), 1022-32.
15. Aarti, H., Jamindar, D., Mahajan, A., & Hardia, A. (2017). Formulation and In-vitro and Skin Permeability Evaluation of Dexamethasone Loaded Niosomal Gel. Asian Journal of Pharmaceutical Research and Development, 5(2), 01-09.
16. Rao, A., Arvapalli, S., Rao, G. S. N., Malothu, N., & Bandaru, N. R. (2021). Design and evaluation of acyclovir niosomes. Research Journal of Pharmacy and Technology, 14(8), 4185-4188.
17. Allam, A., El-Mokhtar, M. A., & Elsabahy, M. (2019). Vancomycin-loaded niosomes integrated within pH-sensitive in-situ forming gel for treatment of ocular infections while minimizing drug irritation. Journal of Pharmacy and Pharmacology, 71(8), 1209-1221.
18. Ramadan, A. A., Eladawy, S. A., El-Enin, A. S. M. A., & Hussein, Z. M. (2020). Development and investigation of timolol maleate niosomal formulations for the treatment of glaucoma. Journal of Pharmaceutical Investigation, 50, 59-70.
19. Mohanty, D., Rani, M. J., Haque, M. A., Bakshi, V., Jahangir, M. A., Imam, S. S., & Gilani, S. J. (2020). Preparation and evaluation of transdermal naproxen niosomes: formulation optimization to preclinical anti-inflammatory assessment on murine model. Journal of liposome research, 30(4), 377-387.
20. Jacob, S., Nair, A. B., & Al-Dhubiab, B. E. (2017). Preparation and evaluation of niosome gel containing acyclovir for enhanced dermal deposition. Journal of liposome research, 27(4), 283-292.
21. Sailaja, A. K., & Shreya, M. (2018). Preparation and characterization of naproxen loaded niosomes by ether injection method. Nano Biomedicine and Engineering, 10(2), 174-180.
22. Abdelbary, A., Salem, H. F., Khallaf, R. A., & Ali, A. M. (2017). Mucoadhesive niosomal in situ gel for ocular tissue targeting: in vitro and in vivo evaluation of lomefloxacin hydrochloride. Pharmaceutical development and technology, 22(3), 409-417.
23. Gugleva, V., Titeva, S., Ermenlieva, N., Tsibranska, S., Tcholakova, S., Rangelov, S., & Momekova, D. (2020). Development and evaluation of doxycycline niosomal thermoresponsive in situ gel for ophthalmic delivery. International Journal of Pharmaceutics, 591, 120010.
24. Siswanto, A., Fudholi, A., Nugroho, A. K., & Martono, S. (2015). In vitro release modeling of aspirin floating tablets using DDSolver. Indonesian Journal of Pharmacy, 26(2), 94.
25. Shirsand, S. B., & Keshavshetti, G. G. (2019). Recent advances in niosomal drug delivery—A review. Research Journal of Life Sciences, Bioinformatics, Pharmaceutical and Chemical Sciences, 3, 514-531.

26. Bnyan, R., Khan, I., Ehtezazi, T., Saleem, I., Gordon, S., O'Neill, F., & Roberts, M. (2018). Surfactant effects on lipid-based vesicles properties. Journal of pharmaceutical sciences, 107(5), 1237-1246.

27. Nava-Arzaluz, M. G., Piñón-Segundo, E., & Ganem-Rondero, A. (2019). Lipid nanocarriers as skin drug delivery systems. In Nanoparticles in Pharmacotherapy . William Andrew Publishing. pp.311-390

28. Yeo, L. K., Olusanya, T. O., Chaw, C. S., & Elkordy, A. A. (2018). Brief effect of a small hydrophobic drug (cinnarizine) on the physicochemical characterisation of niosomes produced by thin-film hydration and microfluidic methods. Pharmaceutics, 10(4), 185.

29. Akbari, V., Abedi, D., Pardakhty, A., & Sadeghi-Aliabadi, H. (2015). Release studies on ciprofloxacin loaded non-ionic surfactant vesicles. Avicenna journal of medical biotechnology, 7(2), 69.

30. Fouda, N. H., Abdelrehim, R. T., Hegazy, D. A., & Habib, B. A. (2018). Sustained ocular delivery of Dorzolamide-HCl via proniosomal gel formulation: in-vitro characterization, statistical optimization, and in-vivo pharmacodynamic evaluation in rabbits. Drug delivery, 25(1), 1340-1349

31. Sahu, A. K., Mishra, J., & Mishra, A. K. (2020). Introducing Tween-curcumin niosomes: Preparation, characterization and microenvironment study. Soft matter, 16(7), 1779-1791.

32. Barani, M., Hajinezhad, M. R., Sargazi, S., Rahdar, A., Shahraki, S., Lohrasbi-Nejad, A., & Baino, F. (2021). In vitro and in vivo anticancer effect of pH-responsive paclitaxel-loaded niosomes. Journal of Materials Science: Materials in Medicine, 32, 1-13.

Current Trends in Biotechnology and Pharmacy
Vol. 19(1) 2204-2210, January 2025, ISSN 0973-8916 (Print), 2230-7303 (Online)
DOI: 10.5530/ctbp.2025.1.9

Computational Analysis of HSP90 Isoforms Identifies Differential Sensitivity Towards Specific Inhibitors

Shravanthi Ravula[1#], Sai Charitha Mullaguri[1#], Sree Kanth Sivan[2], Sravani Akula[1], Vijjulatha Manga[2] and Rama Krishna Kancha[1*]

[1] Molecular Medicine and Therapeutics Laboratory, CPMB, Osmania University, Hyderabad-500007.
[2] Department of Chemistry, Osmania University, Hyderabad-500007.

Corresponding author: ickrishna@gmail.com

Abstract

The heat shock protein 90 (HSP90) protein family consists of cytosolic HSP90-alpha, HSP90-beta and mitochondrial TRAP1. As HSP90 facilitates the activation and stabilization of many oncogenic proteins in cancer cells, it emerged as a potential therapeutic target in cancer treatment. Although many HSP90 inhibitors are under various phases of clinical trials, the efficacy of these inhibitors on each isoform is largely unknown. This study aims to determine the sensitivity profiles of HSP90 isoforms towards various natural and synthetic HSP90 inhibitors. Molecular docking analysis was performed for HSP90 inhibitors along with ATP and ADP over three isoforms HSP90-alpha, HSP90-beta and TRAP1. Our results indicate variable isoform-specific sensitivity towards HSP90 inhibitors. The predicted sensitivity profiles are in line with the limited available experimental data indicating the utility of molecular docking approach. In addition, potential interactions between the inhibitors and residues within the HSP90 isoforms were identified. The data generated in the current study may provide valuable insights for the design of isoform-specific HSP90 inhibitors with improved efficacy and specificity towards the HSP90 isoforms. Further, our study revealed critical residues in each of these isoforms for specific targeting by novel inhibitors.

Keywords

HSP90 isoforms, HSP90 inhibitors, molecular docking, binding affinity, drug sensitivity, ligand interactions.

Introduction

HSP90 is an important molecular chaperone that assists in the folding, maturation and activation of a large number of client proteins, which are critical for cellular homeostasis and various biological processes such as signal transduction, cell cycle regulation, and stress responses (1,2). HSP90 stabilizes several oncogenic proteins that promote tumor development and survival, thus offering an important cellular target for cancer treatment (3,4,5). HSP90 has multiple isoforms such as HSP90-alpha, HSP90-beta and TRAP1, each located in different cellular compartments and performing specific functions. HSP90-alpha and HSP90-beta are mainly cytoplasmic with HSP90-alpha being expressed in response to stress while HSP90-beta is constitutively expressed (6,7). TRAP1 is localized in the mitochondria and is involved in protecting cells from apoptotic stress (8). Although these isoforms share functional similarities, they have structural differences that may affect their interactions with inhibitors. This structural diversity offers a possibility for designing selective inhibitors that target specific HSP90 isoforms, potentially reducing off-target effects and enhancing therapeutic efficacy (9,10). Until now, many inhibitors have been developed that target the ATP-binding domain at the N-terminus of HSP90 to interfere with its chaperone activity and induce the degradation of its clients. However, the effects of these inhibitors on different HSP90 isoforms are not fully

understood. Molecular docking methods offer a valuable approach to study the binding affinities and specificities of HSP90 inhibitors for different isoforms, which can help in the development of more selective drugs (11,12). The aim of the current study is to perform molecular docking analysis to determine the sensitivities of HSP90 isoforms towards various natural and synthetic HSP90 inhibitors.

Material and Methods

HSP90-alpha (PDB: 1YES) (13), HSP90-beta (5UC4) (14) and TRAP1 (4Z1F) (15) isoforms were analysed for their sensitivities towards HSP90 inhibitors. Using Schrodinger Glide XP (extra precision) docking method (16), these structures were docked with adenosine triphosphate (ATP), adenosine diphosphate (ADP) and twenty HSP90 inhibitors collected from the PubChem (17): alvespimycin (17-DMAG), BIIB021, derrubone, gambogic acid, ganetespib, gedunin, geldanamycin, herbimycin, hypericin, IPI504 (retaspimycin hydrochloride), luminespib, macbecin, monocillin, onalespib, pochonin A, pochonin D, PU-H71 (Zelavespib), radicicol, sansalvamide A and tanespimycin (17-AAG) (18). The binding affinity of each receptor-ligand was measured as an XP score and the sensitivity profile of each HSP90 isoform towards the inhibitors was estimated. Additionally, multiple sequence alignment among HSP90-alpha, HSP90-beta and TRAP1 was carried out using Clustal Omega (19), and the interactions between the ligands and the HSP90 isoforms were collected and analysed. Interactions of each isoform with inhibitors that showed higher binding affinity were compared with the available experimentally determined co-crystal structures: HSP90-alpha with ganetespib (PDBs: 3TUH, 6LSZ and 8W8K) (20), TRAP1 with BIIB021 (PDB: 4Z1G) (15), and TRAP1 with PU-H71 (PDB: 4Z1F) (15).

Results and Discussion

A total of 66 molecular dockings were carried out using 20 HSP90 inhibitors, ATP and ADP against HSP90-alpha, HSP90-beta and TRAP1. Both ADP and ATP showed the highest binding affinities towards TRAP1 when compared to HSP90-alpha and HSP90-beta (Figure 1). Importantly, seven inhibitors (alvespimycin, derrubone, geldanamycin, hypericin, IPI-504, luminespib and monocillin) showed higher binding affinity towards HSP90-beta than HSP90-alpha and TRAP1 (Figure 1). Interestingly, BIIB021, gedunin and PU-H71 showed significantly higher binding affinity towards TRAP1 than HSP90-alpha and HSP90-beta; gambogic acid, macbecin and pochonin D showed slightly higher binding affinity towards TRAP1 when compared to HSP90-alpha and HSP90-beta (Figure 1). The greater sensitivity of TRAP1 towards PU-H71 further corroborates with the available experimental data when PU-H71 availability in mitochondria was increased (15). Ganetespib showed slightly higher binding affinity towards HSP90-alpha when compared to HSP90-beta and TRAP1 (Figure 1). Herbimycin showed similar binding affinities towards all three isoforms while onalespib, pochonin A, radicicol, sansalvamide A and tanespimycin showed higher binding affinities towards both HSP90-beta and TRAP1 when compared to HSP90-alpha (Figure 1).

All the interactions between HSP90 isoforms and the inhibitors were summarized in Figure 2 and the residues that interact with the ligands were highlighted in Figure 3. Analysis of the ligand-isoform complexes revealed that amino acid stretches ELI (HSP90-alpha: 47-49; HSP90-beta: 42-44; TRAP1: 115-117), GIGMT (HSP90-alpha: 95-99; HSP90-beta: 90-94; TRAP1: 160-164), GVGFY (HSP90-alpha: 135-139; HSP90-beta: 130-134; TRAP1: 202-206) and GTK (HSP90-alpha: 183-185; HSP90-beta: 178-180; TRAP1: 250-252) were interacting with at least one ligand in each isoform and are conserved among the isoforms (Figure 3). Interestingly, residues N51, M98, N106 and F138 (HSP90-alpha numbering) were shown to interact with all ligands in all three HSP90 isoforms (Figure 3). For individual isoforms, all the ligands showed interactions with (i) N51, A55, K58, I96, G97, M98, N106, L107 and F138 of HSP90-alpha; (ii) N46, A50, M93, N101, L102, F133 and

Current Trends in Biotechnology and Pharmacy
Vol. 19(1) 2204-2210, January 2025, ISSN 0973-8916 (Print), 2230-7303 (Online)
DOI: 10.5530/ctbp.2025.1.9

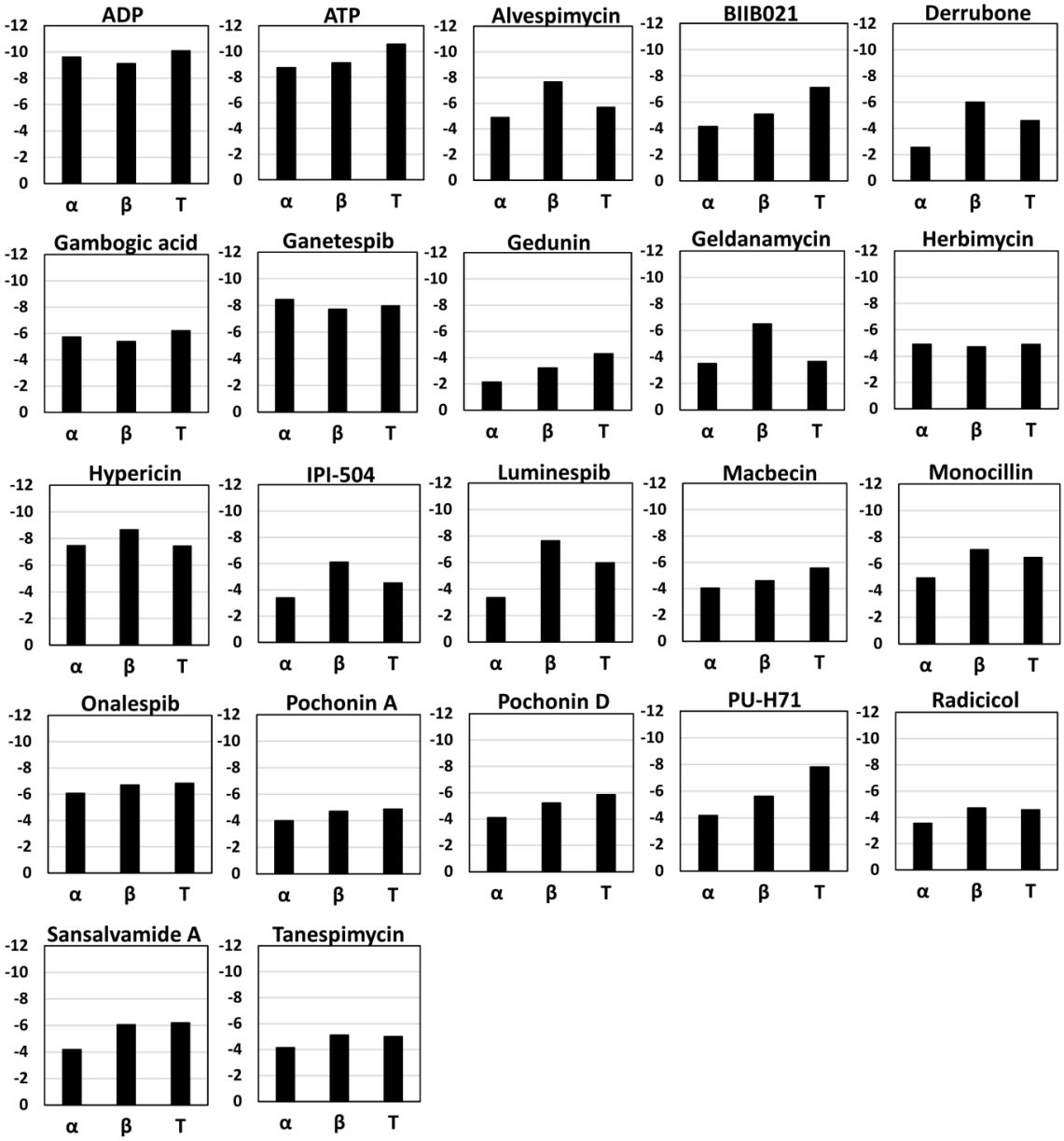

Figure 1. Predicted drug sensitivity profiles of HSP90 isoforms towards HSP90 inhibitors. Binding affinities of ADP, ATP and twenty inhibitors with each HSP90 isoform were measured in terms of XP scores and graphs were plotted. α: alpha; β: beta; T: TRAP1.

T179 of HSP90-beta; (iii) N119, M163, N171, G202, V203, F205, T251 and I253 of TRAP1 (Figures 2 and 3). Among these, A55, I96, M98 and L107 of HSP90-alpha, A50, M93 and L102 of HSP90-beta, and M163, V203 and I253 of TRAP1 formed Vander Waal interactions with all the ligands (Supplementary Figures 1-11).

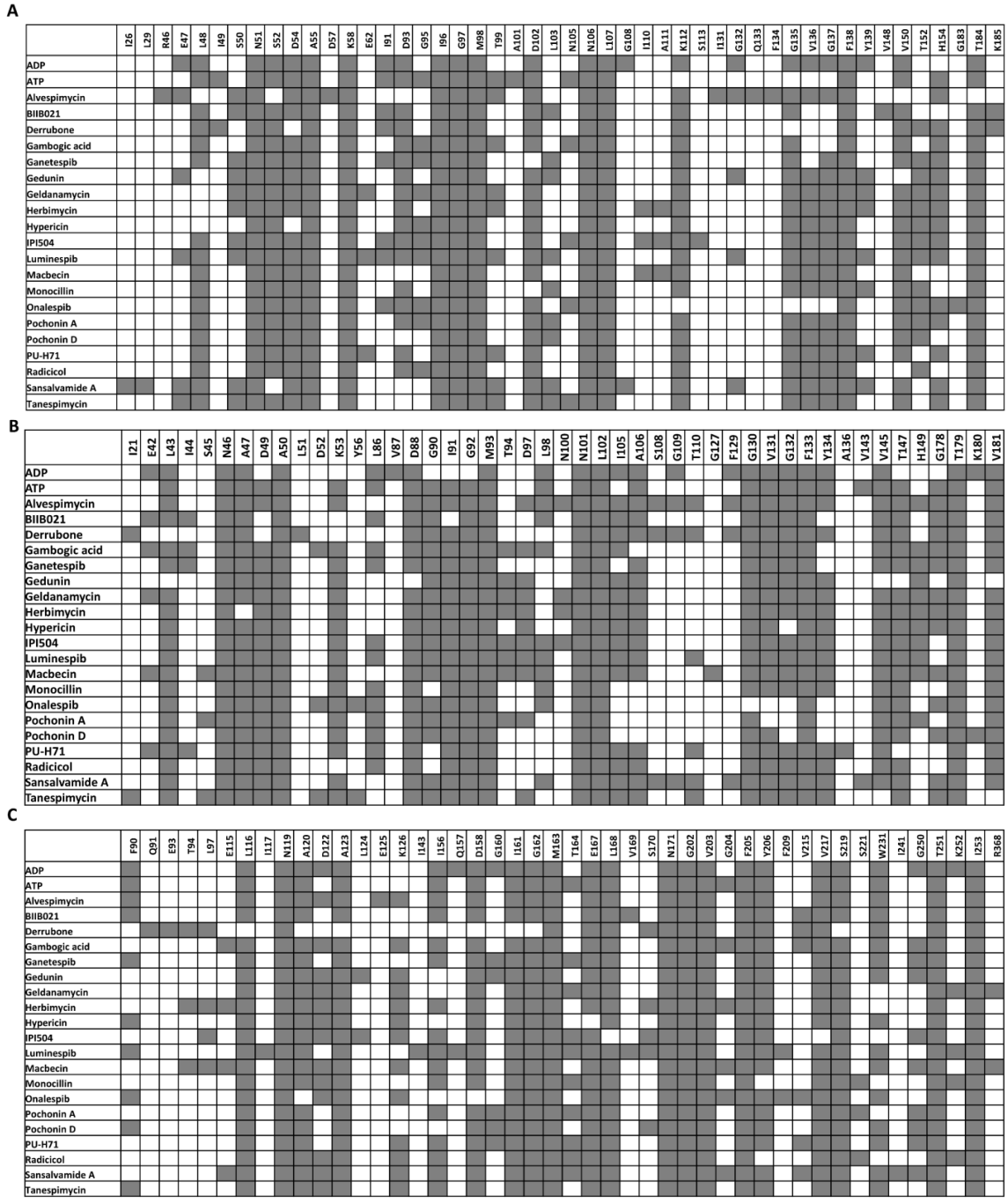

Figure 2. Receptor-ligand interactions between HSP90 isoforms, and ADP, ATP and twenty HSP90 inhibitors. Amino acids in HSP90-alpha (A), HSP90-beta (B) and TRAP1 (C) that are interacting with each ligand were shaded.

Computational analysis of HSP90 isoforms identifies differential sensitivity towards specific inhibitors

```
HSP90-alpha   1   MPEETQTQDQ PMEEEEVETF AFQAEIAQLM SLIINTFYSN KEIFLRELIS NSSDALDKIR  60
HSP90-beta    1   MPEE-----V HHGEEEVETF AFQAEIAQLM SLIINTFYSN KEIFLRELIS NASDALDKIR  55
HSP90-trap1  69   EPLHSIISST ESVQGSTSKH EFQAETKKLL DIVARSLYSE KEVFIRELIS NASDALEKLR  128

HSP90-alpha   61  YESLTDPSKL DSGKELHINL IPNKQDRTLT IVDTGIGMTK ADLINNLGTI AKSGTKAFME  120
HSP90-beta    56  YESLTDPSKL DSGKELKIDI IPNPQERTLT LVDTGIGMTK ADLINNLGTI AKSGTKAFME  115
HSP90-trap1  129  HKLVSDGQAL ---PEMEIHL QTNAEKGTIT IQDTGIGMTQ EELVSNLGTI ARSGSKAFLD  185

HSP90-alpha   121 ALQAGA--DI SMIGQFGVGF YSAYLVAEKV TVITKHN--D DEQYAWESSA GGSFTVRTDT  176
HSP90-beta    116 ALQAGA--DI SMIGQFGVGF YSAYLVAEKV VVITKHN--D DEQYAWESSA GGSFTVRADH  171
HSP90-trap1   186 ALQNQAEASS KIIGQFGVGF YSAFMVADRV EVYSRSAAPG SLGYQWLSDG SGVFEIAEAS  245

HSP90-alpha   177 GEPMGRGTKV ILHLKEDQTE YLEERRIKEI VKKHSQFIGY PITLFVEKER DKEVSDDEAE  236
HSP90-beta    172 GEPIGRGTKV ILHLKEDQTE YLEERRVKEV VKKHSQFIGY PITLYLEKER EKEISDDEAE  231
HSP90-trap1   246 G--VRTGTKI IIHLKSDCKE FSSEARVRDV VTKYSNFVSF PLYLN-----  ----------  288

HSP90-alpha   237 EKEDKEEEKE KEEKESEDKP EIEDVGSDEE EEKKDGDKKK KKKIKEKYID QEELNKTKPI  296
HSP90-beta    232 EEKG---EKE EEDKDDEEKP KIEDVGSDEE DDSGKDKKKK TKKIKEKYID QEELNKTKPI  288
HSP90-trap1   288 ----------  ----------  ----------  ----------  ----------  GRRMNTLQAI  298

HSP90-alpha   297 WTRNPDDITN EEYGEFYKSL TNDWEDHLAV KHFSVEGQLE FRALLFVPRR APFDLFENRK  356
HSP90-beta    289 WTRNPDDITQ EEYGEFYKSL TNDWEDHLAV KHFSVEGQLE FRALLFIPRR APFDLFENKK  348
HSP90-trap1   299 WMMDPKDVRE WQHEEFYRYV AQAHDKPRYT LHYKTDAPLN IRSIFYVPDM KPSMFDVSRE  358

HSP90-alpha   357 KKNNIKLYVR RVFIMDNCEE LIPEYLNFIR GVVDSEDLPL NISREMLQQS KILKVIRKNL  416
HSP90-beta    349 KKNNIKLYVR RVFIMDSCDE LIPEYLNFIR GVVDSEDLPL NISREMLQQS KILKVIRKNI  408
HSP90-trap1   359 LGSSVALYSR KVLIQTKATD ILPKWLRFIR GVVDSEDIPL NLSRELLQES ALIRKLRDVL  418
```

Figure 3. Schematic representation of HSP90 residues interacting with inhibitors. Multiple sequence alignment was performed for the HSP90 isoforms. All the residues that were interacting with at least one ligand in each isoform were highlighted in yellow. Residues in each isoform that were interacting with all the 22 ligands were coloured in red.

Comparison of co-crystal structures (3TUH, 6LSZ and 8W8K) of HSP90-alpha and ganetespib complexes with the molecular docking analysis revealed many common interactions: hydrogen bonds with K58 and G97, and non-bonded interactions with L48, S52, A55, D93, I96, M98, L107, F138 and V186 (Supplementary Figure 4). All the interactions observed in the experimental co-crystals except G108 and T109 were present in the HSP90-alpha and ganetespib complex (Supplementary Figure 4). Further, the common interactions between co-crystal structure (4Z1G) and TRAP1-BIIB021 complex (Supplementary Figure 2) include hydrogen bonds with D158 and T251, and non-bonded interactions with N119, A123, I161, G162, M163, L168, G202 and F205. Similarly, common interactions between co-crystal structure (4Z1F) and TRAP1-PU-H71 complex (Supplementary Figure 10) include hydrogen bonding with D158, non-bonded interactions with N119, A123, I161, G162, M163, E167, N171, G202, F205, W231 and T251. All the interactions present in the co-crystals of TRAP1 with BIIB021 (4Z1G) and PU-H71 (4Z1F) were observed in the complexes obtained through molecular docking indicating the usefulness of computational approach in predicting the drug sensitivities of HSP90 isoforms.

Conclusion

The current study established the sensitivity profiles of HSP90 isoforms towards various natural and synthetic inhibitors. Among

the HSP90 isoforms, TRAP1 was observed to be more sensitive towards PU-H71, which is in line with the previously reported experimental data. Additionally, the interactions observed in the available experimental co-crystal structures were largely present in the complexes obtained from our molecular docking analyses indicating the effectiveness of this approach in predicting drug sensitivities of HSP90 isoforms.

Availability of data

All the data are included in the supplementary files.

Acknowledgements

RKK acknowledges funding from ICMR-Ad-hoc grant (F.No. 58/31/2020/PHA/BMS). SR acknowledges fellowship from the Council of Scientific & Industrial Research (File No. 09/132(0884)/2019-EMR-I). SCM acknowledges salary from ICMR-Ad-hoc grant (F.No. 58/31/2020/PHA/BMS).

Conflict of interest

The authors declare that they have no known competing financial interests or personal relationships that could have appeared to influence the work reported in this paper.

References

1. Schopf, F.H., Biebl, M.M. and Buchner, J., 2017. The HSP90 chaperone machinery. Nature reviews Molecular cell biology, 18(6), pp.345-360.

2. Neckers, L. and Workman, P., 2012. Hsp90 molecular chaperone inhibitors: are we there yet?. Clinical cancer research, 18(1), pp.64-76.

3. Kancha, R.K., Bartosch, N. and Duyster, J., 2013. Analysis of conformational determinants underlying HSP90-kinase interaction. PLoS One, 8(7), p.e68394.

4. Sreedhar, A.S. and Csermely, P., 2004. Heat shock proteins in the regulation of apoptosis: new strategies in tumor therapy: a comprehensive review. Pharmacology & therapeutics, 101(3), pp.227-257.

5. Jhaveri, K. and Modi, S., 2012. HSP90 inhibitors for cancer therapy and overcoming drug resistance. Advances in pharmacology, 65, pp.471-517.

6. Marzec, M., Eletto, D. and Argon, Y., 2012. GRP94: An HSP90-like protein specialized for protein folding and quality control in the endoplasmic reticulum. Biochimica et Biophysica Acta (BBA)-Molecular Cell Research, 1823(3), pp.774-787.

7. Barabutis, N., 2020. Heat shock protein 90 inhibition in the inflamed lungs. Cell Stress and Chaperones, 25(2), pp.195-197.

8. Gesualdi, N.M., Chirico, G., Pirozzi, G., Costantino, E., Landriscina, M. and Esposito, F., 2007. Tumor necrosis factor-associated protein 1 (TRAP-1) protects cells from oxidative stress and apoptosis. Stress, 10(4), pp.342-350.

9. Prodromou, C., 2016. Mechanisms of Hsp90 regulation. Biochemical Journal, 473(16), pp.2439-2452.

10. Chen, B., Piel, W.H., Gui, L., Bruford, E. and Monteiro, A., 2005. The HSP90 family of genes in the human genome: insights into their divergence and evolution. Genomics, 86(6), pp.627-637.

11. Miyata, Y., Nakamoto, H. and Neckers, L., 2013. The therapeutic target Hsp90 and cancer hallmarks. Current pharmaceutical design, 19(3), pp.347-365.

12. Taipale, M., Jarosz, D.F. and Lindquist, S., 2010. HSP90 at the hub of protein homeostasis: emerging mechanistic insights. Nature reviews Molecular cell biology, 11(7),

pp.515-528.

13. Stebbins, C.E., Russo, A.A., Schneider, C., Rosen, N., Hartl, F.U. and Pavletich, N.P., 1997. Crystal structure of an Hsp90–geldanamycin complex: targeting of a protein chaperone by an antitumor agent. Cell, 89(2), pp.239-250.

14. Khandelwal, A., Kent, C.N., Balch, M., Peng, S., Mishra, S.J., Deng, J., Day, V.W., Liu, W., Subramanian, C., Cohen, M. and Holzbeierlein, J.M., 2018. Structure-guided design of an Hsp90β N-terminal isoform-selective inhibitor. Nature communications, 9(1), p.425.

15. Lee, C., Park, H.K., Jeong, H., Lim, J., Lee, A.J., Cheon, K.Y., Kim, C.S., Thomas, A.P., Bae, B., Kim, N.D. and Kim, S.H., 2015. Development of a mitochondria-targeted Hsp90 inhibitor based on the crystal structures of human TRAP1. Journal of the American Chemical Society, 137(13), pp.4358-4367.

16. Friesner, R.A., Murphy, R.B., Repasky, M.P., Frye, L.L., Greenwood, J.R., Halgren, T.A., Sanschagrin, P.C. and Mainz, D.T., 2006. Extra precision glide: Docking and scoring incorporating a model of hydrophobic enclosure for protein− ligand complexes. Journal of medicinal chemistry, 49(21), pp.6177-6196.

17. Kim, S., Chen, J., Cheng, T., Gindulyte, A., He, J., He, S., Li, Q., Shoemaker, B.A., Thiessen, P.A., Yu, B. and Zaslavsky, L., 2023. PubChem 2023 update. Nucleic acids research, 51(D1), pp.D1373-D1380.

18. Ravula, S., Akula, S. and Kancha, R.K., 2024. Natural and Synthetic Inhibitors of Heat Shock Protein 90 Chaperone in Cancer Treatment. Indian journal of pharmaceutical education and research, 58(2), pp.401-410

19. Madeira, F., Madhusoodanan, N., Lee, J., Eusebi, A., Niewielska, A., Tivey, A.R., Lopez, R. and Butcher, S., 2024. The EMBL-EBI Job Dispatcher sequence analysis tools framework in 2024. Nucleic Acids Research, p.gkae241.

20. Xu, C., Zhang, X., Zhao, L., Verkhivker, G.M. and Bai, F., 2024. Accurate Characterization of Binding Kinetics and Allosteric Mechanisms for the HSP90 Chaperone Inhibitors Using AI-Augmented Integrative Biophysical Studies. JACS Au, 4(4), pp.1632-1645.

Current Trends in Biotechnology and Pharmacy
Vol. 19(1) 2211-2221, January 2025, ISSN 0973-8916 (Print), 2230-7303 (Online)
DOI: 10.5530/ctbp.2025.1.10

The Effect of Ursodeoxycholic Acid on Parkinson's Disease: A Systematic and Meta-Analysis of Randomized Controlled trials

Aswin Krishnamurthy, Nandhini Sundaresan*, Vivekananthan G, Sanjay R, Monish S

[1]Department of Pharmacognosy, Sri Ramachandra Faculty of Pharmacy, Sri Ramachandra Institute of Higher Education and Research (DU), Porur, Chennai- 600 116.

Corresponding author: ickrishna@gmail.com

Abstract

Parkinson's disease (PD) is a progressive degenerative disorder involving dopaminergic neurons in the substantia nigra. Along with motor activity impairment, PD patients also have a range of neuropsychiatric, cognitive, and autonomic problems. Ursodeoxycholic acid (UDCA) has been used to treat a wide range of liver-related ailments, including gallstones, cholestatic diseases, and primary biliary cirrhosis (PBC). In addition to this, randomised control trials on the effects of Parkinson's disease have been conducted on UDCA. In the present study, we validate the effect of UDCA on Parkinson disease using meta-analysis. Various electronic databases such as Web of Science, PubMed/ Medline, Cochrane library and Scopus were used for search of articles. The randomized control trials (RCTs) for the effect of interventions of UDCA on Parkinson disease was evaluated using meta-analysis (Review Manager 5.4) software. A total of 304 articles were identified, of which 3 met the inclusion criteria. When compared to patients receiving the control medication, the UDCA-treated patients had higher concentrations of inorganic phosphate (Pi) and ATP. The z scores of UDCA on Pi and ATP concentration were determined to be 0.08 and 0.71 with p-values of 0.00001 and 0.0001, respectively. UDCA might increase brain mitochondrial activity and cellular ATP availability and could possibly have therapeutic disease-modifying effects. Ursodeoxycholic acid administrations in PD significantly increase the concentration of Pi and ATP and maintain ATP homeostasis by increasing ATPase activity and ATP production.

Keywords: Parkinson's disease, ursodeoxycholic acid, meta-analysis, ATP concentration.

Introduction

Parkinson's disease (PD) is a neurological condition characterized by the premature death of dopaminergic neurons in substantia nigra pars compacta. The depletion of dopamine level in basal ganglia result in the movement disorder with symptoms similar to that of Parkinsonism. One third of the elderly population older than 75 is affect with Parkinson disease, still the causes of disease is unknow (1,2). Searching for novel treatment targets is expanding with the vast study being done on the molecular pathways underlying the cause and progression of Parkinson's disease (3). Mitochondrial dysfunction, particularly the selective suppression of complex I is another factor responsible for dopaminergic neuron depletion (4). Magnetic resonance spectroscopy is a powerful tool for non- invasively studying of metabolic alterations and bioenergetic changes in the brain of the patients with neurodegenerative condition. These techniques can directly measure the intracellular pH, free Magnesium and

phosphorus metabolites such as ATP, inorganic phosphate, phosphocreatine, glycerophosphocholine and phosphoethanolamine. As a result, in vivo 31P MRS provides essential insights into relationship between energy failure and neurodegenerative process (5-9).

Mitochondrial dysfunction can induce oxidative stress, as decrease ATP and increase in the production of 'reactive oxygen species (ROS)', further damaging dopaminergic neuron in the mitochondria (10). Various risk factors, including obesity, hypertension and dyslipidemia contribute to the rise in non-communicable disease (11). This causes the accumulation of misfolded α-synuclein, which binds to the electron transport chain (ETC) there by increase in the production of ROS, which promotesmitochondrial DNA damage, this decreases the ATP production. The damage of the ETC reduces Complex I activity, which includes opening of MPTP (Mitochondrial Permeability Transition Pore), releasing cytochrome c and Ca2+, increase inflammatory response through Succinate and Mitochondrial DAMP release, including apoptosis (12-14). Enhanced Drp1-mediated fission of mitochondria and its interactions with MFN1/2 and OPA1 proteins contribute to Parkinson's disease-related mitochondrial fragmentation. Moreover, Parkin and PINK1 mitophagy protein mutations cause defective mitophagy with autosomal recessive early-onset Parkinson's disease (15).

A naturally occurring hydrophilic bile acid called ursodeoxycholic acid (UDCA) has been demonstrated a neuroprotective agent for Parkinson's disease (16). For more than 30 years, UDCA has been approved to treat PBC (primary biliary cholangitis) at a dosage of 15mg/kg. Based on the choleretic actions and capacity to shield hepatocytes from hydrophobic bile acids, UDCA was first given FDA approval for the treatment of numerous cholestatic liver conditions. UDCA and TUDCA can inhibit the apoptosis, prevent mitochondrial dysfunction and reduces oxidative stress (17,18). Previous studies have demonstrated UDCA's ability to partially counteract the effects of the various agents on mitochondrial activity and reactive oxygen species formation. By controlling the PI3K- Akt/PKB pathways, UDCA can prevent the programmed cell death process from killing SH-SY5Y cells (19). UDCA can affect signaling pathway that causes the programmed cell death in neuronal cell lines. In order to further evaluate its neuroprotective potential in PD, the international Linked Clinical Trials (iLCT) designated UDCA as its most highly prioritized neuroprotective chemical for research in clinical studies in 2015 (20). In this study, we aim to validate UDCA effect on Parkinson's disease patients and healthy volunteers using statistical analysis.

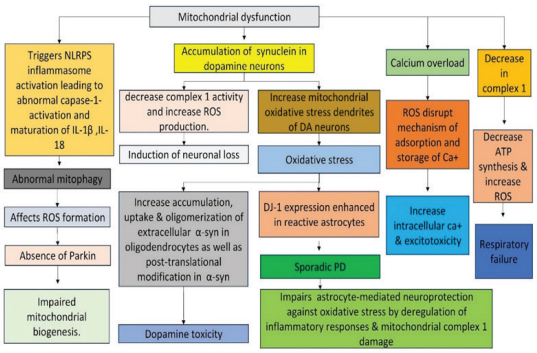

Fig. 1. Flowchart of Mitochondrial dysfunction on Parkinson's disease.

Materials and Methods

Eligibility criteria

We assess the PICO (Population, Intervention, Comparison, and Outcomes) framework: Population: Parkinson's disease-affected persons older than 60 (diagnosed by Pi concentration and ATP concentration using P-MRS); Intervention: Ursodeoxycholic acid (UDCA); Comparison: healthy volunteers, gender, severity, UDCA dosage, and Duration: 6 weeks; Outcomes: Increase in ATP concentration/ decreased dopaminergic neuron death and clinical signs.

Literature search

Literature search systematically from the EMBASE (https://www.elsevier.com/en-in/products/embase), Medline (https://www.medline.com/), Drug Bank (https://go.drugbank.com/), Clinical Trial Gov (https://clinicaltrials.gov/), Google Scholar (https://scholar.google.com/), and Cochrane Central Register of Controlled Trials (CENTRAL) (https://www.cochranelibrary.com/central/about-central) was performed. Futhermore comprehensive survey for references was directed over 2 months, using querying and databases (PubChem, therapeutic target database, toxin target database) reviews, index searches of proceedings, backtracking references, conversations with colleagues, and internet searching. We screened clinical trials and published reviews to find appropriate studies. We searched using the keywords Parkinson Disease, UDCA on PD, Randomized control trials for Parkinsonism, Treatment of PD using UDCA, UDCA for Mental illness, ATP concentration in PD, ROS on mitochondria in PD. There was only English language studies included.

Screening and collection of data

Certainly, potentially eligible RCTs was screened, with disagreements fixed by consensus. For study inclusion, we screened data concerning study characteristics, baseline characteristics, people with unstable circumstances, people with other neurological illnesses, people who were unable to undergo a 7-Tesla P MRS scan (21,22), Multiple systems atrophy (MSA) (23), drug-induced parkinsonism (24), progressive supranuclear palsy (PSP) (25), dystonic or essential tremor (26), intervention and outcomes of interest. We combined all of the data from a trial that was presented in several journals and discrepancies were resolved over discussion.

Homogeneity and transitivity assessment

The trail characteristics and study examination across all qualified studies was evaluated through methodological and clinical heterogeneity. So then methods utilized for classifying disease severity, baseline disease severity and duration of interventions are considered as the chief outcome modifiers across the assessments and measured via distribution following this that any participant comprised in the network could be randomized to any of the accessible interventions are adopted through NMA rationality.

Data synthesis and analysis

We analyzed observational studies and randomized controlled trials individually. For obtaining a continuous variable (Population, Age, Sex, UDCA dose), modification from baseline in UDCA vs. control groups, we measured the standard mean differences (SMDs) or efficacy mean differences (MDs) and 95% confidence intervals (CIs). Inverse variance method was adopted for pooling SMDs and MD. We calculated 95% confidence intervals and risk ratios (RR) using the Mantel-Haenszel method. Statistical heterogeneity was observed by Chi square test and I 2 statistic (27). Using random effects model regardless of heterogeneity all the meta-analyses were performed. We have intended 2 subgroup analysis to evaluate the effect of UDCA on PD patient. Subgroup 1; Effect of UDCA on inorganic phosphate (Pi) concentration in P-MRS (UDCA vs Placebo); Subgroup 2; Effect of UDCA on ATP concentration in P-MRS (UDCA vs Placebo). Sensitivity analyses was carried out, by using alternative effect which subsequently measures (OR vs. RR), alternative pooling methods, and statistical models regarding heterogeneity (random vs. fixed effects). Publication bias was noticed by visually inspecting symmetry of forest plot and funnel plots. The calculations were done using RevMan 5.4 software (28).

Risk of bias

Using Cochrane tool the risk of bias was evaluated, to calculate the included studies for bias. Five areas of bias such as selection bias, reporting bias, detection bias, attrition bias, and

performance bias were used to evaluate the total risk of bias for each of the included studies (29,30). The risk of the decisions was categorised as high, low, or uncertain. Two reviewers completed the assessment independently. A third reviewer was consulted in the case that the options varied.

Confidence in the evidence

Using the web application and Confidence in Network Meta-Analysis (CINeMA) (31,32) framework the confidence was assessed. CINeMA is a version of GRADE approach (Grading of Recommendations, Assessment, Development and Evaluation) for NMA. Each domain was categorized by uniting the direct evidence with statistical contributions to the network to obtain a confidence. Considering the completeness of the study search publication bias was evaluated. However, assessment of funnel plot symmetry was not resolved due to small-study effects and add to uncertainty.

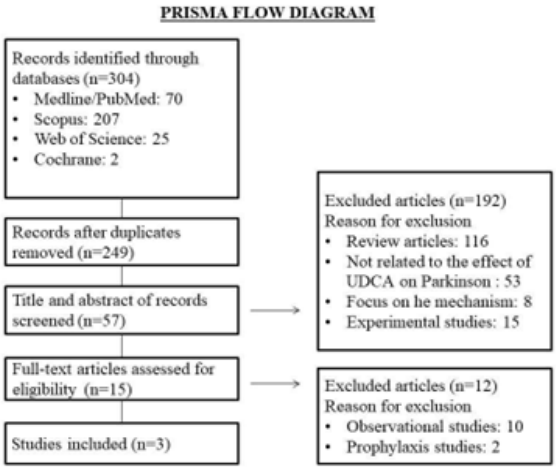

Fig. 2. PRISMA flowdiagram of the included articles.

Results and Discussion

Overall, we recognized 304 references through electronic databases. After rejecting duplicates and references that did not satisfied our inclusion criteria, 15 references were qualified for the qualitative data synthesis; 3 references fulfilled inclusion criteria for the meta-analysis (Tables 1 and 2). The treatment duration is 6 weeks and the subjects provided with ~50mg/kg/day (based on the usage of 250 and 500mg capsules) of UDCA to be allocated into 3 equal daily doses and titrated up over ~3 weeks to a stable dose for 6 weeks. UDCA and the control group's ATP and Pi concentrations were measured using 31-Phosphorus Magnetic Resonance Spectroscopy, clinically which has the potential for neurological practice due to its safe in-vivo evaluation of energy metabolism in cells and the indirect analysis of intracellular pH, Mg 2+, ATP concentration, and phospholipid composition of the cell membrane.

Risk of bias assessment

One study out of the three evaluated ones, as shown in Table 1, was determined to have a high RoB due to missing exclusion criteria (33). Due to bias resulting from the randomization method, deviations from the intended volunteers, incomplete outcome data, and bias in the selection of the reported result, the remaining two studies were identified as having & quot;certain concerns & quot; (Tables 1 and 2).

Assessment of clinical transitivity and heterogeneity

Certainly, we are not able to analyze and assess transitivity and heterogeneity by considering only one research per comparison. Variability in clinical parameters was not detected from the data provided within any of the included trials. It was determined that there was substantial heterogeneity for pairwise comparisons of any intervention vs control (I 2 = 94 and 97%); However, this assessment should not be taken too seriously because there were not enough trials to carry out a more thorough heterogeneity estimation and therefore it may be erroneous.

Pairwise and network meta-analysis

To examine the variations in intervention (UDCA) for each outcome measure, a me-

Current Trends in Biotechnology and Pharmacy
Vol. 19(1) 2211-2221, January 2025, ISSN 0973-8916 (Print), 2230-7303 (Online)
DOI: 10.5530/ctbp.2025.1.10

ta-analysis was conducted. The forest plot (Fig 3 and 4) was created to make the similarities between the ATP and Pi concentration in UDCA and control more clearly. We examined the impact of UDCA on ATP concentration using two trials (Abishek G. Sathe et al. and Xiao-Hong Zhu et al) and Pi concentration using two trials (Bruno Barbiroli et al. and Xiao-Hong Zhu et al) (Table 1 and 2).

Table-1: Characteristics of the Included Studies

Title	First Author's Name	Year of Publication	Country	Type of Study Design	References
Phosphorus Magnetic Resonance in Multiple System Atrophy and Parkinson's Disease	Bruno Barbiroli	1999	Italy	Clinical trail	[34]
Pharmacokinetics, Safety, and Tolerability of Orally Administered Ursodeoxycholic Acid in Patients With Parkinson's Disease- A Pilot Study	Abhishek G	2020	United States	Clinical trail	[14]
Quantitative Assessment of Occipital Metabolic and Energetic Changes in Parkinson's Patients, Using *In-vivo* 31P MRS-Based Metabolic Imaging at 7T	Xiao-Hong Zhu	2021	United States and United Kingdom	Clinical trail	[35]

Table-2: Detailed characteristics of the studies

Author	Population	Sex		Eligibility	Exclusion	Severity	Primary Outcome	Secondary Outcome	Intervention	
		Male	Female						Case (UDCA Dose/ Duration)	Control
Abhishek G Sathe et.al..,	5	4	1	18 years and older (adult, older adult) with Parkinson's disease	Pregnant and lactating women, people with unstable circumstances , people with other neurological illness. People who unable to undergo a 7- Telsa P-MRS scan.	Mild to moderate	Change in the ATP concentration	UDCA pharmacokinetics	50mg/ kg/ day/ Orally for 6weeks	Healthy volunteers
Bruno Barbiroli et.al..,	29	17	12	42-85 years	Multiple system atrophy (MSA), olivopontocerebellar atrophy (OPCA) and straitonigral degeneration variant (SND)	Mild to moderate	Estimation of Pi concentration using P-MRS	Estimation of ATP concentration	UDCA	Healthy volunteers
Xiao-Hong Zhu et.al..,	38	18	20	60-64 years	-	Mild to moderate	Determination of ATP,PCr, Pi, PE and GPC concentration	Cerebral Phosphorus Metabolite	50mg/ kg/ day/ Orally for 6weeks	Healthy volunteers

Inorganic phosphate concentration (Pi)

16 healthy participants and 13 people with Parkinson's disease were recruited by Bruno Barbiroli et al. Brain Pi level was considerably (1.63 mM 0.21 vs. 1.29 mM 0.13; p 0.0001) greater in PD patients than in controls (34). Pi has changed, according to research by Xiao-Hong Zhu et al. ([Pi]PD = 0.90 0.12 mM, [Pi] CT = 1.01 0.11 mM, n = 19, p = 0.007) (35). The UDCA, as compared to the control, favours a rise in the inorganic phosphate concentration (Pi), by statistical analysis with the z score = 0.08 (Fig 3).

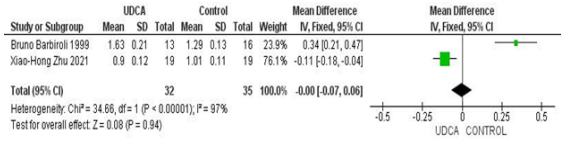

Fig. 3. Effect of UDCA on Pi concentration.

The outcome of ATP concentration

Parkinson's disease patients had lower brain adenosine triphosphate (ATP) levels than age-matched, healthy controls, according to preliminary findings. Totally 5 individuals were taken into the study and P- MRS data were collected from the occipital lobes of three research subjects. The data from the other 2 individuals was either not captured or was useless due to the scanner's technical issue. In subjects 1, 2, and 4, the ATP concentrations were tested under pre-UDCA (2.68, 2.76, and 2.72) and post-UDCA(2.73, 2.79 and 2.75) circumstances. In the first two patients, we also saw a decrease in the metabolic rate of the ATPase reaction, followed by a rise in the metabolic rate of the creatine kinase reaction. The corrective effect of the UDCA therapy may be responsible for these observations. Statistically significant differences were detected in concentrations of ATP ([ATP] PD = 2.62 ± 0.17 mM, [ATP]CT = 2.82 ± 0.14 mM, n = 19, p = 0.0004) (20). The UDCA, as compared to the control it favours a rise in the ATP concentration, by statistical analysis with z score=0.71 (Fig 4).

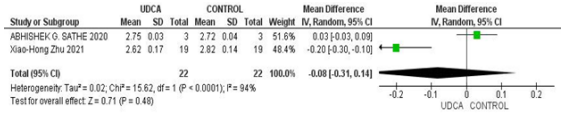

Fig. 4. Effect of UDCA on ATP concentration.

Confidence in the evidence

Due to research limitations, heterogeneity, uncertain, oblique, and publication bias (Tables 1 and 2), confidence in estimates for changes in mean Pi and ATP concentration is regarded as minimal to extremely low (Tables 1 and 2). Due to the short sample size and lack of mixed data, the prediction interval estimate and inconsistency assessment could not be completed, and inconsistency was reduced as a result. The fundamental idea of transitivity may have been weakened by the lowering of inconsistency to account for variance in one impact modification discovered. Because of bias in the choice of the reported outcome, publication bias has been lowered. The evaluation of small-study impacts was not successful.

Discussion

As Parkinson's disease is an entire brain disease, extranigral parts of the brain includes cerebral cortex, show evidence of neuro degeneration as progresses (36, 37). UDCA demonstrated to prevent rotenone-induced apoptosis by increasing mitochondrial action by increasing ATP levels. UDCA altered Bcl-2 and Bax mutations, and decreasing the activities of caspase-3, 8, 9 and modifying the intrinsic and extrinsic pathways. These effects are most likely associated with dopamine production and mitochondrial control. UDCA not only retained its membrane around the mitochondria integrity but also retained its energy production, as UDCA-treated rats had higher levels of ATP in the striatum (38-41). High dosages of UDCA (upto 50mg/kg/day) have been shown to be safe and tolerable in individuals with ALS (amyotrophic lateral sclerosis), and established that UDCA capable of crossing the BBB, with attainable levels in the CSF that correlate with serum levels (42). UDCA is a hydrophilic bile acid and has

been given FDA approval to treat primary biliary cholangitis. Several investigations employing PD cell lines and pre-clinical animal studies revealed its mitochondria-protective and anti-apoptotic properties. It is commonly acknowledged that NAD+ not only controls ATP energy production via NAD+/NADH reactions, also acts as the primary substrate for several NAD+-dependent enzymes responsible for diverse cellular signaling pathways. These enzymes activity is influenced by NAD+, and NAD+ deficiency linked to a variety of neurological diseases (43-45).

Mortiboys et al demonstrated that UDCA restores mitochondrial dysfunction in parkin-mutant fibroblasts derived from Parkinson's disease patients (46). According to the 'UP Study' of phase 2, a two-centered, double blind, randomized, placebo-controlled trial an increase in mean midbrain Pi by +0.02 in the UDCA group and a decrease by 0.006 in the placebo group is consistent with higher ATP hydrolysis in the UDCA treatment group. This Study proved that UDCA at 30 mg/kg is safe and well tolerated in Parkinson's disease, with no SAEs and only minor, temporary side effects recorded in the UDCA treatment group (20). 3 patients were found to have increased ATP levels in occipital cortical region, who had baseline and post UDCA P-MRS assessments. As a result, outcomes support that UDCA enhance the mitochondrial action in Parkinson's disease, and the metabolic rate was decreased in ATPase reaction in the first two participants, while the metabolic rate was increased in creatine kinase reaction in the similar brains. UDCA proved to be quite safe and approved, and this is the first report on UDCA pharmacokinetics in patients with Parkinson's disease (14). Xiao-Hong Zhu et al anticipated that the patients with Parkinson's disease, probably cause DNA damage or cellular abnormalities which change enzyme activities and decrease intracellular NAD+ content, thereby causing a drop in ATP content. As a result, activation of mitochondrial ATP synthase is anticipated to occur in order to increase ATP generation and energy requirements of brain cells (43). A recent clinical study had provided an understanding about the dopaminergic neurons in the substantial nigra are particularly vulnerable to the cellular dysfunctions observed in Parkinson's disease. The findings suggested that the greater susceptibility of nigral dopamine neurons can be directly related to their unique structural and bioenergetic properties leading to a greater basal energy necessity and reduced energy storing capacity. Consequently, they are more vulnerable to cellular stressors that affect energy production in mitochondria (47,48). Clinical trials in large population are required to confirm these discoveries and in contrast to examine the UDCA effect on Parkinson's disease (49). Investigating UDCA in combination with existing PD treatments, such as levodopa or other neuroprotective agents could provide synergistic benefits or enhanced therapeutic effects. We compared the effect of UDCA with the control (healthy volunteers) using P-MRS of the ATP and inorganic phosphate (Pi) concentrations using the meta-analysis software Review Manager 5.4. The ATP and Pi concentrations increased in the UDCA group as compared to the control. Considering its efficacy in animal models and human safety profile, UDCA appears to be a promising treatment for Parkinson's disease (50).

Conclusion

UDCA at the higher doses is safe and endorse in early stage of PD patients. It has the excellent safety profile at 30 mg/kg, combined with the 31P-MRS-based evidence. The meta-analysis highlights promising preliminary findings regarding UDCA's effects on ATP concentration and mitochondrial activity in PD, future research should focus on expanding these findings through rigorous clinical trials, mechanistic investigations, and personalized medicine approaches. This comprehensive approach will be crucial for advancing UDCA from experimental evidence to clinically validated therapeutical intervention for Parkinson's disease and potentially on other neurological conditions.

Author Contributions:

All authors contributed to the study conception and design. Material preparation, data collection and analysis were performed by [Aswin Krishnamurthy], [Nandhini Sundaresan], [Vivekananthan G], [Sanjay R], and [Monish S]. All authors read and approved the final manuscript.

Ethics Approval and Consent to Participate: Not Applicable.

Acknowledgment:

The administration of Sri Ramachandra Faculty of Pharmacy, Sri Ramachandra Institute of Higher Education and Research in Tamilnadu is thanked for their assistance and encouragement.

Funding: This research received no external funding.

Conflict of Interest: The authors declare no conflicts of interest.

References

1. Kalia LV, Lang AE., (2015). Parkinson's disease. Lancet, 386:896-912.
2. Schapira AH, Olanow CW, Greenamyre JT, Bezard E., (2014). Slowing of neurodegeneration in Parkinson's disease and Huntington's disease: future therapeutic perspectives. Lancet, 384:545-555.
3. Abdelkader NF, Safar MM, Salem HA., (2016). Ursodeoxycholic acid ameliorates apoptotic cascade in the rotenone model of Parkinson's disease: modulation of mitochondrial perturbations. Mol Neurobiol, 53:810-817.
4. de Oliveira Junior ER, Truzzi E, Ferraro L, Fogagnolo M, Pavan B, Beggiato S, et al., (2020). Nasal administration of nanoencapsulated geraniol/ursodeoxycholic acid conjugate: towards a new approach for the management of Parkinson's disease. Journal of Control Release, 321:540-552.
5. Weiduschat N, Mao X, Beal MF, Nirenberg MJ, Shungu DC, Henchcliffe C., (2015). Usefulness of proton and phosphorus MR spectroscopic imaging for early diagnosis of Parkinson's disease. J Neuroimaging, 25:105-110.
6. Rango M, Bonifati C, Bresolin N., (2006). Parkinson's disease and brain mitochondrial dysfunction: a functional phosphorus magnetic resonance spectroscopy study. Journal of Cerebral Blood Flow Metabolism, 26:283-290.
7. Jensen, I., Heine, J., Ruf, V.C., Compta, Y., Porcel, L.M., Troakes, C., Vamanu, A., Downes, S., Irwin, D., Cohen, J. and Lee, E.B., (2024). Impact of Magnetic Resonance Imaging Markers on the Diagnostic Performance of the International Parkinson and Movement Disorder Society Multiple System Atrophy Criteria. Movement Disorders.
8. Pettegrew, J.W., Klunk, W.E., Panchalingam, K., McClure, R.J. and Stanley, J.A., (1997). Magnetic Resonance Spectroscopic Changes in Alzheimer's Disease a. Annals of the New York Academy of Sciences, 826(1):282-306.
9. Mortiboys, H., Macdonald, R., Payne, T., Sassani, M., Jenkins, T. and Bandmann, O., (2018). Translational approaches to restoring mitochondrial function in Parkinson's disease. FEBS letters, 592(5):776-792.
10. Rodríguez-Varela, C. and Labarta, E., (2020). Clinical application of antioxidants to improve human oocyte mitochondrial function: a review. Antioxidants, 9(12):1197.
11. Bhatti, J.S., Bhatti, G.K. and Reddy, P.H., (2017). Mitochondrial dysfunction and oxidative stress in metabolic disorders—A step towards mitochondria based thera-

peutic strategies. Biochimica et Biophysica Acta (BBA)-Molecular Basis of Disease, 1863(5):1066-1077.

12. Exner, N., Lutz, A.K., Haass, C. and Winklhofer, K.F., (2012). Mitochondrial dysfunction in Parkinson's disease: molecular mechanisms and pathophysiological consequences. The EMBO journal, 31(14):3038-3062.

13. Moradi Vastegani, S., Nasrolahi, A., Ghaderi, S., Belali, R., Rashno, M., Farzaneh, M. and Khoshnam, S.E., (2023). Mitochondrial dysfunction and Parkinson's disease: pathogenesis and therapeutic strategies. Neurochemical research, 48(8):2285-2308.

14. Sathe, A.G., Tuite, P., Chen, C., Ma, Y., Chen, W., Cloyd, J., Low, W.C., Steer, C.J., Lee, B.Y., Zhu, X.H. and Coles, L.D., (2020). Pharmacokinetics, safety, and tolerability of orally administered ursodeoxycholic acid in patients with Parkinson's disease—a pilot study. The Journal of Clinical Pharmacology, 60(6):744-750.

15. Vang, S., Longley, K., Steer, C.J. and Low, W.C., (2014). The unexpected uses of urso-and tauroursodeoxycholic acid in the treatment of non-liver diseases. Global advances in health and medicine, 3(3):58-69.

16. Ikegami, T. and Matsuzaki, Y., (2008). Ursodeoxycholic acid: mechanism of action and novel clinical applications. Hepatology Research, 38(2):123-131.

17. Kumar, D. and Tandon, R.K., (2001). Use of ursodeoxycholic acid in liver diseases. Journal of Gastroenterology and Hepatology, 16(1):3-14.

18. Amaral, J.D., Viana, R.J., Ramalho, R.M., Steer, C.J. and Rodrigues, C.M., (2009). Bile acids: regulation of apoptosis by ursodeoxycholic acid. Journal of lipid research, 50(9):1721-1734.

19. Chun, H.S. and Low, W.C., (2012). Ursodeoxycholic acid suppresses mitochondria-dependent programmed cell death induced by sodium nitroprusside in SH-SY5Y cells. Toxicology, 292(2-3):105-112.

20. Payne, T., Appleby, M., Buckley, E., van Gelder, L.M., Mullish, B.H., Sassani, M., Dunning, M.J., Hernandez, D., Scholz, S.W., McNeill, A. and Libri, V., (2023). A Double-Blind, Randomized, Placebo-Controlled Trial of Ursodeoxycholic Acid (UDCA) in Parkinson's Disease. Movement Disorders, 38(8):1493-1502.

21. Keith, G.A., Woodward, R.A., Hopkins, T., Allwood-Spiers, S., Trinder, J., Muir, K.W., Porter, D.A. and Fullerton, N.E., (2024). Towards clinical translation of 7 Tesla MRI in the human brain. IPEM-Translation, 9:100025.

22. Arachchige, A.S.P.M., Meuli, S., Centini, F.R., Stomeo, N., Catapano, F. and Politi, L.S., (2024). Evaluating the role of 7-Tesla magnetic resonance imaging in neurosurgery: Trends in literature since clinical approval. World Journal of Radiology, 16(7):274.

23. Jellinger, K.A., (2024). The Pathobiology of Behavioral Changes in Multiple System Atrophy: An Update. International Journal of Molecular Sciences, 25(13).

24. Calzetti, S. and Negrotti, A., (2024). Outcome of Drug-Induced Parkinsonism in the Elderly: A Permanent Nonprogressive Parkinsonian Syndrome May Occur Following Discontinuation of Cinnarizine and Flunarizine. Annals of Pharmacotherapy, 10600280241263592.

25. Currens, L. and Pantelyat, A., (2024). Progressive Supranuclear Palsy Diagnosis and Treatment. Current Treatment Options in Neurology, 26(4):97-114.

26. Rajan, R., Anandapadmanabhan, R., Vishnoi, A., Latorre, A., Thirugnanasam-

bandam, N., Dipani, A., Biswas, D., Radhakrishnan, D.M., Srivastava, A. and Bhatia, K.P., (2024). Essential tremor and essential tremor plus are essentially similar electrophysiologically. Movement Disorders Clinical Practice, 11(2):136-142.

27. Ufondu, A.N., Shukla, U.C., Stambaugh, C., Huber, K.E. and Stambaugh, N., (2023). Categorical variable analyses: Chi-square, Fisher's exact, Mantel–Haenszel. In Translational Radiation Oncology, Academic Press,165-170.

28. Tantry, T.P., Karanth, H., Shetty, P.K. and Kadam, D., (2021). Self-learning software tools for data analysis in meta-analysis. Korean Journal of Anesthesiology, 74(5):459-461.

29. Nikolakopoulou, A., Higgins, J.P., Papakonstantinou, T., Chaimani, A., Del Giovane, C., Egger, M. and Salanti, G., (2020). CINeMA: an approach for assessing confidence in the results of a network meta-analysis. PLoS medicine, 17(4):e1003082.

30. Papakonstantinou, T., Nikolakopoulou, A., Higgins, J.P., Egger, M. and Salanti, G., (2020). Cinema: software for semiautomated assessment of the confidence in the results of network meta-analysis. Campbell systematic reviews, 16(1):e1080.

31. Higgins, J.P., Savović, J., Page, M.J., Elbers, R.G. and Sterne, J.A., (2019). Assessing risk of bias in a randomized trial. Cochrane handbook for systematic reviews of interventions, 205-228.

32. Lundh, A. and Gøtzsche, P.C., (2008). Recommendations by Cochrane Review Groups for assessment of the risk of bias in studies. BMC medical research methodology, 8:1-9.

33. Ufondu, A.N., Shukla, U.C., Stambaugh, C., Huber, K.E. and Stambaugh, N., 2023. Categorical variable analyses: Chi-square, Fisher's exact, Mantel–Haenszel. In Translational Radiation Oncology, Academic Press, 165-170.

34. Barbiroli, B., Martinelli, P., Patuelli, A., Lodi, R., Iotti, S., Cortelli, P. and Montagna, P., (1999). Phosphorus magnetic resonance spectroscopy in multiple system atrophy and Parkinson's disease. Movement disorders: official journal of the Movement Disorder Society, 14(3):430-435.

35. Zhu, X.H., Lee, B.Y., Tuite, P., Coles, L., Sathe, A.G., Chen, C., Cloyd, J., Low, W.C., Steer, C.J. and Chen, W., (2021). Quantitative assessment of occipital metabolic and energetic changes in Parkinson's patients, using in Vivo 31P MRS-based metabolic imaging at 7T. Metabolites, 11(3):145.

36. Mak, E., Su, L., Williams, G.B., Firbank, M.J., Lawson, R.A., Yarnall, A.J., Duncan, G.W., Owen, A.M., Khoo, T.K., Brooks, D.J. and Rowe, J.B., (2015). Baseline and longitudinal grey matter changes in newly diagnosed Parkinson's disease: ICICLE-PD study. Brain, 138(10):2974-2986.

37. Milivojac, T., Grabež, M., Krivokuća, A., Maličević, U., Gajić Bojić, M., Đukanović, Đ., Uletilović, S., Mandić-Kovačević, N., Cvjetković, T., Barudžija, M. and Vojinović, N., (2024). Ursodeoxycholic and chenodeoxycholic bile acids attenuate systemic and liver inflammation induced by lipopolysaccharide in rats. Molecular and Cellular Biochemistry, 1-14.

38. Cavusoglu Nalbantoglu, I., Sevgi, S., Kerimoglu, G., Kadıoglu Duman, M. and Kalyoncu, N.I., (2024). Ursodeoxycholic acid ameliorates erectile dysfunction and corporal fibrosis in diabetic rats by inhibiting the TGF-β1/Smad2 pathway. International journal of impotence research,1-10.

39. Raad, Y. and Jwaid, A.H., (2024). Evaluation of the possible effect of Ursodeoxycholic Acid to treat rheumatoid arthritis in-

duced in the Rat model in comparison with Diclofenac.

40. Li, H., Wang, M., Chen, P., Zhu, M. and Chen, L., (2024). A high-dose of ursodeoxycholic acid treatment alleviates liver inflammation by remodeling gut microbiota and bile acid profile in a mouse model of non-alcoholic steatohepatitis. Biomedicine & Pharmacotherapy, 174:116617.

41. Rodrigues, C.M. and Steer, C.J., (2001). The therapeutic effects of ursodeoxycholic acid as an anti-apoptotic agent. Expert opinion on investigational drugs, 10(7):1243-1253.

42. Bell, S.M., Barnes, K., Clemmens, H., Al-Rafiah, A.R., Al-Ofi, E.A., Leech, V., Bandmann, O., Shaw, P.J., Blackburn, D.J., Ferraiuolo, L. and Mortiboys, H., (2018). Ursodeoxycholic acid improves mitochondrial function and redistributes Drp1 in fibroblasts from patients with either sporadic or familial Alzheimer's disease. Journal of molecular biology, 430(21):3942-3953.

43. Houtkooper, R.H., Cantó, C., Wanders, R.J. and Auwerx, J., (2010). The secret life of NAD+: an old metabolite controlling new metabolic signaling pathways. Endocrine reviews, 31(2):194-223.

44. Lu, M., Zhu, X.H., Zhang, Y. and Chen, W., (2014). Intracellular redox state revealed by in vivo 31P MRS measurement of NAD+ and NADH contents in brains. Magnetic resonance in medicine, 71(6):1959-1972.

45. Ma, Y., Chen, H., He, X., Nie, H., Hong, Y., Sheng, C., Wang, Q., Xia, W. and Ying, W., (2012). NAD+ metabolism and NAD+-dependent enzymes: promising therapeutic targets for neurological diseases. Current drug targets, 13(2);222-229.

46. Mortiboys, H., Furmston, R., Bronstad, G., Aasly, J., Elliott, C. and Bandmann, O., (2015). UDCA exerts beneficial effect on mitochondrial dysfunction in LRRK2 G2019S carriers and in vivo. Neurology, 85(10):846-852.

47. Pacelli, C., Giguère, N., Bourque, M.J., Lévesque, M., Slack, R.S. and Trudeau, L.É., (2015). Elevated mitochondrial bioenergetics and axonal arborization size are key contributors to the vulnerability of dopamine neurons. Current Biology, 25(18):2349-2360.

48. Ciocca, M. and Pizzamiglio, C., (2024). Clinical Benefits of Therapeutic Interventions Targeting Mitochondria in Parkinson's Disease Patients. CNS & Neurological Disorders Drug Targets, 23(5):554.

49. Tonkin, P.G., Miller, T.D., Hartmann, T.E. and Skein, M., (2023). The effects of exercise on non-motor experiences of daily living experienced in Parkinson's Disease: A systematic review and network meta-analysis. Clinical Parkinsonism & Related Disorders, 9:100203.

50. Baroli, B.M., Loi, E., Solari, P., Kasture, A., Moi, L., Muroni, P., Kasture, S., Setzu, M.D., Liscia, A. and Zavattari, P., (2019). Evaluation of oxidative stress mechanisms and the effects of phytotherapic extracts on Parkinson's disease Drosophila PINK1B9 model. The FASEB Journal, 33(10):11028-11034.

Current Trends in Biotechnology and Pharmacy
Vol. 19(1) 2212-2222, January 2025, ISSN 0973-8916 (Print), 2230-7303 (Online)
DOI: 10.5530/ctbp.2025.1.11

Traditional Herbs as Effective Natural Remedies for Treating Urinary Tract Ailments

Venkata Kanaka Srivani Maddala

Department of Chemistry, Vignans Foundation for Science Technology and Research Vadlamudi, Guntur 522 213, Andhra Pradesh

Corresponding author:Sriani77@gmail.com*

Abstract

Urinary tract infections have become quite chronic currently. Approximately 150 million people are affected with urinary tract infections (UTIs) annually. The prevalence of urinary tract infections is high among the women population in comparison with men. It is coexistent with high mortality as well as morbidity. Urinary tract infections may exert their influence on any part of the tract such as urethra, ureters and kidneys. Synthetic drugs are being administered unrestrained to control such diseases leading to many impediments. Frequent administration of antibiotics causes adverse effects and impairs healthy bacteria in the body. Under such circumstances, traditional herbs as an efficacious alternative therapy has surfaced and playing a central role. This review explores the efficacy of some of these traditional herbs and the critical role that they play in managing urinary tract infections among the populace. It is advocated that herbal medicines can be a potential, sustainable alternative therapy for managing urinary tract infections.

Keywords: Alternative therapies, Sustainable approach, Traditional herbs, Treatment, Urinary tract infections

Introduction

Urinary tract infection (UTI) is a severe public health problem and involves any part of the urinary system. UTI is caused by both Gram-positive and Gram-negative bacteria such as *Enterococcus faecalis*, *Escherichia coli*, *Klebsiella pneumonia*, *Proteus mirabilis*, and *Staphylococcus saprophyticus*. The common symptoms of UTI include pain during urination and in the lower back. Fifty per cent of women are affected by such infections (1). Other complications like fever, myalgia, frequent urination, blood in the urine, protein in the urine may occur if the microbes reach the gastrointestinal tract, urethra, bladder or kidney (2). Spread of UTI occurs due to sexual intercourse, unhygienic practices, and lack of adequate intake of water. UTIs can also occur while using a catheter or during chemotherapy (3). Antibiotics are prescribed to prevent recurrence of UTIs (4). Antibiotic therapies can control these UTI infections but the pathogenic strains develop resistance overtime via efflux pumps or by other biochemical mechanisms. Prevention of recurrence of disease is therefore of paramount importance (5). Reoccurrence of UTI can be prevented by antibiotic treatment and non-antibiotic measures (vitamins, hygienic measures, vaccines, oestrogens) that are of poor quality and ineffective (6). Drugs like trimethoprim- sulphamethoxazole or fosfomycin and nitrofurantoin (7,8) are used to treat Escherichia coli, Proteus, Klebsiella and Staphylococcus saprophyticus infection and lead to side effects. An overview of the utilization of traditional herbs to treat the infections is depicted in the figure 1. Many antibiotics were used in treating UTIs. Adverse effects were noticed depending

Current Trends in Biotechnology and Pharmacy
Vol. 19(1) 2212-2222, January 2025, ISSN 0973-8916 (Print), 2230-7303 (Online)
DOI: 10.5530/ctbp.2025.1.11

on the type of specific antibiotics used, and the duration of treatment. Some of the common antibiotics with their adverse effects are shown in the Table 1. Trimethoprim-sulfamethoxazole was used to treat common complicated UTI, but it caused severe joint pains and fever. Trimethoprim-sulfamethoxazole and fluoroquinolones showed little effect on vaginal and fecal anaerobic flora, but resulted in skin rashes, urticaria, angioedema/laryngeal edema, nausea, vomiting, abdominal pain, neuromuscular and gastrointestinal problems tendinopathy, respiratory problems, and pneumonia (9).

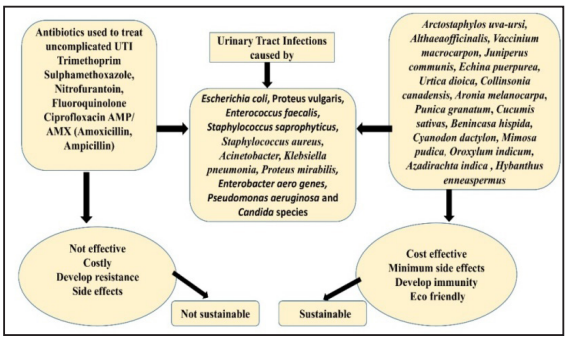

Fig. 1: An overview of urinary tract infection, causal organisms, herbs that can be effectively used to treat UTI are shown in the figure.

Complicated and uncomplicated urinary tract infections

UTI is of two types; complicated and uncomplicated. Complicated UTI occurs in people having abnormalities in any part of genitourinary tract and lead to serious issues compared to uncomplicated UTI. Uncomplicated UTI infections occur in the absence of abnormalities (10). An uncomplicated urinary tract infection is the bacterial infection of bladder and its structure. Uncomplicated UTI is known as cystitis or as lower UTI. Treatment of UTI helps to control the kidney infection or pyelonephritis that may lead to the destruction of delicate structures in nephrons and cause hypertension. UTI is the most common and approximately 800 million are affected with at least one urinary tract infection in every year (11,12). The prevalence of the UTI in women is five times higher than in men (13). According to the Ahmad et al 80% of uro- pathogens have shown resistance to two antibiotics (14). Whenever the pathogens cause UTI, they enter the urinary tract via urethra. Bacteria enter in to urethra from the bowel they colonize and attach to the bladder and form a biofilm that make the pathogens to escape the host immune response (15). Pathogens can enter in to urinary tract due to improper urogenital area via sexual intercourse, feminine products and contraceptives. In the urinary tract, the pathogens develop and cause infections. Pathogens may enter blood stream and migrates to kidney or bladder that lead to infection (16). In uncomplicated infection, the infection of healthy patient responds to antibiotic treatment. But, complicated infections occur in the people having abnormal urinary tract and often obstructed by stones or bladder ureter reflux. Isolated infection occurs at an interval of six months without the connection between two episodes and it represents the mother infection. Unresolved infection does not respond to any antibiotic treatment and reinfection recurrence is the last stage of urinary tract infection. In this type of infection, the patient is infected again with the same pathogen after treating urinary tract infection. Different stages of UTI are shown in the figure 2. Long term usage of antibiotics to treat the urinary tract infection is leading to the development of resistant microbial strains which persist in the environment up to six months. This leaves a window for us to develop and use the effective alternative therapies like that of herbal medicines. Nearly 40% of the population, mostly tribal folk and people living in rural areas are still dependent on such herbs for many treatments.

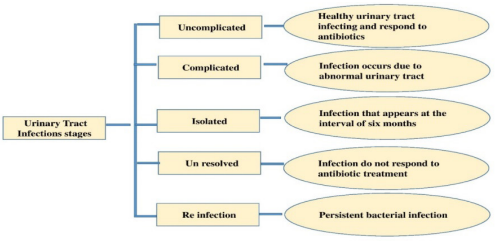

Fig. 2: Various stages of urinary tract infections

Table 1. Antibiotics and their unpropitious effects on urinary tract

Name of the antibiotics	Adverse effects
Trimthoprim-sulfamethoxazole and Fluroquinolones	Little effect on vaginal and faecal anaerobic flora
Nitrofurantoin Fluroquinolone Trimethoprim-sulfamethoxazole AMP/ AMX (Amoxicillin, Ampicillin)	Skin rash
Nitrofurantoin Fluroquinolone Trimethoprim-sulfamethoxazole AMP/AMX (Amoxicillin, Ampicillin)	Urticaria (skin reaction itchy welts) angioedema/laryngeal edema, nausea, vomiting, abdominal pain, neuromuscular and gastrointestinal problems, tendinopathy, respiratory problems, pneumonia
Amoxicillin	Nausea, diarrhea and rash
Fosfomycin	Diarrhoea, head ache and abdominal pain
Trimethoprim-sulfamethoxazole Applied to treat common complicated UTI	Joint pains, fever
Ciprofloxacin	Headache, nausea, dizziness

Symptoms

UTI can be diagnosed by the symptoms like urinary frequency, hematuria, dysuria or suprapubic pain. Such a condition can be confirmed by microscopic observations of urine and by culturing the urine sample. For complicated UTI in addition to above symptoms other symptoms like fever, chills, sepsis can be seen in patients. Burning sensation associated with urine, foul smell from urine, pain in lower abdomen back and pelvic area in women (17), change in urine color are common. If kidney gets infected then it causes fever, nausea, vomiting and back pain (18). Continuous use of antibiotics lead to vaginal candidiasis and gastrointestinal symptoms and it is difficult to prevent the recurrence of infections. *E. coli* causes gastrointestinal diseases and diarrhea (19). If these infections are not treated, they lead to pyelonephritis an infection of kidneys, and sepsis which may leads to threaten the life, and damage to the kidneys. UTI can be controlled by using antibiotics and the choice of antibiotics depends on the type of the bacteria involved. UTI infections can be prevented by taking good hygiene especially after sexual intercourse. Drinking excess water can drain the bacteria out of the urinary tract. However, use of catheter can complement the use of bacteria.

Significance of traditional herbs

Traditional herbs have been found as effective natural remedies in managing many UTIs Traditional herbs can support the body against infections, control inflammation, diuresis, help in the proper functioning of kidneys, build up immunity and reduce clinical symptoms. Garlic, ginger and turmeric show anti-microbial properties and are generally consumed in one form or the other. Peppermint tea can sooth the bladder and prevents discomfort. Chamomile tea, willow bark and liquorice roots control inflammation and reduce symptoms. Dandelion and burdock also show diuretic properties by flushing out the toxins and fluids from the body and thus play a vital role in managing UTI. Cranberry shows antioxidant properties and supports proper functioning of kidneys. Traditional herbs have been used since time immemorial to treat UTIs. Herbs such as *Arctostaphylos uva-ursi, Althaea officinalis, Vaccinium macrocarpon, Ju-*

niperus communis, Echina puerpurea, Urtica dioica, Collinsonia canadensis help in alleviating the symptoms of urinary tract infections without any adverse effects. Further, they are cost-effective and sustainable.

Role of traditional plants in treating UTI

Herbal traditional medicine is helpful to treat UTI infections with minimum adverse effects (20). According to the World Health Organization, multi drug resistant (MDR) bacteria can cause many deaths by the year 2050. In contrast, plants have been used since ages to treat UTI. Approximately, 80 per cent of population from developing countries utilizes plant as medicine to treat multiple infections (21) which are safer than the synthetic drugs (22). Diverse plant parts like bark, leaves, flowers, fruits, seeds, stems, and roots are used for therapeutic purposes which generally consist of several bioactive compounds with pharmacological properties (23,24). Some of the important taxa used in the treatment of UTI include *Aptosimum procumbens*, *Cardiospermum halicacabum*, *Cissampelos capensis*, *Zantedeschia albomaculata*, *Hydrastis canadensis* (golden seal), *Agathosma betulina* (Buchu), *Equisetum arvense* (horse tail), *Arctostaphylos uva-ursi* (bear berry), *Vaccinium macrocarpon* (crane berry), *Echinaceae purpures* (cone flower) and others (24,25,26). Long term administration of these medicinal plants has been found safe for therapy (27). *Punica granatum* (pomogranate), *Cornus mas* (cornelian cherry), *Aronia melanocarpa* (black chock berry) and their extracts are being used currently to cure UTI. So, herbal products being prepared from plant material are highly important and eco-friendly. Research findings have demonstrated the therapeutic properties of many plants which could be attributed to the presence of phytochemical components like terpenoids, tannins, sterols, anthraquinones, saponins, phenols, phytosterols, flavonoids, sesquiterpenes and glycosides. *Cortex dictamni* is the Chinese traditional drug that helps to cure both skin and urinary tract infections. An alkaloid called dictamine extracted from *Cortex dictamni* shows anti-bacterial, anti-cancer and anti-fungal properties (28,29,30). Leaf extract of *Arctostaphylos uva-ursi* consists of flavonoids, terpenoids, tannins, iridoids, arbutin (a glycoside) and show anti-bacterial activity. Byproducts of the *P. granatum* fruit consists of anti-microbial compounds like punicalagin, penicillins, allagic acid and gallic acid and flavonols like myricetin, quercetin and anthocyanins exhibited antibacterial activity (31,32) and its seed extract has the properties of urobactericidal activity against *E. coli*. The fruits of *Aronia melanocarpa* have polyphenols that contain antioxidant and antimicrobial properties. Arona berries consist of quinic acid, which helps in treating UTI (33). Whole plants of *Cinnamomum verum* have antioxidant and antibacterial properties due to the presence of trans-cinnamaldehyde, eugenol and others. Trans-cinnamal acetate and proanthocyanidins help in treating UTIs. *Hybanthus enneaspermus* showed *in vitro* anti-bacterial activity against *E. coli*, *P. aeruginosa*, *K. pneumoniae*, *P. mirabilis*, *E. faecalis* and *S. aureus*. The ethanolic extract of these plants consists of bioactive compounds such as flavonoids, terpenes, alkaloids that can help in mitigating UTIs.

Arctosta phylosuvaursi (Uva-ursi), *Juniperus* spp., (Juniper), leaves and fruits of *Vaccinium macrocarpon* (crane berry) contain antimicrobial compounds that act against microbes and protect the humans against acute and chronic UTIs (34). Berberine is the important drug present in the roots of *Mahonia aquitolium* (dragon grape, belongs to the family Berberidaceae) and *Hydrastis canadensis* kill bacteria and fight against infections to prevent *E. coli* and *Proteus* species from adhering to the host cell (35). Aqueous extraction of *Zea mays* can prevent the symptoms of UTI by reducing the number of RBC pus cells in urine (36). *Gundelia tournefortil*, *Eruca sativa* and *Organum syriacum* increase the activity of clarithrombycin against resistant strains of *E. coli*. Plant extracts coupled with antibiotics regulate MDR *E. coli* infection (37). Whole plant extracts from *Hemidesmus indicus* show urobactericidal activity against different uro-

pathogens clinically isolated from patients suffering from UTI such as *E. coli*, *Enterococcus faecoli*, *Staphylococcus aureus* and *Klebsiella pneumoniae* (38,39,40). Whole plant extracts of *Euphorbia thymifolia* controlled hematuria (41). Leaf extracts of *Agathosma capensis* also can treat urinary ailments. Root extracts of *Withania somnifera* effectively control urinary bladder infections. Root and leaf extracts of *Withania somnifera* also treats the bugs bacteria (extended spectrum beta - lactamases) present in bowel (42). Bark, leaves and flowers of *Urena lobata* control burning sensation in the urethra and other urinary troubles. Decoction prepared from *Abutilon indicum* root, *Vitis vinifera* fruit and water mixture given twice can efficaciously cure dysuria, thirst, and syphilitic fever (43). Fruit extracts of *Benincasa hispida* remediate fever, burning sensation during urination. Seed extracts of *Cucumis sativa* cures dysuria, urethritis, urolithiasis, and burning micturition (43). Some plant species like *Parietaria officinalis*, *Cucurbita maxima*, *Hordeum vulgare*, *Citrus limon*, *Allium cepa*, *Olea europaea* are used alone or mixture of these species with olive oil, goat milk and honey treats urinary diseases (44). A mixture of *Glycyrrhiza glabra* + cow milk + ghee + sugar relieves burning micturition in urethra and restores health. Similarly, *Cyanodon dactylon* roots with white pepper and butter milk reduces burning micturition, anal discomfort and dysuria. *Cyanodon dactylon* leaves show antibacterial activity and inhibit the growth of pathogenic bacteria. Gram negative bacteria were more sensitive compared to Gram positive bacteria (45).

Flower bud and flower extract of *Hibiscus rosa sinensis* can control burning micturition. Tannins present in the flower extract act as antimicrobial agents (46). Epicarp extract of *Cucumis melo* prevents stones in kidney, and UTIs (47). Leaves and roots of *Mimosa pudica* are being used to treat urinary infection, burning urination (48,49). The roots of *Asparagus racemosus* prevent many kinds of urinary troubles (50). The extract of *Solidago canadensis* controls prostrate diseases, urolithiasis and treats UTI. Stem extracts of *Equisetum ramosissimum* (horsetail) exhibit antioxidant and antibacterial properties (51) and expels stones from kidney, help in mitigating skin infections, repairs bone fracture, and relieves joint pains (52). The Chinese herb *Coptis chinensis* (Huandluam) shows *in vitro* inhibitory and anti-inflammatory effects against uropathogenic strains. It consists of berberine, coptisine and palmatine alkaloids that inhibit *E. coli* (54). *Armoracia rusticana* prevents recurrence of UTI in pediatric patients. This herb consists of isothiocyanates which display antibacterial activities against UTI (55). Several phytopharmaceuticals like flavonoids, isoflavonoids, lycopenes, carotenoids, terpenoids, omega 3-fatty acids have been shown to exhibit antibacterial and antimicrobial activity (56), and display minimal adverse effects (56). Many plants that help to treat urinary infections are listed in Table 2.

Table 2. Traditional plants to treat urinary tract infections

Botanical name of the plant	Common name	Plant parts used	Benefits
Agathosmacapensis (L.)	Spicy buchu	Leaves	Controls urinary ailments
Ballota africana	Cat herb	Leaves	Treats bladder and kidney ailments (53)
Withania somnifera (L.)	Ashwagandha/ winter cherry	Roots	Treats urinary bladder infections (42)
Euphorbia thymifolia	Laghu dudhidika / chotidudhi	Complete plant	Controls blood in urine (41)
Mimosa pudica L	Sensitive plant	Leaves and roots	Treats urinary infection and burning urination (48, 49)

Urena lobate L	Caesar weed	bark, leaves and flowers	Relieves from burning sensation and urine trouble
Abutilon indicum	Country mallow	Decoction consisting of Abutilon indicum root, Vitis vinifera fruit and water mixture	Cures dysuria, thirst, syphilitic fever (43)
Benincasa hispida	Winter melon	Fruit extract	Controls fever, burning sensation during urination. Fruit extract inhibits bacterial and fungal growth
Cucumis sativas	Cucumber	Seeds	Cures dysuria, urethritis. Seeds cure urolithiasis, burning micturition
Parietaria officinalis Cucurbita maxima Hordeum vulgare Citrus limon Allium cepa Olea europaea	Pellitory Cucumber Barley Lemon Onion Olive	Mixture of these species with olive oil, goat milk and honey	Treats urinary diseases (44)
Glycyrrhiza glabra Linn	Licorice	Glycyrrhiza glabra + cow milk + ghee + sugar	Treats burning micturition
Cyanodon dactylon	Bermuda grass	Decoction	Decoction of Cyanodon dactylon roots with white pepper and butter milk reduces burning micturition, anal discomfort and dysuria. Cyanodon dactylon leaves show antibacterial activity and inhibit the growth of pathogenic bacteria (Gram negative and positive) (45)
Hibiscus rosa sinensis	Chinese hibiscus	Flower bud Flower extract	Relieves burning micturition. Flower extracts act as antimicrobial agents (46)
Hygrophila aruculata	Kokilaksha	Seeds	Effective against syphilis and burning micturition in urethra
Oroxylum indicum	Midnight horror	Whole plant	Effective against uropathogens
Vitis negundo	Chinese chaste tree	Roots	Effective against uropathogens (57)
Cucumis melo L.	Melon	Epicarp	Expels stones from kidney, and controls urinary tract infections (47)

Euphorbia thymifolia L.	Laghududhika	Whole plant	Controls blood in urine
Azadirachta indica	Neem	Leaves	Urinary trouble
Argemone mexicana L	Mexican poppy	Root	Urinary trouble (58)
Adiantum lunulatum Burm.F	Hamsapadi	Roots	Controls hematuria (59)
Asparagus racemosus wild	Satawar	Roots	Cures urinary troubles (50)
Nyctanthes arbortristis	Tree of sadness	Leaf juice	Acts as diaphoretic, laxative and diuretic (60)
Arctostaphylos uva ursi	Uva ursi	Leaf extract	Urinary anti-septic and diuretic
Solidago canadensis, S. virgaurea and S. gigantea	Canadian golden rod	Extract	Controls prostrate diseases, urolithiasis and treats UTI (61)
Equisetum ramosissimum	Horse tail	Stem extract	Exhibits antioxidant and anti-bacterial properties (51)
Hybanthus enneaspermus	Spade flower	Ethanol extract	Regulates many UTIs
Punica granatum	Pomegranate	Seed extract	Urobactericidal activity against E. coli
Anthocephalus cadamba	Burflower tree	Bark	Antibacterial properties against uropathogens (E. coli) (62)
Armoracia rusticana	Horse radish	Whole herb	Prevents recurrence of UTI in pediatric patients. Antibacterial activities against UTI (55)

Conclusion

UTI is a serious health concern among the mankind. Proper diagnosis and therapeutic intervention at the right time is therefore indispensable. Traditional herbs play a pivotal role in nursing and managing the UTI by reinforcing the life's innate immunity. Traditional herbs minimize inflammation, support proper functioning of kidneys and relieve the symptoms with minimal adverse effects. They are potent with proven efficacy. The dose, combination of herbs, and length of treatment must however be recorded properly for their bona fide medicament. On the negative side, it is believed that not all the traditional herbs are efficacious and give relief from the clinical symptoms to the people and cannot unfasten all the infections compared to modern medical treatment or antibiotics. So, further research in the usage of herbs for treating UTIs is warranted and many innovative methods need to be developed based on the insights generated thus far and critical analysis. Herbs can certainly serve as a sustainable resource too.

Acknowledgement

I like to thank the management of VFSTR (deemed to be university) for their encouragement and moral support.

Conflict of interest

Author declares no conflicts of interest.

Funding

No grants were received by any external and internal funding sources or agencies to acrry out this research and the manuscript has been prepared independently.

Data availability

Not applicable.

References

1. Klein, R.D., Hultgren, S.J. (2020). Urinary tract infections: microbial pathogenesis, host– pathogen interactions and new treatment strategies. Nature Reviews Microbiology,18: 211-226.

2. Foxman, B., Barlow, R. D., Arcy, H., Gillespie, B., Sobel, J.D. (2000). Urinary tract infection: Self-reported incidence and associated costs. Ann. Epidemiol, 10: 509-515.

3. Lo, E., Nicolle, L. E., Coffin, S. E., Gould, C., Maragakis, L. L., Meddings, J., ... and Yokoe, D. S. (2014). Strategies to prevent catheter-associated urinary tract infections in acute care hospitals: 2014 update. Infection Control & Hospital Epidemiology, 35(5): 464-479.

4. Tamadonfar, K.O., Omattage, S. N., Spauldine, C.N., Hultgren, S. J. ON. (2019). Reaching the End of the Line: Urinary Tract Infections. In C.R. Pascale Cossart, Bacteria and Intracellularity. Microbiol. Spectr, 2019: 83-99.

5. Silverman, J.A., Schreiber, H.L., Hooton, T.M., Hultgren, S.J., (2013). From physiology to pharmacy: developments in the pathogenesis and treatment of recurrent urinary tract infections. Curr Urol Rep, 14: 448-456.

6. Pigrau, C., & Escolà-Vergé, L. (2020). Recurrent urinary tract infections: from pathogenesis to prevention. Medicina Clínica (English Edition), 155(4) 171-177.

7. Stein, G. E. (1999). Comparison of single-dose fosfomycin and a 7-day course of nitrofurantoin in female patients with uncomplicated urinary tract infection. Clinical Therapeutics, 21(11): 1864-1872.

8. Little, P., Moore, M. V., Turner, S., Rumsby, K., Warner, G., Lowes, J. A., ... & Mullee, M. (2010). Effectiveness of five different approaches in management of urinary tract infection: randomized controlled trial. Bmj, 340:1-6.

9. Butler, A. M., Durkin, M. J., Keller, M. R., Ma, Y., Powderly, W. G., & Olsen, M. A. (2022). Association of adverse events with antibiotic treatment for urinary tract infection. Clinical Infectious Diseases, 74(8):1408-1418.

10. Johansen, T. E. B., Botto, H., Cek, M., Grabe, M., Tenke, P., Wagenlehner, F. M., & Naber, K. G. (2011). Critical review of current definitions of urinary tract infections and proposal of an EAU/ESIU classification system. International Journal of Antimicrobial Agents, *38*: 64-70.

11. Medina, Martha, and Edgardo Castillo-Pino (2019) An introduction to the epidemiology and burden of urinary tract infections. Therapeutic Advances in Urology 11: 1756287219832172.

12. Flores-Mireles, A. L., Walker, J. N., Caparon, M., & Hultgren, S. J. (2015). Urinary tract infections: epidemiology, mechanisms of infection and treatment options. Nature Reviews Microbiology, 13(5): 269-284.

13 Storme, O., Tirán Saucedo, J., Garcia-Mora, A., Dehesa-Dávila, M., & Naber, K. G. (2019). Risk factors and predisposing conditions for urinary tract infection. Therapeutic Advances in Urology, 11, 1756287218814382.

14. Ahmed, S. S., Shariq, A., Alsalloom, A. A., Babikir, I. H., & Alhomoud, B. N. (2019). Uropathogens and their antimicrobial resistance patterns: Relationship with urinary tract infections. International Journal of Health Sciences, 13(2):48.

15. Salvatore, S., Salvatore, S., Cattoni, E., Siesto, G., Serati, M., Sorice, P., & Torella, M. (2011). Urinary tract infections in women. European Journal of Obstetrics & Gynecology and Reproductive Biology, 156(2):131-136.

16. Al Lawati, H., Blair, B. M., & Larnard, J. (2023). Urinary tract infections: core curriculum 2024. American Journal of Kidney Diseases,83.1:90-100.

17. Ebana, R. U. B., Edet, U. O., Ekaneme-

sang, U. M., Etok, C. A., Ikon, G. M., & Noble, M. K. (2016). Phytochemical screening and antimicrobial activity of three medicinal plants against urinary tract infection pathogens. Asian Journal of Medicine and Health, 1(2):1-7.

18. Abu-Naser, S. S., & Shaath, M. Z. (2016). Expert system urination problems diagnosis. World-wide Journal of Multidisciplinary Research and Development, 2(5):9-19.

19 Khalil, I. A., Troeger, C., Blacker, B. F., Rao, P. C., Brown, A., Atherly, D. E., & Reiner, R. C. (2018). Morbidity and mortality due to shigella and enter toxigenic Escherichia coli diarrhoea: the Global Burden of Disease Study 1990-2016. The Lancet Infectious diseases, 18(11): 1229-1240.

20 Naylor, N. R., Pouwels, K. B., Hope, R., Green, N., Henderson, K. L., Knight, G. M., & Deeny, S. R. (2019). The health and cost burden of antibiotic resistant and susceptible *Escherichia coli* bacteremia in the English hospital setting: a national retrospective cohort study. PloS one, 14(9): e0221944.

21 Nirmal, S. A., Pal, S. C., Otimenyin, S. O., Aye, T., Elachouri, M., Kundu, S. K., & Mandal, S. C. (2013). Contribution of herbal products in global market. Pharma Rev, 95-104.

22 Nisar, B., Sultan, A., & Rubab, S. L. (2018). Comparison of medicinally important natural products versus synthetic drugs-a short commentary. Nat. Prod. Chem. Res, 6(2):308.

23 Ifesan, B. O. T., Fashakin, J. F., Ebosele, F., & Oyerinde, A. S. (2013). Antioxidant and antimicrobial properties of selected plant leaves. European Journal of Medicinal Plants, 3(3): 465-473.

24 Ferdosh, S. (2023). Ethnobotanical Review of Selected Medicinal Plants in Guam for the Treatment of Urinary Tract Ailments and Their Pharmacological Properties. Scientia Pharmaceutica, 91(3): 43.

25 Mhlongo, L. S., & Van Wyk, B. E. (2019). Zulu medicinal ethnobotany: New records from the Amandawe area of KwaZulu-Natal, South Africa. South African Journal of Botany, 122: 266-290.

26 Moteetee, A., & Van Wyk, B. E. (2011). The medical ethnobotany of Lesotho: a review. Bothalia, 41(1): 209-228.

27 Mabona, U., & Van Vuuren, S. F. (2013). Southern African medicinal plants used to treat skin diseases. South African Journal of Botany, 87:175-193.

28 Yang, G., & Chen, D. (2008). Alkaloids from the roots of *Zanthoxylum nitidum* and their antiviral and antifungal effects. Chemistry & biodiversity, 5(9): 1718-1722.

29 Huang, H. Y., Ishikawa, T., Peng, C. F., Tsai, I. L., & Chen, I. S. (2008). Constituents of the root wood of *Zanthoxylum wutaiense* with antitubercular activity. Journal of Natural Products, 71(7):1146-1151.

30 Wang, J. Y., Wang, Z., Li, M. Y., Zhang, Z., Mi, C., Zuo, H. X., ... & Jin, X. (2018). Dictamnine promotes apoptosis and inhibits epithelial-mesenchymal transition, migration, invasion and proliferation by downregulating the HIF-1α and Slug signaling pathways. Chemico-Biological Interactions, 296:134-144.

31 Fahmy, H., Hegazi, N., El-Shamy, S., & Farag, M. A. (2020). Pomegranate juice as a functional food: A comprehensive review of its polyphenols, therapeutic merits, and recent patents. Food & Function, 11(7): 5768-5781.

32 Pirzadeh, M., Caporaso, N., Rauf, A., Shariati, M. A., Yessimbekov, Z., Khan, M. U., & Mubarak, M. S. (2021). Pomegranate as a source of bioactive constituents: A review on their characterization, properties and applications. Critical reviews in food

science and nutrition, 61(6): 982-999.

33 Smeriglio, A., Barreca, D., Bellocco, E., & Trombetta, D. (2017). Proanthocyanidins and hydrolysable tannins: occurrence, dietary intake and pharmacological effects. British Journal of Pharmacology, 174(11): 1244-1262.

34 Yarnell, E. (2002). Botanical medicines for the urinary tract. World journal of urology, 20:285-293.

35 Amin, A. H., Subbaiah, T. V., & Abbasi, K. M. (1969). Berberine sulfate: antimicrobial activity, bioassay, and mode of action. Canadian journal of microbiology, 15(9):1067-1076.

36 Sahib, A. S., Mohammed, I. H., & Hamdan, S. J. (1970). Use of aqueous extract of corn silk in the treatment of urinary tract infection. Journal of Complementary Medicine Research, 1(2):93-93.

37 Darwish, R. M., & Aburjai, T. A. (2010). Effect of ethnomedicinal plants used in folklore medicine in Jordan as antibiotic resistant inhibitors on *Escherichia coli*. BMC complementary and alternative medicine, 10, 1-8.

38 Das, S., Naik, P., Panda, P. (2017). Effect of *Hemidesmus indicus* R.Br. root extract on urinary tract infection causing bacteria. Int J Herbal Med, 5: 160-168.

39 Das, S., Panigrahi, S., & Panda, P. (2018). Antiurobacterial activity of *Punica granatum* L. seed extract. European Journal of Medicinal Plants, 22(2): 1-12.

40 Das, S., Sahoo, K. R., & Parida, B. (2018). Bactericidal activity of *Hemidesmus indicus* R. Br. root extract against clinically isolated uropathogens. J Med Plant Studies, 6(6): 180-192.

41 Aminuddin, G. R. (1993). Observations of the ethnobotany of the Bhunjia–a tribe of Sonabera plateau. Ethnobot, 5: 83-86.

42 Kapur, A., & John, S. A. (2015). Prevalence of Extended-Spectrum Beta-Lactamase-Producing Pathogens from Urinary Tract Infected Samples and Their Sensitivity Pattern Against *Withania somnifera* L. International Journal of Infection, 2(1): 1-4.

43 Kumarasamy, S., & Radhakrishnan, M. (2022). Traditional Siddha Medicinal Herbs Used in the Treatment Urinary Tract Infection (Muthira Kiricharam)-A Narrative Review. International Journal of Ayurveda and Pharma Research, 104-112.

44 Taibi, K., Abderrahim, L. A., Boussaid, M., Taibi, F., Achir, M., Souana, K., & Said, K. N. (2021). Unraveling the ethnopharmacological potential of medicinal plants used in Algerian traditional medicine for urinary diseases. European Journal of Integrative Medicine, 44: 101339.

45 Chaudhari, Y., Mody, H. R., & Acharya, V. B. (2011). Antibacterial activity of Cynodon dactylon on different bacterial pathogens isolated from clinical samples. *International* Journal of Pharmaceutical Studies and Research, 1: 16-20.

46 Ruban, P., & Gajalakshmi, K. (2012). In vitro antibacterial activity of Hibiscus rosa–sinensis flower extract against human pathogens. Asian Pacific Journal of Tropical Biomedicine, 2(5): 399-403.

47 Brahmam, M., Dhal, N. K., & Saxena, H. O. (1996). Ethnobotanical studies among the Tanla of Malyagiri hills in Dhenkanal district, Orissa, India. Ethnobiology in Human Welfare. Deep Publications, 393-396.

48 Girach, R. D., Aminuddin, A., Ahmed, M., Brahmam, M., & Misra, M. K. (1994). Native phytotherapy among rural population of district Bhadrak Orissa.

49 Dash, S. S., & Misra, M. K. (1999). Plant diversity and sustainable development in a Tribal village eco-complex on the Eastern Ghats of Orissa. Journal of Human Ecolo-

gy, 10(5-6): 415-419.

50 Bhattarai, S., Chaudhary, R. P., Taylor, R. S., & Ghimire, S. K. (2009). Biological activities of some Nepalese medicinal plants used in treating bacterial infections in human beings. Nepal Journal of Science and Technology, 10: 83-90.

51 Sureshkumar, J., Amalraj, S., Murugan, R., Tamilselvan, A., Krupa, J., Sriramavaratharajan, V., ... & Ayyanar, M. (2021). Chemical profiling and antioxidant activity of *Equisetum ramosissimum* Desf. stem extract, a potential traditional medicinal plant for urinary tract infections. Future Journal of Pharmaceutical Sciences, 7: 1-11.

52 Sureshkumar, J., Ayyanar, M., & Silambarasan, R. (2021). Ethnomedicinal uses, phytoconstituents and pharmacological importance of pteridophytes used by Malayalis in Kolli hills, India: A quantitative survey. Journal of Herbal Medicine, 25: 100418.

53 Hulley, I. M., & Van Wyk, B. E. (2019). Quantitative medicinal ethnobotany of Kannaland (western Little Karoo, South Africa): Non-homogeneity amongst villages. South African Journal of Botany, 122: 225-265.

54 Godaly, G., Ambite, I., & Svanborg, C. (2015). Innate immunity and genetic determinants of urinary tract infection susceptibility. Current opinion in infectious diseases, 28(1): 88-96.

55 Williams, G., & Craig, J. C. (2009). Prevention of recurrent urinary tract infection in children. Current opinion in infectious diseases, 22(1):72-76.

56 Maddala, V. K. S., Asha, S., & Singh, S. (2022). Phytopharmaceuticals of Medicinal Plants for the Treatment of Common Illnesses. Phytopharmaceuticals and Biotechnology of Herbal Plants, 201-211.

57 Maddala, V. K. S., Asha, S., & Singh, S. (2022). Phytopharmaceuticals of Medicinal Plants for the Treatment of Common Illnesses. Phytopharmaceuticals and Biotechnology of Herbal Plants, 201-211.

57Mishra, S., Mekap, S. K., Patra, S., Dhal, N. K., & Sahoo, S. (2015). Antioxidant and anti-infective potential of Oleanolic acid acetate vis-à-vis *Vitex negundo* Linn. and *Oroxylum indicum* Vent. against human pathogens causing infections of UT, GIT and skin. Oriental Pharmacy and Experimental Medicine, 15:73-82.

58 Nayak, A., Das, N. B., & Nanda, B. (1998). Utility of some tribal drugs of Keonjhar and Similipal area. journal of teaching and research in chemistry, 5:53-59.

59 Girach, R. D. (1992). Medicinal plants used by Kondh tribe of district Phulbani (Orissa) in Eastern India. Ethnobotany, 4(1):53-66.

60 Verma, N. S., Dwivedi, S., Panigrahi, D., & Gupta, S. K. (2011). Anti-bacterial activity of root bark of *Nyctanthes arbor-tristis* Linn. International Journal of Drug Discovery and Herbal Research, 1(2): 61-62.

61 Meyer, B., Schneider, W., & Elstner, E. F. (1995). Antioxidative properties of alcoholic extracts from Fraxinus excelsior, *Populus tremula* and *Solidago virgaurea*. Arzneimittel-forschung, 45(2):174-176.

62. Mishra, M. P., & Padhy, R. N. (2013). In vitro antibacterial efficacy of 21 Indian timber-yielding plants against multidrug-resistant bacteria causing urinary tract infection. Osong public health and research perspectives. *4*(6): 347-357.